



HAL
open science

Study of cerebellar synaptic deficits in two rodent models of schizophrenia

Maxime Veleanu

► **To cite this version:**

Maxime Veleanu. Study of cerebellar synaptic deficits in two rodent models of schizophrenia. *Neurons and Cognition [q-bio.NC]*. Sorbonne Université, 2020. English. NNT : 2020SORUS362 . tel-03378196

HAL Id: tel-03378196

<https://theses.hal.science/tel-03378196>

Submitted on 14 Oct 2021

HAL is a multi-disciplinary open access archive for the deposit and dissemination of scientific research documents, whether they are published or not. The documents may come from teaching and research institutions in France or abroad, or from public or private research centers.

L'archive ouverte pluridisciplinaire **HAL**, est destinée au dépôt et à la diffusion de documents scientifiques de niveau recherche, publiés ou non, émanant des établissements d'enseignement et de recherche français ou étrangers, des laboratoires publics ou privés.

Sorbonne Université

Ecole doctorale Cerveau, Cognition, Comportement (Ed158)

Centre de Recherche Interdisciplinaire en Biologie, UMR7241/U1050, collège de France

Etude des déficits synaptiques cérébelleux dans deux modèles murins de schizophrénie.

Par Maxime Veleau

Thèse de doctorat de Neurosciences

Dirigée par Fekrije Selimi

Présentée et soutenue publiquement le 17 septembre 2020.

Devant un jury composé de :

Lohof Ann, PU, présidente du jury

Vaudry David, CR-HDR, rapporteur

Laumonier Frédéric, CR-HDR, rapporteur

Becamel Carine, MCU-HDR, examinatrice

Jamain Stéphane, CR, examinateur

Selimi Fekrije, DR, directrice de thèse

Remerciements

Tout d'abord, je souhaiterais remercier les membres du jury Ann Lohof, David Vaudry, Frederic Laumonier, Carine Becamel, et Stephane Jamain, d'avoir pris le temps d'assister à ma thèse, et à Ann Lohof et Stéphane Jamain d'avoir suivi mes travaux durant ces divers comités de suivi.

Merci à Fekrije de m'avoir permis de réaliser cette thèse, pour ton expertise, de m'avoir formé intensivement à la rigueur, à la précision et l'organisation, qui m'étaient un peu trop ésotériques, de m'avoir permis d'acquérir de nombreuses connaissances dans de nombreux domaines, et d'avoir souvent traduit mes questions en quelque chose de compréhensible pour le commun des mortels lors de présentations.

Merci à Shayan pour ton aide récurrente, et nos discussions incongrues dénuées de tout filtres, Maëla de répendre une bonne atmosphère, et pour notre agréable cohabitation en salle 17, Séverine d'être un pilier pour l'équipe, Mélanie pour tes éclats d'enthousiasmes, Elsa pour ta gentillesse, aux voisins d'étage, Adrien, Shahab, pour les discussions-café, à Flora pour m'avoir permis de revêtir le rôle clairement usurpé de mentor aux échecs, et toutes les autres personnes que j'ai pu cotoyer au labo.

Merci à Aurore, pour ta présence indispensable, et en plus d'être une parfaite accompagnante à la contrebasse, d'avoir égayé les rares moments de temps libre. Merci à ma famille, de m'avoir supporté et épaulé toutes ces années.

Merci aux amis, Mehdi et Nolwenn pour les beuveries en sortie de labo, Jaffar pour les excursions improvisées, de servir d'aimant à rencontres, et de m'avoir permis d'être dans un jury de thèse de pharma (un peu usurpé, aussi), à Yacine d'avoir contribué à vider la Norvège de ses saumons lors de nos japonais à volonté bimensuels depuis 5 ans, à Jean, Nico, Clément, et les autres amis de pharma.

Intuition has to lead knowledge, but it can't be out there alone." –

Bill Evans

Table des matières

Remerciements	3
Table des matières	5
Table des figures	7
Abbreviations	9
Resumé étendu de la these en Français.....	11
Introduction	17
1) Schizophrenia, a major neurodevelopmental disorder	19
1.1) History and pathophysiology.....	19
1.2) The disconnection theory in Schizophrenia	20
1.3) A multi-factorial disease	21
1.4) Modeling schizophrenia in animals	23
2) Schizophrenia, a synaptopathy?	25
2.1) Synaptic changes in schizophrenia, evidence from postmortem tissue analysis	25
2.1.1) A reduction in grey matter volume	25
2.1.2) Synaptic changes	28
2.2) Synaptic deficits in schizophrenia: evidence from genetic studies.....	30
2.2.1) Rare variants	31
2.2.2) Common variants.....	33
2.3) Synaptic deficits: Functional consequences on neural network	37
2.4) Electrophysiological deficits in mice model of schizophrenia	38
2.5) Synaptic loss in schizophrenia: developmental perspective	40
2.5.1) Deficits of synapse formation	40
2.5.2) Deficits of synapse elimination.....	41
3) The olivo-cerebellar system: a powerful model to study circuit development	45
3.1) Global structure of the cerebellum and inferior olive	45
3.1.1) Cerebellar anatomy	45
3.1.2) Histology of the cerebellum.....	47
3.1.3) Connectivity on Purkinje Cells	49
3.2) Development of the Olivo-cerebellar network.....	54
3.2.1) Development of the Parallel Fiber/Purkinje Cell synapses.....	54
3.2.2) Development of the Climbing Fiber/Purkinje Cell synapses.....	56
4) The cerebellum, an underrated actor in schizophrenia	59
4.1) The cerebellum, a major structure for motor coordination	59

4.2) The cognitive cerebellum.....	60
4.2.1) From motor function to cognition	60
4.2.2) Decoding the cognitive role of cerebellum: studies on animals.....	64
4.3) The cerebellum and schizophrenia	66
4.3.1) Cerebellar injury can induce symptoms relevant to schizophrenia.....	66
4.3.2) Schizophrenic patients have cerebellar deficits	67
Results	71
Part 1: Afferent-specific deficits in cerebellar Purkinje cell synapses in the PCP developmental model of schizophrenia	75
Abstract/Summary	77
Introduction	78
Results.....	81
Discussion.....	85
Materiel and method	91
References	95
Figures.....	105
Supplementary Information.....	114
Part 2: No deficits in cerebellar synapses in a genetic model of schizophrenia.	127
Abstract.....	129
Introduction	130
Results.....	131
Discussion.....	133
Material and methods.....	134
References	138
Figures.....	141
General discussion	149
Summary of the main results	151
What is the effect of PCP subchronic injections during development on climbing fiber/Purkinje cell synapses?	153
Does <i>Ctgf</i> overexpression cause synaptic alterations in the neonatal PCP model?	154
Hypothesis for the link between PCP, neuronal activity and synaptic alterations in cerebellar Purkinje cells	157
Neuronal activity, a potential actor of neurodevelopmental and synaptic disorders?	162
How this study could contribute to the understanding of schizophrenia physiopathology?	163
Relevance of cerebellar synaptic deficits in schizophrenia?	165
Bibliography	167
Annexe	199

Table des figures

Introduction

Figure 1: Dendritic spines of pyramidal cells in the prefrontal cortex of schizophrenic patients compared to healthy subjects	27
Figure 2: Many representative genes are potentially implicated in schizophrenia, in pre and post-synaptic sides.	36
Figure 3: Computational model for homeostatic neuroadaptation.	43
Figure 4 Development of the synapses and alterations in schizophrenia: schematic summary of current knowledge.	44
Figure 5: The olivo-cerebellar network.	46
Figure 6: The cerebellar cortex.	48
Figure 7: Olivo-cerebellar topography.	49
Figure 8: Electron micrograph of excitatory synapses of Purkinje Cells	51
Figure 9: Climbing fiber histology	53
Figure 10: Scheme of the postnatal development of the cerebellar cortex.	58
Figure 11: Cerebellum and cognition: theory and functional evidences.	63

Resultats

Partie 1: Afferent-specific deficits in cerebellar Purkinje cell synapses in the PCP developmental model of schizophrenia

Figure 1. Normal global cerebellar morphology in juvenile mice treated neonatally with PCP.	105
Figure 2. Normal spontaneous spiking of cerebellar Purkinje Cells in PCP-treated mice.	107
Figure 3. Afferent-specific alterations of CF presynaptic boutons morphology are lobule-specific.	109
Figure 4. Normal molecular layer interneurons number and presynaptic boutons morphology in PCP mice	110
Figure 5. Subchronic neonatal PCP induces transient gene expression changes of the neuronal surfaceome in the cerebellum	112
Figure Supplementary 1. Experimental design and recording areas.	114
Figure Supplementary 2. Subchronic neonatal PCP induced gene expression changes of the surfaceome in the cerebellum and brainstem at P30 and the brainstem at P11.	115
Figure Supplementary 3. <i>Ctgf</i> expression after PCP injection and during normal postnatal development in the cerebellum and brainstem	116
Supplementary table 1: Results of the RT-PCR, represented in fold change of the mean value in the PCP-treated group compared to saline-treated group.	117
Supplementary table 2: Results of the RT-PCR, in the four extracts.	121
Supplementary table 3 : R script for gene expression analysis	125

Partie 2: No deficits in cerebellar synapses in a genetic model of schizophrenia.

Figure 1. Normal global cerebellar morphology in P30 LgDel mice.	141
Figure 2. Normal spontaneous electrophysiological activity of Purkinje Cells in the cerebellar cortex of LgDel +/- mice.	142

Figure 3. Normal climbing fiber presynaptic boutons morphology in LgDel mice..... 143
Figure 4. Normal parallel fiber synaptic density in LgDel mice. 145
Figure LgDel 5. Normal Molecular Layer Interneurons presynaptic boutons morphology in LgDel mice. 147

Discussion

Figure S1 : Preliminary results for the role of activity in PCP-elicited deficits 158
Figure S2: Hypothesis for a potential mechanism for PCP induced cerebellar synaptic deficits. 161

Abbreviations

ACSF: Artificial Cerebrospinal fluid

AMPA: α -amino-3-hydroxy-5-methyl-4-isoxazolepropionic acid

ASD: Autism Spectrum Disorder

BDA: Biotinylated Dextran Amines

BDNF: Brain-Derived Neurotrophic Factor

BMP: Bone Morphogenetic Protein

CaBP: Calcium-Binding Protein

CAM: Cell Adhesion Molecule

CCAS: Cerebellar Cognitive Affective Syndrome

CNO: Clozapine-N-Oxide

CNS: Central Nervous System

CNV: Copy Number Variants

COMT: Catechol-O-methyltransferase

CR: Cysteine-Rich

CT: C-terminal

CTGF: Connective Tissue Growth Factor

DAO: dorsal accessory olivary nuclei

DCN: Deep cerebellar nuclei

DISC1: Disrupted In Schizophrenia 1

DLSN: Dorso Lateral Septum Nucleus

DMC: dorsomedial cell column

DMN: Default Mode Network

DWI: Diffusion Weighted Imaging

EGL: External Granular Layer

EPSC: Excitatory Post-Synaptic Currents

GABA: gamma-aminobutyric acid

GFP: Green Fluorescent Protein

GPCR: G protein-coupled receptors

GWAS: Genome-Wide association studies

IGF: insulin-like growth factor

IGFBP: Insulin-like Growth Factor Binding protein

IGL: Internal Granular Layer

IPSC: Inhibitory Post-Synaptic Currents

IQ: Intellectual coefficient

ISI: Interspike interval

KD: Knock Down

KO: Knock out

LgDel: Large Deletion

LSD: Lysergic acid diethylamide

LTD: Long-term depression

LTP: Long-term potentiation

MAO: Medial accessory olive nuclei

MEA: Microelectrode arrays

MHC: Major Histocompatibility Complex

MNTB: Medial Nucleus of the Trapezoid Body

MRI: Magnetic Resonance imaging

NMDA: N-methyl-D-aspartic acid

NMDAR: NMDA Receptor

OR: Odds Ratio

PC: Purkinje cell

PCP: Phenyl Cyclohexyl Piperidine, or Phencyclidine

PET: Positron Emission Tomography

PFA: Paraformaldehyde

PPI: Prepulse inhibition

PSA-NCAM: polysialic acid neural cell adhesion molecule

PBS: Phosphate buffered saline

RELN: Reelin

SD: Standard Deviation

SEM: Standard Error Mean

SNP: Single Nucleotide Polymorphism

TGF: Transforming Growth Factor

UCT: Universal Cerebellar Transform

VGCC: Voltage-gated Calcium Channel

VLO: ventrolateral outgrowth

VOR: vestibulo-ocular reflex

VWC: Willebrand factor type C

WT: Wild Type

Resumé étendu de la these en Français

La schizophrénie est une des pathologies psychiatriques les plus fréquentes et invalidantes, avec une prévalence estimée entre 0,7 et 1%. Cette pathologie est caractérisée par un ensemble de symptômes, classés selon trois catégories : les symptômes dits positifs ou « productifs », tels que les délires, la paranoïa, ou les hallucinations sensorielles ; les symptômes négatifs ou déficitaires comprenant un isolement social, un appauvrissement affectif et émotionnel ; et des symptômes dissociatifs, se définissant par une désorganisation de la pensée et de la parole associée à des déficits cognitifs. Il est maintenant bien connu que cette pathologie est d'origine multifactorielle. Elle est causée à la fois par des facteurs génétiques induisant une « vulnérabilité » accrue durant l'adolescence, mais aussi conjointement par des facteurs environnementaux favorisant comme le stress ou la consommation de drogues. Si la symptomatologie de la schizophrénie a été largement décrite depuis plusieurs décennies, de nombreuses questions restent en suspens concernant les mécanismes neurobiologiques qui la sous-tendent.

Un des éléments les plus incriminés dans la schizophrénie est la synapse. De nombreuses études post-mortem et génétiques ont décelé des anomalies synaptiques chez les patients. Notamment, les patients présentent fréquemment une baisse de la densité des épines dendritiques, siège de l'établissement des synapses excitatrices, dans de nombreuses régions du système nerveux central. De plus, la quantification de certains marqueurs synaptiques ainsi que l'expression de nombreux gènes synaptiques ont également révélé des anomalies fréquentes chez les patients schizophrènes. Par ailleurs, les études génétiques ont, elles, décelé de nombreuses mutations significativement associées à la schizophrénie, et parmi ces gènes, de nombreux codent pour des protéines synaptiques, ou étant impliquées dans la fonction synaptique. Cependant, prises séparément, ces mutations ne sont associées qu'à un faible surrisque de développer la maladie, n'ayant, par conséquent, pas permis de déceler un candidat synaptique majeur pour expliquer la pathologie. Au contraire, l'élévation du risque induite par des facteurs génétiques serait causée par une accumulation de nombreuses mutations à faible impact, menant à un réseau neuronal anormal, et potentiellement plus sensible à des facteurs environnementaux. Ainsi, à ce jour, il n'y a pas de candidats précis identifiés comme cause des anomalies synaptiques dans la schizophrénie, et les potentielles altérations du développement synaptique restent encore peu connues.

Au niveau des structures cérébrales impliquées dans la schizophrénie, si le cortex préfrontal et l'hippocampe concentrent la majeure partie des recherches, d'autres structures pourraient avoir une implication, telles que le cervelet. En effet, bien que le cervelet soit habituellement considéré comme une structure essentiellement motrice, il est maintenant reconnu comme ayant également une implication dans des processus cognitifs. De plus, les patients schizophrènes présentent fréquemment des anomalies morphologiques cérébelleuses telles qu'une diminution de son volume, et un ensemble de symptômes dans lesquels le cervelet joue un rôle, tels que des « signes neurologiques mineurs », par ailleurs associés à un mauvais pronostic. Le cortex cérébelleux a une architecture cellulaire stéréotypée : les cellules de Purkinje, les neurones principaux du cervelet et unique voie de sortie du cortex cérébelleux, reçoivent 4 afférences synaptiques : deux excitatrices, les fibres parallèles, provenant des neurones granulaires et les fibres grimpantes provenant des neurones de l'olive inférieure dans le tronc cérébral ; et deux inhibitrices, provenant des neurones en étoile et en panier. Chacune de ces afférences possède des propriétés morphologiques et fonctionnelles distinctes, mises en place selon des mécanismes développementaux précis. Ces afférences peuvent être étudiées indépendamment, faisant ainsi du cortex cérébelleux une structure de choix pour l'étude du développement synaptique à l'échelle synapse-spécifique.

Ce projet de thèse s'est organisé autour de trois grandes questions. Premièrement, l'étude des propriétés morphologiques et fonctionnelles globales du cervelet dans deux modèles murins de schizophrénie a pour but de décrire d'éventuelles altérations cérébelleuses pouvant participer à l'étiologie de la schizophrénie. Deuxièmement, l'étude des déficits synaptiques cérébelleux dans deux modèles murins de schizophrénie a pour but de déceler et de décrire d'éventuels déficits à l'échelle synapse-spécifique. Enfin, l'étude des mécanismes moléculaires pourrait permettre de trouver de nouveaux candidats et de nouvelles voies de signalisations impliquées dans le développement synaptique.

Afin de répondre à ces questions, nous avons utilisé deux modèles murins développementaux couramment utilisés pour mimer la schizophrénie : un modèle pharmacologique, consistant en l'injection de Phencyclidine (PCP), un antagoniste NMDA connu pour provoquer une symptomatologie de type psychotique proche de celle rencontrée chez les patients schizophrènes, et un modèle génétique, le modèle LgDel, mimant la délétion 22q11.2 connue pour provoquer chez l'homme un risque 25 à 30 fois plus élevé de devenir schizophrène. L'utilisation de deux modèles permet d'étudier deux différentes stratégies

d'induction de la pathologie, à savoir une environnementale (PCP) et une génétique (LgDel) et d'étudier leur impact respectif sur le cervelet et son développement synaptique.

Dans un premier temps, je me suis concentré sur le modèle PCP. Après avoir injecté le PCP durant la seconde semaine postnatale, j'ai étudié les propriétés morphologiques et fonctionnelles du cervelet à P30 (30 jours après la naissance). La quantification de la surface de tranches sagittales de cervelet n'a pas permis de détecter de différences significatives chez les souris PCP comparées aux contrôles, et l'analyse extracellulaire *ex-vivo* de l'activité spontanée des cellules de Purkinje a révélé des propriétés électrophysiologiques normales chez les souris PCP, suggérant que le traitement PCP néonatal n'induit pas de différences majeures de la morphologie du cervelet et de l'activité spontanée du cortex cérébelleux.

Nous avons ensuite étudié la morphologie des différentes afférences de la cellule de Purkinje à P30 en utilisant des marqueurs d'immunohistochimie spécifiques de chacun des boutons présynaptiques et nous avons détecté des différences spécifiques d'un seul type de synapse. En effet, si les afférences inhibitrices, et les fibres parallèles, ne semblent pas affectées dans le modèle PCP, les boutons présynaptiques des fibres grimpantes sont significativement plus petits chez les souris PCP, et sont localement présents en plus grand nombre dans un des deux lobules étudiés, suggérant que le modèle PCP induit des déficits synapse-spécifique au niveau de la fibre grimpante, possiblement en perturbant la maturation synaptique et les mécanismes d'élimination synaptique durant le développement.

Nous avons ensuite voulu étudier les mécanismes moléculaires pouvant expliquer ces déficits. Pour ce faire, nous avons quantifié l'expression de certains gènes codant pour des protéines membranaires et sécrétées pouvant potentiellement jouer un rôle dans le développement synaptique. En effet, ces deux familles de molécules comprennent de nombreux acteurs tels que les cadhérines, les ephrines, ou les protéines du complément, connues pour réguler la formation, la maturation, l'élagage synaptique, ou encore participer à la spécificité du contact synaptique entre deux neurones. Nous avons quantifié l'expression génique à deux différentes périodes : à P11 immédiatement après la dernière injection de PCP, afin de déceler des altérations moléculaires aiguës et transitoires, puis à l'adolescence à P30, afin de déceler d'éventuelles altérations moléculaires durables. Alors que nos analyses n'ont pas détecté de différences à P30, 30 gènes sont transitoirement dérégulés dans le cervelet à P11. Parmi ces gènes, nous avons trouvé un certain nombre de candidats pouvant potentiellement expliquer les déficits synaptiques, dont *Ctgf*, un gène codant pour une protéine de la matrice extracellulaire,

précédemment identifiée en tant que potentiel biomarqueur dans la schizophrénie, et interagissant fonctionnellement avec de nombreux acteurs de la formation, maturation et élimination synaptique. Enfin, nous avons montré que l'injection de PCP perturbe l'activité du réseau neuronal dans le cervelet, en faveur d'une augmentation. De plus, nos résultats préliminaires montrent que l'augmentation de l'activité des neurones granulaires durant la seconde semaine postnatale est suffisante pour reproduire l'augmentation de l'expression de *Ctgf*, nous menant à suggérer l'hypothèse que les déficits synaptiques cérébelleux induits par le PCP sont médiés par une sécrétion activité-dépendante de *Ctgf* dans le cervelet durant une période critique du développement synaptique. Afin de vérifier cette hypothèse, deux expériences complémentaires vont être réalisées, pour déterminer si l'augmentation durant la seconde semaine postnatale de l'expression de *Ctgf* d'une part, et de l'activité des neurones granulaires d'autre part, suffisent à reproduire les déficits synaptiques cérébelleux du modèle PCP.

Pour le second modèle, le modèle génétique *LgDel*, nous avons reproduit les analyses morphologiques et électrophysiologiques globales réalisées sur le modèle PCP. Nos résultats montrent que cette délétion génétique n'induit pas à P30 de déficits majeurs de la morphologie du cervelet, ni de l'activité spontanée de cellules de Purkinje, et que la morphologie des différents boutons présynaptiques est normale, suggérant que le développement des synapses dans le réseau olivo-cérébelleux n'est pas affecté dans ces souris.

Pour conclure, ce travail de thèse a pu mettre en avant des déficits synapse-spécifique dans l'établissement du réseau synaptique de la cellule de Purkinje dans un modèle environnemental de schizophrénie, alors que le modèle génétique présente un réseau synaptique normal, pouvant suggérer que des facteurs environnementaux précoces dans le développement pourraient induire une désorganisation de la micro circuiterie synaptique. De plus, notre étude moléculaire a permis d'identifier différents candidats, et en particulier la protéine sécrétée CTGF, pouvant potentiellement expliquer les déficits synaptiques induits par le PCP, et ainsi être un nouvel acteur de la formation et maturation du réseau synaptique. Enfin, l'activité neuronale pouvant être influencée par des facteurs environnementaux, nous avons émis l'hypothèse qu'une perturbation environnementale à une période critique du développement synaptique peut induire des altérations au long terme de l'architecture synaptique, via, notamment, une dérégulation activité-dépendante de l'expression de molécules synaptogéniques.

Introduction

1) Schizophrenia, a major neurodevelopmental disorder

1.1) History and physiopathology

Schizophrenia is one of the most famous psychiatric disorders, and it has raised many questions and debates for almost one century. But its mechanisms are still poorly understood.

This disease is one of the most important public health priorities in psychiatric disorders, because of its high prevalence (0.7 to 1% of the population (Saha et al., 2005)) and the severity of the symptoms, classically separated into positive symptoms, which include hallucinations, delusions, paranoia; negative symptoms, with anhedonia, social withdrawal; and cognitive symptoms. Schizophrenia affects young subjects, from adolescence to early adulthood (Rapoport et al., 2005), leads to a progressive loss of autonomy and marginalization, and a decreased life expectancy by around 20 years (Olfson et al., 2015). Despite numerous drugs having been released on the market to treat schizophrenia, failure rate is high: more than 40% of patients are re-hospitalized, engaging an important human and economic cost for health care systems (Vos et al., 2017).

While the symptomatology of schizophrenia had been described since the beginning of the XIXth century by the German psychiatrist Emil Kraepelin under the term of “*precocial demencia*”, the first neuropathological hypothesis came only 50 years after. In 1951, Laborit made the fortuitous discovery that an antihistaminic drug, Chlorpromazine, initially used to treat anaphylactic shock, has a huge “calming” effect on patients and moderates their psychotic crisis (Laborit et al., 1952). This gave birth to the first effective treatment for schizophrenic patients: neuroleptics. This discovery has been at the root of the understanding of schizophrenia physiopathology, but also of modern neuropharmacology. This drug successfully treats positive symptoms of schizophrenia, and because it is known to block post-synaptic D2 dopaminergic receptors, researchers hypothesized a hyperdopaminergic state in schizophrenia (Carlsson and Lindqvist, 1963). This hypothesis was further strengthened by the observation that dopaminergic enhancer drugs, like amphetamines and cannabinoids, could induce psychotic symptoms (Lieberman et al., 1987). At end of the 80s, the discovery that dopamine metabolites were not universally elevated in the schizophrenic brain, brought the idea of a regional specificity of dopaminergic defects. Weinberger proposed that 1. dopaminergic receptors D1 are principally located in the prefrontal cortex and under-activated, while D2 receptors are mainly subcortical and overactivated, and 2. the cortical hypodopaminergia may be responsible

for negative symptoms, while subcortical hyperdopaminergia may be responsible for positive symptoms (Weinberger, 1987).

However, the dopaminergic hypothesis does not seem sufficient to explain schizophrenia pathophysiology, given the high rate of resistance to neuroleptic treatment and relapse rate reaching 50% (Gilbert et al., 1995). The observation that some psychotomimetic drugs like phencyclidine (PCP), a noncompetitive N-méthyl-D-aspartate (NMDA) antagonist, are inducing acute symptoms mimicking negative, cognitive, and positive symptoms of schizophrenia on healthy subjects (Pradhan, 1984), introduced glutamatergic receptors as potential actors of schizophrenia. Consistent with this hypothesis, postmortem studies on brains of patients with schizophrenia show altered expression levels of several NMDAR and α -amino-3-hydroxy-5-methyl-4-isoxazolepropionic acid (AMPA) receptor subunit (reviewed in part 2.3). Moreover, these receptors play a role in dopamine release: chronic administration of PCP induces a decrease of prefrontal dopaminergic activity, and an increase of subcortical dopaminergic activity—consistent with the dopaminergic hypothesis (Carlsson and Carlsson, 1990). While administration of NMDA antagonists is sufficient to induce a wide range of schizophrenia-like symptoms, schizophrenia seems to be much more than just a global hypoglutamatergic state. Since NMDA is a major excitatory neurotransmitter, blockade of NMDA receptors is supposed to induce a decrease of neuronal activity. Yet, *in vivo* electrophysiology recordings in the medial Prefrontal Cortex (mPFC) of rodents has shown that injection of PCP (or ketamine, another NMDA antagonist), induces, on the contrary, an increase of the activity of this structure, suggesting a neuronal or regional specificity of the pharmacological effect of PCP. Later studies confirmed that NMDA inhibition acts preferentially on afferent hippocampal GABAergic interneurons and induces a disinhibition of prefrontal pyramidal neurons (Homayoun and Moghaddam, 2007; Jodo et al., 2005). The glutamatergic hypothesis of schizophrenia opened a new axis of research in schizophrenia, allowing the emergence of several animal models, useful to study pathophysiological mechanisms at the neuronal and molecular level.

1.2) The disconnection theory in Schizophrenia

Researchers and psychiatrists have hypothesized since the beginning of the 20th century that schizophrenia may implicate a “disruption” or “dissociation” of different mental processes that may be caused by an anatomical disruption or splitting in the brain (Wernicke, 1906) or an “uncoupling of the brain normally integrated processes” (Bleuler, 1950). In turn, that may

perturb the interconnections of different brain areas and thus the integration and coordination of higher order cognitive processes. More modern conceptions of these functional connectivity deficits between brain areas gave birth to several models of brain connectivity deficits in schizophrenia, for example the “cognitive dysmetria “of Andreasen (Andreasen et al., 1999), defined as “a disruption in the fluid coordination of mental activity that is the hallmark of normal cognition “, and centered on cortico-subcortico-cerebellar system. This disequilibrium could in turn lead to aberrant representation of internal thought and sensory experience.

However, the first concretization of these conceptual intuitions came only at the end of the 20th century, with the development of *in vivo* brain connectivity studies (termed “connectomic”), such as functional Magnetic Resonance imaging (fMRI) and Positron Emission Tomography (PET) or Diffusion Weighted Imaging (DWI). These techniques allow the imaging of the co-activation of different brain regions reflecting communication between them during resting state or during a behavioral task. Studies of functional connectivity disturbances in schizophrenia reported many alterations, especially in the Default Mode Network (DMN), a resting state network involved in introspective processing (Forlim et al., 2020; Fornito et al., 2012; Whitfield-Gabrieli et al., 2009), but also during cognitive tasks (Godwin et al., 2017; Ilzarbe et al., 2019; Kasperek et al., 2012). While the causal mechanisms of functional connectivity deficits in schizophrenia are not fully understood yet, there are several evidences for the implication of synaptic plasticity deficits (Crabtree and Gogos, 2014; Stephan et al., 2009).

1.3) A multi-factorial disease

Results from many epidemiological studies accumulated for decades suggest that schizophrenia may be, at least in part, facilitated by early environmental stressors during childhood, or even in utero. For example, exposure of a fetus to maternal infection, malnutrition, drug abuse, or smoking, results in increased schizophrenia incidence (Brown and Susser, 2008; Mednick et al., 1988; Quinn et al., 2017). This hypothesis is strengthened by results from animal models reproducing these early environmental stressors showing the induction of cognitive behavioral abnormalities and neurobiological alterations relevant to schizophrenia (Labouesse et al., 2015). Longitudinal studies on children who will develop later schizophrenia, and retrospective studies highlighted some mild alterations in childhood/adolescence compared to typical children. For example, mild cognitive deficits,

attention disorder, neurological soft signs, and IQ reduction are frequently found before schizophrenia onset (George et al., 2017). Early neurobiological alteration due to early environmental stress may thus perturb normal brain development and induce mild neurobiological abnormalities that will contribute to the progressive emergence of schizophrenia later in early adulthood. Several environmental stressors in adolescence or early adult age, like intense stress or drug abuse (mainly cannabis, LSD or amphetamine), are also known to “trigger” the onset of schizophrenia, and are often causing the first psychotic episode of schizophrenic patients (Stilo and Murray, 2019).

However, despite being clearly associated with an increased risk of developing schizophrenia, environmental stressors are not sufficient to explain the pathogenicity of schizophrenia, and are not exclusive to this pathology. Genetic predisposition factors also play an important role in schizophrenia. It is known since the first half of the XXth century that schizophrenia risk is higher in relatives (Kallmann, 1938; Schulz, 1933) than in unaffected family. Moreover, studies on twins revealed a very high concordance rate of illness in monozygotic and dizygotic twins, respectively around 40% and 17% (Gottesman, 1991). Another evidence for a genetic factor in schizophrenia came from the study of a Scottish pedigree harboring a genetic translocation in the gene *DISC1* (*Disrupted in Schizophrenia 1*). This translocation is associated with a high segregation of schizophrenia and other psychiatric diseases cases (Sachs et al., 2005; St Clair et al., 1990). Calculation of the heritability of schizophrenia, which is the part of the variability of a phenotype due to genetics, has been estimated to 80% (Hilker et al., 2018).

Several genomic strategies tried to identify causal genes for schizophrenia, that could be classically described as rare, but penetrant (meaning inducing a strong risk to develop schizophrenia), and common but accounting for a poor risk (Rees et al., 2015). Large scale Genome Wide Association Studies (GWAS), which are unbiased analysis of millions of common Single Nucleotide Polymorphisms (SNPs) in a case-control study design, have identified a large number of susceptibility loci of very small individual effects. One meta-analysis study combined available GWAS samples and identified 108 risk loci, accounting for a small increase in the risk of developing schizophrenia, with an odds ratio (a statistical calculation allowing the estimation of the association between a risk factor and a clinical result) inferior to 1.3 (Schizophrenia Working Group of the Psychiatric Genomics Consortium, 2014). In addition to SNPs, a few rare variants (Copy Number Variants, CNVs) have been found, with a much higher odds ratio (for example, the 22q11.2 deletion has an OR of 25) (Murphy et al.,

1999). These genetic studies failed to detect a major risk variant for schizophrenia. Rather, they point to a polygenic model where multiple genes create a predisposition to developing schizophrenia (Fanous et al., 2012; Levinson et al., 2012). All this evidence suggests that schizophrenia is caused by the interaction between polygenetic predisposition factors and early environmental stressors, and that this multifactorial origin should be taken into account for studying and modeling schizophrenia.

1.4) Modeling schizophrenia in animals

Because of the limitations of studies in humans, numerous efforts have been made to model diseases in animals. Many strategies have been used to model schizophrenia pathophysiology, mostly using rodents, by trying to reproduce different factors supposed to be causal, or to participate to the disease. There are four main different types of animal models of schizophrenia: pharmacological, genetic, lesion, and gestational.

First, pharmacological models are trying to reproduce the neurochemical alterations seen in patients. As described, the dopamine and glutamatergic neurotransmitter systems are likely dysregulated in schizophrenia. This gave birth to the amphetamine model, mimicking the hyperdopaminergia of schizophrenia, and the NMDA antagonist models. Serotonin and GABA models also exist, but are much less used (Jones et al., 2011). Pharmacological models using NMDA antagonists, such as phencyclidine (PCP) or ketamine, were some of the first models created, and are still in use. These models are based on the observation that PCP administration in humans successfully reproduce a wide range of cognitive, positive, and negative symptoms (Pradhan, 1984). While it is challenging to monitor in rodents the behavioral alterations typical of schizophrenic patients that are really specific of humankind (hallucination, dissociation, delirium...), several neuropathological alterations are encouragingly reproduced. For example, chronic PCP models induce mesolimbic system hyperresponse to amphetamines (Jentsch, 1999), decreased synaptic spines in frontal cortex neurons (Flores et al., 2007) and a reduced number of cortical and hippocampal parvalbumin interneurons (Jenkins et al., 2008; Reynolds et al., 2004). There are several different schemes of injections of NMDA antagonist, all aiming to answer different questions. While acute adult models are useful to study psychotic symptoms resulting directly from the glutamatergic alteration such as hallucinations, chronic neonatal models are required to study developmental mechanisms occurring during childhood and adolescence.

The second main class of animal models of schizophrenia aims to reproduce the genetic susceptibility of people at high risk for developing the disease. The DISC1 mutant mouse was designed to reproduce the balanced chromosomal translocation found in a large Scottish family, and this translocation has been widely linked to schizophrenia (Millar et al., 2000). This mouse is known to have several behavioral deficits, such as Prepulse Inhibition (PPI) deficit, alterations in spontaneous locomotor activity, and impairment of working memory (Gómez-Sintes et al., 2014; Kvajo et al., 2008a).

Another genetic model mouse widely used in schizophrenia is the LgDel mouse, or the similar Df(16)A+/-, reproducing the 22q11.2 microdeletion, a genetic risk factor leading to a 25 to 30-fold increased risk of developing schizophrenia (Gur et al., 2017; Murphy et al., 1999). LgDel mice show cognitive deficits and working memory impairment relevant to schizophrenia (Karayiorgou et al., 2010; Nilsson et al., 2018), and have a decreased density of dendritic spines and glutamatergic synapses (Mukai et al., 2008).

There are two last classes of models, that won't be further detailed in this thesis: gestational models inducing early prenatal environmental insults, such as the gestational MAM (methylazoxymethanol, an anti-mitotic and anti-proliferative agent) or prenatal maternal immune activation, aiming to induce precocial alteration of brain development; and lesion models: neonatal and adult ventral hippocampal lesion (Lodge, 2013; Macêdo et al., 2012).

2) Schizophrenia, a synaptopathy?

Several neurodevelopmental disorders, such as Autism Spectrum Disorders or intellectual disability, are now considered as synaptopathy, disease of the synapse. Several lines of evidence suggest that this is also the case for schizophrenia.

2.1) Synaptic changes in schizophrenia, evidence from postmortem tissue analysis

2.1.1) A reduction in grey matter volume

Neuroanatomical studies have brought important knowledge on neurobiological deficits in psychiatric disorders. Postmortem studies have been an important source of histopathological information, despite their evident limitations and bias—usually from old subjects, no longitudinal studies possible, variable quality of the tissues... However, most of earlier postmortem discoveries on schizophrenic patients have been replicated and completed using neuroimaging that also brought the possibility of tracking the evolution of anatomical changes across the progression of the disease.

It has frequently been shown that schizophrenia is associated with a decrease in cerebral volume: postmortem studies estimated a reduction of 3% (Heckers et al., 1991; Pakkenberg, 1987), and several meta-analyses of MRI measurements calculated an overall volume decrease of 2% (Haijma et al., 2013; Wright et al., 2000). This decrease was region-specific, and numerous neuroimaging studies have found a decrease of the volume of the prefrontal cortex, the paralimbic cortex (Goldstein et al., 1999), the temporal cortex (Wright et al., 2000) the cerebellum, the hippocampus and the thalamus, with a significant increase of the volume of ventricles (Haijma et al., 2013).

This decrease is mainly associated to a significant decrease of the gray matter volume of around 6%, a result that has been widely replicated in both postmortem and neuroimaging studies (Kasai et al., 2003; Sporn et al., 2003; Takahashi et al., 2010; van Haren et al., 2008). This result has also been replicated in drug-free patients, and young patients after their first psychotic episode, suggesting that this decrease in gray matter volume may be part of the pathology rather than a consequence of the treatment (Lawrie, 2018). A decrease of the cortical gray matter suggests neuronal loss. However, histopathological postmortem studies failed to identify any deficit in neuronal population number (Pakkenberg, 1993), and two studies have

shown an increase of the neuronal density coupled with a decreased volume in the dorsolateral prefrontal cortex (Selemon et al., 1998, 1995). These results suggest a decrease in the global volume of neurons rather than neuronal loss. Postmortem histological studies indeed identified a reduction of the volume of pyramidal cells in the hippocampus (Benes et al., 1991), pyramidal cells in the prefrontal cortex (Zaidel et al., 1997) and cerebellar Purkinje cells (Tran et al., 1998).

The volume of neurons depends on the volume of their soma, dendritic arborization and dendritic spine density. If some studies have noticed a decrease of the soma size in schizophrenic patients (Rajkowska et al., 1998), the most consistent finding concerns the dendritic arborization. Several postmortem studies have detected consistent reduction in dendritic arborization and dendritic spine density in the temporal and frontal cortex of schizophrenic patients (Garey et al., 1998). This deficit is the most consistent and the most frequently reproduced in the neocortex, particularly in layer 3 (Garey et al., 1998; Glantz and Lewis, 2000; Sweet et al., 2009). Furthermore, ultrastructural studies suggest that there is a 30% decrease of the size of striatal spines (Roberts et al., 1996). However, in non-cortical areas results seem more heterogeneous. Some studies found a decreased spine density in the subiculum (Rosoklija et al., 2000) and the striatum (Roberts et al., 1996), but an increase in the caudate, putamen and the patch (Roberts et al., 2015). This heterogeneity of the dendritic spine defect across the brain suggests a regionalization of the synaptic deficits, which correlates with the regionalization of neurochemical deficits described earlier.

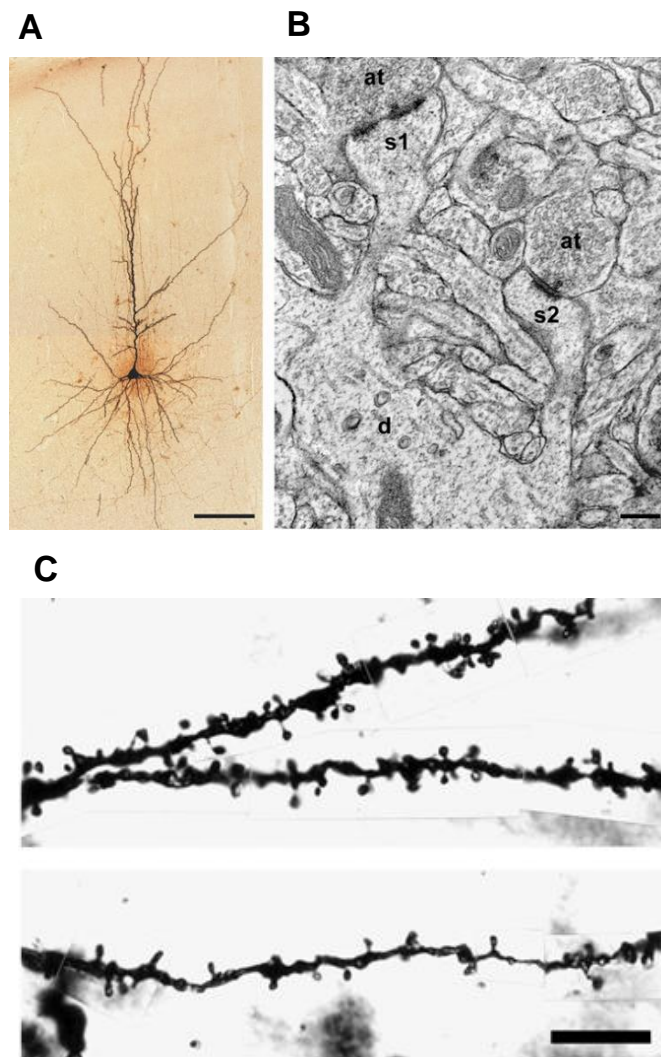


Figure 1: Dendritic spines of pyramidal cells in the prefrontal cortex of schizophrenic patients compared to healthy subjects

A) Light micrograph of a biocytin-filled pyramidal cell showing the cell body, and basilar and apical dendritic shafts (Adapted from Glausier et Lewis, 2013). Scale bar is 100 μm

B) Electron micrograph showing two spines (s1, s2) protruding from a dendritic shaft (d). Spine s1 is receiving a perforated asymmetric (presumably glutamatergic) synapse. Scale bar 200 nm (Adapted from Glausier et Lewis, 2013)

C) Decreased layer 3 spine density in the dorsolateral prefrontal cortex: Golgi-impregnated basilar dendrites and spines from healthy subjects (top) and schizophrenic patient (bottom). Scale bar is 10 μm) (Adapted from Lewis and Gonzalez-Burgos (2008))

2.1.2) Synaptic changes

Because most of the excitatory synapses are located on dendritic spines, the changes in dendritic spine density and sizes suggest an excitatory synaptic deficit in schizophrenia. Interestingly, a recent study using positron emission tomography looked for the first time at *in vivo* synaptic dysfunction in humans. Using a radiotracer specific for SV2A, a presynaptic protein, they found a significant decrease of the volume of distribution in schizophrenic patients compared to control in the frontal cortex and *nucleus accumbens*, confirming *in vivo* a quantitative loss of synapses in schizophrenia (Onwordi et al., 2020).

To assess specifically synaptic changes, many studies performed immunostaining, western blots and mRNA gene expression quantification for well-known synaptic proteins in postmortem brain tissues from schizophrenic patients. These synaptic markers included synapsin, a protein located in the presynaptic compartment known for its role in the formation and maintenance of synapses (Ferreira and Rapoport, 2002), synaptophysin and synaptobrevin, two proteins necessary for exocytosis, or proteins of the SNARE complex, essential for calcium-dependent exocytosis. Postsynaptic proteins such as PSD95, one of the major excitatory post synaptic scaffold protein, were also widely studied. Decreased mRNA was shown for synaptophysin, SNAP25, VGLUT1, Complexin II, Syngap1 (Funk et al., 2009), PSD95 and synapsin in the hippocampus (Eastwood and Harrison, 2005; Young et al., 1998) and Synaptophysin, VGLUT1 and Complexin II in the prefrontal cortex (Eastwood and Harrison, 2005; Gray et al., 2010; Scarr et al., 2006; meta-analysis by Osimo et al., 2019). Quantitative western blot and immunostaining analysis also found a reduced level of Synapsin 1 (Browning et al., 1993), and PSD95 in the hippocampus (Matosin et al., 2016), and a reduced density of synapsin 1, synaptophysin and SNAP25 clusters in the prefrontal cortex (Glantz and Lewis, 1997; Karson et al., 1999). A deficit of Syntaxin1 phosphorylation by the Casein Kinase2 has been described in schizophrenic patient postmortem brains, suggesting changes in the binding to other proteins of the SNARE complex and presynaptic dysfunction (Castillo et al., 2010).

Although the vast majority of the published studies suggest that schizophrenia is characterized by a reduced expression of excitatory synaptic proteins and reduced excitatory synaptic density, a few reports have also shown an increase of excitatory presynaptic proteins in several brain regions: for example an increase of SNAP25, synaptophysin and syntaxin immunostaining in the cingulate cortex (Gabriel et al., 1997) or an increase of synaptobrevin 1, SNAP 25 and Syntaxin1 mRNA expression in the left superior temporal gyrus (Sokolov et al.,

2000). Protein levels of the Vesicular Glutamate Transporter 2 (vGLUT2), which is found in subcortical glutamatergic neurons, are also increased in the *nucleus accumbens* and the *substantia nigra* (Roberts et al., 2020).

Many alterations of glutamatergic postsynaptic receptors have been found in postmortem studies, straightening the glutamatergic hypothesis of schizophrenia. However, results are very diverse in the literature, depending on the localization or the subunit (**Table 1**), and sometime results are conflicting.

	AMPA	NMDA	Kainate	Metabotropic
mPFC	<p>↓ GluA1 ↓ GluA2 expression (Corti et al., 2011)</p> <p>↑ GluA2 ↑ GluA4 expression (Dracheva et al., 2005)</p>	<p>↑ GluN2D ↓ GluN2C expression (Akbarian et al., 1996a)</p> <p>↓ GluN1 ↓ GluN2A ↓ GluN2C expression (Beneyto and Meador-Woodruff, 2008)</p>	<p>↔ GluK4 ↓ GluK2 expression (Meador-Woodruff et al., 2001)</p>	<p>↓ mGluR3 expression (Ghose et al., 2009)</p> <p>↑ mGluR1 ↑ mGluR2 ↑ mGluR3 expression (Gupta et al., 2005)</p> <p>↔ mGluR3 (Gupta et al., 2005; Ohnuma et al., 1998)</p>
Hippocampus	<p>↓ GluA1 ↓ GluA2 ↓ GluA3 protein (Eastwood et al., 1997) & expression (Eastwood et al., 1995; Harrison et al., 1991)</p>	<p>↓ GluN1 ↑ GluN2B expression (Gao et al., 2000)</p>	<p>↓ GluK2 ↓ GluK5 (Porter et al., 1997)</p>	

Table 1: Summary of glutamate receptor subunit deregulation in schizophrenic patients found in postmortem studies.

There are four main classes of glutamatergic receptors: three ionic receptors: NMDA, AMPA, and Kainate, and the metabotropic receptors or glutamate.

These inconsistent results could arise from different causes: it could be due to the heterogeneity of the patients, of their age, and some of the studies didn't separate treatment free patients from those treated with neuroleptic. Nevertheless, these results suggest a dysregulation of glutamatergic receptors as a core feature in schizophrenia, that could come from different origins.

Inhibitory synapses alterations are also a common feature of schizophrenia. Several authors have detected a significant decrease of the expression of the GAD67 mRNA (Glutamic Acide Decarboxylase 67, an enzyme responsible for GABA synthesis) in the human prefrontal cortex (Akbarian et al., 1996b; Hashimoto et al., 2003; Knable et al., 2002) and the cerebellar cortex (Hosseini Fatemi et al., 2005), suggesting that the presynaptic secretion of GABA may be reduced. The expression of the GABA Transporter 1 (Gat-1) mRNA, responsible for the reuptake of GABA, is also reduced in diverse prefrontal regions (Hashimoto et al., 2008). At the post-synaptic side, several postmortem studies noticed an increase of the GABA_A receptor subunit in the Axon Initial Segment of Pyramidal neurons (Benes et al., 1996), possibly as a compensation mechanism for the diminished presynaptic GABAergic activity (de Jonge et al., 2017).

Altogether these results suggest that synaptic deficits, both at excitatory and inhibitory synapses, are characteristic of schizophrenia and are heterogeneous amongst the brain region analyzed, similarly to the neurotransmitter deficits. A key remaining question is whether these synaptic defects are at the origin of the disease, or whether they are caused by the pathology or the treatment.

2.2) Synaptic deficits in schizophrenia: evidence from genetic studies

As described earlier, there is now compelling evidence that genetic factors contribute strongly to increased risk of schizophrenia. While current genetic studies still have not identified strong causal genes that could explain the pathology, they have identified numerous potential candidates for understanding physiopathological mechanisms. Interestingly, most of the literature points to several synaptic genes or pathways, even without a priori or focus into synapses, suggesting that synaptic genes have a central role in the genetic predisposition to schizophrenia. The current knowledge in the genetic of schizophrenia could be classified into

two categories: common mutation that have a small effect on the risk of developing schizophrenia, and rare variants of larger effect. The main results are summarized in **Figure 2**.

2.2.1) Rare variants

Familial genetic and DNA sequencing studies allowed to detect rare genetic variants such as Copy Number Variations (CNVs) or indels (insertion or deletion of a nucleotide sequence), that could be both inherited or *de novo* mutations. These rare variants have a potentially large effect on the risk of developing schizophrenia, and can help to identify targets that have a large effect, and that could be more easily linkable to the pathology.

CNVs Copy Number Variants (CNVs) currently represent the main source of known rare variants for schizophrenia, and it has been shown that large and rare (<1%) CNVs occur more frequently in schizophrenic patients than in controls (Kirov et al., 2009), and confer substantial risk (odds ratios between 3 and 30) to develop schizophrenia. Several of these CNVs involve synaptic genes. Some of the first discovered and most well-known inherited chromosomal anomalies of high penetrance for schizophrenia have been detected on familial studies, and two CNVs are of particular importance: the 22q11 microdeletion syndrome, and the DISC1 (Disrupted in Schizophrenia 1). The 22q11 microdeletion syndrome is a recurrent deletion of three megabases, which increases by 25 to 30-fold the risk for schizophrenia (Murphy et al., 1999), and is frequently associated with cognitive deficits even in non-schizophrenic patients (Philip and Bassett, 2011). This deletion covers several genes that are either synaptic or interfering with synapse regulation, such as the Catechol-O-Methyl Transferase (COMT), responsible for the degradation of dopamine and other catecholamines in the synaptic cleft, or SNAP29 whose polymorphism has been associated with schizophrenic patients (Saito et al., 2001). Regarding the high rate of schizophrenia in 22q11 microdeletion carriers, it is plausible that the haploinsufficiency of one or more genes in this region may be bringing a susceptibility to develop schizophrenia.

DISC1 encodes a protein involved in synaptic regulation (Maher et al., 2012; Malavasi et al., 2018) and was identified as the gene disrupted by a balanced reciprocal translocation in a Scottish family with schizophrenia and other psychiatric disorders (St Clair et al., 1990).

Other well-described CNVs affect the neurexin/neuroligin pathway. Neurexins are presynaptic cell adhesion molecules, forming transsynaptic complexes with the neuroligin, and are crucial for synapse function (Südhof, 2008) and glutamatergic transmission (Kattenstroth et al., 2004). For example, one well-known CNV at the locus 2q32 directly affects the NRXN1

gene, coding for the neurexine 1 protein. This locus has been associated with autism (Onay et al., 2016; Walsh et al., 2008) and schizophrenia (Rujescu et al., 2009; Vrijenhoek et al., 2008; T. Walsh et al., 2008) (**Figure 2**). Moreover, two other genes of the neuroligin pathway, *ErbB4* and *MAGI2*, have been found disrupted in schizophrenia by CNVs (Walsh et al., 2008).

More recent DNA sequencing studies on schizophrenia subjects has identified several proteins associated with an increased risk of developing schizophrenia, often converging on synaptic proteins. For example, a recent study focused on ultra-rare variants (URVs), defined as alleles that have a frequency of about 1/100 000 (Genovese et al., 2016), that could be even specific for one single subject. The authors found that schizophrenia patients have a significantly superior proportion of URVs than controls, and a significant enrichment in sets of genes coding for synaptic proteins. Similarly, a study focusing on rare *de novo* CNVs identified several synaptic proteins strongly associated with schizophrenia, including *DLG1*, *DLGAP1*, *DLG2*, members of the Membrane Associated Guanylate Kinases (MAGUKs) family, which are associated with NMDA receptors (Kirov et al., 2009).

Finally, exome sequencing strategies focused on coding parts on the genome, and some found a polygenic burden from rare mutations distributed across many genes, with a high enrichment of the post-synaptic ARC associated proteins, *PSD95*, and Voltage-gated calcium channels (Purcell et al., 2014). A meta-analysis by the Schizophrenia Exome Sequencing Meta-analysis (SCHEMA) consortium, one of the largest exome sequencing database (more than 100 000 individuals) allowed the identification of several rare variants with significant association to schizophrenia, including proteins associated with synapse formation, maturation or function (Unpublished data extracted from <https://schema.broadinstitute.org/>, summarized in **Table 2**)

Altogether, results on common variants suggest that while the genetic variants associated with an increased risk for developing schizophrenia are very diverse, many converge on synaptic or synapse-associated genes.

SetD1A	Histone methyltransferase,	Knock out on mice induces alterations in axonal branching and cortical synaptic dynamics (Mukai et al., 2019)
Cullin-1	E3 ubiquitin ligases	Synapse elimination (Ding et al., 2007)
HERC1	E3 ubiquitin ligases	Dendritic development (Pérez-Villegas et al., 2018)
<i>Trio</i> Rho Guanine Nucleotide Exchange Factor	GTPase	Dendritic branching and synaptic strength (Ba et al., 2016)
GRIN2A	NMDA receptor subunit	
GRIA3	AMPA receptor subunit	
CACNA1G	Calcium channel	
SP4	Transcription factor	Control dendritic patterning in cerebellar granule cells (Ramos et al., 2007)

Table 2: Summary of genes extracted from the Schizophrenia Exome Sequencing Meta-analysis (SCHEMA) consortium database significantly associated with schizophrenia (unpublished data, results found at <https://schema.broadinstitute.org/>)

2.2.2) Common variants

Genome Wide Association Studies (GWAS) have been a major breakthrough in genetic studies, allowing very high throughput genetic analysis and identification of several potential pathways in genetic diseases. GWAS are looking mainly at Single Nucleotide Polymorphisms (SNPs), which are frequent (>1% of the population) variation of only one nucleotide, but can also identify copy number variations (CNVs). The detection of common variants that have small but additive effects on the risk of developing schizophrenia can help to identify several

pathways instead of one precise gene. Some authors hypothesize that around 23% of the variance in schizophrenia is explained by common SNPs (Cross-Disorder Group of the Psychiatric Genomics Consortium et al., 2013; Lee et al., 2012).

Several GWAS studies found SNPs inside genes (or in regulatory regions) coding for synaptic proteins. A SNP located in the Dysbindin (*DTNBP1*) gene in the 6p24-22 locus has been linked to schizophrenia by several studies (Schwab et al., 2003; Straub et al., 2002), and its expression is decreased in schizophrenia in the dorsolateral prefrontal cortex (Koh et al., 2003; Talbot et al., 2004). The Dysbindin protein is located in synaptic sites, and has been implicated in regulation of exocytosis and vesicle biogenesis (Chen et al., 2008). Other synaptic genes identified by older genetic studies comprise *mGLUR3* (Lohmueller et al., 2003), *Neuregulin1* (Stefansson et al., 2002) and the nicotinic receptor gene *CHRNA7* (Freedman et al., 2001). One of the biggest and most recent GWAS databases for schizophrenia currently comes from the psychiatric genomics consortium (PGC2) who identified 108 loci significantly associated with schizophrenia (Ripke et al., 2014). In this study, rather than identifying directly genes related to schizophrenia, the authors identified large loci, containing several genes, and several molecular pathways or family of molecules specifically enriched—suggesting that some pathway or process potentially of relevance to schizophrenia could be dysregulated by different SNPs.

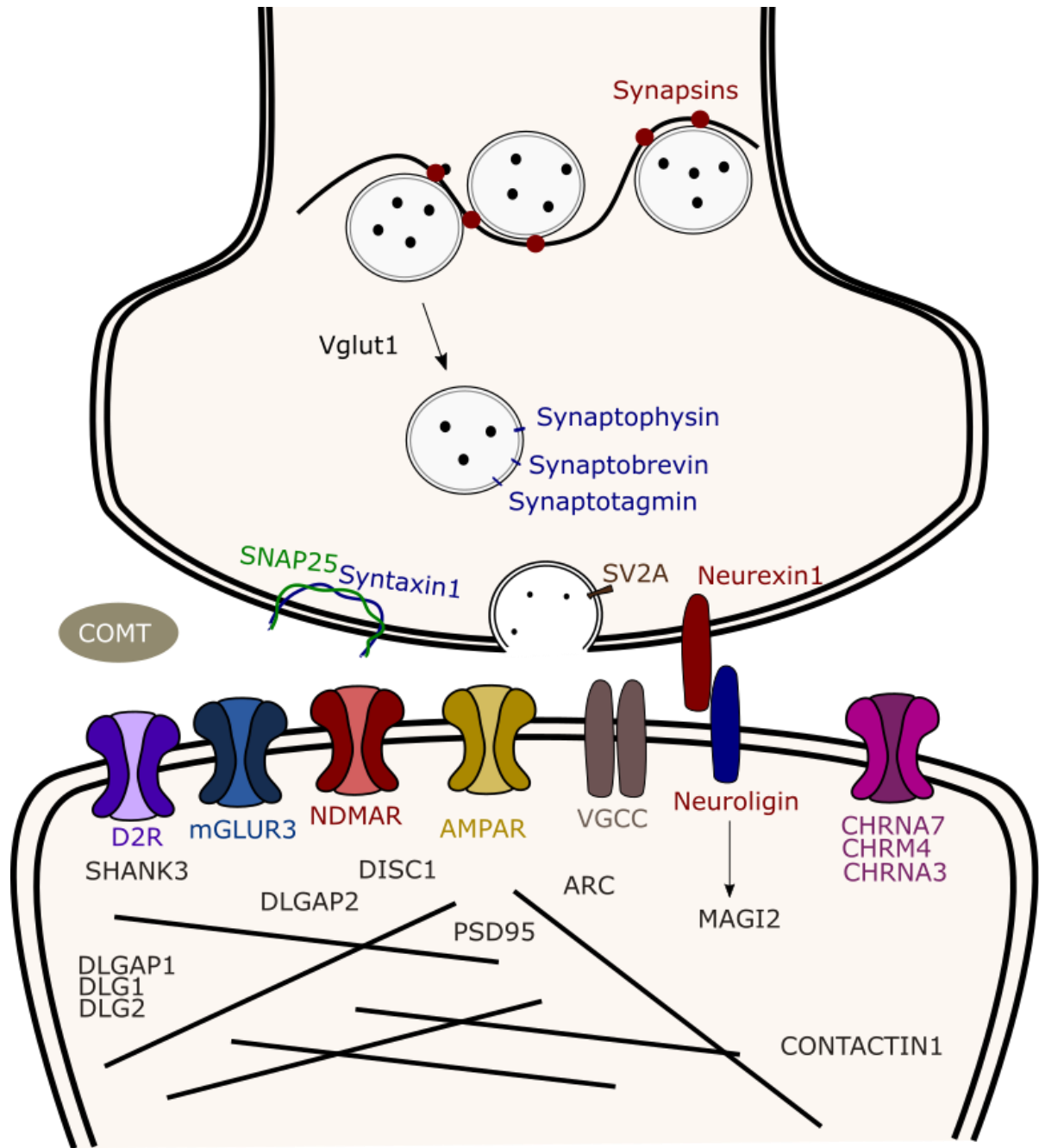
Interestingly, several families of proteins related to synapses were extracted from these GWAS: The D2R dopaminergic receptor and several glutamate receptor subunits *GRIA1*, *GRIA4*, *GRIN2B*, *GRM5*, in good correlation with the hypothesis of glutamate dysregulation in schizophrenia (cf. above). The voltage-gated calcium channels family (VGCC) is also well represented in this study, with a significant association with schizophrenia of *CACNA1C*, *CACNB2* and *CACNA1I*. VGCC proteins are well-known ion channels with permeability to calcium, and are regulators of neuronal excitability, and plays a major role in synaptic transmission. VGCC are also known to interact with NMDA receptors on post-synaptic dendrites (Hou et al., 2002).

The GWAS study from Ripke et al., has been taken as a basis by several in silico analysis trying to extract relevant risk genes or pathways from these loci by different prediction approaches, with different results. (Gaspar and Breen, 2017; Ma et al., 2018; Ripke et al., 2014; Schijven et al., 2018). Different proteins related to synapses have been found, such as the cholinergic receptor subunits *CHRM4*, *CHRNA3*, or *FGFR1*, a protein implicated in synapse

formation (Cambon et al., 2004), MARK1, implicated in neuronal polarity and axon-dendrite specification (Maussion et al., 2008), NOS1, implicated in glutamatergic and GABAergic plasticity (Gaspar and Breen, 2017; Hardingham et al., 2013), or GPM6A, MMP16, TCK4 and CNTN4. Pathway analysis of this GWAS also found several synaptic signaling pathways enriched from these SNPs (Schijven et al., 2018) targeting the dopaminergic synapse, the cholinergic synapse and long-term potentiation pathway.

Finally, one of the strongest association loci extracted from these studies is situated in the chromosome 6, and contains the MHC region, particularly of interest because of its implication in synapse elimination (Sekar et al., 2016), as detailed below.

To conclude this part, many evidences coming from histological studies, neuroimaging, transcriptomic, and genetic studies, are converging to suggest that synaptic deficits are very likely a major actor in schizophrenia.



2.3) Synaptic deficits: Functional consequences on neural network

As review above, morphological and quantitative synaptic deficits have been well described in schizophrenic patients, and genetic studies searching for association between gene alteration and an increased risk of developing schizophrenia often converge to synaptic genes. However, understanding what are the functional consequences of these synaptic deficits, and describing how the synaptic function may be altered remains challenging. Although not directly a measure of synaptic functions, functional imaging and neural oscillation EEG (Electro Encephalogram) allows to discover functional deficits that could be a reflect/consequence of synaptic dysfunction.

EEG recordings on humans are used to monitor oscillations from neural sources that span a range of frequencies and are conventionally classified into delta (0.5–4 Hz), theta (4–7 Hz), alpha (8–12 Hz), beta (12–30 Hz), and gamma (30–80 Hz) (Sun et al., 2011). Neural oscillations are thought to be associated with several cognitive functions, including sensory processing, attention, working memory, which are all deficitary in schizophrenia (Uhlhaas et al., 2008). Oscillations recorded by EEG are a reflect of large scale synchronous neuronal activity that results from internal coordination of spike timing of a neuronal population that is important for information encoding (Buzsáki and Draguhn, 2004; Singer, 1999).

In resting state, EEG studies have shown controversial results, some report found an increase of gamma power in frontal and temporal regions (Venables et al., 2009) or a decrease in the posterior region of the medial parietal cortex (Rutter et al., 2009). In behavioral paradigms, schizophrenic patients show consistent decrease of gamma power, in sensory gating tasks (Johannessen et al., 2005) or mental arithmetic (Kissler et al., 2000). Some authors hypothesis that these oscillation deficits may be caused by excitation inhibition imbalance (Krystal et al., 2017; Uhlhaas, 2018) which is thought to be an important feature in schizophrenia. Indeed, *in vitro* studies have shown that gamma oscillations rely highly on Fast Spiking GABAergic interneurons that are synchronizing their output through fast mutual inhibition (Bartos et al., 2007), and that they are affected by GABA and AMPA, NMDA and metabotropic glutamate receptors (Faulkner et al., 1999; Whittington et al., 1995). Consequently, deficits of GABA neurons inhibition may play a role in gamma oscillation deficits in schizophrenia (Gonzalez-Burgos et al., 2010).

This suggests that gamma oscillations deficits could potentially be a neurobiological marker of schizophrenia (Sun et al., 2011), and that this network disorganization could be a consequence of synaptic deficits in schizophrenia.

At another scale, fMRI studies on humans found several deficits of functional connectivity (the temporal correlation between two neurophysiological events in different regions, supposed to be coupled to each other) in schizophrenia, mostly involving prefrontal brain regions (Cole et al., 2011; Fornito et al., 2012), that are implicated in cognitive functions, interception, salience processing (Palaniyappan et al., 2013). Moreover, the default mode network, which is involved in introspective processing (Whitfield-Gabrieli et al., 2009) is particularly suspected to be disrupted in schizophrenia.

Another paradigm used to study functional connectivity deficits in schizophrenia is based on Mismatch Negativity (MMN) tasks in patients. MMN is a brain response to violations of a rule, established by a sequence of sensory stimuli, and is used to reflect synapse plasticity (Harms et al., 2020; Stephan et al., 2006). Schizophrenic patients present deficits in MMN, that correlate well with the disease severity and cognitive dysfunction (Baldeweg et al., 2004), which suggest a role of synaptic plasticity deficit in schizophrenia (Stephan et al., 2006). Finally, that mechanism is thought to be dependent of NMDA receptors (Javitt et al., 1996; Umbricht et al., 2000).

To conclude this part, in humans, studies of different scales of functional connectivity deficits, by different methods, show that schizophrenic patients have a disorganized and inefficient neuronal network. They improperly integrate and treat complex cognitive tasks, and this could be explained in part by synaptic deficits, in particular glutamatergic and GABAergic.

2.4) Electrophysiological deficits in mice model of schizophrenia

The study of precise synaptic properties, complicated in humans, requires the use of animal models of schizophrenia, allowing to study the electrophysiological properties of synapses. As mentioned in chapter 1.2, several models of schizophrenia exist, from pharmacological models trying to reproduce neurobiological alterations seen on patients, to genetic models that aims to reproduce the genetic susceptibility of patients at high risk to develop schizophrenia.

In the pharmacological Phencyclidine model, several studies have shown a disruption of prefrontal and hippocampal synchrony, which corroborates with the data on patients detailed

above. In the mPFC, chronic injection of PCP in adult rats under anesthesia induces consistent reductions in theta oscillations and an abnormal cortical synchronization in pyramidal cells (Young et al., 2015). On the other hand, in the hippocampus, acute injections of PCP in mice induce an increase of hippocampal gamma waves (Ehrlichman et al., 2009; Ma and Leung, 2000). Similarly, the Df16^{+/-} mice, a model mimicking the 22q11.2 human deletion syndrome also presents deficit of gamma waves (Hamm et al., 2017) and theta hippocampal-prefrontal oscillations (Sigurdsson et al., 2010).

In order to assess whether there are electrophysiological deficits in models of schizophrenia, several authors used patch clamp recordings in rodents. In mPFC slices, subchronic PCP treatment induces different synaptic deficits, with a depolarized resting membrane potential, a decrease of the paired pulse facilitation, a significant increase of excitatory postsynaptic current variance and a hypersensitive response of mPFC pyramidal cells to NMDA (Arvanov and Wang, 1999; Ninan, 2003). In another neuronal region, the Dorso Lateral Septum Nucleus (DLSN), implicated in the regulation of emotional responsiveness, there is a dysfunction of the NMDA regulation after chronic PCP treatment (Yu et al., 2002). Yu and collaborators have shown a significant enhancement of NMDA mediated EPSC caused by an upregulation of post-synaptic NMDA receptors. The same study of Yu and collaborators showed that GABAergic mediated synaptic currents were depressed following chronic PCP, possibility mediated by hypofunctional GABA_A synaptic receptors. Another study in the hippocampus of subchronically treated adult mice, found no difference in AMPA and NMDA mediated EPSC, but an impairment of the LTP in CA1 neurons, and an enhanced inhibitory synaptic transmission (Nomura et al., 2016). They conclude that enhanced GABAergic input to the CA1 underlies the LTP deficit. Similar LTP deficits have been obtained with the use of MK801 (Wiescholleck and Manahan-Vaughan, 2013) and Ketamine (Yang et al., 2018), two other NMDA antagonists.

Pharmacological models of schizophrenia show deficit of synaptic transmission and plasticity, although one could argue that these deficits could be explained by the direct effect of the pharmacological agent, rather than specific of schizophrenia. However, several genetic models of schizophrenia also point to transmission and plasticity deficits. Functional analysis of synaptic transmission in Disc1 mutant mouse has detected a deficit of short-term plasticity in CA3/CA1 synapses (Kvajo et al., 2008b), and deficits of LTP in hippocampal neurons, consistent with findings in the PCP model (Kuroda et al., 2011). In Df16A^{+/-} mice, electrophysiological recordings reveal several deficits of hippocampal synaptic transmission: a

decrease of inhibitory transmission onto CA2 pyramidal neurons, a more hyperpolarized resting potential of pyramidal neurons, and an impaired plasticity at inhibitory synapses in CA2 area (Piskorowski et al., 2016). Interestingly, similar synaptic alterations have been linked to cognitive behavioral deficits (Manahan-Vaughan et al., 2008) and some of these deficits are effectively reversed by some neuroleptics (Ninan, 2003), the therapeutic class used to treat schizophrenia.

To conclude, although mouse models of schizophrenia show evident limitations and may not reflect the complete physiopathology of the disease, the fact that several models of schizophrenia have various deficit in synaptic transmission and plasticity, correlate well with the various genetic alterations of synaptic genes and the morphological synaptic deficits seen in schizophrenic patients. Altogether, this strengthens the hypothesis that schizophrenia is a synaptopathy, and that abnormal synaptic organization and function may be a core feature of schizophrenia physiopathology.

2.5) Synaptic loss in schizophrenia: developmental perspective

One of the most consistent synaptic deficits in schizophrenia concerns the synaptic loss in the brain of patients, as suggested by the loss of gray matter and the decrease in dendritic spine density. However, this decrease could arise from two sources: either a deficit of synaptogenesis, or an increase in synaptic pruning.

2.5.1) Deficits of synapse formation

Several genes found in genetic studies of schizophrenia could be implicated in synapse formation: SHANK3 mutation is associated with deficits in synaptogenesis (Gouder et al., 2019); RELN gene coding for reelin protein, is implicated in synapse formation, maturation, elimination, and plasticity (Bosch et al., 2016). Several genes coding for Cell Adhesion Molecules (CAM) are found in studies of de novo mutation (Fromer et al., 2014), including EPHB3, EPHA1, CDH5, PCDH10, PCDHAC2 and PCDHA11, and CAMs are thought to be largely implicated in synapse formation (Südhof, 2018).

A recent transcriptomic study in normal brains from in utero life to adulthood has evaluated the expression profile of several genes with de novo mutations in schizophrenic patients, and assessed whether these genes form co-expression/protein interaction network in a

particular brain region and developmental period. A significant enriched network was found in the dorsolateral and ventrolateral prefrontal cortex during development. Interestingly, many genes mostly function in neuronal migration, synaptic transmission, signaling, suggesting that prefrontal neuronal development during fetal life could play a role in the pathophysiology of schizophrenia (Gulsuner et al., 2013). Skene et al. studied the expression of many genes during the lifespan of humans and mice, and found a significant “shift” in early adulthood of the expression of many proteins implicated in synaptic function, and they thus defined a “genetic calendar” (Skene et al., 2017). They postulate that schizophrenia onset is associated with a misexpression of many genes during that critical shift. They found that *de novo* mutations from Gulsuner et al. were indeed associated with that critical expression shift in early adulthood, suggesting that these mutations may affect late synapse maturation and may play a role in schizophrenia onset.

There are currently few real evidences for a deficit of synaptogenesis in schizophrenia. This might be due to technical difficulties since it requires the quantification of synapse density in very young subjects or before birth. Further studies in genetic and prenatal models of schizophrenia at different ages may possibly bring some answers.

2.5.2) Deficits of synapse elimination

Synaptic pruning was revealed by the electron microscopy studies (Huttenlocher and Dabholkar, 1997) on postmortem brains from healthy humans, showing that synaptic density reaches a maximum at 2-4 years of age, and decreases during the adolescence to reach half at the adult age. A recent transcriptomic study on thousands of genes in the prefrontal cortex across the human lifespan reported that many genes involved in synapse function peak during fetal life, and then decrease during infancy and adolescence. (Colantuoni et al., 2011). The hypothesis of a change in synapse elimination in schizophrenia was born in 1982 when Feinberg speculated that schizophrenia might result from an excess of synapse elimination programmed to occur during adolescence.

Neuroimaging studies of young patients with first episode schizophrenia, and longitudinal studies on children detected as “at high risk of developing schizophrenia” allowed to target earlier developmental stages. Interestingly, these studies showed that schizophrenic patients have a significant decrease in cortical gray matter compared to controls, which occurs

around the onset of schizophrenia, at a time which coincides with the time of synaptic pruning (Andreasen et al., 2011).

However, mechanistic evidence for pruning deficits in schizophrenia were lacking, until a recent study in 2016, showing the implication of the gene coding for the complement protein C4 in schizophrenia. Interestingly, the gene coding for C4 is located in the MHC locus, which has the strongest risk association for schizophrenia. In the paper, the authors (Sekar et al., 2016) identified four alleles of the C4 genes, and found a strong association between the alleles and the risk for schizophrenia. Moreover, they have shown that each allele is associated to a different level of C4A protein expression, and that the level of expression is correlated with the risk for schizophrenia. They have shown that the C4A RNA expression levels were increased in the brain tissue of schizophrenia patients, and that C4 human protein localized to neuronal synapses, dendrites, axons and cell bodies. Finally, by using a mouse model of retinogeniculate synapse refinement, they have shown that the deletion of C4 protein leads to reduced pruning. Another study published in 2019 strengthen this hypothesis: in this paper the authors used a reprogramed *in vitro* model of microglia mediated synapse engulfment, using human derived microglia like cells. They have demonstrated an increase of synapse elimination (Sellgren et al., 2019) in schizophrenic patients derived cultures compared to control, and showed that this effect was associated to patients carrying a risk-associated locus of the C4 protein.

A computational model by Krystal et al., schematized in Figure 3, proposed a hypothesis linking glutamate synaptic dysfunction, neural oscillation abnormalities, excitation/inhibition imbalance, and synapse elimination (**Figure 3**) (Krystal et al., 2017). Following the increased excitation, synaptic downscaling mechanisms will occur, leading to synapse elimination.

Recursive Compounded Allostatic Neurodevelopmental Processes

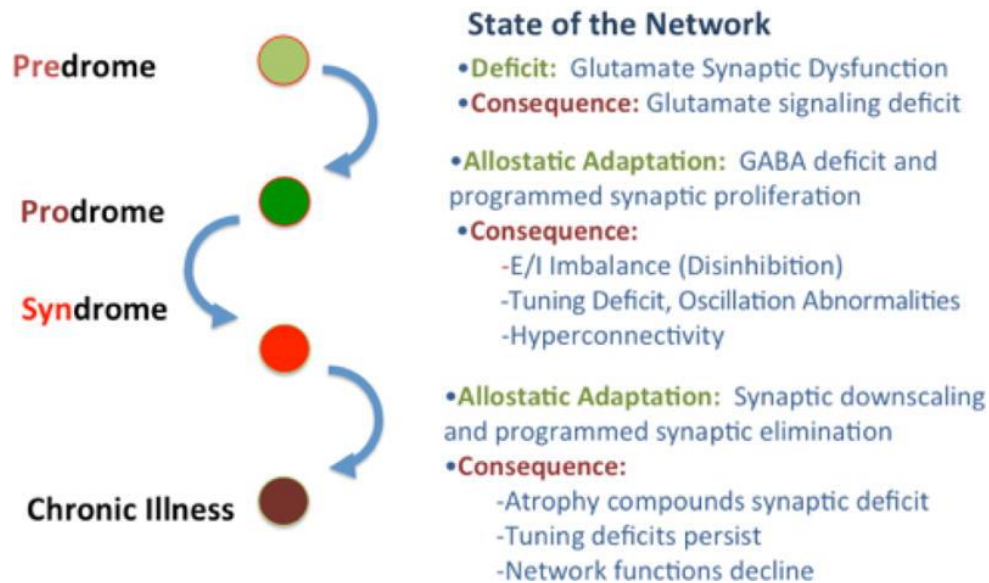


Figure 3: Computational model for hemostatic neuroadaptation (From Krystal and Anticevic, 2015).

This model proposes that initial glutamatergic synaptic dysfunction (as suggested by the convergence of many genetic studies) may alter glutamate signaling (predrome phase). Then allostatic adaptation may occur during the prodromic phase (before the apparition of symptoms), downregulating inhibitory GABAergic activity, leading to impaired excitation/inhibition imbalance, oscillation abnormalities and hyperconnectivity, that could be responsible for an increased risk of declaring schizophrenia. A last allostatic adaptation would then appear, corresponding to the onset of the pathology, with an increased synaptic elimination, leading to a decline of network functions.

To conclude this part, most of the current evidence for synaptic deficits in schizophrenia concerns synaptic maturation, elimination, function and plasticity, which take place between childhood and early adulthood, consistent with the developmental hypothesis of schizophrenia (Murray and Lewis, 1987; Weinberger, 1987). While there are relatively few evidences for precocial or prenatal synaptogenesis deficits (**Figure 4**), some genetic studies suggest that there could possibly be alterations of early synapse formation (Gulsuner et al., 2013) that need to be studied at earlier stages of the synaptic development.

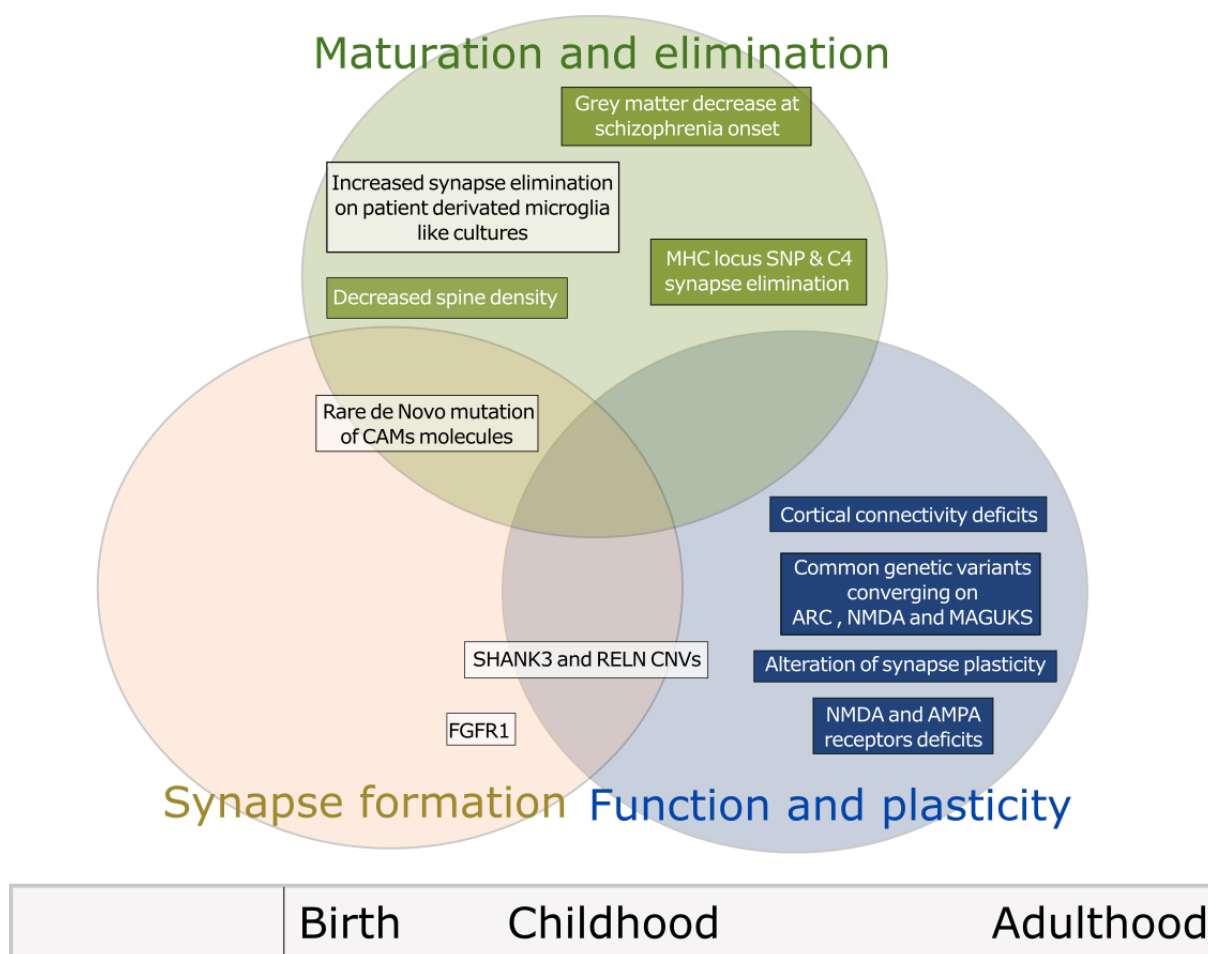


Figure 4 Development of the synapses and alterations in schizophrenia: schematic summary of current knowledge.

Synaptic development has been divided into 3 main categories: synapse formation, with the establishment of synapse contact, synapse maturation and elimination, and synapse function and plasticity. Most of the post mortem and genetic alterations affect synapse maturation, elimination, and synapse function and plasticity. Up to date, except the identification of a few genes known to play a role in synapse formation, there are few clear evidences for deficits of synapse formation in schizophrenia.

3) The olivo-cerebellar system: a powerful model to study circuit development

The olivo-cerebellar system, composed by the cerebellum and the inferior olive in the brainstem, has been used for a long time to study the development and plasticity of synapses. Its unique architecture and the extensive characterization of its circuitry, molecular composition, and physiology stems from knowledge accumulated over decades of research; and make it a structure of choice for studying various properties of synapses. First, the cerebellar cortex has a well-defined histological structure, and each neuron type has its own properties; second, researchers can use several morphological, genetic, and electrophysiological markers to study each actor independently.

3.1) Global structure of the cerebellum and inferior olive

3.1.1) Cerebellar anatomy

The cerebellum, “little brain” in Latin, is located in the posterior cranial fossa, and is the biggest part of the hindbrain. It is composed of two main parts: the cerebellar cortex, and the Deep Cerebellar Nuclei (DCNs). The cerebellar cortex is composed in the mediolateral axis of two hemispheres, joined by a central part called vermis. In the anteroposterior axis, the cerebellum is divided into 3 lobes: the anterior, posterior, and flocculo-nodular, the first two separated by the primary fissure, the last two by the posterolateral fissure (**Figure 5**). Three different nuclei compose the DCNs: the fastigial (medial), the interposed, and the dentate (lateral), located in the depth of the cerebellar hemispheres, close to the fourth ventricle.

The inferior olive is located in the brainstem, and is divided into three main parts: the principal olivary nucleus (PO), the medial accessory olivary nucleus (MAO) and the dorsal accessory olivary nucleus (DAO) (**Figure 5E**). 4 subnuclei are also described: the *subnucleus* β , the dorsomedial cell column (DMC), the dorsomedial group (DMG) and the ventrolateral outgrowth (VLO).

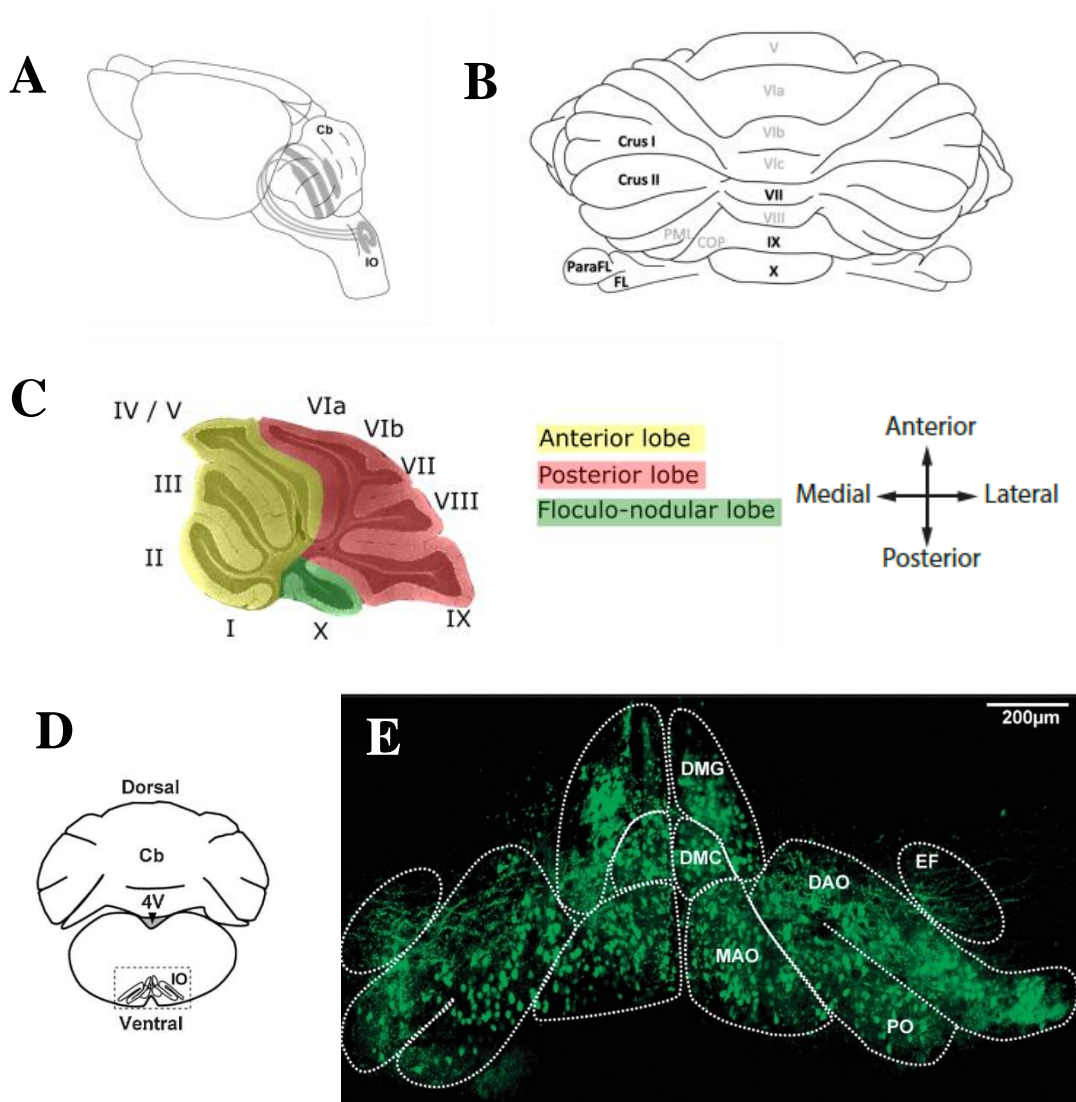


Figure 5: The olivo-cerebellar network.

- A) Projection from the inferior olive (brainstem) to the cerebellum (from Reeber et al., 2013),
- B) Representation of the different lobules of the rodent cerebellum (from Rondi-Reig et al., 2014).
- C) Sagittal view of the lobes and lobules in the vermis of the rodent cerebellum. Each lobe is separated into several lobules: in the vermis, the anterior is composed of the lobules I, II, III, IV and V, the posterior by the lobules VI, VIIA, VIIB, VIII and IX, and the flocculo-nodular lobe by the lobule X. In the lateral hemispheres, the lobule VIIA is replaced by two structures called Crus I and Crus II.
- D) Representation of the rodent cerebellum (Cb) and the brainstem containing the Inferior Olive (IO) in a coronal view. 4V = Fourth Ventricle. From Pätz et al., 2018.
- E) The mouse inferior olive and its *subnucleus*, in a sagittal cut. Two-photon fluorescence image of GFP-expressing cells from an IGSF9-GFP mouse. PO = Principal Olive, MAO = medial accessory olivary nucleus, DAO = dorsal accessory olivary nucleus, DMC = dorsomedial cell column, DMG = the dorsomedial cell group, EF = efferent fibers. From Pätz et al., 2018.

3.1.2) Histology of the cerebellum

Ramon y Cajal was the first to describe the histology of the cerebellar cortex 130 years ago, using Golgi-impregnated staining (Cajal, 1888). This work is considered as a pioneer work in unraveling the complexity of the central nervous system cellular organization. He described the organization of the cerebellar cortex in three layers (**Figure 6**): the granule cell layer, the Purkinje Cell Layer, and the Molecular Layer. The granular layer contains mainly the granule cells, which are small (5-8 μ m of diameter), but numerous, excitatory neurons. Although the cerebellum represents only 10% of the volume of the Central Nervous System, the cerebellar Granular Cells represent alone half of all neurons of the brain. The granular layer also contains the Golgi Cells, which are GABAergic neurons, and the Lugaro cells, inhibitory interneurons located at the top of the granular layer and the unipolar brush cells, which are small excitatory interneurons particularly concentrated in lobule IX, X, and in lower density in hemispherical portions of lobules IV-VI (Diño et al., 1999). The Purkinje Cell Layer contains the soma of the Purkinje Cells, and the Molecular layer contains the dendritic tree of the Purkinje Cells and the inhibitory Stellate and Basket cells. Several types of glial cells are also found in the cerebellar cortex: the oligodendrocytes, astrocytes, microglial cells, and Bergmann cells, whose somata are in the Purkinje Cell Layer and processes in the molecular layer.

The cerebellum receives two main inputs. The first input comes from mossy fibers that are excitatory axons coming from different parts of the CNS. They connect different zones of the cerebellum depending on their provenance. The vestibulocerebellum, or flocculo-nodular lobe, receives direct inputs from the vestibular sensory nerve, and from the vestibular nuclei. The spinocerebellum, located in vermal and paravermal zones of the anterior and posterior lobes receives inputs from the spinal cord. The neocerebellum or cerebrocerebellum comprise most of the lateral hemispheres of the cerebellum, and receives the majority of its inputs from the pontine nuclei, a relay nucleus receiving inputs from the majority of the cerebral cortex via corticopontine fibers. The cerebral inputs include the primary motor and premotor cortices of the frontal lobe, the primary and secondary somatic sensory cortices of the anterior parietal lobe, and the secondary visual regions of the posterior parietal lobe. Pontine nuclei also receive collateral axons from layer V pyramidal neurons of the neocortex (Wu et al., 2018).

The mossy fibers form synapses with neurons of the DCNs, and with most of the neurons of the granule cells layer. They connect several granule cells, forming between 400 and 600 synapses called “rosettes” (Palkovits et al., 1972) ; several unipolar brush cells (in the

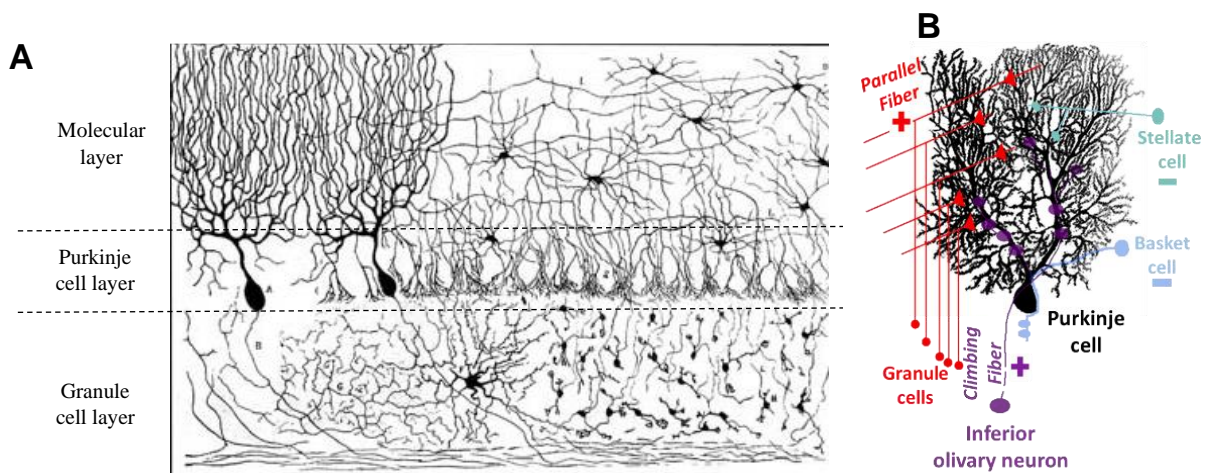


Figure 6: The cerebellar cortex

A) Ramon y Cajal's first drawing published in 1888 illustrating the three layers of the cerebellar cortex: the granule cell layer, containing granule and Golgi cells, the Purkinje cell layer containing the soma of the Purkinje cells, and the molecular layer containing the stellate cells and the dendritic tree of the Purkinje cell, which is in a sagittal plan.

B) B: schematic representation of the Purkinje cell and its 4 afferents.

lobule where they are present), which are innervating granule cells and other unipolar brush cells; and finally, Golgi cells, which are connecting granular cells and unipolar brush cells.

The second cerebellar input is the axons of the Inferior Olivary Neurons, located in the brainstem. The inferior olivary neurons receive afferents from different regions: the superior colliculus, the red nucleus, the raphe nuclei, the sensory trigeminal nuclei, and the spinal cord. The Inferior Olivary Neurons contact directly the Purkinje Cell via a structure called the climbing fiber, and also send collateral to the DCNs. Connections between the inferior olive, the cerebellar cortex, and the DCNs follow a precise topography, forming a complex organization called "modules". The topography between the inferior olive and the cerebellum is also correlated with the presence or absence of the Aldolase C enzyme in the cerebral cortex: Aldolase C staining forms a characteristic band pattern, called "zebrin" (Figure 7, from Sugihara and Shinoda, 2004)

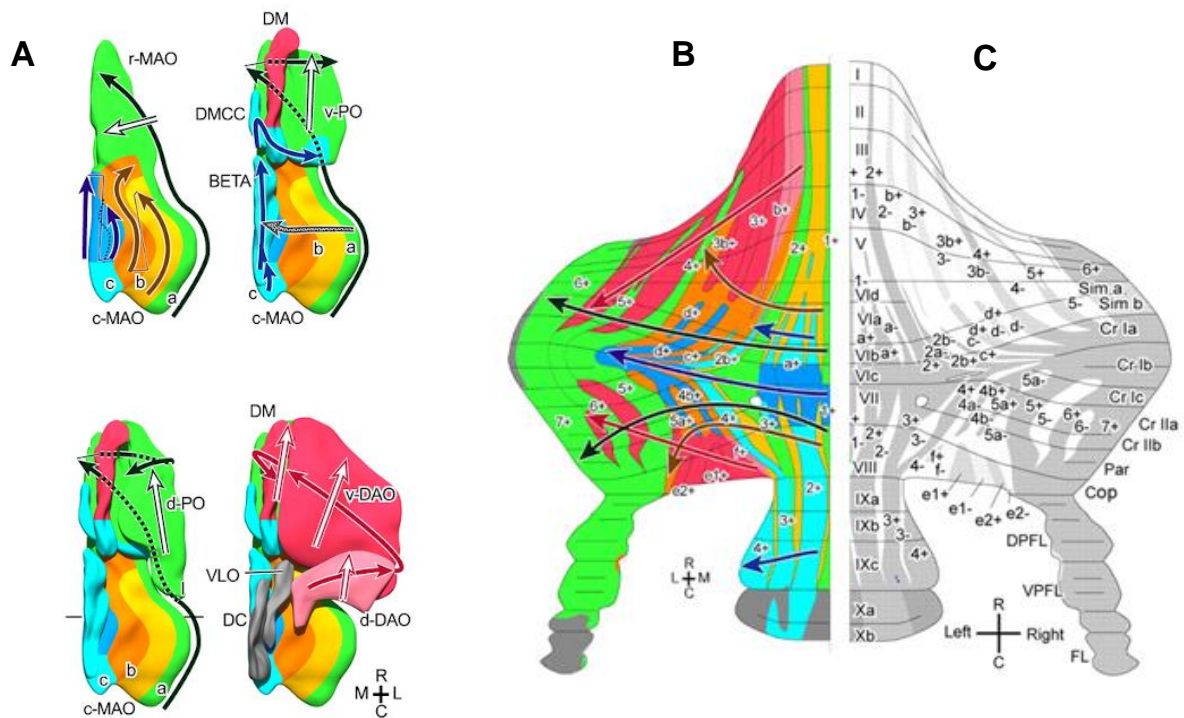


Figure 7: Olivo-cerebellar topography.

A) 3D representations of the inferior olive, from 4 different views.

B) Representation of unfolded cerebellum. The color code represents the localization of the projecting inferior olivary neurons from (A).

C) Representation of the Aldolase C positive (gray) and aldolase C negative (white) bands in the unfolded cerebellar cortex.

3.1.3) Connectivity on Purkinje Cells

The main neuron of the cerebellum is the Purkinje Cell (PC), which is an inhibitory (GABAergic) neuron and the only output of the cerebellar cortex. It has a large soma, and a flat and elaborate dendritic tree in the sagittal plane, with a large number of dendritic spines. The unique axon of PCs projects to the deep cerebellar nuclei (DCN): the PCs of the vermis project to the fastigial DCN (the more medial nucleus), those from the para-vermis (the region between the central vermis and the hemispheres) project to the interposed DCN, the ones from hemispheres innervates the dentate DCN, and those from the flocculus project to the vestibular nuclei. Purkinje Cells also give collateral that innervate other Purkinje Cells and Molecular Layer Interneurons.

The Purkinje Cell receives inputs from 4 different neurons types (**Figure 6B**): two excitatory: The Granule Cells, sending their unique axons called “Parallel Fiber” and the Inferior Olivary Neurons, sending the “Climbing Fiber”.

” The two others are inhibitory GABAergic neurons located in the molecular layer: The Stellate Cells (SC) in the upper molecular layer, and the Basket Cells (BC), close to the Purkinje Cell soma. The different synapses have very distinct electrophysiological properties that can be studied using patch clamp experiments in Purkinje Cells, by stimulating one of the afferents, and recording the repercussion on Purkinje Cell electrical activity.

Purkinje cells have a spontaneous electrical activity, in form of trains of spike both sodium and calcium dependent. These spikes, called “simple spikes” occur at a rate of 17-150hz (Raman and Bean, 1999), but can also be elicited by synaptic activation of the Parallel Fibers (Konnerth et al., 1990). Another type of spike is seen in Purkinje cells: The Complex Spikes, which are slower (1 to 3 Hz), with a much larger amplitude, and followed by a high-frequency burst of smaller amplitude action potential, called “spikelets”. These complex spikes are caused by climbing fiber activation and can involve the generation of calcium mediated action potential in dendrites (Ito and Itō, 1984). The complex spike is typically followed by a “pause,” stopping temporarily the simple spike activity.

Parallel Fiber/Purkinje Cell Synapse

The parallel fibers are the axons of the Granular cells. A unique axon arises from the Granular Cell, then enters in the molecular layer and split into two parallel fibers, forming a “T-shape”. The Parallel Fiber are orthogonal to the dendritic tree of the Purkinje, in a coronal plan. A Purkinje Cell can receive up to 200 000 parallel fibers, which forms one or two *en passant* synapses (Harvey and Napper, 1991) via varicosities that are formed at intervals along the length of the fibers. A parallel fiber can contact several hundred Purkinje Cells as it travels across the cerebellum (Napper and Harvey, 1988). Fibers are small in diameter (from 0,15μm to 0,7μm) but long (several millimeters). Parallel fibers are occupying the majority of the dendritic tree, with a very high density of around 8×10^8 synapses per mm^3 . These fibers make asymmetric glutamatergic synapses, with relatively small varicosities, with a diameter of 300 to 400 nm. (Napper and Harvey 1998) (**Figure 8A**).

It has been shown that an electrical response of the Purkinje cell to parallel fiber input requires the activation of around 50 parallel fibers, to produce a simple spike (Barbour, 1993). Synaptic transmission can be elicited by an electrical stimulation in the molecular layer, that

will activate multiple Parallel Fibers, and elicit an Excitatory Post Synaptic Current (EPSC). This EPSC is proportional to the strength of the stimulation, and to the number of PFs activated, and is called “smoothly graded stimulus-response” (Konnerth et al., 1990).

Short term plasticity is a temporary plasticity mechanism that can occur immediately after spike generation and last typically from hundreds to thousands of milliseconds. It can be either facilitation or depression mechanisms, respectively an increase of the release probability of the neurotransmitters caused by an influx of calcium into the axon terminal, or a decreased released probability caused by a depletion of neurotransmitters at the synaptic cleft. In the case of parallel fibers, when the PF-EPSC is elicited twice and when the interval between two stimuli is smaller than 300ms, the second PF-EPSC present an increased amplitude. This paired pulsed facilitation mechanisms are typical of this synapse type (Konnerth et al., 1990). Parallel fiber/Purkinje cell synapses are subjected to long-term plasticity mechanisms, both long-term potentiation (LTP)(Hoxha et al., 2016) and climbing-fiber dependent Long -term depression (LTD) (Ito and Kano, 1982), which requires the co-activation of the PF and CF and implicates different molecular actors. This phenomenon is induced by a climbing-fiber elicited complex spike, producing a Ca^{++} influx through voltage-gated Ca^{++} channels, and endocytosis of AMPA receptors, which reduces PF/PC synapse strength.

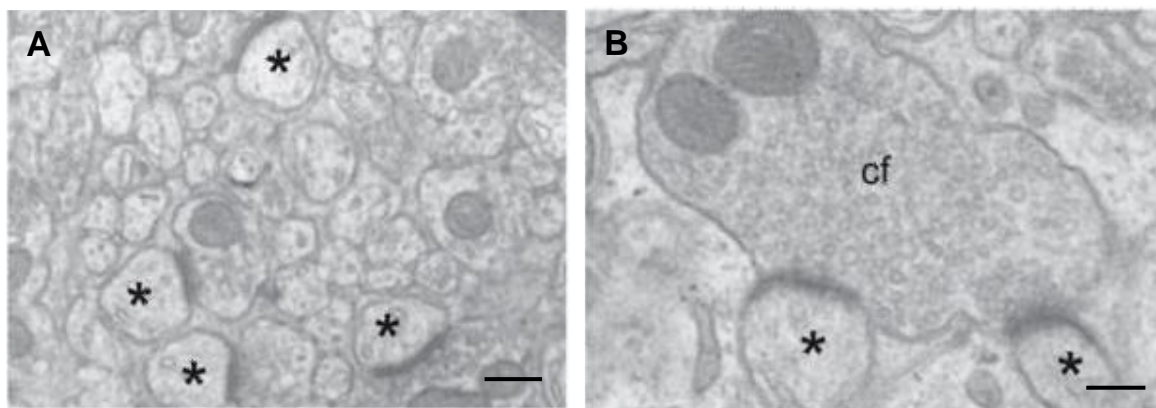


Figure 8: Electron micrograph of excitatory synapses of Purkinje Cells (from Wulff et al., 2009)

- (A) Asymmetric synapses between parallel fiber and Purkinje Cell spines (marked by a star). Scalebar 500nm.
- (B) Asymmetric synapse between one climbing fiber (cf) and Purkinje cell. Scalebar 360nm.

Climbing Fiber/Purkinje Cell Synapse

The climbing fiber arises from the axon of the inferior olivary neurons, and forms around 300 synapses on a Purkinje Cell. The Climbing fiber is quite thick (up to 1 μm diameter (Castejon and Sims, 2006)), and contrary to the parallel fibers, climbing fibers make synapses only on the proximal dendrites of the Purkinje Cell. Climbing fiber/Purkinje cell synaptic boutons are much bigger than PF's ones, with a diameter range from 0.5–2 μm (Brown et al., 2012; Sugihara et al., 2000). A climbing fiber can be morphologically separated into 3 main parts: the primary branch, the tendril branch and distal branch. The last two parts are providing the biggest number of synapses. However, primary branches, despite having lower synapse density, may be important for providing fast and reliable signals, because of their proximity to PC's soma and their low axial resistance. The density of CF boutons is smaller than PF one: On average CFs form a bouton every 8.7 μm , which is less than all the boutons from other synapse type in the cerebellum (Shepherd et al., 2002). One of the most important particularities about CFs is their one-to-one relationship with Purkinje cells, in the adult cerebellum. The loss of this relationship is often associated with motor impairments such as ataxia (Kano et al., 1995; Levenes et al., 1997; Mariani et al., 1977).

At the electrophysiological level, climbing fibers elicit a typical “all or none” response in PCs following stimulation. The climbing Fiber–Purkinje cell synapse is characterized by a different form of short-term plasticity than PF-PC synapses: paired-pulse depression, which is detected as a decrease of the amplitude of the second CF-EPSC when the interstimulus interval is shorter than 5s (Konnerth et al., 1990). CF/PC synapses can also show LTD (Hansel and Linden, 2000) but not LTP at adult age. CF/PC LTP seems to be specific to a short developmental period from P5 to P8, and to be important for CF developmental mechanisms that will be explained below.

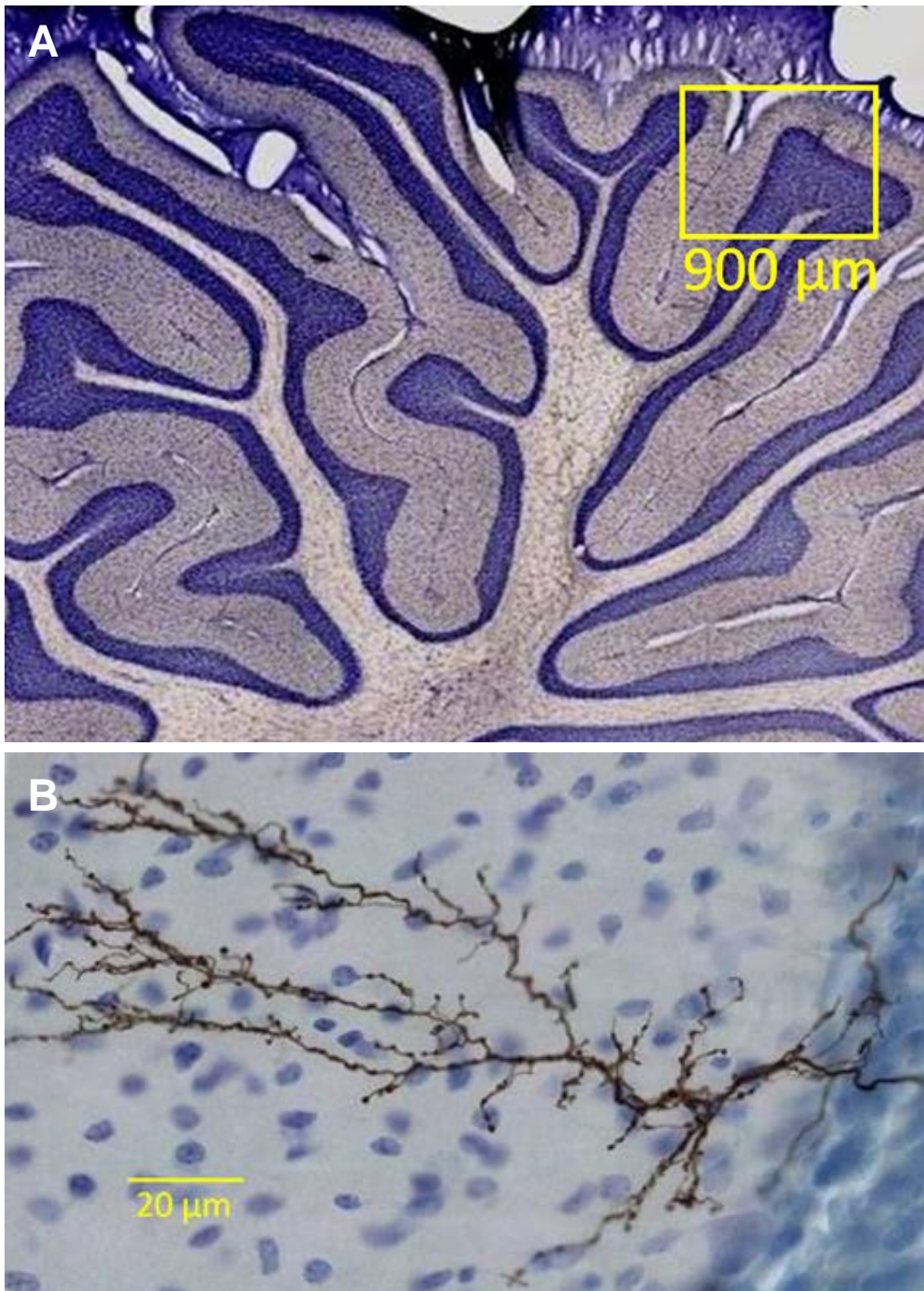


Figure 9: Climbing fiber histology

- A) Sagittal slice of a rat cerebellum, nucleus counterstained with thionine (blue).
- B) Climbing fiber anterogradely labeled using biotinylated Dextran Amine (BDA). From Brown et al., 2012.

Inhibitory synapses

Inhibitory synapses on PCs arise from two types of Molecular Layer Interneurons: the Stellate cells and Basket cells. Stellate cells are the only cell type of the upper third of the ML. They extend their multiple axons in the parasagittal plane of the cerebellar cortex (the plane of the PC dendrites, perpendicular to parallel fibers), and send vertical collaterals innervating different Purkinje cells (Palay and Chan-Palay, 2012). Basket cells, on the contrary, are located in the lower half of the Molecular layer, and target Purkinje cell soma, forming a pericellular nest, and axon initial segment, forming pinceaux. Stellate and basket cells form classical GABAergic symmetric synapses with Purkinje Cells, and the global density of synaptic boutons is intermediate between climbing fiber and parallel fiber synapses (Shepherd et al., 2002).

Molecular layer interneurons have an intrinsic activity, their stimulation in patch clamp experiments elicit classical Inhibitory Post Synaptic Currents (IPSC) in Purkinje cells, and they mainly act as regulators of PC activity. A recent study has shown a different effect of Basket and Stellate cells on PC firing: a selective suppression of stellate cells increased the regularity of simple spikes and the frequency of complex spikes, while basket cell depletion increases simple spike firing and decreases complex spike frequency (Brown et al., 2019).

3.2) Development of the Olivo-cerebellar network

The olivo-cerebellar network is one of the most studied systems for deciphering synaptic development and circuit assembly, benefiting of the highly distinguishable afferent.

3.2.1) Development of the Parallel Fiber/Purkinje Cell synapses

The high degree of specialization of each synapse type of the cerebellar cortex, the different morphology and functional properties and the specific subcellular localization of each afferent obviously requires complex developmental mechanisms. Indeed, how each afferent axon contact a Purkinje Cell, and how they “share” the dendritic territory has been one of the major questions in the cerebellar development field.

The first neurons generated in the cerebellar cortex are the Purkinje Cells, born around E11 and E13 (Embryonic day 11 and 13), and migrate between E12 and E15 to the cerebellar plate. Granule cells originate from neuronal progenitors called Rostral Rhombic lip progenitors (which also give birth to some ventral neurons in the rostral hindbrain region), which begin to proliferate around E10. By E15, Granule Cells precursors migrate in the External Granular layer

(located in the superficial zone of the cerebellar cortex, above the molecular layer). There, mitotic granule cells precursors replicate and expand, and then begin to migrate tangentially in both rostral-caudal and medio-lateral axes (Komuro et al., 2001). After their tangential migration, post-mitotic granule cells initiate a radial migration of their soma, passing through the molecular layer along the fibers of the Bergmann Glia, in the dorso-ventral axis, to reach around P15 their final destination, the Granule Cell layer. The EGL then finally disappears.

The development of parallel fiber synaptic inputs and the formation of thin terminal branches of the Purkinje cell dendritic arborization, called “spiny branchlets” occurs in a concomitant manner, and depend on the integrity of both Granule Cells and Purkinje Cells. The study of several mutant mice provided evidence for this interplay. For example, in the agranular *weaver* mouse (a mouse mutant in which granule cells die before migrating, hence lacking parallel fibers) Purkinje Cell dendritic development is severely impaired; PCs have a decreased dendritic tree length and no spiny branchlets (Sotelo, 1978), suggesting that PC dendritic arborization requires the presence of its presynaptic partner. However, the study of the *staggerer* mutant, a mouse almost completely lacking parallel fiber/Purkinje cell synapses, suggest that spine formation may also have intrinsic developmental mechanisms. In these mice, although granule cells were present during the development and able to migrate and form parallel fibers, they were not able to form synapses, thus leading to a degenerative process and granule cell death. In this mutant, PC dendritic tree also have a greatly reduced size, but they have spines on the soma and primary branches, suggesting that these spines were able to develop without granule cells, while the organization and pattern may be modulated by cellular interactions with the presynaptic inputs.

Formation of Parallel fiber/Purkinje cell synapses is initiated during the first postnatal weeks, and depends on several molecular factors, called “synaptic organizers.” It has been shown that granule cells express Wnt-7a from postnatal day 6 (P6) to P22 and that it regulates axon outgrowth and branching, associated to an augmentation and a clustering of Synapsin 1, a presynaptic protein implicated in synapse formation (Lucas and Salinas, 1997). Cerebelin-1 (Cbln1), a protein secreted by the Granule Cells, has been identified as a crucial factor for establishment and maintenance of PF/PC synapses, forming a tripartite complex with Glur δ 2 and Neurexin (Hirai et al., 2005; Ito-Ishida et al., 2008; Matsuda et al., 2010; Uemura et al., 2010).

3.2.2) Development of the Climbing Fiber/Purkinje Cell synapses

At the “creeper stage”, Climbing fibers begin to contact Purkinje Cells protrusions around embryonic day E19 (Chedotal and Sotelo, 1993). However, these contacts are immature: they disappear during remodeling of Purkinje Cells, and don't provide any detectable electrophysiological response before P3 (Crepel, 1971). Similar to Parallel Fibers, some “synaptic organizers” have been found for CF, including BAI3 receptor on PC dendrites and its presynaptic ligand C1QL1, which are crucial for CF/PC synaptogenesis (Kakegawa et al., 2015; Sigoillot et al., 2015).

At birth, each ION produces ~100 immature CFs that contact several somato-dendritic immature processes of one Purkinje Cell. At this stage, each Purkinje Cell is innervated by three to five CFs, eliciting EPSCs with similar amplitudes until P3. The maximum of multi-innervation is reached at P5, at which age electrophysiological recordings are able to record 3 to 5 climbing fibers per Purkinje Cells. In the second postnatal week, the CF-EPSC recorded from each PC are differentiated into one large CF-EPSC and several small CF-EPSCs, suggesting a strengthening of one CF input over the other (Hashimoto and Kano, 2013; Letellier et al., 2009). The “strongest” CF is selectively strengthened and this phase is called the functional differentiation. From P6-P7, CF synapses are progressively eliminated. The strengthened climbing fiber translocates from the soma of the PC to the dendrites, around P9 and thereafter, while the others, restricted around the soma of PCs, are progressively eliminated. Supernumerary climbing fiber elimination occurs through two distinct phases: the “early” phase, from P6-P7 to P12, and the “late” phase, from P12 to P17. Both phases implicate different mechanisms, and are regulated by different actors (**Figure 10**).

Early phase of climbing fiber elimination

During homosynaptic competition, beginning around P6–P7, and lasting until P12, climbing fiber number progressively decrease, even in hypo granular cerebellar, suggesting that this phase is independent of granule cells (Crepel et al., 1981). Moreover, in GluR δ 2 Knockout mice lacking half of functional PF/PC synapses, two phases of CF synapse elimination can be distinguished. In the first one, from P5 to P11, KO mice exhibit a similar number of CFs than WT, but this value became significantly larger than in WT from P12 to P14 (Hashimoto et al., 2009). However, a recent study by Bailly et al. show that strong irradiation of granule cells, restricted to P5 or P6 completely abolishes climbing fiber synaptic elimination, which suggests that even the early phase of climbing fiber elimination requires the presence of granule cells (Bailly et al., 2018a). CF homosynaptic competition depends on PC and CF activity. This has

been shown by two sets of experiments: first, by lowering the excitability of PCs at P9, Lorenzetto et al. have shown that almost 80% of PC remain innervated by two CFs in adult mice (Lorenzetto et al., 2009). Second, a pharmacological blockage of the activity of Climbing Fiber from P9 to P12 induces a persistent multi-innervation (Andjus et al., 2003).

During this phase, the “loser” CFs, that form synapses on the soma, progressively disappear, and synapses are eliminated, leaving only the dendritic synapses of the “winner” CF. It has been shown that the strengthening of one CF is dependent on molecular factors, including *Sema3A*, *PlxnA4*, *IGF1*, and *progranulin sort1* (Uesaka et al., 2014). For example, *IGF-1* overexpression has been shown to strengthen/maintain both the strongest and weaker CF synapses (Kakizawa et al., 2003).

Late phase of climbing fiber elimination

The second phase of CF synapse elimination starts around P12 and is dependent on the proper formation of granule cells/Purkinje cells synapses. The deletion of *GluD2* or *Cbln1*, two proteins crucial for proper PF-PC synapse formation, or mice with a hypogranular cerebellum, all show deficits of climbing fiber elimination (Hirai et al., 2005; Kano et al., 1995). In particular, *Glurδ2* KO mice show a persistence of perisomatic multiple CF innervation, but also an aberrant CF innervation of distal PC dendrites, in a territory that is supposed to be restricted to PFs. Several other molecular actors have been identified, including *mGluR1* and its downstream signaling cascade (*PLCb4*, *PKCγ*..), as mice lacking these molecules all show impaired CF synapse elimination, specific of the third postnatal week. (Hashimoto et al., 2000; Kano et al., 1995; Offermanns et al., 1997).

This phase is also characterized by a competition of PF and CF for PC dendritic territory. This competition has been shown by experiments on *Glurδ2* or *Cbln1* knockout mice: in the absence of a normal occupation of PF-PC synapses, there is an apparition of ectopic CF synapses in the distal dendrites, a territory normally reserved for PFs (Hirai et al., 2005; Ichikawa et al., 2002).

Altogether, this suggests that granule cells are important for the late phase of climbing fiber elimination, both by restricting the CF territory to proximal dendrites, and by participating to the elimination of supernumerary perisomatic CF synapses. This phase lasts until the complete regression of supernumerary climbing fibers, normally reached around P18.

Finally, a study has shown that a massive elimination of PF/PC synapses on proximal dendrites occurs after the late phase of CF/PC elimination from P18 to P30, suggesting that Purkinje Cells synaptic wiring reach an equilibrium after up to four weeks of complex synapse competition and elimination (Ichikawa et al., 2016).

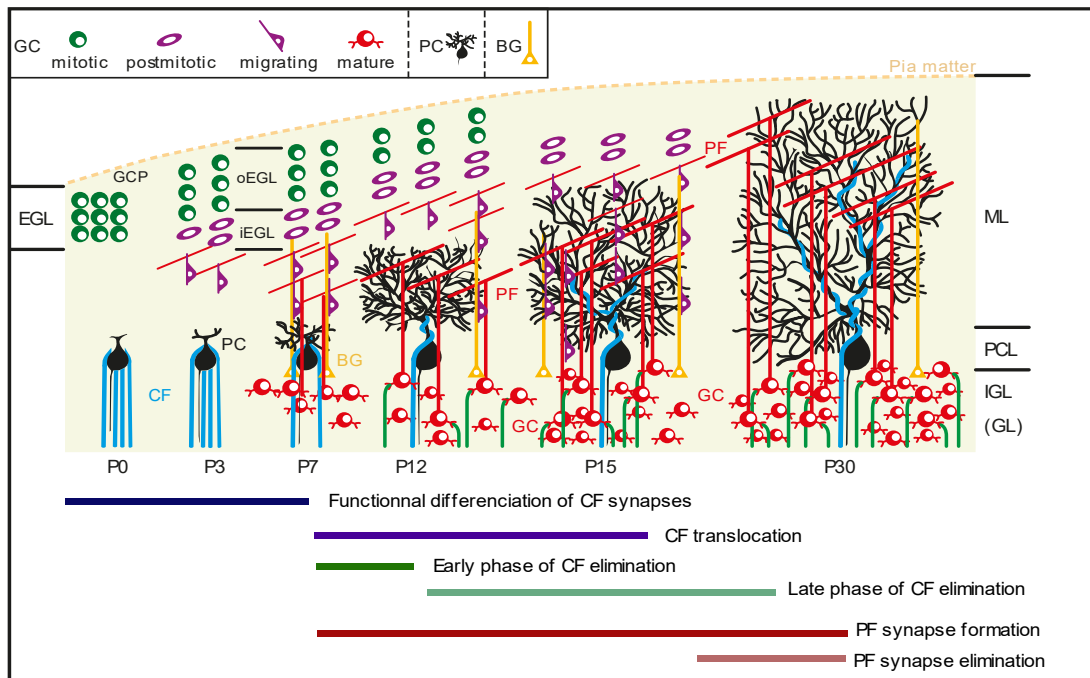


Figure 10: Scheme of the postnatal development of the cerebellar cortex.

At birth, a Purkinje cell is contacted by several climbing fibers, up to five. Until P7 occurs the “functional differentiation” phase of climbing fiber, with a strengthening of one CF over the other. Supernumerary climbing fibers are progressively eliminated, through the early (P7 to P11) and late (P12 to P18) phase of CF elimination. Granule Cells progenitors, in green, divide in the External Granular Layer (EGL). They start differentiating and migrate tangentially from the outer EGL to the inner EGL. Then, from P7 to P15, they migrate radially (dorso-ventral axis) along Bergmann Glia fibers, to reach their final destination: The Granule Cell Layer (also referred as Internal Granular Layer (IGL)). Parallel fibers are formed from P7, and are eliminated from P18 to early adulthood.

4) The cerebellum, an underrated actor in schizophrenia

Many studies tried to decipher the functional role of the cerebellum by linking its physiology to behavior, but until recently, its implication has been restricted to motor behavior and motor pathology such as ataxia. However, it is now known that the cerebellum is also implicated in complex cognitive processes. Since most of the theories concerning the implication of the cerebellum in cognitive processes are extrapolated from cerebellar control of motor coordination, this will be quickly described in the first part. Then, the main theories for the “cognitive cerebellum” will be described, to finally explain the evidences for cerebellar implication in schizophrenia.

4.1) The cerebellum, a major structure for motor coordination

The cerebellum has been known for decades as a major structure for motor function, after the observation at the beginning of the nineteenth century that humans and animals presenting cerebellar lesions or dysfunction show evident motor alterations, with imprecise movement and poor coordination (Ataxia) (Glickstein et al., 2009). Following studies described much broader motor functions for the cerebellum, with the discovery that the cerebellum is implicated in sensorimotor synchronization and oculomotor control (Ito, 1972; Manto et al., 2012; Zee et al., 1980), but has also a role in motor learning, by improving the motor performance using error and correction mechanisms (Ito and Itō, 1984).

Performing accurate voluntary movement requires internal planification of the movement, but also the integration of a wide variety of sensory inputs. Many different models have been created to try to link the cytoarchitecture of the cerebellum with motor control (Apps and Garwicz, 2005). To initiate a movement, the motor command is sent to the spinal cord from the neocortex, and a copy is sent to the cerebellum, named “efferent copy” (Wolpert et al., 1998). The cerebellum also receives real-time sensory information, either visual, auditory, or somesthetic. Then, the cerebellum is thought to process two types of corrections: the “forward internal model” and the “inverse internal model”. In the “forward internal model” the cerebellum compares the internal representation of the motor commands to the actual situation of the body (that could derive from the expected situation, because of the “noise”, the external environment, of the imperfectness of the body sensors). Next, the cerebellum computes a real-

time movement correction. On the contrary, in the “inverse internal model”, the cerebellum is thought to use a prediction of the potential deviation, without sensory feedback (Ito, 2008; Wolpert et al., 1998). These internal models are thought to be treated in defined cerebellar “modules”, which are “loops” between the cerebellar cortex, the deep cerebellar nuclei, and the inferior olivary neurons, receiving sensory inputs through mossy fibers. The feedback signal is provided by the climbing fiber, which brings the “correction” to the internal model via its activity on the Purkinje Cell.

The cerebellum is also implicated in motor learning. For example, the cerebellum, and more precisely the plasticity of the cerebellar cortex, controls the vestibulo-ocular reflex (VOR), an ocular reflex used to compensate the head movement during the visual pursuit of a target, as suggested by the deficits in VOR in mice lacking Parallel Fiber LTP (Gutierrez-Castellanos et al., 2017).

4.2) The cognitive cerebellum

Despite the fact that the most visible defects induced by cerebellar lesions concern motor behavior, the idea that the cerebellum could be implicated in cognitive functions was popularized by Schmahmann in the '90s after the observation that cerebellar patients were unable to precisely control their thoughts and have diverse cognitive deficits. (Schmahmann, 1991).

4.2.1) From motor function to cognition

Several theories emerge to explain the role of the cerebellum in cognitive processes, some of them as an extrapolation of its motor functions. One of the first and most famous one is the “Dysmetria of thought” theory (**Figure 11A**) from Schmahmann. He’s stating that the cerebellum “*regulates the rate, rhythm, force and the accuracy of movements, so does it regulate the speed consistency, capacity, and appropriateness of mental or cognitive processes*” (Schmahmann, 2019, 1991). One particularity of this model is that it unifies the implication of the cerebellum in sensorimotor function, cognition, and emotion, around one universal role/process that could be applied to all mental functions, rather than having separate roles for motor or cognitive functions. This theory is based on the fact that the general architecture of the cerebellum is stereotypical, while the cerebellar connections with other cerebral structures are organized topographically. In other terms, the homogenous architecture

of the olivo-cerebellar loop may reflect a universal computation role, that Schmahmann named “Universal Cerebellar Transform (UCT)”, by which the cerebellum integrates implicitly internal representations (memory, thoughts, motor planification) with external stimuli (sensorial information), and this role applies to different functions depending on the region of the cerebellum.

Several evidences converge for a regionalization of the cerebellum. First, it can be deduced from the provenance of the fiber tracts: the anterior lobe receives connections from the spinal cord and sensorimotor areas, suggesting a role in sensorimotor processes, the posterior vermis receive limbic inputs, and the lobule VI/VII and lateral areas are connected with associative areas of the cerebral cortex (the prefrontal cortex, posterior parietal cortex, cingulate gyrus), presenting higher cognitive functions (Stoodley and Schmahmann, 2010). This regionalization correlate well with the defect that could be seen on patients: while anterior lesions bring motor deficits (ataxia, eye movement deficits), lesions of the posterior lobe bring cognitive deficits (Schmahmann et al., 2009).

Second, several neuroimaging studies confirmed this regionalization well, and strengthened the hypothesis of a cognitive cerebellum. Functional Magnetic Resonance Imaging studies (fMRI) in humans (**Figure 11B**) allow visualizing the activation of cerebellar structures during different motor and cognitive tasks, and thus to deduct the functional topography of the human cerebellum (Stoodley and Schmahmann, 2009). Tasks such as moving the arm or the leg, expected to be essentially sensorimotor, activate the anterior lobe and adjacent parts of the lobule VI, and the second sensorimotor area in lobule VIII (**Figure 11 B**). On the contrary, cognitive paradigms activate different regions of the posterior cerebellum. For example, language and verbal working memory tasks activate the lobule VI and Crus I, executive functions such as organizing, working memory, or strategy formation activates the Crus 1 and lobule VIIB, and finally tasks involving emotional processing activate vermal lobules VI and VII.

Interestingly, these studies showed that some tasks are lateralized, for example language seem restricted to the right cerebellum, while spatial functions concern the left cerebellum, which is the opposite of what is seen in the cerebral cortex, suggesting crossed cerebro-cerebellar projections (Guell et al., 2018). Another example of cerebellar implication in language is brought by a language comprehension task conducted in healthy volunteers, in which participants had to listen to a sentence and link the last word to one of four images

presented, in two conditions: when the sentence brings a context predicting the final word, and when the sentence doesn't give any clue. In this task, acute disruption of the right cerebellar hemisphere by transcranial magnetic stimulation specifically slowed down saccade reaction time in the predictive condition, thus confirming the causal role for the right hemisphere of the cerebellum. in prediction of semantic content (Miall et al., 2016).

To conclude, these studies confirmed that the cerebellum is implicated in a wide range of motor and cognitive tasks, organized in an antero-posterior sensorimotor-to-cognitive gradient, similar to what is seen in the cerebral cortex (Guell et al., 2018, 2015). The “new” cognitive role for the cerebellum opened a new door for cerebellar research, and several studies tried then to decipher how the cerebellum encodes cognitive information, notably using animal models.

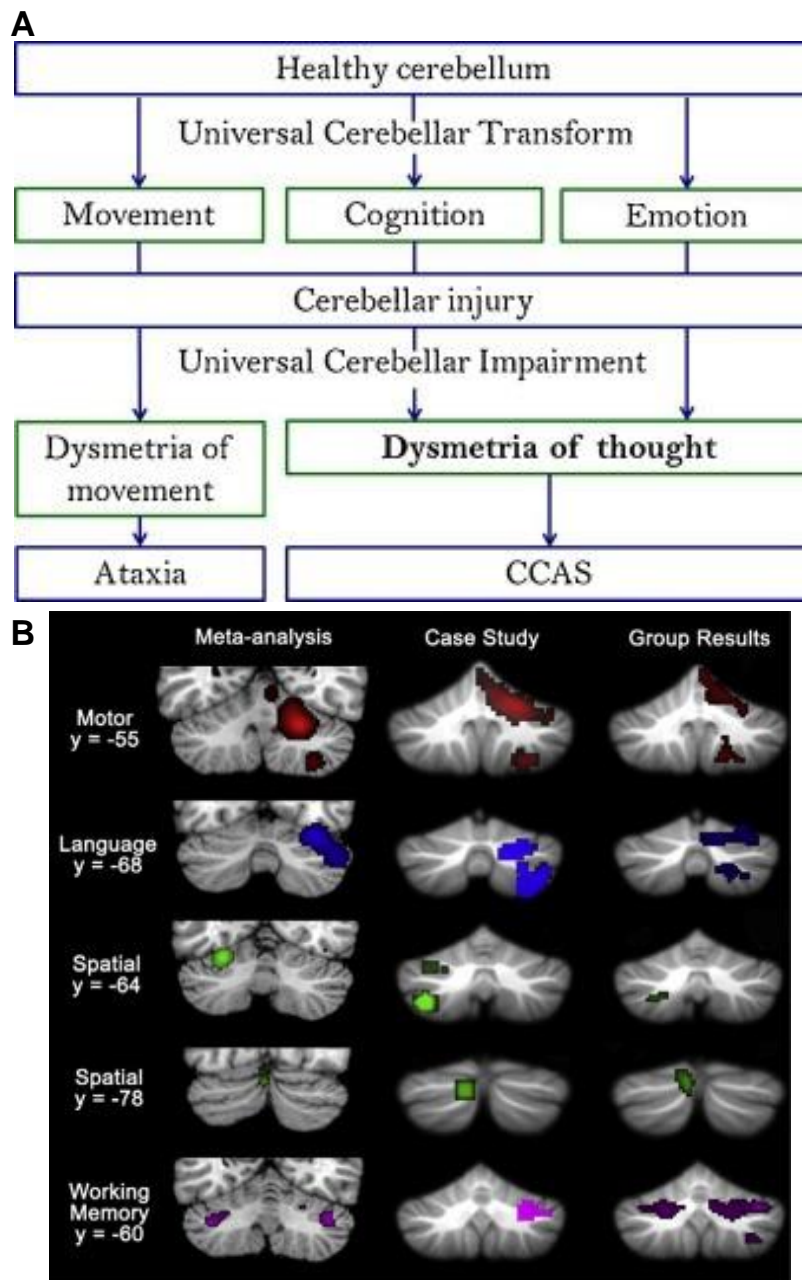


Figure 11: Cerebellum and cognition: theory and functional evidences.

A) Scheme of Schmahmann dysmetria of thoughts and universal cerebellar transform theories

(From Guell et al., 2015)

B) Functional topography in the human cerebellum revealed by task-based fMRI, from a meta-analysis (left), a single case study (middle) and a group of 9 subject (right), shows the different pattern of activation of different areas of the cerebellum

(From Schmahmann, 2019).

4.2.2) Decoding the cognitive role of cerebellum: studies on animals

As a consequence of the recent enthusiasm concerning the implication of the cerebellum in cognitive processes, several researchers aimed to decipher its role in animal models by selectively modulating cerebellar function and assessing the consequences in different cognitive and behavioral paradigms.

Cerebellar implication in spatial navigation

One of the earlier studies tested whether the cerebellum could be implicated in spatial navigation, based on the hypothesis that spatial navigation requires the integration of the internal representation of the environment with self-motion sensorimotor information. In other words, if the spatial map is known to be the role of hippocampal place cells, the cerebellum is an ideal candidate for integration of visual and vestibular sensory inputs that may place the movement of the body in the spatial map.

In their paper published in 2011, Rochefort and collaborators have shown that the cerebellar Purkinje cells are functionally linked to hippocampal place cells, using a mouse model with selective impairment of LTD at Parallel fiber/Purkinje Cell synapses in a spatial navigation behavioral paradigm (Rochefort et al., 2011). In these mice, while navigation performances in light condition (using external clues) were normal, the performances in dark condition were significantly impaired (using internal clues). While in daylight, mice can navigate using visual cues, navigation in the dark requires the use of internal self-motion cues, the own representation of their body. This suggests that integration of self-motion cues was impaired in those mice. *In vivo* freely moving recordings of hippocampal place cells during the behavioral tasks have correlated this behavioral deficit with the activity of place cells, which were disrupted only in the dark condition. In other terms, the disruption of Purkinje cell long term plasticity was sufficient to perturb the activity of hippocampal place cells, and manifest specific deficits in integrating self-motion cues, in absence of any prior motor, motivational, or vestibular deficits.

The cerebellum, reward, and learning reinforcement

Another recently found cognitive function of the cerebellum is its role in reward processing. In their pioneer work in 2017, Wagner and collaborators found that the cerebellar granule cells encode the expectation of reward. By using two-photon imaging, they were able to record specifically granule cells activity, during several reward-related behavioral paradigms (Wagner et al., 2017). In particular, they found three different populations of granule cells, across all the lobules they recorded (VIa, VIb, and simplex): one encoding for the obtention of

the reward, another encoding reward anticipation and active after a stimulus or after the mice produce an action they previously learned to generate a reward, and the last one reacting to reward omission, meaning the absence of an expected reward. They postulate that the neuronal response is unlikely linked to sensorial or motor stimulation, as the activity of both reward anticipation and reward omission neurons is specific to the reward, and is reproducible across different behavioral tasks involving different motor or sensorial stimuli. This brings one of the first direct evidence for an active participation of the cerebellum to reward processing.

Another more recent paper has strengthened the evidence for cerebellar implication in reward-related reinforcement learning (Sendhilnathan et al., 2020). By recording the activity of a single Purkinje Cell in monkeys, during a learned behavioral task, the authors have shown that the Purkinje cell participate to the learning of the task through reinforcement of an error signal. The simple spike activity of Purkinje cells was modulated during the learning of the task only, not when the monkey is trained enough to know accurately the outcome of their action, suggesting an implication specifically in the learning process. Moreover, this result seems to be independent of sensorimotor parameters. They further have shown that Purkinje cells activity is keeping in memory the result of the previous decision only (but not the N-2). This memory of the previous decision is brought by a peak simple spike activity of Purkinje cells during a define period of hundreds of milliseconds between two trials (called “delta epoch”) and could be divided into two kinds of neurons: Purkinje cells keeping the memory of “wrong decision” and those memorizing the right one. Moreover, this “wrong or right” signal decrease with improving performances during trials. Therefore, this mechanism could be seen as a learning-based error signal, similar to what can be seen for a motor-related task in the cerebellum. Interestingly, on the contrary to the hypothesis concerning motor learning, the signal error isn’t conveyed by the climbing fiber, as complex spike activity is totally uncorrelated with the reward.

Another study using optogenetic in the DCNs, has shown that modulation of DCNs neurons directly modulate reward circuitry, through direct monosynaptic connection to the Ventral Tegmental Area (VTA) (Carta et al., 2019). In this article, the authors were able to activate VTA dopaminergic neurons by optogenetic stimulation of DCNs neurons, and this stimulation was able to change the place preference of the mouse, suggesting that stimulation is rewarding. The inhibition of DCN neurons was also altering social preference of the mouse, suggesting an implication of the cerebellum in social behavior. Moreover, regarding the

importance of the dopaminergic system in schizophrenia, this study shows that the cerebellum could act directly on a well-recognized circuit for schizophrenia.

Finally, the cerebellum exerts an influence on the development of cognition and social behavior as suggested by a study in which the authors modulated the activity of the cerebellar Molecular Layer Interneurons during late brain development, and noticed long-term deficits in several cognitive tasks. Using chemogenetic DREADDs inactivation, they specifically inhibited the activity of cerebellar MLI in lobules VI, VII, Crus 1 and Crus2 from P21 to P56 (a period corresponding to adolescence). This manipulation of activity induced long-term deficits in eye-blink conditioning (a cerebellar-dependent associative learning task), and a deficit in cognitive flexibility in a reversal learning paradigm (in a Y-maze, the mice had to learn to find the localization of a reward, and after they learned the rule, the experimenter exchanged the arms, forcing the mouse to relearn the new rule). Moreover, developmental inhibition of the activity of Crus2 MLI induces social deficits, as in a 3-chamber task, social preference over an object was abolished. These experiments suggest that a normal cerebellar development is required for cognitive and social capabilities, and that several subregions of the cerebellum may be part, together with other more well-recognized cerebral structures such as the prefrontal cortex, of a cognitive neuronal network. Together, these studies bring strong arguments for the implication of the cerebellum in cognitive processes, and show its active participation to high order cognitive processes such as rewards, spatial navigation, or social behavior.

4.3) The cerebellum and schizophrenia

The cognitive role of the cerebellum logically raises the question of a potential implication of the cerebellum in mental disorders, such as schizophrenia, especially since cerebellar deficits have been described in the context of psychiatric disorders.

4.3.1) Cerebellar injury can induce symptoms relevant to schizophrenia

Following the recent evidence concerning a cognitive role of the cerebellum, researchers and psychiatrists began to envision that the cerebellum could be playing a role in psychiatric disorders such as schizophrenia. One of the first evidence came from the characteristic behavioral symptomatology that some posterior cerebellar lesions could induce.

Schmahmann defined the “Cerebellar Cognitive Affective Syndrome” (CCAS), or Schmahmann’s syndrome, as a set of cognitive impairments following cerebellar injury

(surgery, stroke, hemorrhage), characterized by impairments in executive functions, affective dysregulation (aggressivity, inappropriate behavior, disinhibition, etc.), language deficits (decrease verbal fluency, mutism, abnormal syntax), working memory deficits, impaired ability to multitask, poor mental flexibility, etc. (Schmahmann and Sherman, 1998). Interestingly, a range of symptoms of the CCAS are classified into the psychosis spectrum, such as illogical thought, paranoia, hallucinations, lack of empathy, and are symptoms classically present in schizophrenic patients, suggesting that in some cases cerebellar injury could be sufficient to induce schizophrenia-like symptoms. Similarly, a few reports found an association between psychosis and cerebellar injury, comprising cerebellar tumors (Madhusoodanan et al., 2015), and a rapid psychotic onset after cerebellar strokes (Bielawski and Bondurant, 2015; Neufeld et al., 2016).

4.3.2) Schizophrenic patients have cerebellar deficits

Schizophrenic patients have a reduced cerebellar volume, detected both in neuroimaging (Jacobsen et al., 1998; Keller et al., 2003; Moberget et al., 2018; Nopoulos et al., 1999) and postmortem studies (Weinberger et al., 1980), and are also seen in drug-naïve and first onset patients. Interestingly, cerebellar volume reduction was amongst the most pronounced compared to other brain structures, occupying the third place after the hippocampus and the pallidum. Moreover, deficits in the posterior cerebellum and hemisphere, in particular lobule VI and Crus1/2, present the biggest correlation with psychotic symptoms (Moberget et al., 2019), coherent with the cognitive role of these structures. At the histological level, the linear density and the size of Purkinje cells is decreased in patients (Reyes and Gordon, 1981; Tran et al., 1998). While studies at the molecular level in cerebellum of schizophrenic patients are rare, several synaptic proteins have been found decreased in the cerebellar granule cells, with a 30% decrease of synaptophysin and a 36% decrease of Complexin 1 (Eastwood et al., 2001).

Moreover, as mentioned before, schizophrenic patients have a decreased blood flow in the cerebellum in several cognitive tasks, including memory, attention, social cognition (Andreasen et al., 1996; Crespo-Facorro et al., 2001), suggesting that cerebellar function in cognitive tasks is deficient. Schizophrenia patients show several deficits that could be reflective of cerebellar impairment, including impaired eyeblink conditioning, impaired adaptation of vestibulo-ocular reflex, dyscoordination, or neurological soft signs, which are a set of motor coordination, equilibrium and sensory integration items that have a high prevalence on schizophrenic patients (Picard et al., 2008). A resting state fMRI study screening for whole-

brain connectivity deficits in schizophrenic patients found a significant correlation between negative symptoms in schizophrenia and diminished connectivity between dorsolateral prefrontal cortex and vermal posterior cerebellum (Brady et al., 2019). Interestingly, after applying transcranial magnetic stimulation in the cerebellum of these patients, they were able to increase prefrontal cortex-cerebellum connectivity and to improve negative symptoms severity, suggesting that this connection may be at least partially causative in some negative symptoms of schizophrenia. The volume of the cerebellum has also been correlated with cognitive functions in schizophrenia, including verbal memory (Toulopoulou et al., 2004) or global IQ (Nopoulos et al., 1999). However, while it is now clear that some cerebellar injuries can lead to schizophrenia-like symptoms, and that many schizophrenic patients have cerebellar deficits, the precise role of the cerebellum in the diverse physiopathology of schizophrenia remains largely unknown.

How could the cerebellum play a role in schizophrenia?

One of the pioneer theories trying to explain the implication of the cerebellum in schizophrenia is Andreasen's "cognitive dysmetria" theory. The cerebellum is functionally connected with the thalamus and the cerebral cortex through the "Cerebro-cortico-thalamo-cortical circuit (CCTCC). This theory postulates that the cerebellum is at the center of the synchrony/coordination of thoughts and actions, and that this synchrony may be underpinned by a fast interconnection between the cerebellum and the cerebral cortex, passing through the thalamus (Andreasen et al., 1998). The cerebellum could play an important role in this loop. The cerebellar cortex receives many inputs from other parts of the brain, through mossy fibers and climbing fibers, information that converge to the Purkinje Cell, that could discriminate and recognize specific input condition. Moreover, the cerebellum is a powerful prediction structure, with strong error-correction capabilities. In schizophrenic patients, this pattern and error detection could be altered, leading to an improper mixture of for example internal stimuli (memory, imagination) with external sensorial stimuli. For example, the auditory information from the auditory cortex could be misinterpreted as "coming from outside" rather than being internal, leading to auditory hallucinations. This hypothesis is strengthened by PET imaging studies, showing that schizophrenic patients have lower blood flow in the cerebellum and thalamus compared to controls in a variety of cognitive tasks (Andreasen et al., 1996; Andreasen and Pierson, 2008; Volkow and Fowler, 1992). Finally, if not all the schizophrenic patients have cerebellar deficits, cerebellar dysfunction has been associated with a poor prognosis, with a negative correlation between the cerebellar volume and negative symptoms,

duration of psychotic symptoms, and greater psychosocial impairments (Wassink et al., 1999). Altogether, this suggests a potential role of the cerebellum in schizophrenia pathophysiology, or at least in a subpopulation of patients, which raises the question of defining endophenotypes in schizophrenia (Picard et al., 2008), a population of patients presenting a more homogenous group of symptoms.

To conclude this chapter, it seems now clear that the cerebellum should now be considered as an actor of cognitive processes. The theories of cerebellar functioning, both coming from new insight and from an extension of the cerebellar role in motor coordination, depict the cerebellum as a powerful neuronal machine, able to compute and integrate a vast variety of internal and external information, and have a role in learning and prediction mechanisms that could be applied to many complex cognitive processes. That functioning fits well with a part of schizophrenia symptomatology, hence disruption of cerebellar circuitry could partially explain—or at least participate to some cognitive deficits and dissociative symptoms. If animal studies recently tried to decipher the cognitive role of the cerebellum at the neuronal level, a lot of efforts remains to be done in order to fully understand by which pathophysiological mechanisms the cerebellum could play a role in the etiology of schizophrenia.

Results

Deficits of the quantity, morphology, function, but also molecular architecture of synapses have been detected in both patients and animal models of various neuropsychiatric deficits, such as schizophrenia. These deficits likely contribute to the behavioral phenotype seen in patients with schizophrenia and other psychiatric disorders. Consistent with this hypothesis, many synaptic cell adhesion molecules important for synapse formation, maturation, specificity, and pruning, such as cadherins, neuroligins, or LRR proteins, are implicated with social behavior (for review see (Taylor et al., 2020)). As reviewed by Taylor et al., disruption of these molecules in rodents is often associated with impairment of social affiliative behavior (meaning engagement of a social reciprocal interaction with a conspecific). However, despite the great progress made in the field, there are several limitations: first, most of the studies are done at the brain region scale, not the synapse-specific scale. Thus, deficits specific of one synapse type could be missed. Second, many questions remain unanswered concerning the mechanisms that could be disrupted in schizophrenia, which likely occur in a defined period of synaptic development.

The olivo-cerebellar network, because of its well-described cytoarchitecture and synaptic organization, is a powerful model to study the formation of neural circuits at the synapse-specific level. Moreover, despite the fact that schizophrenia was primarily thought to implicate deficits of the prefrontal cortex or hippocampus, the cerebellum has recently emerged as a potential actor of this pathology.

My work was organized around two main questions. The first one was to study the potential synaptic alterations in mice models of schizophrenia at the afferent-specific level, and deciphering the mechanisms leading to these defects. Second, this work aims to highlight the potential role of cerebellar malfunctioning in schizophrenia, and especially of its synaptic circuitry.

Schizophrenia is a highly complex disease, and may not implicate one unique causal factor, but rather many potential genetic and environmental actors, eventually cumulative. I thus studied two different widely used developmental models of schizophrenia.

The first one, the subchronic neonatal phencyclidine (PCP) model, consists in several injections during the second postnatal week of the NMDA antagonist PCP. This drug is known to induce acutely psychotic symptoms in humans, resembling those seen in patients with schizophrenia, suggesting an important role of the glutamatergic circuit in this disease. Perhaps more interestingly in the context of this work, the use of this drug in the early development of

the mouse induces long-term behavioral and neuropathological alterations potentially relevant to schizophrenia. This model is thought to mimic active environmental disruption of brain development. In this part, using morphological and *ex vivo* extracellular electrophysiological analysis, I have shown that the PCP model doesn't induce any major deficit in cerebellar cytoarchitecture and in global Purkinje cells activity, but induces a general decrease of the volume of climbing fiber presynaptic boutons, and an increase of synaptic contacts between climbing fiber in certain subpopulations of PCs, while other afferents of Purkinje cells are not affected. Moreover, using high-throughput gene expression analysis, we detected several genes transiently deregulated during the PCP treatment, which could eventually explain the synaptic phenotype.

The second model is a genetic one, the LgDel (Large Deletion) model. It mimics the genetic deletion 22q11.2, that is responsible in humans for a 40% increased risk of developing schizophrenia. While the direct mechanism of the alterations and its relationship with schizophrenia is still unknown, its relatively high penetrance suggests that some anomalies of the neuronal network may generate an increased susceptibility to develop the pathology. This model might more reflect cumulative genetic predisposition factors seen in patients. Using the same set of morphological and electrophysiological tools than for the PCP model, I didn't find any changes either in the global cerebellar morphology and PC activity, or in synaptic morphology. It suggests that the establishment of the synaptic network in the cerebellar cortex may not be affected by this large genetic deletion, and that eventual defects, if any, might concern other parameters of circuit function or occur later during development.

**Part 1: Afferent-specific
deficits in cerebellar
Purkinje cell synapses in the
PCP developmental model of
schizophrenia**

Afferent-specific deficits in cerebellar Purkinje cell synapses in the PCP developmental model of schizophrenia

Veleanu M.¹, Sigoillot S.M.¹, Becamel C.², Selimi F.^{1*}

Affiliations:

¹ Center for Interdisciplinary Research in Biology (CIRB), College de France, CNRS, INSERM, PSL Research University, Paris, France

² Institute for Functional Genomics (IGF), University of Montpellier, CNRS, INSERM, Montpellier, France

*Corresponding author: fekrije.selimi@college-de-france.fr

Abstract/Summary

Synaptopathies are diseases of the brain that are caused by or related to dysfunctions of synapses. Schizophrenia is now considered a synaptopathy due to the discovery of numerous synaptic deficits in postmortem tissues, and of many mutations affecting synaptic genes in schizophrenic patients. While global synaptic loss and synaptic gene misexpression have been described in the prefrontal cortex and hippocampus of schizophrenic patients, very little is known about the specific synaptic deficits that could alter neuronal circuits in schizophrenia. Using a developmental pharmacological mouse model of schizophrenia, the chronic neonatal Phencyclidine (PCP) treatment, we found specific alterations of some types of synapses in the olivo-cerebellar circuit. The suchronic injection of PCP also induced a significant transient misregulation of the expression of several membrane and secreted genes, suggesting a transient modification of the neuronal surfaceome in the PCP model. In particular, *Ctgf*, a gene coding for a secreted extracellular matrix protein known to interact with synaptic organizers, was transiently upregulated both in the cerebellum and brainstem. This overexpression could potentially interfere with the normal development of the olivocerebellar circuit. Moreover, our results show the presence of synaptic deficits in the cerebellum of a mouse model of schizophrenia, strengthening the recent recognition that the cerebellum may be an actor of this disease.

Introduction

The specificity of connectivity between different neurons is at the base of brain function. The development of specific synapses involves the fine regulation of complex mechanisms of recognition between pre- and post-synaptic neurons, the specialization of the pre- and post-synaptic compartments, and the refinement of the network through selective synapse elimination and stabilization (Sanes and Yamagata, 2009; Sanes and Zipursky, 2020; Südhof, 2018). All these steps depend on the timely regulation of multiple molecular actors, in particular proteins at the neuronal surface. Membrane proteins such as cadherins, immunoglobulins, ephrins, or semaphorins have been implicated in synaptogenesis (Pasterkamp, 2012; Sanes and Yamagata, 2009). Secreted extracellular molecules are also important actors of synapse formation and specificity. For example, the WNT protein family is associated with synapse formation, and modulates axon guidance (Salinas, 2012), and timely regulated expression of Sonic Hedgehog (Shh) is necessary for the formation of cortical microcircuitry (Harwell et al., 2012). Secreted proteins of the C1Q family, cerebellins and C1QL proteins, have been identified as major organizers of excitatory synapses in the brain (Kakegawa et al., 2015; Sigoillot et al., 2015; Südhof, 2018). In the cerebellum, CBLN1 mediates the formation of parallel fiber/Purkinje cell synapses, and C1QL1 regulates the development of climbing fiber/Purkinje cell synapses through their respective receptors GluRdelta2 and the adhesion GPCR BAI3 (Kakegawa et al., 2015; Sigoillot et al., 2015; Uemura et al., 2010).

Schizophrenia spectrum disorders are now considered as synaptopathies (Howes et al., 2020; Osimo et al., 2018; Sekar et al., 2016; Sellgren et al., 2019; Yin et al., 2012). Many synaptic deficits have been described in the brains of schizophrenic patients. Postmortem studies have revealed a loss of dendritic arborization associated with a decreased spine density (Glantz and Lewis, 2000; Roberts et al., 1996; Rosoklija et al., 2000) and a decrease in many synaptic proteins such as synapsin, PSD95, SNAP25, and several subunits of glutamate receptors, in various brain areas (Eastwood and Harrison, 2005; Glantz and Lewis, 1997; Karson et al., 1999; Scarr et al., 2006, meta-analysis by Osimo et al., 2019). Although most described deficits concern excitatory synapses, inhibitory deficits are also found in schizophrenia, with decreased mRNA levels for GAD65, Gat-1, and GABA_A in several brain regions of schizophrenic patients (Akbarian et al., 1996; Hashimoto et al., 2008; Vawter et al., 2002), and an increase of GABA_A receptor binding in the prefrontal cortex (Benes et al., 1996). Genetic studies also suggest defects in synaptic development and/or function in patients with

schizophrenia. A large Genome Wide Association study identified 108 significant schizophrenia associated loci with Single Nucleotide Polymorphisms (SNPs) in some synaptic genes, such as the dopaminergic receptor D2R, the glutamate receptor subunits GRIA1, GRIA4, GRIN2B, GRM5, or the voltage-gated calcium channels proteins CACNB2 CACNA1C and CACNA11 (Ripke et al., 2014). Exome sequencing studies have identified several rare *de novo* or inherited variants of stronger penetrance, with a high enrichment of the post-synaptic ARC-associated proteins, PSD95, and voltage-gated calcium channels (Purcell et al., 2014). While schizophrenia is a highly complex disease that is likely to involve a combination of potential genetic and environmental causes, these various post-mortem and genetic susceptibility studies suggest that dysfunction at glutamatergic synapses may be one of the major causal features of schizophrenia.

NMDA antagonists in rodents are extensively used to model environmental disruptions that might be involved in the etiology of schizophrenia and to mimic several relevant physiopathological alterations (Jones et al., 2011). In particular, these drugs are associated with psychotic-like symptoms similar to those seen on schizophrenic patients. In the neonatal subchronic phencyclidine (PCP) model, the drug is administered subcutaneously to rodent pups during the second postnatal week, a critical period of the development of the rodent brain. This period is particularly sensitive to early environmental stressors that could lead to increased risk of developing schizophrenia (Rapoport et al., 2012). PCP neonatal injections in rodents induce a wide range of behavioral and neuropathological alterations in the adult. Prepulse inhibition of the startle response, a sensorimotor gating task used both in animal models and humans as a behavioral marker of psychiatric disorders such as schizophrenia, is found defective in several studies (Anastasio and Johnson, 2008; Kjaerby et al., 2013; Wang et al., 2001), while one found it unchanged (Boctor and Ferguson, 2009). Other behavioral deficits include spatial memory deficits (Nakatani-Pawlak et al., 2009; Wang et al., 2001), and a deficit in social novelty discrimination (Clifton et al., 2013; Meffre et al., 2012; Terranova et al., 2005). At the neuronal level, studies have reported a reduction of Parvalbumin (PV) expression in fast spiking PV cortical interneurons (Kaalund et al., 2013; Mouri et al., 2007), a decreased number of PV neurons, and a decreased spine density in the frontal cortex, nucleus accumbens and hippocampus (Nakatani-Pawlak et al., 2009). These mice have also several other synaptic deficits, such as a reduction in the expression of the synaptic protein PSA-NCAM (polysialic acid neural cell adhesion molecule), known to promote stabilization of synapses during early synaptogenesis (Dityatev et al., 2000) and synaptophysin, a well-known presynaptic marker.

Finally, mice have likely impaired function of both excitatory and inhibitory synapses: some studies found a significant enhancement of NMDA mediated Excitatory Post Synaptic Currents (EPSC) (Yu et al., 2002), an impairment of Long Term Plasticity (LTP) in CA1 neurons (Nomura et al., 2016) and reduced mini Inhibitory Post Synaptic Currents (mIPSCs) in cortical layer II/III pyramidal neurons (Kjaerby et al., 2014).

A key remaining question is whether all synapses are affected similarly in neurodevelopmental diseases such as schizophrenia. To answer this question, we are using the olivo-cerebellar network as a model due to its well-described cytoarchitecture and synaptic organization. In particular, Purkinje cells, the unique output of the cerebellar cortex, receive two types of excitatory inputs: parallel fibers (from cerebellar granule cells) and climbing fibers (from inferior olivary neurons), and two types of inhibitory inputs (from cerebellar basket and stellate cells), which form synapses with distinct morphologies, subcellular localization, and functions. Moreover, while schizophrenia was primarily thought to implicate deficits of the prefrontal cortex or hippocampus, the cerebellum has emerged as a potential actor in this pathology. Schizophrenic patients often present a decreased cerebellar volume (Andreasen et al., 1996; Moberget et al., 2019; Weinberger et al., 1980), as well as neurological soft signs, a type of sensorimotor impairment that implicates the cerebellum (Hirjak et al., 2016). Interestingly, neurological soft signs have been correlated with a poor outcome and greater negative and cognitive symptoms (Picard et al., 2008; Prikryl et al., 2007; Wassink et al., 1999). Furthermore, while initially thought to be a motor-related structure, it is now well established that the cerebellum also plays a role in cognitive processes (Schmahmann, 1991; Stoodley and Schmahmann, 2010) such as spatial navigation (Rochefort et al., 2011), language (Guell et al., 2015), reward (Wagner et al., 2017) and social cognition (Badura et al., 2018).

In this study, we used morphological and electrophysiological analysis to describe synaptic characteristics in an afferent-specific manner in the PCP neonatal model. PCP was delivered through systemic subcutaneous injections of the drug at postnatal day 7 (P7), P9 and P11 (**Figure S1A**) and analysis was performed at P30. Our results show that PCP neonatal injections induce long-lasting synaptic deficits specifically at climbing fiber/Purkinje cell synapses, one of the two excitatory synapse types of Purkinje cells, while no major deficit is detected in other PC synapses, cerebellar cytoarchitecture and spontaneous Purkinje cell activity. Using high-throughput gene expression analysis, we detected a transient PCP-induced misregulation of several genes coding for membrane and secreted proteins, and in particular identified CTGF overexpression as a potential actor of PCP induced synaptic changes.

Results

Global cerebellar cytoarchitecture and spontaneous electrophysiological properties of Purkinje cells are normal in juvenile mice in the PCP model

Schizophrenic patients often present a decreased cerebellar volume (Moberget et al., 2019; Weinberger et al., 1980). We thus first analyzed whether the neonatal injection of PCP induces any lasting defects in global cerebellar morphology. Calbindin immunostaining revealed a normal cerebellar cortex cytoarchitecture in PCP treated mice with a stereotypical organization in layers. In particular it revealed the molecular layer, which contains the dendritic tree of the Purkinje cells that receives all the excitatory inputs and inhibitory inputs from stellate interneurons. No change in the mean total area of sagittal slices of the cerebellum and the mean thickness of the molecular layer were detected at P30 between mice treated with PCP or vehicle (**Figure 1A and 1B**), suggesting the absence of major deficits in granule cell and Purkinje cell genesis and differentiation.

Postmortem analysis of cerebral tissue of patients with schizophrenia have revealed deficits in the expression of Parvalbumin, a calcium-binding protein characteristic of a subpopulation of inhibitory interneurons, and a decrease in inhibitory Parvalbumin interneurons density in the prefrontal cortex (Jenkins et al., 2008; Reynolds et al., 2004). Quantification of Parvalbumin protein expression and the number of inhibitory interneurons did not reveal any change in the cerebellum of the PCP model (**Figure 1C and 1D**).

The Purkinje cells have an intrinsic spontaneous electrophysiological activity, which lead to a characteristic simple spike activity and is modulated by Purkinje cell's synaptic afferents. Using microelectrode arrays (MEA), we recorded the spontaneous activity of Purkinje cells in whole cerebellar slices *ex vivo* (**Figure 2A**), to measure the mean firing rate and the regularity of spiking activity (**Figure 2B**). The mean firing rate represents the mean activity of each recorded neuron during a whole recording. The regularity of the spiking is estimated using two statistical parameters: the Coefficient of Variation (CV) measuring the mean variance of interspike intervals during the whole recording, and the CV2 measuring the variability of spiking between two adjacent interspike intervals (Holt et al., 1996), thus less sensitive to rate fluctuations during the recording. None of these parameters showed any statistical difference between PCP treated mice versus controls (**Figure 2C**). Altogether, these results show that the neonatal PCP treatment does not affect the development of the

cytoarchitecture of the cerebellar cortex and the differentiation of cerebellar Purkinje cells in a major and long-lasting manner.

Neonatal PCP treatment induces synapse-specific morphological deficits in cerebellar Purkinje cells

The cerebellar cortex is organized into different zones, according to the connectivity with other brain areas that are involved in sensory-motor to higher cognitive functions (Stoodley, 2012), thus defining a functional topography of the cerebellum. We focused our study in lobules engaged in various functions relevant for schizophrenia: lobule VI (engaged in language tasks, working memory paradigms, and spatial navigation) and lobule VIII (engaged in sensorimotor tasks) (Stoodley and Schmahmann, 2010) (**Supplementary figure S1B**). The Purkinje cells receive two excitatory inputs, the climbing fibers coming from inferior olivary neurons in the brainstem, and the parallel fibers coming from the granule cells in the granular layer of the cerebellar cortex, and two inhibitory inputs coming from stellate and basket cells in the cerebellar cortex. To analyze potential synaptic deficits in PCP treated mice, we used immunolabeling of markers specific of the presynaptic terminal of each of these afferents: VGLUT2 for climbing fiber presynaptic boutons (**Figure 3A and 3C**), VGLUT1 for parallel fibers presynaptic boutons (**Figure 3E**) and GAD65 for inhibitory contacts (**Figure 4A**).

During the second postnatal week, the climbing fiber translocates along the dendritic tree of the Purkinje cell to form a few hundred synapses along the proximal dendrites and occupy a territory that extends up to approximately 80% of the height of the molecular layer. In lobule VI, the extension of climbing fiber synaptic territory was unchanged in PCP- versus vehicle-treated mice, but the density of the VGLUT2 puncta was significantly increased by 33% (**Figure 3B and 3D**). In lobule VIII, a small (7%) but statistically significant increase in the extension of CF synaptic territory was detected while VGLUT2 puncta density remained unchanged (**Figure 3B and 3D**). 3D quantification revealed a 20 % decrease in the mean volume of the VGLUT2 puncta in PCP-treated mice compared to vehicle, in both lobules (**Figure 3D**). To analyze synapses from the second excitatory afferent, the parallel fibers, we measured the mean intensity of VGLUT1 labeling (Zhang et al., 2015) in the molecular layer because an adequate segmentation and quantification of these presynaptic boutons is difficult due to their small size and extremely high density. Our results revealed no difference between PCP- and vehicle-treated mice (**Figure 3E and 3F**), suggesting no effect of PCP treatment on the number of parallel fiber/Purkinje cell synapses. While glutamatergic alterations are one of

the most widely highlighted physiopathological deficits in schizophrenia, there are also numerous evidence for inhibitory deficits (Gonzalez-Burgos et al., 2010; Radhu et al., 2015). Quantification of inhibitory synapses labeled with GAD65 revealed a normal synaptic density (**Figure 4A and 4B**) and no change in the volume of the GAD65 boutons (**Figure 4C and 4D**) in the molecular layer of PCP mice.

Altogether, our results show that PCP neonatal treatment induces the presence of specific synaptic deficits in the olivocerebellar circuit in juvenile mice: a general decrease in the volume of climbing fiber presynaptic boutons, sometimes accompanied by an increase in synapse density, while other PC synapses are unaffected. This suggests first that the perturbation induced by PCP during postnatal development affects synapses in an afferent-specific manner in a neuron type, and second that there might be lobule-specific changes in the cerebellum.

Neonatal PCP induces transient misregulation of the neuronal surfaceome

Neuronal activity is well known to control gene expression (Ebert and Greenberg, 2013) and thus injection of an NMDA antagonist could affect circuit development through the modulation of the expression of genes controlling synapse formation and/or maturation. We thus performed an analysis of the expression of genes that could be involved in olivo-cerebellar synaptic development and maintenance. In particular, we focused on genes that could contribute to excitatory synapse formation and maintenance in cerebellar Purkinje cells, first because we did not find any inhibitory synaptic deficits and second because climbing fiber/Purkinje cell synapse development is dependent on both homosynaptic and heterosynaptic mechanisms (Bailly et al., 2018; Ichikawa et al., 2016; Miyazaki et al., 2004). Previous work has shown that the establishment of proper connectivity involves the expression of secreted and membrane proteins that are specific for each PC afferent (Hirai et al., 2005; Kakegawa et al., 2015; Sigoillot et al., 2015). A comparative analysis of the gene expression profiles of granule cells and inferior olivary neurons using the bacTRAP strategy allowed us to determine the sets of genes specifically enriched in each of these PC afferents and coding for cell surface proteins that could participate in the specific molecular synaptic code (unpublished data). We identified 324 differentially expressed genes coding for secreted and membrane proteins in these two neuronal populations, 250 for inferior olivary neurons and 74 for granule cells (Iyer et al. unpublished data). To identify changes induced by PCP treatment, we quantified the expression of these genes using high throughput quantitative RT-PCR in cerebellar and brainstem extracts

from P11 animals, right after the last PCP injection to identify acute effects, and from P30 animals to detect long-lasting changes (**Figure 5A**). At P30, hierarchical clustering analysis of the 324 selected genes revealed no cluster with consistent over or under-expression in the PCP group (**Figure 5B, right panel**). At P11, the same analysis did not find any cluster in the brainstem, but revealed two clusters in the cerebellum: 11 genes were globally over- expressed after PCP treatment and 27 genes were downregulated, (**Figure 5B, left panel**). In a second series of analysis, multiple t test comparison was performed in each of the four groups. At P30, no genes reached significance in both cerebellar and brainstem extract after multiple t test comparison and Benjamini-Hochberg False Discovery Rate (FDR) correction (Benjamini and Hochberg, 1995) (**Figure 5C**). At P11, no gene was significantly dysregulated in the brainstem, but in the cerebellar extracts 3 genes reached significance for FDR threshold set to 5%: *Ctgf*, *Gal*, and *Rab29*, and 2 other genes were found when FDR threshold was set to 10%: *Ier3* and *Ly6h*. (**Figure 5C**). Overall, these analyses show that the most consistent change in gene expression after PCP injection is found at P11 in the cerebellum, where 2 genes are significantly overexpressed, and 1 is significantly downregulated.

What are the functions of the products of these misregulated genes and what could be their role in the long-lasting synaptic changes observed in the PCP treated mice? Analysis of protein-protein interactions using the string database (<https://string-db.org/>) revealed significant interaction enrichment in our dataset, suggesting that some of the proteins are biologically connected, at least partially. This database allows to predict protein-protein interactions, including direct (physical) and indirect (functional) association, from curated databases and derived from four sources: systematic co-expression analysis, text-mining from scientific literature, detection of shared selective signals across genomes, and interaction knowledge based on gene orthology between species (Szklarczyk et al., 2017).

For this analysis, we decided to perform a less stringent analysis and selected genes with a fold change of at least 10% and that reached significance in multiple t tests without correction for FDR, thus accepting a higher rate of false positive (**Figure S2A**). 41 genes were included in the string database analysis. Predicted interaction was found between 7 genes *Cxcl12*, *Cnr1*, *Gal*, *Oprl1*, *Ctgf*, *Rock2* and *Igfbp5* (**Figure S2B**). Interestingly, this set of genes includes the one with the strongest misregulation in our data: the gene coding for Connective Tissue Growth Factor (CTGF, also known as CCN2), whose mRNA levels were increased 5 times in the cerebellum (**Figure S2B and S3A**). CTGF is a secreted protein implicated in tissue repair, extracellular matrix remodeling, cell survival, cell adhesion, dendritogenesis, and the formation

of the neuromuscular junction (Hoshijima et al., 2006; Khodosevich et al., 2013; Ohkawara et al., 2020; Ramazani et al., 2018; Song et al., 2017; Yu et al., 2019).

Cxcl12, *Cnr1*, *Gal* and *Oprl1* were all found in the same curated database from Reactome Pathway (Ligand: GPCR complexes that activate Gi:Heterotrimeric G-protein Gi). Functional interaction between CTGF and CXCL12 has previously been shown in the human lung fibroblasts: CXCL12 leads to overexpression of CTGF (Lin et al., 2014). This relationship does not match with our results (*Cxcl12* is under-expressed while *Ctgf* is over-expressed). However, it doesn't exclude that these two proteins interact differently in the cerebellum, and that *Cxcl12* could be a functional node between our PCP-induced *Ctgf* over-expression and the consistent molecular abnormality of Gi complex ligand pathway. Interestingly, these 5 genes have already been associated with schizophrenia, either as a biomarker, or in genetic studies (Frederiksen et al., 1991; Khan et al., 2018; Lin et al., 2016; Schwarz et al., 2010; Sun et al., 2015; Ujike et al., 2002; Zhang et al., 2020).

Altogether, our results show that the neonatal PCP model induces transient deficits in the expression of several genes coding for membrane and secreted proteins, including genes associated with schizophrenia and neural network development.

Discussion

Schizophrenia is considered a synaptopathy, because of the evidence for synaptic deficits found in postmortem and association with mutations in synaptic genes found in genetic studies. While it is considered that schizophrenia has a developmental origin (Weinberger, 2017), little is known about the precise developmental mechanisms leading to synaptic deficits in this disease. To fill this gap, we studied synaptic deficits in the cerebellum of the neonatal subchronic phencyclidine model, a pharmacological developmental model widely used to mimic partially the schizophrenia physiopathology. Our analysis revealed morphological deficits in the climbing fiber/Purkinje cell synapse but not for the other types of synapses received by Purkinje cells, suggesting a synapse type-specific alteration in Purkinje cell connectivity. Moreover, we have shown that the PCP neonatal treatment induces a transient misregulation of the neuronal surfaceome in the cerebellum, including a strong increase in the expression of *Ctgf*, a gene involved in synaptic development at the neuromuscular junction

(Ohkawara et al., 2020) and that has been found as a biomarker in schizophrenia (Li et al., 2015; Schwarz et al., 2010).

Neonatal PCP induces afferent specific deficits in synaptogenesis in cerebellar Purkinje cells

Our results show a decrease in the mean volume of climbing fiber presynaptic boutons in both lobules analyzed. This presynaptic bouton atrophy may reflect a deficit of the maturation of climbing fiber synapses, that could potentially lead to weakened climbing fiber synapse function. Similar deficits have been described in several models of cerebellar developmental disruption, such as early postnatal alcohol exposure (Pierce et al., 2011), in a knock-down of postsynaptic protein BAI3 (Sigoillot et al., 2015), in a conditional knock-out of neuroligins (Zhang et al., 2015), or Gao subunit knockout (Cha et al., 2019), suggesting that climbing fiber atrophy could be a feature of several pathological conditions. Electrophysiological patch-clamp recordings will assess whether climbing fiber synaptic function is altered in PCP mice.

While the decreased volume of climbing fiber boutons suggests a deficit of climbing fiber maturation, the increased density may reflect a deficit of synaptic pruning. Indeed, similarly to other synapses, climbing fiber synapses are massively eliminated in the early postnatal life, through activity-dependent mechanisms. Immature Purkinje cell receives inputs from up to five climbing fibers. These supernumerary inputs are progressively eliminated from P6 to P21, to reach a mature state of one climbing fiber per Purkinje cell (Kano et al., 2018). This elimination of supernumerary climbing fibers is processed through two phases. The first one, the “early phase”, from P6 to P11, is dependent of climbing fiber activity, consists in a progressive strengthening of one “winner” climbing fiber that translocates along the Purkinje cell dendritic tree, while the other “loser” climbing fibers remain on the soma and proximal dendrites. The “late phase”, from P11 to P21, consists in the elimination of synapses from the “loser” climbing fibers, and is dependent on the activity of parallel fibers. Increased density of VGLUT2 clusters is found only in the lobule VI, and not in lobule VIII. One possible explanation would come from the fact that the cerebellum has an asynchronous development: it has been shown that the dendritogenesis in lobules I and X occur earlier than in lobules VI, VII, and VIII (Sotelo, 2004). Here, we injected PCP at three precise time points of the development, separated by 48 hours. Because of the relatively low half-life of the phencyclidine, which has been estimated at 36,8 minutes in the brain of rats chronically treated with the same dose of phencyclidine (Nabeshima et al., 1987a), it is plausible that these injections might perturb differentially each region of the cerebellum because of their

asynchronous maturation. Hence, the increased climbing fiber synaptic density that we see in our results could be caused by a lobule-specific impairment of climbing fiber synapse elimination induced by PCP perturbation of activity in the network.

Perturbations of Climbing fiber synaptic development correlate with the deregulation of the neuronal surfaceome in PCP mice

The establishment of a complex synaptic network requires the precise regulation of synapse formation and the fine selection of synaptic partners, mechanisms that implicate, amongst others, the regulation of the expression of membrane and secreted proteins such as neurexins, pentraxins, ephrins, or C1q-containing proteins (reviewed by Südhof, 2018). Moreover, several cell adhesion molecules that are important for the development of synapses are regulated by neuronal activity (Ebert and Greenberg, 2013; Fields and Itoh, 1996). The PCP, as an NMDA antagonist, is expected to block the binding of glutamate, one of the main excitatory neurotransmitters, and thus to affect neuronal activity, suggesting that it could modulate the expression of activity-dependent genes. Moreover, cerebellar network development, including climbing fiber synapse elimination, implicates activity dependent mechanisms (Hashimoto and Kano, 2013). To understand the molecular mechanisms that could underlie the effects of the PCP treatment on the cerebellar synaptic network, we thus performed a gene expression analysis focusing on genes coding for membrane and secreted proteins that could potentially regulate the development of Purkinje cell excitatory connectivity.

Our results revealed a subset of genes coding for membrane or secreted proteins that are transiently misregulated by PCP treatment. This misregulation occurs during the second postnatal week at a critical period of the development when the synaptic network is set up (Hashimoto and Kano, 2013). Functional protein association network and pathway analysis revealed a significant enrichment of protein-protein interactions in our dataset and identified 2 potentially relevant signaling pathways (**Figure 5D**). The most represented one in our dataset is the “ligands of GPCR (G Protein-Coupled Receptors), activating the inhibitory Gi protein” group, comprising *Cxcl12*, *Oprl1*, *Gal*, and *Cnr1*, proteins that have previously been implicated in schizophrenia (Frederiksen et al., 1991; Khan et al., 2018; Lin et al., 2016; Schwarz et al., 2010; Sun et al., 2015; Ujike et al., 2002; Zhang et al., 2020). *Cxcl12* has been shown to have a neuroprotective effect through downregulation of the NMDA receptor subunit NR2B (Nicolai et al., 2010). In a rodent model of HIV associated neurocognitive disorders, CXCL12 promotes dendritic spine survival (Festa et al., 2020), suggesting that this gene could play a role in PCP-induced synaptic phenotype. The other pathway found in our dataset is the Hedgehog, with *Cdon* and *Boc*. Altogether, this suggests that the PCP treatment might misregulate several signaling pathways with known developmental roles and thus perturb normal synaptic development.

CTGF, a candidate for PCP-induced cerebellar synaptic deficits

The most strongly misregulated gene in our dataset is the gene coding for CTGF, an extracellular secreted matrix protein known for its implication in tissue repair, cell adhesion, and cell migration (Jun and Lau, 2011; Takigawa, 2017). CTGF has been detected as a plasmatic biomarker in schizophrenia (Li et al., 2015; Schwarz et al., 2010). The expression pattern of *Ctgf* in the cerebellum during development shows an increase in expression from P7, with a peak at P21, followed by a decrease in adulthood (**Figure S3B**). In the brainstem, the developmental profile shows a two-fold increase from birth to P14, followed by a decrease until adulthood. This pattern follows the period of intense synapse formation, maturation, and refinement in the cerebellum during postnatal development (Ichikawa et al., 2016; Kano et al., 2018; Lohof et al., 1996), and suggests that CTGF could play a role in the establishment of connectivity in this structure.

Several recent papers highlight CTGF as a potential synaptic actor, as it regulates dendritic branching of subplate neurons (Yu et al., 2019), and synapse formation at the neuromuscular junction (Ohkawara et al., 2020). Interestingly, Ohkawara et al. have shown that CTGF directly binds to LRP4, a synaptic organizer (Mosca et al., 2017), that it promotes the specialization of the muscle presynaptic terminal and is essential for proper function of the neuromuscular junction. CTGF is known to interact with several proteins that are associated with synaptic elimination such as IGF1 (Abreu et al., 2002; Kakizawa et al., 2003; Kim et al., 1997), BMP4 (Abreu et al., 2002; Higashi et al., 2018; Kalinovsky et al., 2011) or TGF- β 1 (Bialas and Stevens, 2013). TGF- β signaling has a role in synapse formation and maturation, highlighted by studies in the visual system (Stevens et al., 2007) and in the cerebellum (Araujo et al., 2016). Similarly, BMP4 has been linked to synaptic development by several studies in the auditory system (Xiao et al., 2013), and in the cerebellum (Kalinovsky et al., 2011). Interestingly the TGF-beta pathway was also found to be modified by PCP in our gene expression analysis. Further manipulation of CTGF protein expression in the cerebellum during this critical developmental period is necessary to elucidate potential causal link between CTGF overexpression and synaptic deficits in the PCP neonatal model, and its potential contribution to the etiology of schizophrenia.

Finally, our study describes for the first time cerebellar synaptic deficits in a murine mouse model commonly used to mimic schizophrenia physiopathology. While initially thought to be essentially a motor task-related structure, many studies highlight cerebellum role in cognition

(Schmahmann, 2019), and animal studies recently confirmed direct cerebellar implication in reward processing (Sendhilnathan et al., 2020; Wagner et al., 2017), spatial navigation (Rondi-Reig et al., 2014) and social behavior (Badura et al., 2018; Carta et al., 2019). The cerebellum emerges now as a potential actor of psychiatric disorders, such as Autism Spectrum Disorder (ASD) (Becker and Stoodley, 2013; Wang et al., 2014) or schizophrenia (Andreasen and Pierson, 2008). While synaptic deficits in the cerebellum are unlikely totally responsible for schizophrenia symptoms, they could contribute through the wide cerebro-cerebellar network.

Material and method

Antibodies

The following primary antibodies were used: mouse monoclonal anti-CABP (1:1000; swant, Switzerland, #300), rabbit polyclonal anti-CABP (1:1000; swant, #9.03), guinea pig polyclonal anti VGLUT1 (1:5000; Millipore, Massachusetts, USA, #AB5905), guinea pig polyclonal anti-VGLUT2 (1:5000; Millipore, #AB2251), mouse anti-Parvalbumin (1:1000: swant, #PV235) and mouse anti-GAD65 (1:500, abcam, Cambridge, United Kingdom, #ab26113)

The following secondary antibodies were used: donkey polyclonal anti-guinea pig Alexa Fluor 594 (2µg/mL; Invitrogen, California, USA, #A11076), donkey anti-mouse Alexa Fluor 488 (2µg/mL; invitrogen, #R37114), donkey polyclonal anti-Mouse Alexa Fluor 568 (2µg/mL; invitrogen, #A10037), donkey polyclonal anti-Rabbit Alexa Fluor 488 (2µg/mL; invitrogen, #A21206).

Immunohistochemistry

Mice brains were extracted after intracardiac perfusion with 4% Paraformaldehyde (PFA) in Phosphate-buffered saline (PBS) solution. After dissection, the brain was stored in the 4% PFA in PBS 1X solution for one hour at 4°C, and then cryoprotected for 48h into a 30% sucrose in PBS solution at 4°C. After sectioning with a freezing microtome, brain slices were washed three times for five minutes in PBS, then blocked with 4% donkey serum in PBS for 30 minutes at room temperature. The primary antibodies were diluted in PBS, 1% triton X-100, 1% donkey serum, at their respective concentration, and incubated overnight at 4°C under agitation. The sections were then washed three times for five minutes in PBS 1% triton X-100 and incubated for one hour at room temperature in the secondary antibody, diluted in PBS, 1% triton X-100, 1% donkey serum. The sections were then incubated for 15 minutes at room temperature with the nuclear marker Hoechst 33342 (0,2 mg/mL, Sigma, Gothenburg, Sweden, Cat#H6024) in PBS 0.2% triton. The sections were then washed three times for five minutes in PBS 1% triton and recovered in PBS. The sections were finally mounted with Prolong Gold between microscope slides and coverslips.

Image acquisition and quantification

Images for global cerebellar morphology were acquired using a Zeiss Axiozoom V16 microscope, equipped with a digital camera (AxioCam HRm) using a 10x objective (pixel size: 0,650 μ m).

Images for synaptic quantifications were acquired using a Leica SP5 upright confocal microscope, using a 63x objective (63x/1.4 WD: 0.1mm), pixel size 57x57nm. The pinhole aperture was set to one Airy Unit and a z-step of 200 nm was used. Laser intensity and photomultiplier tube (PMT) gain was set in order to occupy the full dynamic range of the detector. Images were acquired in 16-bit range.

All the quantifications were done in blind condition, with the Fiji opensource software (Schindelin et al., 2012).

First, for VGLUT2 and GAD65 quantifications, all the images were normalized using the quantile-based normalization plugin of Fiji (<https://www.longair.net/edinburgh/imagej/quantile-normalization/>). The intensity distribution of the images has been normalized using 256 quantiles for each staining.

Then, the synaptic boutons were extracted from the background using the 3D Weka Segmentation plugin (https://imagej.net/Trainable_Weka_Segmentation) after manual selection of signal and background samples. The plugin extracts the signal from background and produces a binary image. The Fiji built-in plugin 3D object counter was then used in order to count and measure every object (cluster of VGLUT2 or GAD65 positive signal).

For VGLUT1 quantification, the background of the whole image was artificially subtracted using the Fiji built-in subtract background plugin. The signal measured was the raw integrated density (the sum of the values of the pixels in the selection) divided by the area in μ m², thus providing a measure of the mean intensity per μ m².

Total RNA extraction and RT-PCR

For RNA extraction, the animal was first anesthetized with isoflurane 4%, decapitated, and the cerebellum and brainstem were dissected in Hanks balanced salt solution (HBSS) solution. After removal of the meninges, the tissues were stored at -80C°.

Total RNA was then extracted using the Qiagen RNeasy mini kit (Qiagen, Venlo, Netherlands, #74106) following tissue homogenization, according to manufacturer's instruction. Equivalent amounts of total RNA (100 ng) were reverse-transcribed using SuperScript® VILO™ cDNA

Synthesis kit (Life Technologies, California, USA, Cat#11754-250), according to manufacturer's instructions.

High throughput RT-PCR was then done by the microfluidic platform from Genomic Paris center of the IBENS (Institut de Biologie de l'École Normale Supérieure), using a Biomark HD system, IFC Controller AX, HX and MX.

Gene clustering and analysis

The raw data from gene expression analysis were extracted and analyzed using MATLAB.

Hierarchical clustering was done using the Cluster 3.0 open source software (developed by Michael Eisen at Stanford University (<http://bonsai.hgc.jp/~mdehoon/software/cluster/>)). First, gene expression data were log₂ transformed. Then, genes were centered around the median, and hierarchical clustering were performed using spearman rank correlation. A heatmap representation was done by Java treeview.

For the systematic fold change and statistical test analysis, a script was written on R open source software. For each dataset, a multiple t test comparison was performed on the 324 genes, assuming a normal distribution and the equality of variances. Benjamini-Hochberg procedure for multiple correction as been performed

For the pathway analysis, the same multiple t test have been performed, but without correction for multiple testing. Genes found significant (p value > 0.05) were analyzed using the String-database website (<https://string-db.org/>). Line thickness indicates the strength of data support, collected from curated databases, extracted from PubMed abstracts or from gene fusion or co-expression databases.

High density microelectrode array (MEA) analysis of Purkinje cell spiking in acute cerebellar slices

Experiments were performed on acute cerebellar slices obtained from P30 mice in artificial cerebrospinal fluid (ACSF) containing (in mM): NaCl 125, KCl 2.5, D(+)Glucose 25, NaHCO₃ 25, NaH₂PO₄ 1.25, CaCl₂ 2, and MgCl₂ 1, gassed with 5% CO₂/95% O₂. Parasagittal slices (320 μm) were cut at 30°C with a Campden Ci 7000 smz microtome at an advance speed of 0.03 mm/s and vertical vibration set to 0.1–0.3 μm. Slices were then transferred to a chamber filled with oxygenated ACSF at 37°C and allowed to recover for 1 h before recordings.

For recordings, the slices were placed over a high-density microelectrode array of 4096 electrodes (electrode size, 21 × 21 μm; pitch, 42 μm; 64 × 64 matrix; Biocam X, 3Brain, Wädenswil, Switzerland), and constantly perfused with oxygenated ACSF at 37°C.

Extracellular activity was digitized at 17 kHz and data were analyzed with the Brainwave software from 3Brain. The signal was filtered with a butterworth high-pass filter at 200 Hz, spikes were detected with a hard threshold set at -100 μ V, and unsupervised spike sorting was done by the software. We selected units with a firing rate between 15 and 100 spikes per second and we excluded units presenting more than 5% of refractory period violation (set to 3 ms). Firing pattern variability, or regularity, is defined as a measure of the consistency of time intervals between spikes [interspike interval (ISI) = seconds]. To quantify the average variability in firing patterns, the coefficient of variance of the ISI (CV) was calculated as the ratio of the standard deviation (SD) of ISIs to the mean ISI of a given cell. To measure rhythmicity of cells, CV2 was calculated. CV2 measures firing pattern variability within a short period of two ISIs [$CV2 = 2|ISI_{n+1} - ISI_n|/(ISI_{n+1} + ISI_n)$] (Holt and Douglas, 1996).

Statistical Analysis

Data were analyzed using GraphPad Prism for statistics. Values are given as mean \pm SEM.

Normality was estimated using d'Agostino Pearson normality test. The means between two conditions were compared using unpaired Student t test when both data sets follow a normal law, otherwise, they were compared using a Mann-Whitney nonparametric test.

References

- Abreu, J.G., Ketpura, N.I., Reversade, B., De Robertis, E.M., 2002. Connective-tissue growth factor (CTGF) modulates cell signaling by BMP and TGF- β . *Nat. Cell Biol.* 4, 599–604. <https://doi.org/10.1038/ncb826>
- Akbarian, S., Sucher, N., Bradley, D., Tafazzoli, A., Trinh, D., Hetrick, W., Potkin, S., Sandman, C., Bunney, W., Jones, E., 1996. Selective alterations in gene expression for NMDA receptor subunits in prefrontal cortex of schizophrenics. *J. Neurosci.* 16, 19–30. <https://doi.org/10.1523/JNEUROSCI.16-01-00019.1996>
- Anastasio, N.C., Johnson, K.M., 2008. Atypical Antischizophrenic Drugs Prevent Changes in Cortical N-Methyl-D-Aspartate Receptors and Behavior Following Sub-chronic Phencyclidine Administration in Developing Rat Pups. *Pharmacol. Biochem. Behav.* 90, 569–577. <https://doi.org/10.1016/j.pbb.2008.04.017>
- Andreasen, N.C., O’Leary, D.S., Cizadlo, T., Arndt, S., Rezai, K., Ponto, L.L., Watkins, G.L., Hichwa, R.D., 1996. Schizophrenia and cognitive dysmetria: a positron-emission tomography study of dysfunctional prefrontal-thalamic-cerebellar circuitry. *Proc. Natl. Acad. Sci.* 93, 9985–9990.
- Andreasen, N.C., Pierson, R., 2008. The Role of the Cerebellum in Schizophrenia. *Biol. Psychiatry* 64, 81–88. <https://doi.org/10.1016/j.biopsych.2008.01.003>
- Araujo, A.P.B., Diniz, L.P., Eller, C.M., de Matos, B.G., Martinez, R., Gomes, F.C.A., 2016. Effects of Transforming Growth Factor Beta 1 in Cerebellar Development: Role in Synapse Formation. *Front. Cell. Neurosci.* 10. <https://doi.org/10.3389/fncel.2016.00104>
- Badura, A., Verpeut, J.L., Metzger, J.W., Pereira, T.D., Pisano, T.J., Deverett, B., Bakshinskaya, D.E., Wang, S.S.-H., 2018. Normal cognitive and social development require posterior cerebellar activity. *eLife* 7, e36401. <https://doi.org/10.7554/eLife.36401>
- Badura, A., Verpeut, J.L., Metzger, J.W., Pereira, T.D., Pisano, T.J., Deverett, B., Bakshinskaya, D.E., Wang, S.S.-H., n.d. Normal cognitive and social development require posterior cerebellar activity 36.
- Bailly, Y., Rabacchi, S., Sherrard, R.M., Rodeau, J.-L., Demais, V., Lohof, A.M., Mariani, J., 2018. Elimination of all redundant climbing fiber synapses requires granule cells in the postnatal cerebellum. *Sci. Rep.* 8, 10017. <https://doi.org/10.1038/s41598-018-28398-7>
- Becker, E.B.E., Stoodley, C.J., 2013. Chapter One - Autism Spectrum Disorder and the Cerebellum, in: Konopka, G. (Ed.), *International Review of Neurobiology, Neurobiology of Autism*. Academic Press, pp. 1–34. <https://doi.org/10.1016/B978-0-12-418700-9.00001-0>
- Benes, F.M., Vincent, S.L., Marie, A., Khan, Y., 1996. Up-regulation of GABAA receptor binding on neurons of the prefrontal cortex in schizophrenic subjects [WWW Document]. *Neuroscience*. [https://doi.org/10.1016/0306-4522\(96\)00328-4](https://doi.org/10.1016/0306-4522(96)00328-4)
- Benjamini, Y., Hochberg, Y., 1995. Controlling the False Discovery Rate: A practical and Powerful Approach to Multiple Testing. <https://doi.org/10.1111/j.2517-6161.1995.tb02031.x>
- Bialas, A.R., Stevens, B., 2013. TGF- β signaling regulates neuronal C1q expression and developmental synaptic refinement. *Nat. Neurosci.* 16, 1773–1782. <https://doi.org/10.1038/nn.3560>

- Boctor, S.Y., Ferguson, S.A., 2009. Neonatal NMDA receptor antagonist treatments have no effects on prepulse inhibition of postnatal day 25 Sprague-Dawley rats. *Neurotoxicology* 30, 151–154. <https://doi.org/10.1016/j.neuro.2008.10.011>
- Carta, I., Chen, C.H., Schott, A.L., Dorizan, S., Khodakhah, K., 2019. Cerebellar modulation of the reward circuitry and social behavior. *Science* 363, eaav0581. <https://doi.org/10.1126/science.aav0581>
- Cha, H.L., Choi, J.-M., Oh, H.-H., Bashyal, N., Kim, S.-S., Birnbaumer, L., Suh-Kim, H., 2019. Deletion of the α subunit of the heterotrimeric Go protein impairs cerebellar cortical development in mice. *Mol. Brain* 12, 57. <https://doi.org/10.1186/s13041-019-0477-9>
- Clifton, N.E., Morisot, N., Girardon, S., Millan, M.J., Loiseau, F., 2013. Enhancement of social novelty discrimination by positive allosteric modulators at metabotropic glutamate 5 receptors: adolescent administration prevents adult-onset deficits induced by neonatal treatment with phencyclidine. *Psychopharmacology (Berl.)* 225, 579–594. <https://doi.org/10.1007/s00213-012-2845-3>
- Dityatev, A., Dityateva, G., Schachner, M., 2000. Synaptic strength as a function of post-versus presynaptic expression of the neural cell adhesion molecule NCAM. *Neuron* 26, 207–217. [https://doi.org/10.1016/s0896-6273\(00\)81151-4](https://doi.org/10.1016/s0896-6273(00)81151-4)
- Eastwood, S.L., Harrison, P.J., 2005. Decreased expression of vesicular glutamate transporter 1 and complexin II mRNAs in schizophrenia: further evidence for a synaptic pathology affecting glutamate neurons. *Schizophr. Res.* 73, 159–172. <https://doi.org/10.1016/j.schres.2004.05.010>
- Ebert, D.H., Greenberg, M.E., 2013. Activity-dependent neuronal signaling and autism spectrum disorder. *Nature* 493, 327–337. <https://doi.org/10.1038/nature11860>
- Festa, L.K., Irollo, E., Platt, B.J., Tian, Y., Floresco, S., Meucci, O., 2020. CXCL12-induced rescue of cortical dendritic spines and cognitive flexibility. *eLife* 9, e49717. <https://doi.org/10.7554/eLife.49717>
- Fields, R.D., Itoh, K., 1996. Neural cell adhesion molecules in activity-dependent development and synaptic plasticity. *Trends Neurosci.* 19, 473–480. [https://doi.org/10.1016/S0166-2236\(96\)30013-1](https://doi.org/10.1016/S0166-2236(96)30013-1)
- Frederiksen, S.O., Ekman, R., Gottfries, C.-G., Widerlöv, E., Jonsson, S., 1991. Reduced concentrations of galanin, arginine vasopressin, neuropeptide Y and peptide YY in the temporal cortex but not in the hypothalamus of brains from schizophrenics. *Acta Psychiatr. Scand.* 83, 273–277. <https://doi.org/10.1111/j.1600-0447.1991.tb05539.x>
- Glantz, L.A., Lewis, D.A., 2000. Decreased Dendritic Spine Density on Prefrontal Cortical Pyramidal Neurons in Schizophrenia. *Arch. Gen. Psychiatry* 57, 65–73. <https://doi.org/10.1001/archpsyc.57.1.65>
- Glantz, L.A., Lewis, D.A., 1997. Reduction of Synaptophysin Immunoreactivity in the Prefrontal Cortex of Subjects With Schizophrenia: Regional and Diagnostic Specificity. *Arch. Gen. Psychiatry* 54, 660–669. <https://doi.org/10.1001/archpsyc.1997.01830190088009>
- Gonzalez-Burgos, G., Hashimoto, T., Lewis, D.A., 2010. Alterations of Cortical GABA Neurons and Network Oscillations in Schizophrenia. *Curr. Psychiatry Rep.* 12, 335–344. <https://doi.org/10.1007/s11920-010-0124-8>
- Guell, X., Hoche, F., Schmahmann, J.D., 2015. Metalinguistic deficits in patients with cerebellar dysfunction: empirical support for the dysmetria of thought theory. *Cerebellum Lond. Engl.* 14, 50–58. <https://doi.org/10.1007/s12311-014-0630-z>
- Harwell, C.C., Parker, P.R.L., Gee, S.M., Okada, A., McConnell, S.K., Kreitzer, A.C., Kriegstein, A.R., 2012. Sonic hedgehog expression in corticofugal projection neurons

- directs cortical microcircuit formation. *Neuron* 73, 1116–1126.
<https://doi.org/10.1016/j.neuron.2012.02.009>
- Hashimoto, K., Kano, M., 2013. Synapse elimination in the developing cerebellum. *Cell. Mol. Life Sci.* 70, 4667–4680. <https://doi.org/10.1007/s00018-013-1405-2>
- Hashimoto, T., Arion, D., Unger, T., Maldonado-Avilés, J.G., Morris, H.M., Volk, D.W., Mirnics, K., Lewis, D.A., 2008. Alterations in GABA-related transcriptome in the dorsolateral prefrontal cortex of subjects with schizophrenia. *Mol. Psychiatry* 13, 147–161. <https://doi.org/10.1038/sj.mp.4002011>
- Higashi, T., Tanaka, S., Iida, T., Okabe, S., 2018. Synapse Elimination Triggered by BMP4 Exocytosis and Presynaptic BMP Receptor Activation. *Cell Rep.* 22, 919–929. <https://doi.org/10.1016/j.celrep.2017.12.101>
- Hirai, H., Pang, Z., Bao, D., Miyazaki, T., Li, L., Miura, E., Parris, J., Rong, Y., Watanabe, M., Yuzaki, M., Morgan, J.I., 2005. Cbln1 is essential for synaptic integrity and plasticity in the cerebellum. *Nat. Neurosci.* 8, 1534–1541. <https://doi.org/10.1038/nn1576>
- Hirjak, D., Thomann, P.A., Kubera, K.M., Stieltjes, B., Wolf, R.C., 2016. Cerebellar contributions to neurological soft signs in healthy young adults. *Eur. Arch. Psychiatry Clin. Neurosci.* 266, 35–41. <https://doi.org/10.1007/s00406-015-0582-4>
- Holt, G.R., Douglas, J., 1996. Comparison of Discharge Variability Visual Cortex Neurons. *J. Neurophysiol.* 75, 1806–1814.
- Holt, G.R., Softky, W.R., Koch, C., Douglas, R.J., 1996. Comparison of discharge variability in vitro and in vivo in cat visual cortex neurons. *J. Neurophysiol.* 75, 1806–1814. <https://doi.org/10.1152/jn.1996.75.5.1806>
- Hoshijima, M., Hattori, T., Inoue, M., Araki, D., Hanagata, H., Miyauchi, A., Takigawa, M., 2006. CT domain of CCN2/CTGF directly interacts with fibronectin and enhances cell adhesion of chondrocytes through integrin $\alpha 5\beta 1$. *FEBS Lett.* 580, 1376–1382. <https://doi.org/10.1016/j.febslet.2006.01.061>
- Howes, O., Onwordi, E., Haalf, E., Whitehurst, T., Wells, L., Rabiner, I., Bonsall, D., Vernon, A., 2020. The Synaptic Hypothesis of Schizophrenia: In Vivo PET Evidence in Patients and Preclinical Evidence of the Effects of Antipsychotics. *Biol. Psychiatry* 87, S234. <https://doi.org/10.1016/j.biopsych.2020.02.607>
- Ichikawa, R., Hashimoto, K., Miyazaki, T., Uchigashima, M., Yamasaki, M., Aiba, A., Kano, M., Watanabe, M., 2016. Territories of heterologous inputs onto Purkinje cell dendrites are segregated by mGluR1-dependent parallel fiber synapse elimination. *Proc. Natl. Acad. Sci.* 113, 2282–2287. <https://doi.org/10.1073/pnas.1511513113>
- Jenkins, T.A., Harte, M.K., McKibben, C.E., Elliott, J.J., Reynolds, G.P., 2008. Disturbances in social interaction occur along with pathophysiological deficits following sub-chronic phencyclidine administration in the rat. *Behav. Brain Res.* 194, 230–235. <https://doi.org/10.1016/j.bbr.2008.07.020>
- Jones, C., Watson, D., Fone, K., 2011. Animal models of schizophrenia: Animal models of schizophrenia. *Br. J. Pharmacol.* 164, 1162–1194. <https://doi.org/10.1111/j.1476-5381.2011.01386.x>
- Jun, J.-I., Lau, L.F., 2011. Taking aim at the extracellular matrix: CCN proteins as emerging therapeutic targets. *Nat. Rev. Drug Discov.* 10, 945–963. <https://doi.org/10.1038/nrd3599>
- Kaalund, S.S., Riise, J., Broberg, B.V., Fabricius, K., Karlsen, A.S., Secher, T., Plath, N., Pakkenberg, B., 2013. Differential expression of parvalbumin in neonatal phencyclidine-treated rats and socially isolated rats. *J. Neurochem.* 124, 548–557. <https://doi.org/10.1111/jnc.12061>

- Kakegawa, W., Mitakidis, N., Miura, E., Abe, M., Matsuda, K., Takeo, Y.H., Kohda, K., Motohashi, J., Takahashi, A., Nagao, S., Muramatsu, S., Watanabe, M., Sakimura, K., Aricescu, A.R., Yuzaki, M., 2015. Anterograde C1ql1 signaling is required in order to determine and maintain a single-winner climbing fiber in the mouse cerebellum. *Neuron* 85, 316–329. <https://doi.org/10.1016/j.neuron.2014.12.020>
- Kakizawa, S., Yamada, K., Iino, M., Watanabe, M., Kano, M., 2003. Effects of insulin-like growth factor I on climbing fibre synapse elimination during cerebellar development. *Eur. J. Neurosci.* 17, 545–554. <https://doi.org/10.1046/j.1460-9568.2003.02486.x>
- Kalinovsky, A., Boukhtouche, F., Blazeski, R., Bornmann, C., Suzuki, N., Mason, C.A., Scheiffele, P., 2011. Development of Axon-Target Specificity of Ponto-Cerebellar Afferents. *PLoS Biol.* 9, e1001013. <https://doi.org/10.1371/journal.pbio.1001013>
- Kano, M., Watanabe, T., Uesaka, N., Watanabe, M., 2018. Multiple Phases of Climbing Fiber Synapse Elimination in the Developing Cerebellum. *The Cerebellum* 17, 722–734. <https://doi.org/10.1007/s12311-018-0964-z>
- Karson, C.N., Mrazek, R.E., Schluterman, K.O., Sturmer, W.Q., Sheng, J.G., Griffin, W.S.T., 1999. Alterations in synaptic proteins and their encoding mRNAs in prefrontal cortex in schizophrenia: a possible neurochemical basis for ‘hypofrontality.’ *Mol. Psychiatry* 4, 39–45. <https://doi.org/10.1038/sj.mp.4000459>
- Khan, M.S., Boileau, I., Kolla, N., Mizrahi, R., 2018. A systematic review of the role of the nociceptin receptor system in stress, cognition, and reward: relevance to schizophrenia. *Transl. Psychiatry* 8, 1–12. <https://doi.org/10.1038/s41398-017-0080-8>
- Khodosevich, K., Lazarini, F., von Engelhardt, J., Kaneko, H., Lledo, P.-M., Monyer, H., 2013. Connective Tissue Growth Factor Regulates Interneuron Survival and Information Processing in the Olfactory Bulb. *Neuron* 79, 1136–1151. <https://doi.org/10.1016/j.neuron.2013.07.011>
- Kim, H.-S., Nagalla, S.R., Oh, Y., Wilson, E., Roberts, C.T., Rosenfeld, R.G., 1997. Identification of a family of low-affinity insulin-like growth factor binding proteins (IGFBPs): Characterization of connective tissue growth factor as a member of the IGFBP superfamily. *Proc. Natl. Acad. Sci.* 94, 12981–12986. <https://doi.org/10.1073/pnas.94.24.12981>
- Kjaerby, C., Broberg, B.V., Kristiansen, U., Dalby, N.O., 2014. Impaired GABAergic Inhibition in the Prefrontal Cortex of Early Postnatal Phencyclidine (PCP)-Treated Rats. *Cereb. Cortex* 24, 2522–2532. <https://doi.org/10.1093/cercor/bht109>
- Kjaerby, C., Bundgaard, C., Fejgin, K., Kristiansen, U., Dalby, N.O., 2013. Repeated potentiation of the metabotropic glutamate receptor 5 and the alpha 7 nicotinic acetylcholine receptor modulates behavioural and GABAergic deficits induced by early postnatal phencyclidine (PCP) treatment. *Neuropharmacology* 72, 157–168. <https://doi.org/10.1016/j.neuropharm.2013.04.041>
- Li, Y., Yolken, R., Cowan, D.N., Boivin, M.R., Liu, T., Niebuhr, D.W., 2015. Biomarker Identification and Effect Estimation on Schizophrenia – A High Dimensional Data Analysis. *Front. Public Health* 3. <https://doi.org/10.3389/fpubh.2015.00075>
- Lin, C.-H., Shih, C.-H., Tseng, C.-C., Yu, C.-C., Tsai, Y.-J., Bien, M.-Y., Chen, B.-C., 2014. CXCL12 Induces Connective Tissue Growth Factor Expression in Human Lung Fibroblasts through the Rac1/ERK, JNK, and AP-1 Pathways. *PLoS ONE* 9. <https://doi.org/10.1371/journal.pone.0104746>
- Lin, J.-R., Cai, Y., Zhang, Q., Zhang, W., Nogales-Cadenas, R., Zhang, Z.D., 2016. Integrated Post-GWAS Analysis Sheds New Light on the Disease Mechanisms of Schizophrenia. *Genetics* 204, 1587–1600. <https://doi.org/10.1534/genetics.116.187195>

- Lohof, A.M., Delhaye-Bouchard, N., Mariani, J., 1996. Synapse Elimination in the Central Nervous System: Functional Significance and Cellular Mechanisms. *Rev. Neurosci.* 7. <https://doi.org/10.1515/REVNEURO.1996.7.2.85>
- Meffre, J., Chaumont-Dubel, S., Mannoury la Cour, C., Loiseau, F., Watson, D.J.G., Dekeyne, A., Séveno, M., Rivet, J.-M., Gaven, F., Délérís, P., Hervé, D., Fone, K.C.F., Bockaert, J., Millan, M.J., Marin, P., 2012. 5-HT₆ receptor recruitment of mTOR as a mechanism for perturbed cognition in schizophrenia: 5-HT₆ receptors activate mTOR to control cognition. *EMBO Mol. Med.* 4, 1043–1056. <https://doi.org/10.1002/emmm.201201410>
- Miyazaki, T., Hashimoto, K., Shin, H.-S., Kano, M., Watanabe, M., 2004. P/Q-type Ca²⁺ channel α 1A regulates synaptic competition on developing cerebellar Purkinje cells. *J. Neurosci. Off. J. Soc. Neurosci.* 24, 1734–1743. <https://doi.org/10.1523/JNEUROSCI.4208-03.2004>
- Moberget, T., Alnæs, D., Kaufmann, T., Doan, N.T., Córdova-Palomera, A., Norbom, L.B., Rokicki, J., van der Meer, D., Andreassen, O.A., Westlye, L.T., 2019. Cerebellar Gray Matter Volume Is Associated With Cognitive Function and Psychopathology in Adolescence [WWW Document]. *Biol. Psychiatry*. <https://doi.org/10.1016/j.biopsych.2019.01.019>
- Mosca, T.J., Luginbuhl, D.J., Wang, I.E., Luo, L., 2017. Presynaptic LRP4 promotes synapse number and function of excitatory CNS neurons. *eLife* 6, e27347. <https://doi.org/10.7554/eLife.27347>
- Mouri, A., Noda, Y., Enomoto, T., Nabeshima, T., 2007. Phencyclidine animal models of schizophrenia: Approaches from abnormality of glutamatergic neurotransmission and neurodevelopment. *Neurochem. Int.* 51, 173–184. <https://doi.org/10.1016/j.neuint.2007.06.019>
- Nabeshima, T., Fukaya, H., Yamaguchi, K., Ishikawa, K., Furukawa, H., Kameyama, T., 1987. Development of tolerance and supersensitivity to phencyclidine in rats after repeated administration of phencyclidine. *Eur. J. Pharmacol.* 135, 23–33. [https://doi.org/10.1016/0014-2999\(87\)90753-9](https://doi.org/10.1016/0014-2999(87)90753-9)
- Nakatani-Pawlak, A., Yamaguchi, K., Tatsumi, Y., Mizoguchi, H., Yoneda, Y., 2009. Neonatal Phencyclidine Treatment in Mice Induces Behavioral, Histological and Neurochemical Abnormalities in Adulthood. *Biol. Pharm. Bull.* 32, 1576–1583. <https://doi.org/10.1248/bpb.32.1576>
- Nicolai, J., Burbassi, S., Rubin, J., Meucci, O., 2010. CXCL12 inhibits expression of the NMDA receptor's NR2B subunit through a histone deacetylase-dependent pathway contributing to neuronal survival. *Cell Death Dis.* 1, e33–e33. <https://doi.org/10.1038/cddis.2010.10>
- Nomura, T., Oyamada, Y., Fernandes, H.B., Remmers, C., Xu, J., Meltzer, H., Contractor, A., 2016. Subchronic phencyclidine treatment in adult mice increases GABAergic transmission and LTP threshold in the hippocampus. *Neuropharmacology* 100, 90–97. <https://doi.org/10.1016/j.neuropharm.2015.04.012>
- Ohkawara, B., Kobayakawa, A., Kanbara, S., Hattori, T., Kubota, S., Ito, M., Masuda, A., Takigawa, M., Lyons, K.M., Ishiguro, N., Ohno, K., 2020. CTGF/CCN2 facilitates LRP4-mediated formation of the embryonic neuromuscular junction. *EMBO Rep.* n/a, e48462. <https://doi.org/10.15252/embr.201948462>
- Osimo, E.F., Beck, K., Reis Marques, T., Howes, O.D., 2018. Synaptic loss in schizophrenia: a meta-analysis and systematic review of synaptic protein and mRNA measures. *Mol. Psychiatry*. <https://doi.org/10.1038/s41380-018-0041-5>
- Pasterkamp, R.J., 2012. Getting neural circuits into shape with semaphorins. *Nat. Rev. Neurosci.* 13, 605–618. <https://doi.org/10.1038/nrn3302>

- Picard, H., Amado, I., Mouchet-Mages, S., Olié, J.-P., Krebs, M.-O., 2008. The Role of the Cerebellum in Schizophrenia: an Update of Clinical, Cognitive, and Functional Evidences. *Schizophr. Bull.* 34, 155–172. <https://doi.org/10.1093/schbul/sbm049>
- Pierce, D.R., Hayar, A., Williams, D.K., Light, K.E., 2011. Olivary Climbing Fiber Alterations in PN40 Rat Cerebellum Following Postnatal Ethanol Exposure. *Brain Res.* 1378, 54–65. <https://doi.org/10.1016/j.brainres.2011.01.028>
- Prikryl, R., Ceskova, E., Kasperek, T., Kucerova, H., 2007. Neurological soft signs and their relationship to 1-year outcome in first-episode schizophrenia. *Eur. Psychiatry* 22, 499–504. <https://doi.org/10.1016/j.eurpsy.2007.03.012>
- Purcell, S.M., Moran, J.L., Fromer, M., Ruderfer, D., Solovieff, N., Roussos, P., O’Dushlaine, C., Chambert, K., Bergen, S.E., Kähler, A., Duncan, L., Stahl, E., Genovese, G., Fernández, E., Collins, M.O., Komiyama, N.H., Choudhary, J.S., Magnusson, P.K.E., Banks, E., Shakir, K., Garimella, K., Fennell, T., DePristo, M., Grant, S.G.N., Haggarty, S.J., Gabriel, S., Scolnick, E.M., Lander, E.S., Hultman, C.M., Sullivan, P.F., McCarroll, S.A., Sklar, P., 2014. A polygenic burden of rare disruptive mutations in schizophrenia. *Nature* 506, 185–190. <https://doi.org/10.1038/nature12975>
- Radhu, N., Garcia Dominguez, L., Farzan, F., Richter, M.A., Sernalul, M.O., Chen, R., Fitzgerald, P.B., Daskalakis, Z.J., 2015. Evidence for inhibitory deficits in the prefrontal cortex in schizophrenia. *Brain* 138, 483–497. <https://doi.org/10.1093/brain/awu360>
- Ramazani, Y., Knops, N., Elmonem, M.A., Nguyen, T.Q., Arcolino, F.O., van den Heuvel, L., Levtchenko, E., Kuypers, D., Goldschmeding, R., 2018. Connective tissue growth factor (CTGF) from basics to clinics. *Matrix Biol. J. Int. Soc. Matrix Biol.* 68–69, 44–66. <https://doi.org/10.1016/j.matbio.2018.03.007>
- Rapoport, J., Giedd, J., Gogtay, N., 2012. Neurodevelopmental model of schizophrenia: update 2012. *Mol. Psychiatry* 17, 1228–1238. <https://doi.org/10.1038/mp.2012.23>
- Reynolds, G.P., Abdul-Monim, Z., Neill, J.C., Zhang, Z.-J., 2004. Calcium binding protein markers of GABA deficits in schizophrenia — post mortem studies and animal models [WWW Document]. *Neurotox. Res.* <https://doi.org/10.1007/BF03033297>
- Ripke, S., Neale, B.M., Corvin, A., Walters, J.T.R., Farh, K.-H., Holmans, P.A., Lee, P., Bulik-Sullivan, B., Collier, D.A., Huang, H., Pers, T.H., Agartz, I., Agerbo, E., Albus, M., Alexander, M., Amin, F., Bacanu, S.A., Begemann, M., Belliveau Jr, R.A., Bene, J., Bergen, S.E., Bevilacqua, E., Bigdeli, T.B., Black, D.W., Bruggeman, R., Buccola, N.G., Buckner, R.L., Byerley, W., Cahn, W., Cai, G., Campion, D., Cantor, R.M., Carr, V.J., Carrera, N., Catts, S.V., Chambert, K.D., Chan, R.C.K., Chen, R.Y.L., Chen, E.Y.H., Cheng, W., Cheung, E.F.C., Ann Chong, S., Robert Cloninger, C., Cohen, D., Cohen, N., Cormican, P., Craddock, N., Crowley, J.J., Curtis, D., Davidson, M., Davis, K.L., Degenhardt, F., Del Favero, J., Demontis, D., Dikeos, D., Dinan, T., Djurovic, S., Donohoe, G., Drapeau, E., Duan, J., Dudbridge, F., Durmishi, N., Eichhammer, P., Eriksson, J., Escott-Price, V., Essioux, L., Fanous, A.H., Farrell, M.S., Frank, J., Franke, L., Freedman, R., Freimer, N.B., Friedl, M., Friedman, J.I., Fromer, M., Genovese, G., Georgieva, L., Giegling, I., Giusti-Rodríguez, P., Godard, S., Goldstein, J.I., Golimbet, V., Gopal, S., Gratten, J., de Haan, L., Hammer, C., Hamshere, M.L., Hansen, M., Hansen, T., Haroutunian, V., Hartmann, A.M., Henskens, F.A., Herms, S., Hirschhorn, J.N., Hoffmann, P., Hofman, A., Hollegaard, M.V., Hougaard, D.M., Ikeda, M., Joa, I., Julià, A., Kahn, R.S., Kalaydjieva, L., Karachanak-Yankova, S., Karjalainen, J., Kavanagh, D., Keller, M.C., Kennedy, J.L., Khrunin, A., Kim, Y., Klovins, J., Knowles, J.A., Konte, B., Kucinskis, V., Ausrele Kucinskiene, Z., Kuzelova-Ptackova, H., Kähler, A.K., Laurent, C., Lee Chee Keong, J., Hong Lee, S., Legge, S.E., Lerer, B., Li, M., Li, T., Liang, K.-Y., Lieberman, J.,

- Limborska, S., Loughland, C.M., Lubinski, J., Lönnqvist, J., Macek Jr, M., Magnusson, P.K.E., Maher, B.S., Maier, W., Mallet, J., Marsal, S., Mattheisen, M., Mattingsdal, M., McCarley, R.W., McDonald, C., McIntosh, A.M., Meier, S., Meijer, C.J., Melegh, B., Melle, I., Meshulam-Gately, R.I., Metspalu, A., Michie, P.T., Milani, L., Milanova, V., Mokrab, Y., Morris, D.W., Mors, O., Murphy, K.C., Murray, R.M., Myin-Germeys, I., Müller-Myhsok, B., Nelis, M., Nenadic, I., Nertney, D.A., Nestadt, G., Nicodemus, K.K., Nikitina-Zake, L., Nisenbaum, L., Nordin, A., O'Callaghan, E., O'Dushlaine, C., O'Neill, F.A., Oh, S.-Y., Olincy, A., Olsen, L., Van Os, J., Pantelis, C., Papadimitriou, G.N., Papiol, S., Parkhomenko, E., Pato, M.T., Paunio, T., Pejovic-Milovancevic, M., Perkins, D.O., Pietiläinen, O., Pimm, J., Pocklington, A.J., Powell, J., Price, A., Pulver, A.E., Purcell, S.M., Quested, D., Rasmussen, H.B., Reichenberg, A., Reimers, M.A., Richards, A.L., Roffman, J.L., Roussos, P., Ruderfer, D.M., Salomaa, V., Sanders, A.R., Schall, U., Schubert, C.R., Schulze, T.G., Schwab, S.G., Scolnick, E.M., Scott, R.J., Seidman, L.J., Shi, J., Sigurdsson, E., Silagadze, T., Silverman, J.M., Sim, K., Slominsky, P., Smoller, J.W., So, H.-C., Spencer, C.A., Stahl, E.A., Stefansson, H., Steinberg, S., Stogmann, E., Straub, R.E., Strengman, E., Strohmaier, J., Scott Stroup, T., Subramaniam, M., Suvisaari, J., Svrakic, D.M., Szatkiewicz, J.P., Söderman, E., Thirumalai, S., Toncheva, D., Tosato, S., Veijola, J., Waddington, J., Walsh, D., Wang, D., Wang, Q., Webb, B.T., Weiser, M., Wildenauer, D.B., Williams, N.M., Williams, S., Witt, S.H., Wolen, A.R., Wong, E.H.M., Wormley, B.K., Simon Xi, H., Zai, C.C., Zheng, X., Zimprich, F., Wray, N.R., Stefansson, K., Visscher, P.M., Trust Case-Control Consortium, W., Adolfsson, R., Andreassen, O.A., Blackwood, D.H.R., Bramon, E., Buxbaum, J.D., Børglum, A.D., Cichon, S., Darvasi, A., Domenici, E., Ehrenreich, H., Esko, T., Gejman, P.V., Gill, M., Gurling, H., Hultman, C.M., Iwata, N., Jablensky, A.V., Jönsson, E.G., Kendler, K.S., Kirov, G., Knight, J., Lencz, T., Levinson, D.F., Li, Q.S., Liu, J., Malhotra, A.K., McCarroll, S.A., McQuillin, A., Moran, J.L., Mortensen, P.B., Mowry, B.J., Nöthen, M.M., Ophoff, R.A., Owen, M.J., Palotie, A., Pato, C.N., Petryshen, T.L., Posthuma, D., Rietschel, M., Riley, B.P., Rujescu, D., Sham, P.C., Sklar, P., St Clair, D., Weinberger, D.R., Wendland, J.R., Werge, T., Schizophrenia Working Group of the Psychiatric Genomics Consortium, Psychosis Endophenotypes International Consortium, 2014. Biological insights from 108 schizophrenia-associated genetic loci. *Nature* 511, 421–427. <https://doi.org/10.1038/nature13595>
- Roberts, R.C., Gaither, L.A., Peretti, F.J., Lapidus, B., Chute, D.J., 1996. Synaptic organization of the human striatum: A postmortem ultrastructural study. *J. Comp. Neurol.* 374, 523–534. [https://doi.org/10.1002/\(SICI\)1096-9861\(19961028\)374:4<523::AID-CNE4>3.0.CO;2-3](https://doi.org/10.1002/(SICI)1096-9861(19961028)374:4<523::AID-CNE4>3.0.CO;2-3)
- Rocheffort, C., Arabo, A., Andre, M., Poucet, B., Save, E., Rondi-Reig, L., 2011. Cerebellum Shapes Hippocampal Spatial Code. *Science* 334, 385–389. <https://doi.org/10.1126/science.1207403>
- Rondi-Reig, L., Paradis, A.-L., Lefort, J.M., Babayan, B.M., Tobin, C., 2014. How the cerebellum may monitor sensory information for spatial representation. *Front. Syst. Neurosci.* 8. <https://doi.org/10.3389/fnsys.2014.00205>
- Rosoklija, G., Toomayan, G., Ellis, S.P., Keilp, J., Mann, J.J., Latov, N., Hays, A.P., Dwork, A.J., 2000. Structural Abnormalities of Subicular Dendrites in Subjects With Schizophrenia and Mood Disorders: Preliminary Findings. *Arch. Gen. Psychiatry* 57, 349–356. <https://doi.org/10.1001/archpsyc.57.4.349>
- Salinas, P.C., 2012. Wnt signaling in the vertebrate central nervous system: from axon guidance to synaptic function. *Cold Spring Harb. Perspect. Biol.* 4. <https://doi.org/10.1101/cshperspect.a008003>

- Sanes, J.R., Yamagata, M., 2009. Many Paths to Synaptic Specificity [WWW Document]. <http://dx.doi.org/10.1146/annurev.cellbio.24.110707.175402>.
<https://doi.org/10.1146/annurev.cellbio.24.110707.175402>
- Sanes, J.R., Zipursky, S.L., 2020. Synaptic Specificity, Recognition Molecules, and Assembly of Neural Circuits. *Cell* 181, 1434–1435. <https://doi.org/10.1016/j.cell.2020.05.046>
- Scarr, E., Gray, L., Keriakous, D., Robinson, P.J., Dean, B., 2006. Increased levels of SNAP-25 and synaptophysin in the dorsolateral prefrontal cortex in bipolar I disorder. *Bipolar Disord.* 8, 133–143. <https://doi.org/10.1111/j.1399-5618.2006.00300.x>
- Schindelin, J., Arganda-Carreras, I., Frise, E., Kaynig, V., Longair, M., Pietzsch, T., Preibisch, S., Rueden, C., Saalfeld, S., Schmid, B., Tinevez, J.-Y., White, D.J., Hartenstein, V., Eliceiri, K., Tomancak, P., Cardona, A., 2012. Fiji: an open-source platform for biological-image analysis. *Nat. Methods* 9, 676–682. <https://doi.org/10.1038/nmeth.2019>
- Schmahmann, J.D., 2019. The cerebellum and cognition. *Neurosci. Lett.* 688, 62–75. <https://doi.org/10.1016/j.neulet.2018.07.005>
- Schmahmann, J.D., 1991. An Emerging Concept: The Cerebellar Contribution to Higher Function. *Arch. Neurol.* 48, 1178–1187. <https://doi.org/10.1001/archneur.1991.00530230086029>
- Schwarz, E., Izmailov, R., Spain, M., Barnes, A., Mapes, J.P., Guest, P.C., Rahmoune, H., Pietsch, S., Leweke, F.M., Rothermundt, M., Steiner, J., Koethe, D., Kranaster, L., Ohrmann, P., Suslow, T., Levin, Y., Bogerts, B., van Beveren, N.J., McAllister, G., Weber, N., Niebuhr, D., Cowan, D., Yolken, R.H., Bahn, S., 2010. Validation of a blood-based laboratory test to aid in the confirmation of a diagnosis of schizophrenia. *Biomark. Insights* 5, 39–47. <https://doi.org/10.4137/bmi.s4877>
- Sekar, A., Bialas, A.R., de Rivera, H., Davis, A., Hammond, T.R., Kamitaki, N., Tooley, K., Presumey, J., Baum, M., Van Doren, V., Genovese, G., Rose, S.A., Handsaker, R.E., Schizophrenia Working Group of the Psychiatric Genomics Consortium, Daly, M.J., Carroll, M.C., Stevens, B., McCarroll, S.A., 2016. Schizophrenia risk from complex variation of complement component 4. *Nature* 530, 177–183. <https://doi.org/10.1038/nature16549>
- Sellgren, C.M., Gracias, J., Watmuff, B., Biag, J.D., Thanos, J.M., Whittredge, P.B., Fu, T., Worringer, K., Brown, H.E., Wang, J., Kaykas, A., Karmacharya, R., Goold, C.P., Sheridan, S.D., Perlis, R.H., 2019. Increased synapse elimination by microglia in schizophrenia patient-derived models of synaptic pruning. *Nat. Neurosci.* 22, 374–385. <https://doi.org/10.1038/s41593-018-0334-7>
- Sendhilnathan, N., Ipata, A.E., Goldberg, M.E., 2020. Neural Correlates of Reinforcement Learning in Mid-lateral Cerebellum. *Neuron* 106, 188–198.e5. <https://doi.org/10.1016/j.neuron.2019.12.032>
- Sigoillot, S.M., Iyer, K., Binda, F., González-Calvo, I., Talleur, M., Vodjdani, G., Isope, P., Selimi, F., 2015. The Secreted Protein C1QL1 and Its Receptor BAI3 Control the Synaptic Connectivity of Excitatory Inputs Converging on Cerebellar Purkinje Cells. *Cell Rep.* 10, 820–832. <https://doi.org/10.1016/j.celrep.2015.01.034>
- Song, Y., Kim, J.-S., Choi, E.K., Kim, J., Kim, K.M., Seo, H.R., 2017. TGF- β -independent CTGF induction regulates cell adhesion mediated drug resistance by increasing collagen I in HCC. *Oncotarget* 8, 21650–21662. <https://doi.org/10.18632/oncotarget.15521>
- Sotelo, C., 2004. Cellular and genetic regulation of the development of the cerebellar system. *Prog. Neurobiol.* 72, 295–339. <https://doi.org/10.1016/j.pneurobio.2004.03.004>
- Stevens, B., Allen, N.J., Vazquez, L.E., Howell, G.R., Christopherson, K.S., Nouri, N., Micheva, K.D., Mehalow, A.K., Huberman, A.D., Stafford, B., Sher, A., Litke, A.M.,

- Lambris, J.D., Smith, S.J., John, S.W.M., Barres, B.A., 2007. The Classical Complement Cascade Mediates CNS Synapse Elimination. *Cell* 131, 1164–1178. <https://doi.org/10.1016/j.cell.2007.10.036>
- Stoodley, C.J., 2012. The Cerebellum and Cognition: Evidence from Functional Imaging Studies. *The Cerebellum* 11, 352–365. <https://doi.org/10.1007/s12311-011-0260-7>
- Stoodley, C.J., Schmahmann, J.D., 2010. Evidence for topographic organization in the cerebellum of motor control versus cognitive and affective processing. *Cortex J. Devoted Study Nerv. Syst. Behav.* 46, 831–844. <https://doi.org/10.1016/j.cortex.2009.11.008>
- Südhof, T.C., 2018. Towards an Understanding of Synapse Formation. *Neuron* 100, 276–293. <https://doi.org/10.1016/j.neuron.2018.09.040>
- Sun, L., Cheng, Z., Zhang, F., Xu, Y., 2015. Gene expression profiling in peripheral blood mononuclear cells of early-onset schizophrenia. *Genomics Data* 5, 169–170. <https://doi.org/10.1016/j.gdata.2015.04.022>
- Szklarczyk, D., Morris, J.H., Cook, H., Kuhn, M., Wyder, S., Simonovic, M., Santos, A., Doncheva, N.T., Roth, A., Bork, P., Jensen, L.J., von Mering, C., 2017. The STRING database in 2017: quality-controlled protein-protein association networks, made broadly accessible. *Nucleic Acids Res.* 45, D362–D368. <https://doi.org/10.1093/nar/gkw937>
- Takigawa, M., 2017. The CCN Proteins: An Overview. *Methods Mol. Biol. Clifton NJ* 1489, 1–8. https://doi.org/10.1007/978-1-4939-6430-7_1
- Terranova, J.-P., Chabot, C., Barnouin, M.-C., Perrault, G., Depoortere, R., Griebel, G., Scatton, B., 2005. SSR181507, a dopamine D2 receptor antagonist and 5-HT1A receptor agonist, alleviates disturbances of novelty discrimination in a social context in rats, a putative model of selective attention deficit. *Psychopharmacology (Berl.)* 181, 134–144. <https://doi.org/10.1007/s00213-005-2268-5>
- Uemura, T., Lee, S.-J., Yasumura, M., Takeuchi, T., Yoshida, T., Ra, M., Taguchi, R., Sakimura, K., Mishina, M., 2010. Trans-synaptic interaction of GluRdelta2 and Neurexin through Cbln1 mediates synapse formation in the cerebellum. *Cell* 141, 1068–1079. <https://doi.org/10.1016/j.cell.2010.04.035>
- Ujike, H., Takaki, M., Nakata, K., Tanaka, Y., Takeda, T., Kodama, M., Fujiwara, Y., Sakai, A., Kuroda, S., 2002. CNR1, central cannabinoid receptor gene, associated with susceptibility to hebephrenic schizophrenia. *Mol. Psychiatry* 7, 515–518. <https://doi.org/10.1038/sj.mp.4001029>
- Vawter, M.P., Crook, J.M., Hyde, T.M., Kleinman, J.E., Weinberger, D.R., Becker, K.G., Freed, W.J., 2002. Microarray analysis of gene expression in the prefrontal cortex in schizophrenia: a preliminary study. *Schizophr. Res.* 58, 11–20. [https://doi.org/10.1016/S0920-9964\(01\)00377-2](https://doi.org/10.1016/S0920-9964(01)00377-2)
- Wagner, M.J., Kim, T.H., Savall, J., Schnitzer, M.J., Luo, L., 2017. Cerebellar granule cells encode the expectation of reward. *Nature* 544, 96–100. <https://doi.org/10.1038/nature21726>
- Wang, C., McInnis, J., Ross-Sanchez, M., Shinnick-Gallagher, P., Wiley, J.L., Johnson, K.M., 2001. Long-term behavioral and neurodegenerative effects of perinatal phencyclidine administration: implications for schizophrenia. *Neuroscience* 107, 535–550. [https://doi.org/10.1016/S0306-4522\(01\)00384-0](https://doi.org/10.1016/S0306-4522(01)00384-0)
- Wang, S.S.-H., Kloth, A.D., Badura, A., 2014. The Cerebellum, Sensitive Periods, and Autism. *Neuron* 83, 518–532. <https://doi.org/10.1016/j.neuron.2014.07.016>
- Wassink, T.H., Andreasen, N.C., Nopoulos, P., Flaum, M., 1999. Cerebellar morphology as a predictor of symptom and psychosocial outcome in schizophrenia. *Biol. Psychiatry* 45, 41–48. [https://doi.org/10.1016/S0006-3223\(98\)00175-9](https://doi.org/10.1016/S0006-3223(98)00175-9)

- Weinberger, D.R., 2017. The neurodevelopmental origins of schizophrenia in the penumbra of genomic medicine. *World Psychiatry* 16, 225–226. <https://doi.org/10.1002/wps.20474>
- Weinberger, D.R., Kleinman, J.E., Luchins, D.J., Bigelow, L.B., Wyatt, R.J., 1980. Cerebellar pathology in schizophrenia: a controlled postmortem study. *Am. J. Psychiatry* 137, 359–361. <https://doi.org/10.1176/ajp.137.3.359>
- Xiao, L., Michalski, N., Kronander, E., Gjoni, E., Genoud, C., Knott, G., Schleggenburger, R., 2013. BMP signaling specifies the development of a large and fast CNS synapse. *Nat. Neurosci.* 16, 856–864. <https://doi.org/10.1038/nn.3414>
- Yin, D.-M., Chen, Y.-J., Sathyamurthy, A., Xiong, W.-C., Mei, L., 2012. Synaptic dysfunction in schizophrenia. *Adv. Exp. Med. Biol.* 970, 493–516. https://doi.org/10.1007/978-3-7091-0932-8_22
- Yu, B., Wang, C., Liu, J., Johnson, K.M., Gallagher, J.P., 2002. Adaptation to chronic PCP results in hyperfunctional NMDA and hypofunctional GABAA synaptic receptors. *Neuroscience* 113, 1–10. [https://doi.org/10.1016/S0306-4522\(02\)00163-X](https://doi.org/10.1016/S0306-4522(02)00163-X)
- Yu, I.-S., Chang, H.-C., Chen, K.-C., Lu, Y.-L., Shy, H.-T., Chen, C.-Y., Lee, K.-Y., Lee, L.-J., 2019. Genetic Elimination of Connective Tissue Growth Factor in the Forebrain Affects Subplate Neurons in the Cortex and Oligodendrocytes in the Underlying White Matter. *Front. Neuroanat.* 13. <https://doi.org/10.3389/fnana.2019.00016>
- Zhang, B., Chen, L.Y., Liu, X., Maxeiner, S., Lee, S.-J., Gokce, O., Südhof, T.C., 2015. Neuroligins Sculpt Cerebellar Purkinje-Cell Circuits by Differential Control of Distinct Classes of Synapses. *Neuron* 87, 781–796. <https://doi.org/10.1016/j.neuron.2015.07.020>
- Zhang, Y., You, X., Li, S., Long, Q., Zhu, Y., Teng, Z., Zeng, Y., 2020. Peripheral Blood Leukocyte RNA-Seq Identifies a Set of Genes Related to Abnormal Psychomotor Behavior Characteristics in Patients with Schizophrenia. *Med. Sci. Monit. Int. Med. J. Exp. Clin. Res.* 26, e922426-1-e922426-31. <https://doi.org/10.12659/MSM.922426>

Acknowledgments: Philippe Marin for helpful discussions, Coralie Bertoux for technical help with PCP injections, Bertrand Ducos and Marine Delagrangue for running the high throughput qPCR, Marco Aquila and Alessandro Maccione for technical help with the MEA and the spike sorting, respectively. We acknowledge the Orion imaging facility, CIRB, and also the personnel from the CIRB Animal facility. This work was supported by funding from: ATIP-AVENIR program (RSE11005JSA to FS), Fondation pour la Recherche Médicale Equipe FRM DEQ20150331748 (FS), and European Research Council ERC consolidator grant SynID 724601 (to FS).

Contributions: F.S., M.V. and S.M.S. designed the study and the experiments. M.V. and S.M.S. performed the experiments and collected the data; C.B. provided the first batches of PCP treated mice, M.V. wrote the first draft of the manuscript, all authors read the manuscript and S.M.S. and F.S. revised the manuscript.

Competing interests: Authors declare no competing interests.

Figures

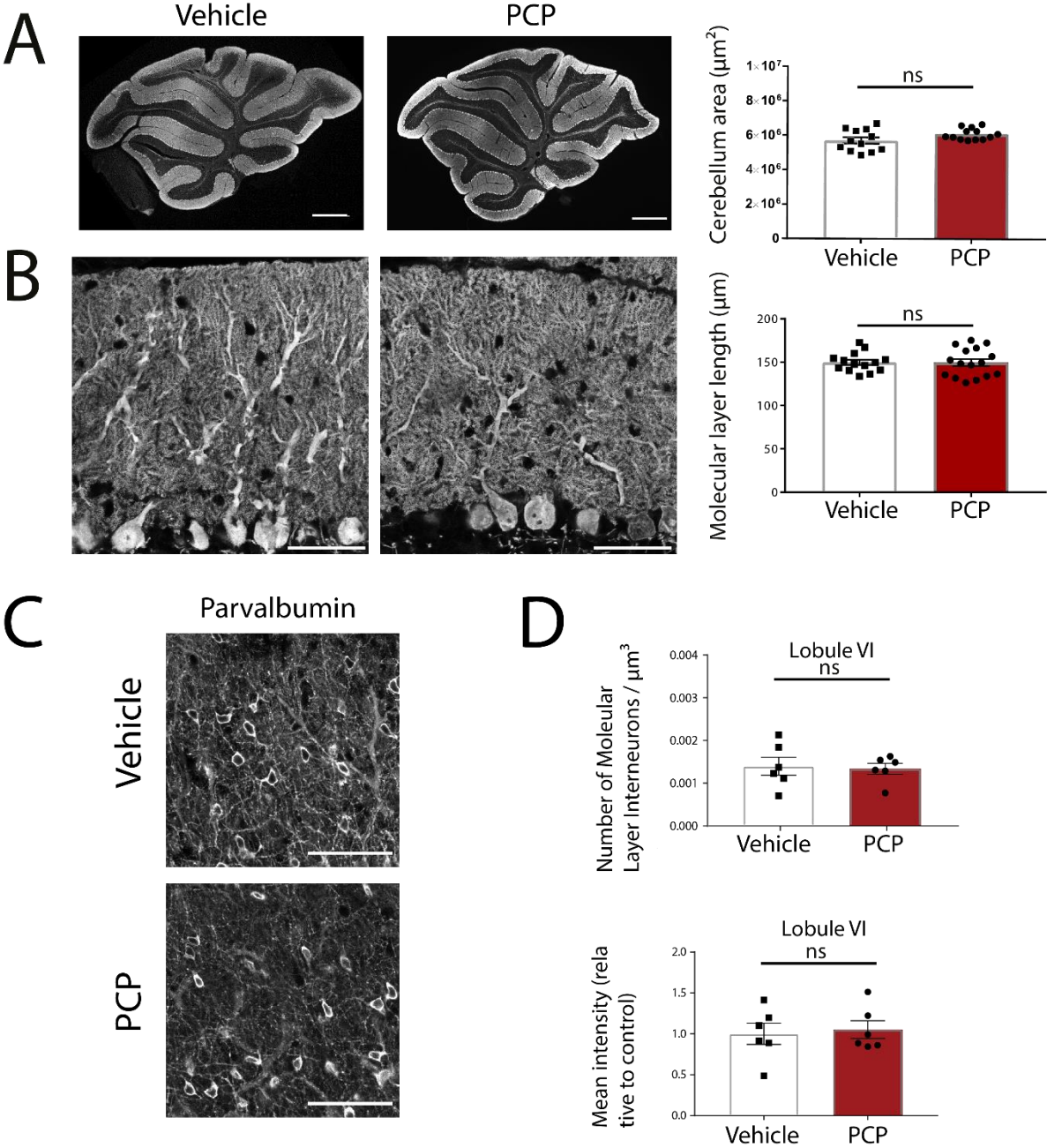


Figure 1. Normal global cerebellar morphology in juvenile mice treated neonatally with PCP.

(A) Sagittal cerebellar slices from P30 vehicle (left) and PCP (right) animals were immunolabeled with an anti-calbindin antibody, which specifically stains Purkinje cells. Scale bar: 1000 μm . Quantification of the mean area of the cerebellar slices show no significant differences

between the two conditions in the vermis. Mean \pm SEM. Vehicle: n=12 animals, PCP: n=13, Unpaired Student's *t* test, ns = not significant.

- (B) Purkinje cells and their dendritic tree were immunostained with an anti-calbindin antibody and imaged in lobule VI of sagittal cerebellar sections from P30 vehicle (left) and PCP (right) animals. The thickness of the molecular layer was measured as the length from the beginning of the primary dendrite of Purkinje cells to the upper extremity of the molecular layer. Scale bar: 50 μ m. No significant differences in the thickness of the molecular layer are found between Vehicle- and PCP-treated animals. Mean \pm SEM. Vehicle: n=14 animals, PCP: n=17, Unpaired Student's *t* test, ns = not significant.
- (C) Molecular layer interneurons labeled using anti-parvalbumin antibody in sagittal cerebellar sections from P30 mice. Scale bar: 50 μ m.
- (D) Quantification of molecular layer interneurons density, and anti-parvalbumin protein mean intensity, revealed that PCP mice have a normal number of inhibitory neurons, and no deficits in parvalbumin protein expression in the molecular layer. Unpaired Student's *t* test, ns = not significant.

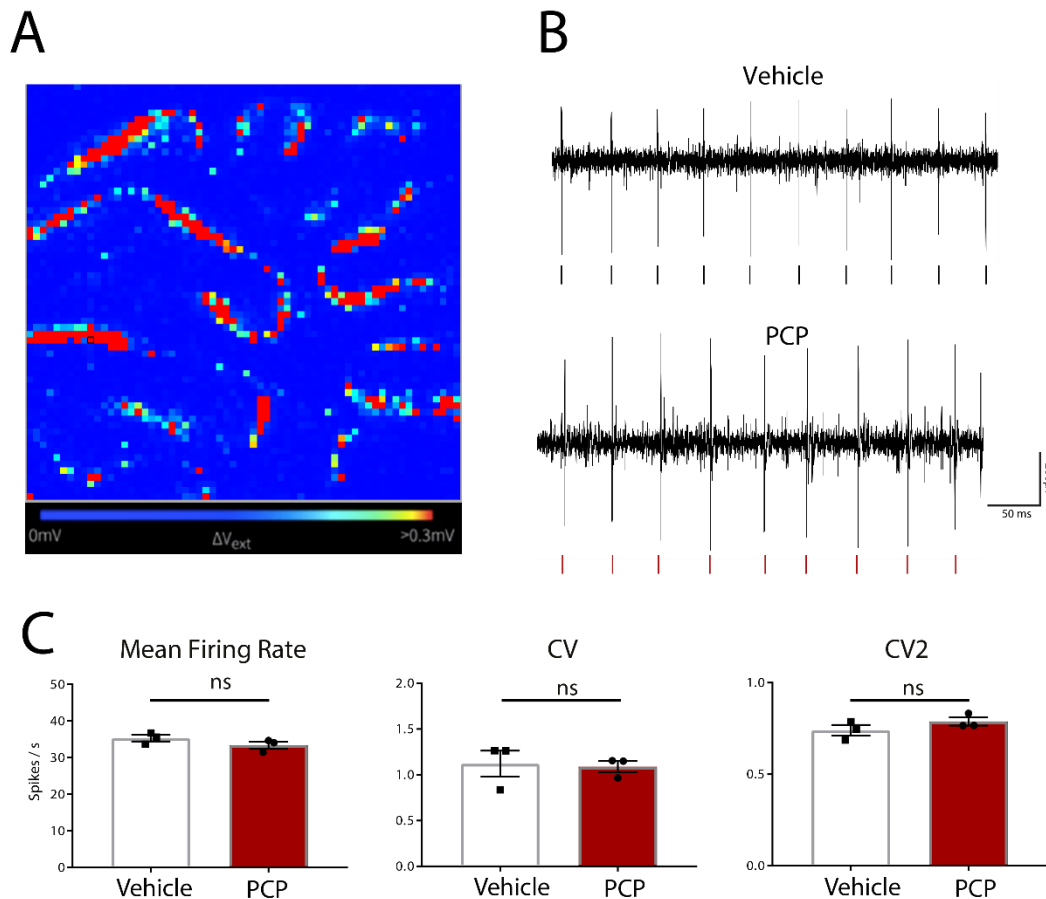


Figure 2. Normal spontaneous spiking of cerebellar Purkinje Cells in PCP-treated mice

(A) High density microelectrode arrays (MEA) were used to record Purkinje cell spiking in acute cerebellar slices from P30 vehicle- and PCP-treated mice. The image is an example of the recorded electrical activity in a cerebellar slice from a vehicle-treated mouse: Each pixel represents one channel, with units showing high activity in red, and low activity in blue.

(B) Representative traces of recordings from one channel for each type of animal. Each colored vertical bar represents an action potential detected by the Brainwave software after spike detection.

(C) Histograms of mean firing rate, coefficient of variation of Inter Spike Intervals (CV) and CV2. Recordings were done on two slices per animal, each slice containing between 20 and 200 active neurons. The software sorted all the detected spikes into clusters called “unit”, based on the similarity of their shapes and their spatial localization. All the units (supposed to represent spiking neurons) from two slices of a same animal are pooled together. Mean \pm SEM. Vehicle: n=3 mice, PCP, n=3 mice Mann-Whitney non-parametric test, ns = not significant.

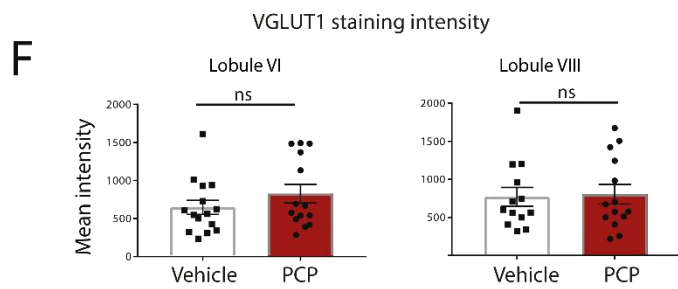
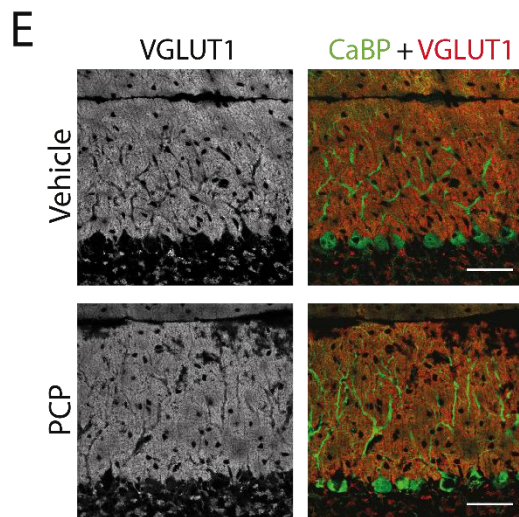
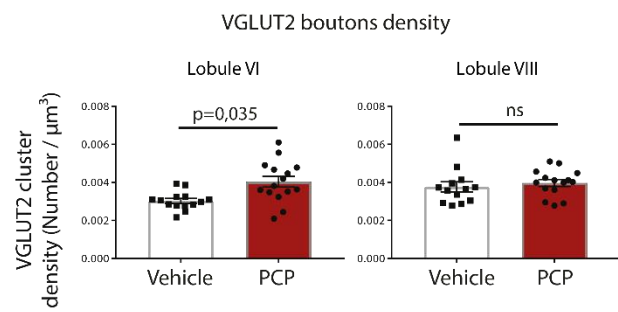
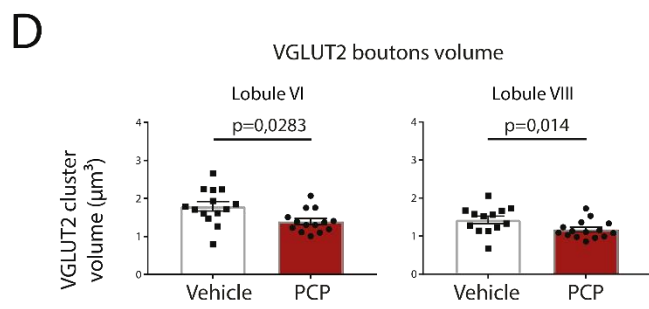
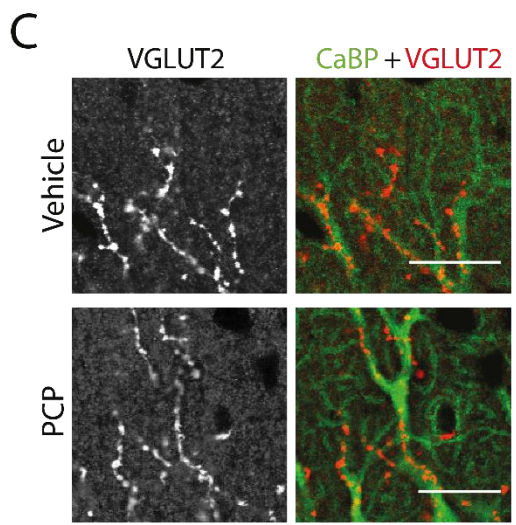
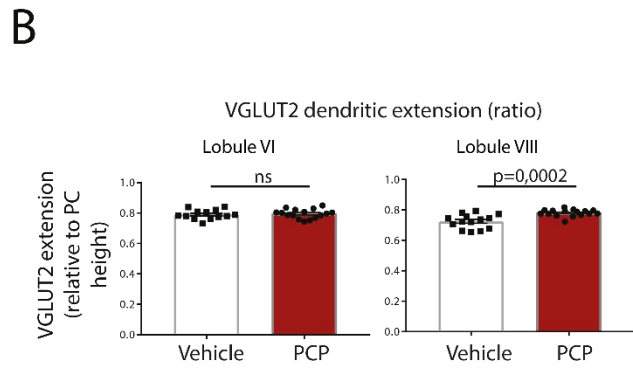
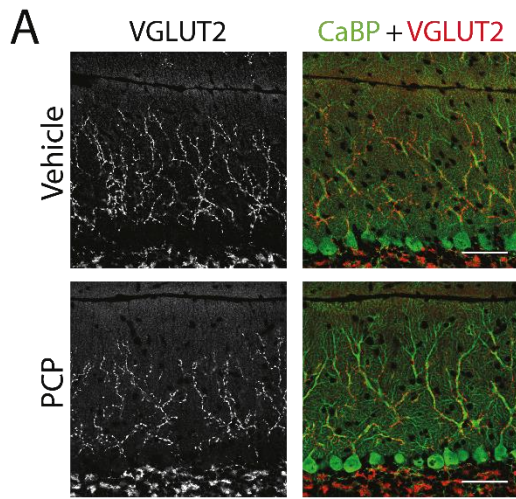


Figure 3. Afferent-specific alterations of CF presynaptic boutons morphology are lobule-specific.

- (A) Climbing fiber presynaptic boutons were immunostained with an anti-VGLUT2 antibody (red), and Purkinje cells and their dendritic tree with an anti-calbindin antibody (green), in parasagittal cerebellar sections from P30 vehicle and PCP mice. Scale bar: 50 μ m.
- (B) The extension of Climbing fiber synaptic territory has been calculated by quantifying the extent of VGLUT2 labelling relative to the height of the Purkinje cell dendritic tree. Climbing fiber extension is significantly increased in lobule VIII, but not lobule VI, in PCP-treated mice compared to control. Vehicle n=13 animals in lobule VI, n=14 in lobule VIII, PCP: n=16 in both lobules. Mean \pm SEM, unpaired Student's *t* test, lobule VI: p=0,38, lobule VIII: p=0.0002.
- (C) High magnification image of VGLUT2 clusters (red) and Purkinje cell dendrites (green) in sagittal cerebellar sections from P30 vehicle and PCP mice labeled as in (A). Scale bar: 20 μ m.
- (D) Top: Quantification of the mean volume of VGLUT2 puncta. Vehicle: n=14 animals in lobule VI, 13 in lobule VIII; PCP: n=14 animals in lobule VI, 15 in lobule VIII. Mean \pm SEM, unpaired Student's *t* test, lobule VI: p=0,0283, lobule VIII: p=0.014.
Bottom: Quantification of the mean density of VGLUT2 puncta revealed a 33% increase in the lobule VI of PCP mice, but not in lobule VIII compared to vehicle mice. Mean \pm SEM. Vehicle: n=14 animals in lobule VI, 13 in lobule VIII, PCP: n=15 animals in lobule VI, 15 in lobule VIII. Unpaired Student *t*-test. Lobule VI: p=0,035, lobule VIII: p=0,523.
- (E) Parallel fiber presynaptic boutons were immunostained with an anti-VGLUT1 antibody (red), and an anti-calbindin antibody was used to stain Purkinje cells and its dendritic tree (green) in parasagittal cerebellar sections from P30 Vehicle and PCP mice. Scale bar: 50 μ m.
- (F) Quantification of the mean intensity of anti-VGLUT1 staining in the molecular layer revealed no change in the PCP model, in both lobules VI and VIII. Vehicle n=15 and 13 animals respectively, PCP n=14 animals. Unpaired Student's *t* test, ns = not significant.

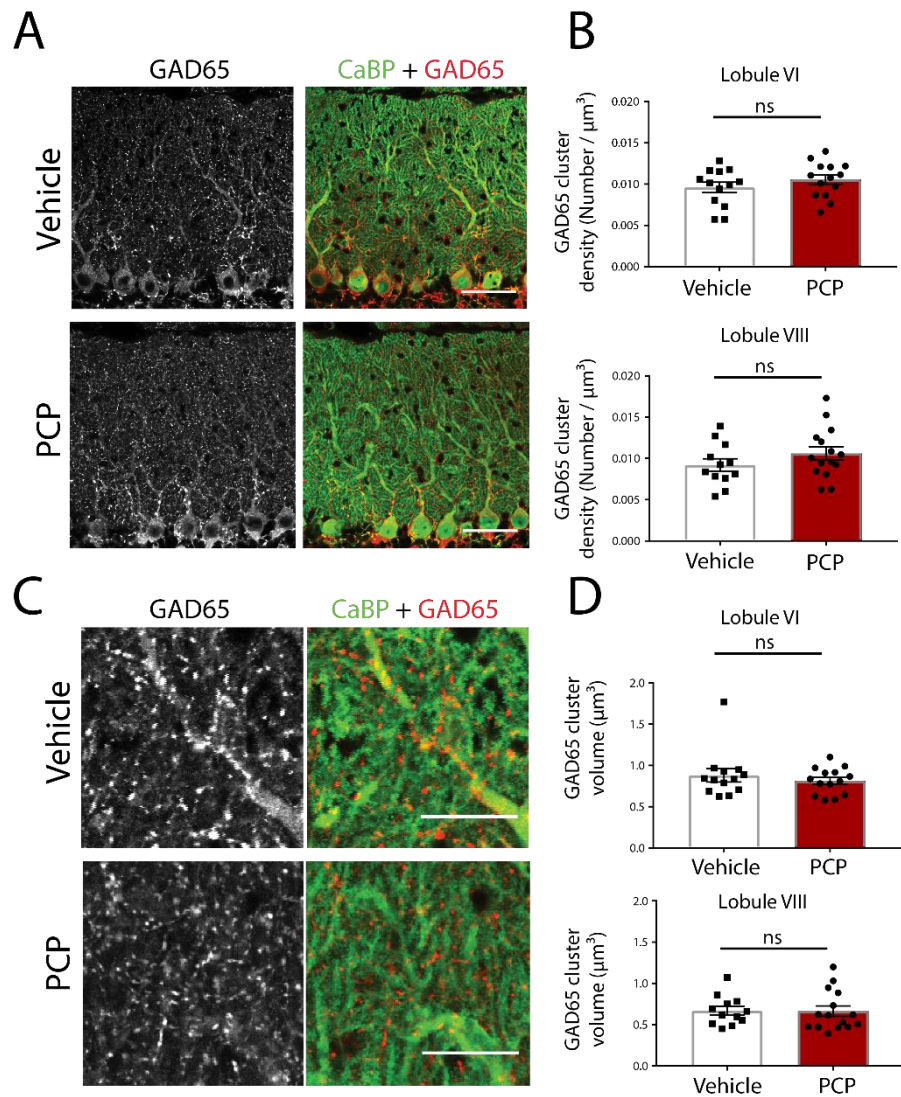


Figure 4. Normal molecular layer interneurons number and presynaptic boutons morphology in PCP mice

- (A) Molecular layer interneurons presynaptic boutons were immunostained with an anti-GAD65 antibody (red), and an anti-calbindin antibody has been used to stain Purkinje cells and its dendritic tree (green), in sagittal cerebellar sections from P30 vehicle and PCP mice. Scale bar: 50 μm .
- (B) Quantification of GAD65 puncta revealed normal presynaptic inhibitory boutons density in the molecular layer of lobules VI and VIII in PCP models. Vehicle n=13 and 12 animals respectively, PCP n=14 and 15 animals, respectively. Unpaired Student's *t* test, ns = not significant.

- (C) High magnification image of GAD65 clusters (red) and Purkinje cell dendrites (green) in sagittal cerebellar sections from P30 vehicle and PCP mice labeled as in (A). Scalebar: 20 μ m.
- (D) Quantification of GAD65 puncta revealed normal presynaptic inhibitory boutons volume in lobules VI and VIII in PCP models. Vehicle n=13 and 12 animals respectively, PCP n=14 and 15 animals, respectively. Unpaired Student's *t* test, ns = not significant.

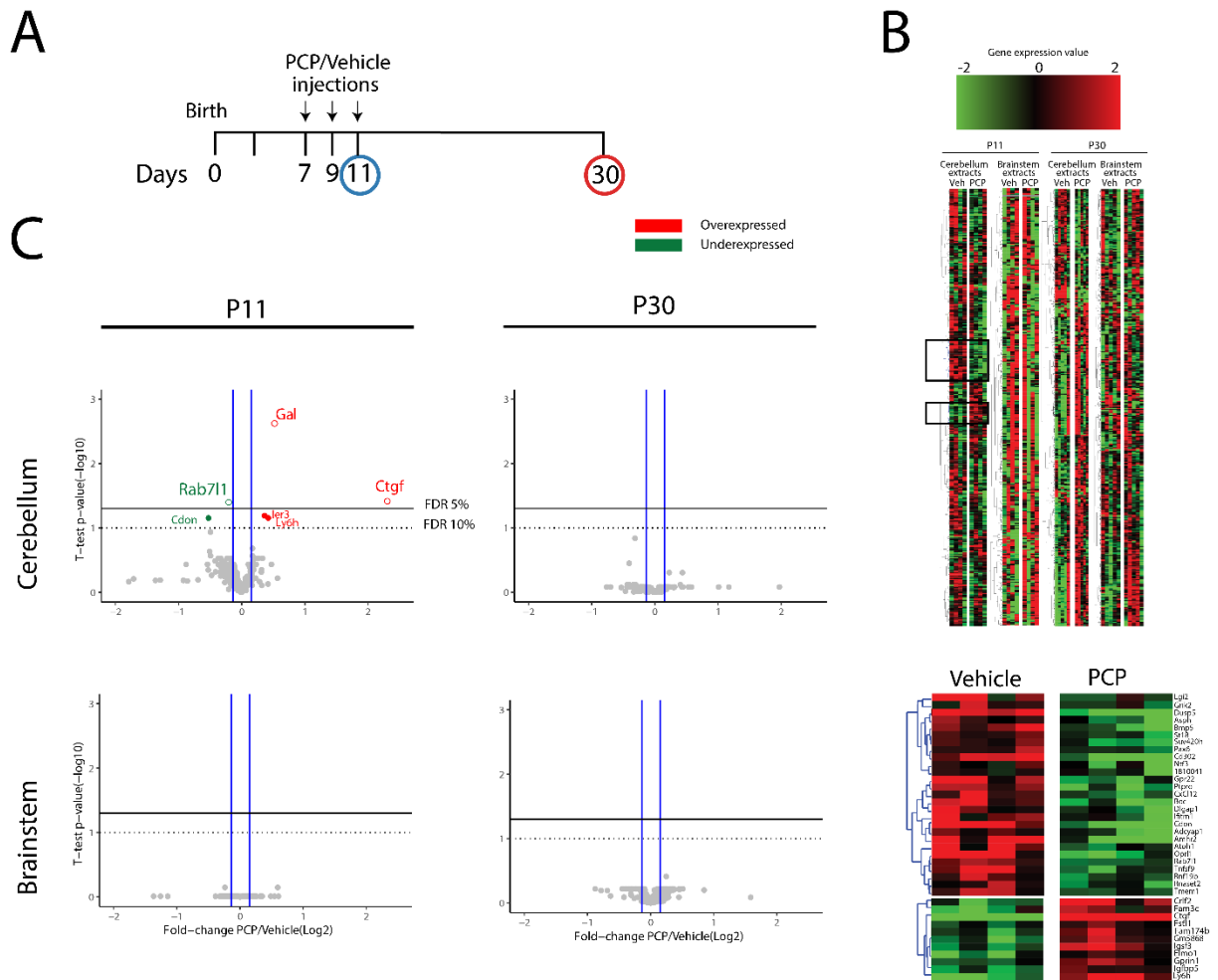


Figure 5. Subchronic neonatal PCP induces transient gene expression changes of the neuronal surfaceome in the cerebellum

- (A) Experimental design. PCP or Vehicle is injected in neonatal mice at P7, P9, P11. Gene expression changes were analyzed from both cerebellum and brainstem at either P11, to detect immediate changes after PCP treatment, or at P30, to detect eventual long-term changes.
- (B) Top: hierarchical clustering analysis of the 324 quantified genes, in cerebellar and brainstem extracts, at P11 and P30. In both P30 extracts, and in the P11 brainstem extracts, no cluster of genes were consistently over-expressed or under-expressed in the PCP group. In the P11 cerebellum extracts, two main clusters were found, one with gene upregulation, one with downregulation.

Bottom: zoom on the two clusters of downregulated genes (27 genes, top) or upregulated (11 genes, bottom) in the PCP model compared to vehicle. For the full list of genes and changes, see supplementary table 1.

(C) Volcano plot representation of the changes in gene expression in the four groups. Each dot represents the fold change for a gene and the corresponding corrected p value (using the Benjamini-Hochberg correction for multiple t test comparison (Benjamini and Hochberg, 1995)). Y axis: $-\log_{10}$ of corrected p values. X axis: Log_2 of gene fold change. The top black horizontal bar corresponds to a false discovery rate (FDR) threshold set to 5%, the bottom dotted bar corresponds to FDR set to 10, and vertical blue bars correspond to a fold change in gene expression level of 10%. Genes with a $\text{FDR} < 5\%$ are represented with empty circles.

Supplementary Information

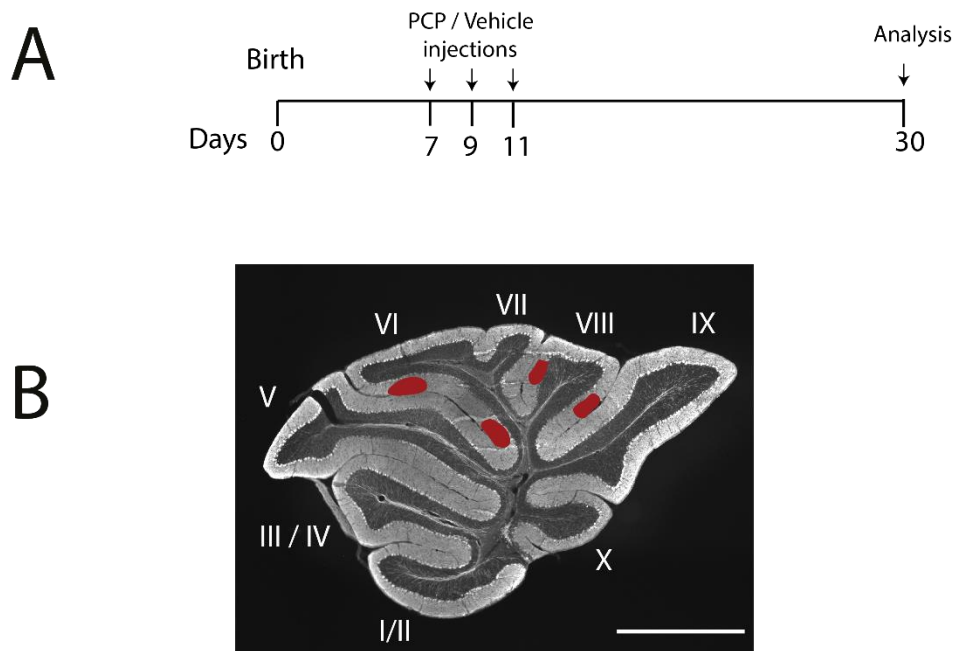


Figure Supplementary 1. Experimental design and recording areas

(A) Experimental design. Subcutaneous injections of vehicle (NaCl 0,9% solution) or PCP (10mg/kg) at postnatal day 7 (P7), P9 and P11. Analyses have been done at P30, when all the major steps of the olivocerebellar circuit development have been completed.

(B) Sagittal slice of a mouse cerebellum with the different lobules in the vermis. The red patches represent the areas in which the morphological analysis above (Fig. 3 and 4) are performed.

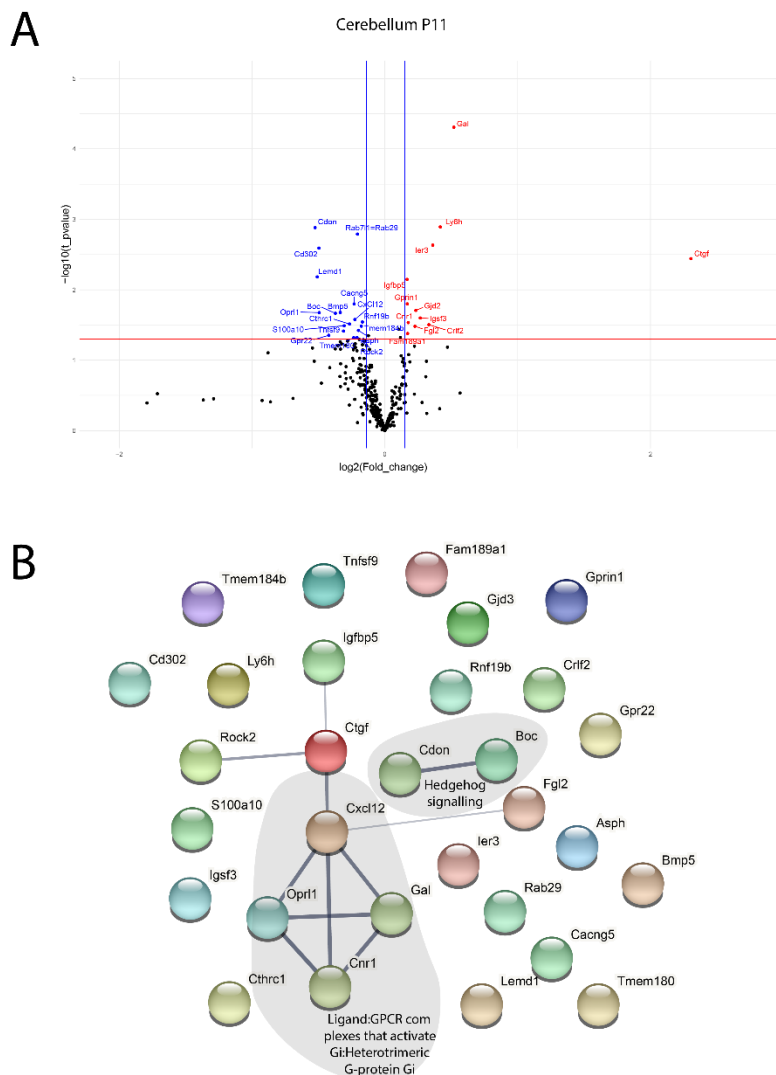


Figure Supplementary 2. In silico analysis predicts potential interactions between *Ctgf* and several other genes potentially misregulated by PCP in the cerebellum.

- (A) Volcano plot representation of the changes in gene expression in the cerebellum P11 group with p values for multiple testing without Benjamini-Hochberg correction. 41 genes have a fold-change of at least 10 % with an uncorrected p lower than 0.05. Y axis: $-\log_{10}$ of corrected p values. X axis: \log_2 of gene fold change. The red horizontal bar corresponds to the selected p value threshold set to 0,05, while vertical blue bars correspond to a fold change of 10%.
- (B) The 41 selected genes transiently misregulated at P11 in the cerebellum and brainstem were mapped in the String-database to represent known and predicted functional interactions between proteins. Line thickness indicates the strength of data support collected from curated databases, extracted from PubMed abstracts or from gene fusion or co-expression databases. *Ctgf* appears to be in the center of a network of several misregulated genes, including *Igfbp5*, *Rock2*, and *Cxcl12*.

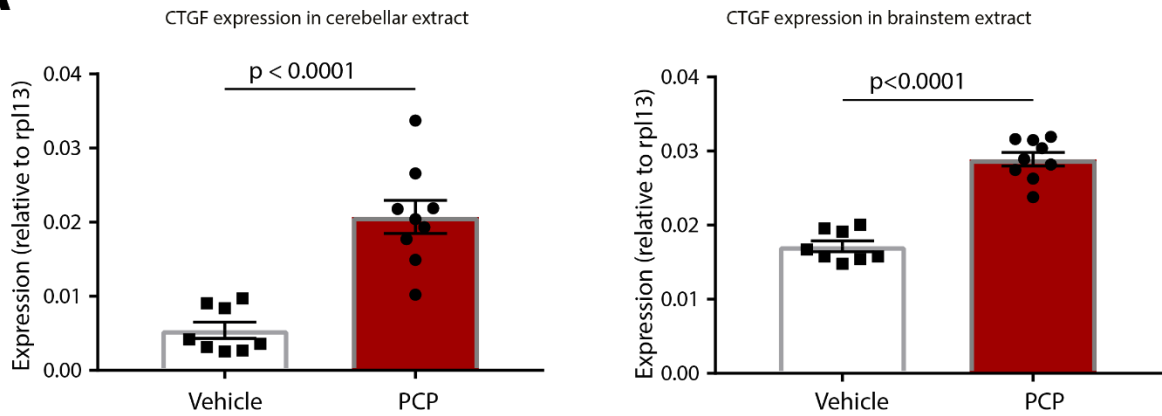
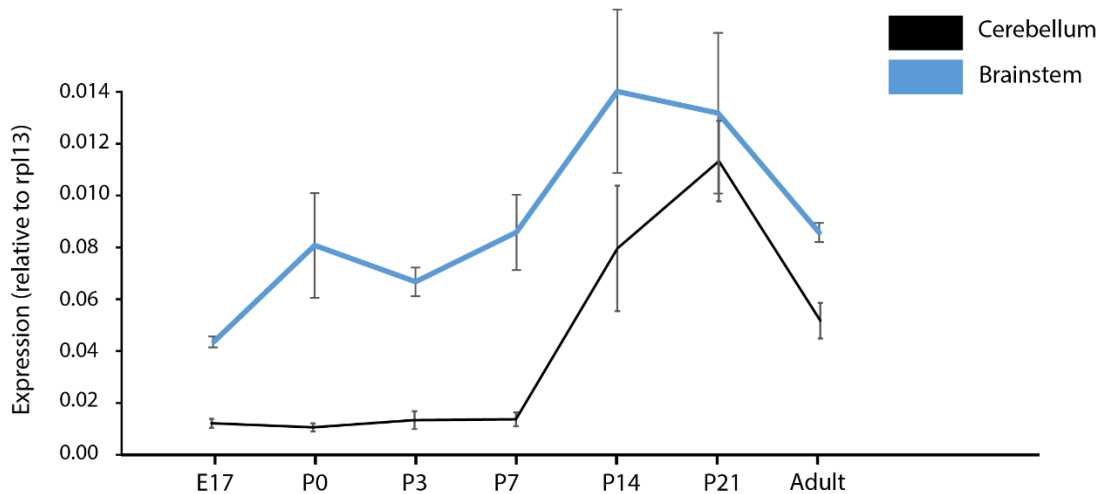
A**B**

Figure Supplementary 3. *Ctgf* expression after PCP injection and during normal postnatal development in the cerebellum and brainstem

- (A) Quantification of *Ctgf* expression in PCP mice following the last injection at P11 compared to vehicle in the cerebellum (left) and brainstem (right) extracts. Unpaired Student's *t* test. Vehicle: n=8 animals, PCP: n=9.
- (B) Expression profile of *Ctgf* during development and in adult extracts in wild type mice. In the cerebellum (black), *Ctgf* expression is low in the first postnatal week, increases massively from P7 to a peak at P21 (with a six-fold change). The expression then decreases by half in adult age. In the brainstem, *Ctgf* expression increases from P3 to P14, and then decrease until adulthood.

Supplementary tables

Supplementary table 1: Results of the RT-PCR, represented in fold change of the mean value in the PCP-treated group compared to saline-treated group.

Gene	Fold change of PCP mice versus control			
	Cerebellum P11	Brainstem P11	Cerebellum P30	Brainstem P30
B2m	0.90417	1.01883	1.14921	0.81699
Bai1	0.98683	0.94455	1.16530	0.90248
Boc	1.04168	1.05346	1.11247	0.77236
Cadps2	0.93276	1.19858	1.16961	0.97618
cc15	0.62264	1.46110	1.07417	0.86486
Chn2	0.98692	0.97451	1.00685	0.81357
Cnh3	0.80612	1.10690	0.90296	1.01490
Crtac1	0.92794	1.00711	1.06750	0.99825
Cthrc1	0.95218	0.96118	1.12837	0.83171
Gabra6	0.22603	0.41804	1.10566	0.81753
Gpr123	0.85252	0.98506	1.00452	0.96201
Gpr22	0.97257	0.94951	1.05034	0.74617
Gpx3	0.99211	1.07435	1.44456	1.02130
Htr5b	0.64450	0.91455	0.83605	0.85427
Ifng2	0.89560	1.08788	0.98146	0.83641
Kit	0.90101	1.00556	1.04286	0.95011
Lg2	0.91889	1.02148	1.07260	0.84901
Lypd1	0.94500	0.97854	1.16184	0.87548
Lyz1	3.00000	1.05277	0.93333	0.40000
Masp1	1.01142	1.09799	1.09044	1.03106
Nell2	0.98658	0.95585	0.98920	0.87862
Nrsn2	0.97652	0.96968	1.04528	0.97439
Nrxn3	0.94176	0.99824	1.08387	0.88878
Olfm2	0.97800	0.99624	1.13655	0.98522
Olfm3	0.93957	0.99283	1.00783	0.68529
Slc24a3	0.97248	1.04156	1.00881	0.94110
Tspan9	0.95895	1.09685	0.95871	0.88793
Abcg2	0.94996	0.98976	1.04891	0.93277
AcsL5	0.93669	1.00475	1.05375	0.93290
Adam11	0.84784	0.94712	0.98755	0.93736
Adam23	1.03197	0.95247	1.06605	0.91633
Ajap1	1.08072	0.95746	0.97935	1.11578
Ap2a2	0.99446	0.95000	1.09039	0.95765
BAI3	1.01466	1.15506	3.02759	0.30338
Chln3	0.54417	0.86901	1.02960	0.88351
Cbln4	0.96376	0.95449	1.49595	0.94935
Cd151	0.94594	0.90013	1.01765	0.92715
Cdh13	0.98014	0.93411	1.07642	0.95655
Cdh9	0.92776	1.00963	1.34275	1.02703
Ctnnap2	0.92867	0.94720	1.01935	0.99324
Crh	0.90571	0.85633	0.90654	0.38755
Efn3	0.99955	1.03684	1.07197	1.04074
Dusp15	0.97853	1.03554	0.99702	1.05678
Dner	0.95787	1.03892	1.06858	0.98799
Dgcr2	0.98869	0.96722	1.03015	0.98996
CxCl12	0.91784	0.83454	1.01103	0.85536
Cx3c11	0.90875	0.94759	1.04301	0.93006
Gal	0.92510	1.08224	2.01526	1.43261
Gab2	0.93739	1.12682	1.07603	1.03645
Fstl1	0.89085	0.85906	0.94466	1.07404
F2r	0.93002	0.92937	1.32201	1.00817
Epha4	0.98256	0.98647	1.13436	1.08120
Egfl7	0.93636	0.95009	1.35315	1.09346
Itgav	1.03497	1.00512	1.06280	0.95677
Inad1	0.95054	0.94184	0.98800	0.93857
Il16	0.73343	0.86032	0.99672	0.95749
Il10b	0.94610	0.89533	1.15873	0.94300
Grid2	0.90914	1.02781	1.04418	1.00864
Gm4980	0.76241	0.93363	1.00989	1.04384
Ntm	0.96600	1.03963	1.04299	0.89793
Nrcam	0.95982	0.85247	1.14220	0.96862
Nell1	0.90597	1.00039	1.24087	0.90837
Lrn5	0.96826	0.98196	1.18531	0.93344
Lin7c	0.92735	1.11366	1.04439	0.99897
Lemd1	0.80879	0.87000	1.35760	0.70318
Ramp3	0.98637	1.11995	1.09973	0.93411
Pvrl2	0.95763	0.91139	1.19083	0.79241
Ptpn	0.89597	0.93431	1.04626	1.01440
Pcdh20	0.97286	0.88455	1.12094	0.94646
Sema4f	0.95389	0.86184	1.17330	0.89830
Sema4a	1.02067	0.95366	1.08667	0.97899
Sdc1	0.98929	1.13042	0.98030	0.96302
Scarb1	0.95514	1.06191	1.14891	0.96131
S100a6	0.97186	1.01645	1.07862	0.94804
S100a10	0.95616	0.84834	0.97664	0.80875

Tnfrsf21	0.93816	0.96386	1.12329	0.90851
Tmem205	0.93828	0.94686	1.11314	0.88418
Tmeff1	0.97993	1.01015	1.07107	0.92115
Thy1	0.93759	0.93158	1.14788	0.87855
Tgfb2	0.92633	0.96072	1.11835	0.89019
Susd4	0.89712	0.97135	1.13963	0.79841
Vstm2b	1.00532	1.11496	1.11846	0.99743
Vegfb	0.93365	1.09755	1.08237	0.88849
Unc13c	0.95747	0.96401	1.16882	0.79389
Tspan31	0.93416	1.18481	0.73808	1.01146
Tspan12	0.93209	0.85026	0.97888	0.95601
Bmp5	1.01478	1.08162	1.13052	0.79256
C3	1.16577	1.27597	0.23766	0.71739
Comp	0.98462	0.80174	1.07221	1.25882
Crlf1	1.36364	0.99302	0.82609	1.06306
Crtam	0.93370	1.18655	0.99525	0.75034
Cxcr7	1.03125	0.38770	0.79221	0.52767
Dusp5	1.21081	1.01634	1.19603	0.67481
Gabrd	1.05574	1.08069	0.99772	0.95701
Gpr64	0.86715	1.00431	1.14815	0.90889
Gpr88	0.93503	0.91928	0.93362	0.61942
Ifitm1	1.05233	0.89227	0.83382	0.79123
Il17re	1.00000	0.94192	1.11755	0.82516
Lgals3	1.27957	1.39986	0.89720	0.99535
Imo2	0.98852	0.99180	0.99085	0.94713
Nf3	0.94545	0.86511	1.01468	0.87979
Pcp4l1	0.94590	1.06528	1.01714	0.91579
Pex5l	0.92565	0.95677	1.00373	0.90273
Slpr3	1.18919	0.82316	0.92171	0.54897
Spint2	1.05188	1.02577	0.99296	1.04252
Tmem204	1.02802	1.09226	1.00161	0.91298
Wnt7a	0.97953	1.04602	1.05785	0.88475
I810041L15Rik	1.02096	1.00615	0.96726	0.93691
Tmem248	0.99382	0.92385	1.00637	1.00704
Mgp	1.11528	1.04302	0.95778	1.02789
Misd6	1.04210	0.97097	1.06200	0.87689
Mboat7	1.03698	0.99865	1.02104	0.96887
March11	1.06022	0.95888	1.12828	0.93594
Ache	0.96813	1.01835	0.99845	0.92794
Ndnf	1.02238	1.02025	0.95730	0.95219
A730017C20Rik	0.93640	1.00075	1.09702	0.92644
6430571L13Rik	0.93086	1.03877	0.92598	0.92611
Vstm5	1.01519	1.05127	1.11214	0.95754
fam210b	0.85983	0.99775	0.93433	1.04637
Aqp6	1.14943	1.25999	1.05205	0.88215
Anxa2	1.02689	0.88953	0.99293	0.93221
Amhr2	1.24432	0.82106	1.35356	0.54741
Alox5ap	0.99085	0.91738	1.06116	0.87969
Adcyap1	0.96680	1.01444	1.22706	0.85705
Adcy2	0.92516	1.05055	0.95398	0.95131
Atp1b1	1.00541	0.94469	1.05408	0.91064
Atp13a2	0.97432	0.99993	0.99442	0.98742
Asph	1.00425	0.97609	0.99727	0.87105
asap1	1.05483	1.01567	1.02410	0.95304
Armxc2	0.97005	1.00872	1.02357	0.89150
Arhgap15	1.02778	0.91255	0.87379	1.29825
Cartpt	1.15973	1.10904	2.25269	1.48329
Cacng5	1.18198	1.09623	1.02481	0.85208
Cacna1g	0.97378	0.96407	1.01822	0.89182
Itbd11	0.97779	1.03736	1.04862	0.84487
Bgn	1.03506	0.87556	0.98385	0.91738
BC048546	1.00000	1.52464	0.85000	1.15789
Cdon	1.10327	1.13378	0.97958	0.69486
Cdh15	1.00559	1.03946	0.99690	0.77204
Cd302	0.97167	1.24530	1.20993	0.70896
Cd24a	1.03735	1.19148	1.09658	0.95613
Cd164l2	0.95918	1.12968	0.90406	0.89042
Casc4	0.94397	1.17318	0.89006	1.16651
Cgrefl	0.97345	1.00604	0.96780	1.06029
Chid1	0.96156	0.93354	0.80982	1.04765
Cklf	0.99631	1.02460	0.87032	1.08030
Clec10a	0.91736	0.83989	1.04561	0.92630
Clu	0.92777	0.89899	0.78256	1.01428
Cnksr2	0.98287	0.90374	0.86227	0.90201
Cnr1	0.98356	0.90156	0.82692	1.12974
Cop2	0.99676	0.96764	0.84881	1.03750

Crf2	0.90402	0.99037	0.73665	1.25878
Crtap	0.95190	0.94765	0.82852	1.06633
Ctgf	1.18312	1.51161	0.82931	4.93957
Ctla2a	1.14752	1.06623	0.94310	1.10623
Ctla2b	1.25000	1.08452	0.85481	0.96557
Cttn1	0.90391	0.94645	0.98125	1.05161
Cttn2	0.98486	0.90912	0.96460	1.07882
Cyb561	0.96175	0.87916	0.81175	0.99309
Cyb561d2	0.96289	0.95269	0.95802	0.98127
Diras2	1.01174	0.89579	0.80145	0.99567
Dirc2	0.97509	0.86555	0.82831	
Dlg4	1.04617	0.85890	0.86170	1.01007
Dlgap1	1.04528	0.89756	0.90099	1.00121
Dnaj4	0.97675	0.91000	0.91232	0.85147
Dnaj15	0.96613	0.88818	0.87445	0.98116
Dock4	1.01060	0.89409	0.89622	0.87992
Dos	0.92842	0.92136	0.85637	0.95928
E130311K13Rik	0.96762	0.88181	0.85967	1.01721
Ecel1	0.97361	0.91873	1.47473	1.23823
Ehd1	0.95712	0.95174	0.82469	1.01795
Elmo1	1.04306	0.82929	0.86789	0.89776
Emb	1.01497	0.99296	0.81583	1.16707
Ewc2	1.01515	0.97053	0.88079	1.13950
Fam174b	0.97979	0.88188	0.85318	1.02361
Fam189a1	0.95183	0.99285	0.97190	1.12650
Fam19a1	0.99105	0.89483	0.90000	1.03356
Fam20c	0.98623	0.94280	0.80863	1.08866
Fam3c	1.02269	0.89179	0.96316	1.04716
Fgl2	0.96481	0.98623	0.75294	1.17057
Fuca2	0.99380	0.88451	0.88082	1.03947
Fxyd1	1.04381	0.94763	0.75485	1.03601
Fxyd7	0.94207	0.85424	0.90773	0.95630
Fzd7	1.00425	0.86249	0.75369	0.90938
Gabra4	0.99210	0.91608	0.94626	0.99951
Gabra5	1.00313	0.94376	1.01629	1.10582
Gabrg1	0.97149	0.85610	0.82217	1.01201
Gpr125	1.03731	0.89324	0.82476	1.05246
Gpr1bb	0.78857	0.86929	0.86724	1.03815
Gng5	0.94176	0.92556	0.79419	1.12111
Gng4	0.97367	0.97318	0.91514	0.89229
Gm5868	0.80635	0.92100	0.72304	1.17555
Gjd2	0.96960	0.93899	0.96581	1.04801
Gpr45	0.99840	0.89553	0.82481	0.81295
Gpr26	0.97289	0.91437	1.05047	1.00804
Gpr25	0.81858	0.83343	0.82812	1.08359
Gpr176	1.05339	0.97170	0.98857	1.09705
Gpr137b-ps	0.98387	0.80857	0.94930	0.85815
Gpr137b	0.95695	0.83899	0.82535	0.90132
Gmn4				

Kcnk12	1,05787	0,95151	1,15036	0,79300
Lypd6b	0,90517	1,25024	1,02833	0,78226
Lyo6h	0,93965	1,06869	1,05590	1,33597
Lypd6	0,97463	1,12931	1,04153	0,87270
Lpl	0,90233	1,00477	0,58954	0,95447
Lphn2	1,01407	1,08486	0,79352	0,96956
Lhfp15	0,91422	0,99953	0,85802	1,10005
Actb	1,05298	1,08321	0,89080	0,99040
C1ql1	0,97759	0,95900	0,89442	1,05598
Cbln1	1,11386	1,08540	0,84178	0,97814
Mmp15	1,04735	1,06160	0,87450	1,00199
Mrv1	1,06425	1,01531	1,15395	0,83204
Nat8l	1,01786	0,91956	0,94951	0,91135
Ninj1	1,07299	0,92822	0,94013	1,13252
Npc2	1,07298	1,00156	0,80988	0,95062
Npnt	0,98520	1,02155	0,81574	1,11281
Npx2	1,03928	1,07494	0,94111	0,91225
Odz3	1,11806	0,97147	0,88133	1,03942
Opr1	1,17514	0,86896	0,89556	0,71002
Oscpl	1,05155	1,02053	0,80955	1,09863
Panx1	1,07660	1,04719	0,86405	0,97560
Pard6b	1,11254	0,91328	0,91210	0,79345
Pcolce	1,14973	0,99486	0,89132	0,95055
Pesk5	1,22935	1,02584	0,83179	1,04167
Pde2a	1,00858	0,93180	0,84635	0,96504
Plp2	1,22739	0,93348	0,78925	0,95454
Plxdc1	1,06078	0,91270	0,87263	0,90029
Pmepa1	1,11324	0,93168	0,99934	0,90634
Popdc3	1,11029	0,91327	1,23188	0,90945
Ppap2c	1,15111	1,14823	0,91570	1,03340
Prmt8	1,04690	1,03234	0,90962	0,94906
Prss23	1,14735	0,96150	0,88183	0,93828
Ptn	1,01511	0,99403	0,86635	0,98660
Ptplad2	0,96368	0,84662	0,88404	0,97336
Qpct1	1,00535	0,99465	0,88779	1,03991
Rab6b	1,18761	1,02818	0,85600	0,95122
Rab71l	1,11190	0,88737	0,90496	0,86706
Rasgrp2	1,08082	1,01938	0,94898	0,91092
Rel2	0,97389	0,98331	0,82658	0,99217
Resp18	1,14155	0,94741	0,95376	0,91256
Rgs19	1,08752	1,04425	0,88606	0,86443
Rhbdd2	1,08644	1,01469	0,91846	0,93383
Rnaset2a	1,15528	1,03828	0,92564	0,89758
Rnaset2b	1,19122	0,95378	0,92652	0,98054
Rnf19b	1,10687	0,99581	0,90032	0,88923
Rock2	1,10291	1,03717	0,94704	0,86470
Rtn4r	0,98828	1,02733	0,83765	0,84843
Rtn4r12	1,07853	0,88236	1,13585	0,94157
S100a4	1,15209	1,07906	0,82966	1,00756
Scn3a	1,12589	1,01596	1,12751	1,00562
Scn3b	1,07973	0,99574	0,98812	1,05853
Serpinf1	1,17739	0,85929	0,91789	0,96353
Sh3gl2	1,03009	0,90643	0,86968	0,93033
Shisa4	1,15981	0,94885	0,84868	0,94939
slc24a5	1,36842	1,07563	1,07684	1,00000
Slc22a23	1,14272	1,02708	0,91078	0,97882
Slc20a1	1,13344	0,87366	0,90261	0,88926
Slc1a4	1,11370	0,96456	0,90334	0,98277
Slc17a7	1,05547	0,76454	0,91902	0,93762
Slc10a4	1,11854	1,01275	3,92381	1,04722
Spns2	1,11326	1,01041	0,87582	1,00646
Smpd13a	1,06227	0,93773	0,86128	0,96287
Sln	0,74627	1,15978	0,94624	0,69152
Slc4a2	1,06382	0,98141	0,82724	0,92308
slc30a10	1,16913	0,99509	0,93746	0,90097
Slc25a1	1,16082	0,95654	0,92795	0,97538
Syng3	1,12207	1,01629	0,93027	0,94494
Stxbp5	1,15315	0,97512	0,93816	0,90355
Stx1a	1,15842	1,02148	1,00000	1,05184
Sbd1	1,18834	0,93618	1,09014	1,24900
Stap2	1,42623	0,81175	0,88351	0,86629
Srgn	1,21786	0,92366	0,90026	0,94404
Tgfb1	1,15703	0,85583	0,89113	1,00761
Tex2l	1,80000	0,45256	0,69136	0,29167
Tctn2	1,29817	0,97719	0,92610	0,98239
Sytl2	1,26304	0,95566	0,85223	0,96598
Syt9	1,27732	1,06640	0,94477	1,02560

Syt12	1,15425	0,98790	0,92590	0,87282
Tmem179	1,22518	1,02023	0,99779	1,02607
Tmem159	1,10220	1,03384	0,87650	0,92627
Tmem14a	1,17522	0,96475	0,92339	0,93260
Tmed10	1,17547	0,98670	0,90108	0,95155
Tm6sf1	1,26945	0,96795	1,00630	0,89671
Timp2	1,12807	1,00499	0,88596	1,04297
Tmem42	1,22460	1,05488	0,90053	0,91244
Tmem191c	1,08840	1,02527	0,86544	1,09217
Tmem19	1,10893	0,93860	0,88474	0,91788
Tmem184b	1,18334	0,99906	0,90045	0,88425
Tmem180	1,16578	0,97483	1,01064	0,85004
Tmem179b	1,02857	1,00525	0,93482	0,82313
Twsg1	1,16630	1,02091	0,92902	0,97349
Tspan6	1,11667	1,04108	1,12197	0,93909
Trhde	1,17871	1,05741	1,12914	0,90640
Tnfsf9	1,37273	0,96582	0,98088	0,80582
Tnfrsf11b	1,21622	0,96854	1,12376	0,81504
Tmie	1,08225	1,15804	0,96772	0,92008
Znrf2	1,26466	1,08008	1,06292	0,99366
Znrf1	1,16838	1,07501	1,08125	
Zdhc22	1,06224	1,01885	0,95506	1,07357
Vstm2l	1,18585	1,04666	1,13142	0,84598
Vstm2a	1,28970	1,09953	0,84571	0,97468
Vps37b	1,11902	0,99360	0,73714	1,38683

Supplementary table 2: Results of the RT-PCR, in the four extracts.

Mean and SEM of RT-PCR values for each gene normalized to rp113. Values are calculated following this formula: $2^{-(CT(\text{gene})-CT(\text{Rp113}))}$. n=5 vehicle and PCP mice for brainstem and cerebellum P30 groups, n=4 vehicle and PCP mice for brainstem and cerebellum P11 groups.

Gene	Brainstem P30				Brainstem P11				Cerebellum P30				Cerebellum P11			
	Mean Vehicle	SEM Vehicle	Mean PCP	SEM PCP	Mean Vehicle	SEM Vehicle	Mean PCP	SEM PCP	Mean Vehicle	SEM Vehicle	Mean PCP	SEM PCP	Mean Vehicle	SEM Vehicle	Mean PCP	SEM PCP
B2m	0.4235	0.0286	0.3829	0.0203	0.2308	0.0114	0.2352	0.0135	0.3084	0.0125	0.3544	0.0178	0.1338	0.0104	0.1093	0.0035
Bai1	0.9080	0.0416	0.8961	0.0348	0.8954	0.0273	0.8458	0.0239	0.7233	0.0639	0.8429	0.0377	0.3578	0.0204	0.3229	0.0098
Boc	0.0854	0.0050	0.0890	0.0096	0.0570	0.0040	0.0601	0.0022	0.5054	0.0438	0.5622	0.0183	0.2458	0.0129	0.1899	0.0081
Cadp2	0.0348	0.0021	0.0325	0.0008	0.0373	0.0034	0.0447	0.0030	0.5330	0.0598	0.6235	0.0269	0.3804	0.0214	0.3714	0.0303
cc15	0.0021	0.0005	0.0013	0.0002	0.0002	0.0000	0.0004	0.0001	0.0008	0.0003	0.0008	0.0002	0.0003	0.0001	0.0002	0.0000
Chn2	0.2064	0.0091	0.2037	0.0055	0.1785	0.0082	0.1740	0.0057	2.9276	0.0848	2.9476	0.1441	0.4964	0.0434	0.4038	0.0133
Cnih3	0.0706	0.0086	0.0569	0.0059	0.0562	0.0030	0.0623	0.0053	0.0223	0.0013	0.0201	0.0010	0.0136	0.0005	0.0138	0.0006
Crtac	0.7489	0.0337	0.6949	0.0260	0.7004	0.0275	0.7054	0.0429	0.0525	0.0043	0.0561	0.0034	0.0716	0.0020	0.0714	0.0036
Cthrc1	0.0816	0.0005	0.0776	0.0029	0.1454	0.0069	0.1398	0.0071	0.0712	0.0058	0.0803	0.0037	0.0448	0.0019	0.0373	0.0014
Fos	0.0677	0.0071	0.0735	0.0027	0.0450	0.0013	0.1020	0.0087	0.1015	0.0538	0.1352	0.0265	0.0200	0.0012	0.0297	0.0025
Gabra6	0.0029	0.0010	0.0007	0.0001	0.0021	0.0006	0.0009	0.0002	4.1480	0.1418	4.5862	0.2786	0.8393	0.0781	0.6862	0.0405
Gpr123	0.3599	0.0177	0.3068	0.0093	0.2855	0.0166	0.2813	0.0160	0.1734	0.0139	0.1742	0.0048	0.0854	0.0047	0.0822	0.0021
Gpr22	0.1035	0.0047	0.1007	0.0046	0.0759	0.0044	0.0720	0.0031	0.4373	0.0157	0.4593	0.0133	0.0467	0.0033	0.0349	0.0011
Gpx3	0.1318	0.0044	0.1307	0.0009	0.1367	0.0045	0.1469	0.0092	0.0094	0.0009	0.0136	0.0041	0.0196	0.0009	0.0200	0.0007
Htr5b	0.0520	0.0136	0.0335	0.0084	0.0320	0.0034	0.0293	0.0034	0.0016	0.0002	0.0013	0.0002	0.0010	0.0001	0.0008	0.0001
Ingr2	0.2632	0.0109	0.2357	0.0137	0.2570	0.0101	0.2796	0.0217	0.2804	0.0095	0.2752	0.0071	0.1780	0.0149	0.1488	0.0046
Kit	0.0596	0.0032	0.0537	0.0011	0.0673	0.0037	0.0677	0.0053	0.2886	0.0133	0.3010	0.0157	0.1008	0.0046	0.0957	0.0031
Lgi2	1.1634	0.0533	1.0691	0.0459	0.6799	0.0372	0.6945	0.0266	0.5759	0.0464	0.6177	0.0460	0.1927	0.0113	0.1636	0.0040
Lypd1	0.1706	0.0082	0.1612	0.0071	0.2183	0.0055	0.2136	0.0099	0.0440	0.0040	0.0511	0.0021	0.0262	0.0010	0.0230	0.0006
Lyz1	0.0001	0.0000	0.0002	0.0001	0.0003	0.0001	0.0003	0.0000	0.0001	0.0000	0.0001	0.0000	0.0001	0.0000	0.0000	0.0000
Masp1	0.1593	0.0026	0.1611	0.0071	0.1020	0.0075	0.1120	0.0039	0.0882	0.0055	0.0962	0.0041	0.0829	0.0028	0.0855	0.0030
Nel1	0.6619	0.0352	0.6530	0.0170	0.9018	0.0536	0.8620	0.0552	1.9605	0.0944	1.9394	0.0691	0.8219	0.0406	0.7222	0.0242
Nrsn2	0.7870	0.0187	0.7685	0.0315	0.5477	0.0215	0.5311	0.0253	0.2706	0.0112	0.2828	0.0081	0.0804	0.0023	0.0784	0.0035
Nrxn3	0.7723	0.0273	0.7273	0.0329	0.5663	0.0369	0.5653	0.0355	2.0733	0.1271	2.2472	0.1181	0.5186	0.0417	0.4609	0.0148
Offm2	0.2427	0.0060	0.2374	0.0099	0.2855	0.0113	0.2845	0.0227	0.0406	0.0030	0.0461	0.0016	0.0365	0.0009	0.0360	0.0010
Offm3	0.1178	0.0030	0.1107	0.0033	0.1660	0.0079	0.1648	0.0072	0.6968	0.0337	0.7022	0.0383	0.0815	0.0085	0.0558	0.0041
Slc24a3	0.2260	0.0077	0.2198	0.0097	0.3049	0.0215	0.3176	0.0169	0.2647	0.0181	0.2671	0.0092	0.0820	0.0038	0.0771	0.0021
Tspan9	0.3347	0.0093	0.3209	0.0228	0.3413	0.0225	0.3744	0.0193	1.4783	0.0840	1.4173	0.0441	0.5229	0.0316	0.4643	0.0239
Ahcg2	0.0556	0.0029	0.0528	0.0039	0.0371	0.0014	0.0367	0.0019	0.0370	0.0036	0.0388	0.0036	0.0300	0.0007	0.0280	0.0008
Acs15	0.0834	0.0024	0.0781	0.0025	0.0686	0.0026	0.0689	0.0034	0.0328	0.0013	0.0345	0.0015	0.0187	0.0007	0.0174	0.0004
Adam11	0.2907	0.0092	0.2465	0.0082	0.1514	0.0059	0.1434	0.0074	0.7657	0.0532	0.7561	0.0269	0.1347	0.0110	0.1262	0.0056
Adam23	0.8778	0.0425	0.9059	0.0269	0.5626	0.0233	0.5359	0.0251	0.8619	0.0381	0.9189	0.0335	0.2833	0.0166	0.2596	0.0103
Aiap1	0.0728	0.0023	0.0787	0.0029	0.1457	0.0048	0.1395	0.0085	0.0714	0.0084	0.0699	0.0045	0.0339	0.0018	0.0378	0.0021
An2a2	0.6032	0.0225	0.5999	0.0243	0.6641	0.0418	0.6309	0.0330	1.2949	0.0722	1.4120	0.0746	0.5793	0.0231	0.5547	0.0223
BAI3	0.0177	0.0072	0.0180	0.0045	0.0204	0.0065	0.0236	0.0080	0.0144	0.0087	0.0437	0.0109	0.0293	0.0017	0.0089	0.0088
Clql1	0.2646	0.0465	0.2207	0.0377	0.3952	0.0331	0.3621	0.0209	0.0384	0.0019	0.0375	0.0010	0.1128	0.0026	0.1250	0.0055
Cbln1	0.1646	0.0054	0.1641	0.0088	0.2015	0.0095	0.2101	0.0191	3.2303	0.0652	3.2134	0.0725	1.1024	0.0718	1.1023	0.0385
Cbln3	0.0057	0.0008	0.0031	0.0002	0.0030	0.0001	0.0026	0.0001	2.7461	0.1632	2.8274	0.1505	0.3268	0.0366	0.2887	0.0257
Cbln4	0.0905	0.0031	0.0872	0.0023	0.1617	0.0079	0.1544	0.0155	0.0039	0.0004	0.0059	0.0013	0.0035	0.0001	0.0033	0.0001
Cd151	0.1913	0.0092	0.1809	0.0098	0.1094	0.0061	0.0985	0.0033	0.1647	0.0044	0.1676	0.0097	0.0649	0.0020	0.0602	0.0010
Cdh13	0.3243	0.0119	0.3178	0.0054	0.6712	0.0308	0.6270	0.0574	0.0092	0.0062	0.1068	0.0060	0.2054	0.0048	0.1965	0.0060
Cdh9	0.0246	0.0006	0.0229	0.0004	0.0330	0.0018	0.0333	0.0023	0.0033	0.0002	0.0045	0.0005	0.0069	0.0002	0.0071	0.0008
Cntnap2	0.2568	0.0085	0.2385	0.0042	0.2046	0.0152	0.1938	0.0156	0.1939	0.0112	0.1977	0.0076	0.0636	0.0035	0.0632	0.0032
Crh	0.2017	0.0355	0.1827	0.0420	0.1316	0.0145	0.1127	0.0093	0.0155	0.0118	0.0140	0.0065	0.0018	0.0009	0.0007	0.0003
Efn3a	0.0895	0.0045	0.0895	0.0050	0.1269	0.0058	0.1316	0.0098	0.0326	0.0021	0.0349	0.0014	0.0249	0.0010	0.0259	0.0013
Dusp15	0.1668	0.0065	0.1632	0.0072	0.1957	0.0026	0.2026	0.0086	0.1209	0.0070	0.1205	0.0022	0.0680	0.0021	0.0719	0.0038
Dner	0.4007	0.0138	0.3838	0.0141	0.5372	0.0278	0.5582	0.0448	1.3678	0.0814	1.4616	0.0671	0.7470	0.0217	0.7380	0.0164
Dger2	0.3007	0.0083	0.2973	0.0098	0.2830	0.0147	0.2737	0.0149	0.6020	0.0373	0.6201	0.0303	0.2948	0.0079	0.2918	0.0093
CxCl12	0.1706	0.0081	0.1566	0.0084	0.1151	0.0062	0.0961	0.0056	0.2576	0.0111	0.2604	0.0132	0.1804	0.0063	0.1543	0.0033
Cx3c11	1.2306	0.0168	1.1183	0.0419	1.2225	0.0856	1.1584	0.0643	0.3434	0.0153	0.3581	0.0300	0.0632	0.0050	0.0588	0.0029
Gal	0.1100	0.0058	0.1018	0.0056	0.0962	0.0064	0.1041	0.0051	0.0034	0.0003	0.0069	0.0024	0.0065	0.0001	0.0093	0.0002
Gab2	0.0447	0.0012	0.0419	0.0010	0.0398	0.0028	0.0448	0.0006	0.0336	0.0031	0.0362	0.0013	0.0194	0.0003	0.0201	0.0008
Fst1	0.4220	0.0160	0.3759	0.0087	0.3782	0.0226	0.3249	0.0157	0.1343	0.0079	0.1269	0.0050	0.1329	0.0022	0.1428	0.0027
F2r	0.0403	0.0019	0.0375	0.0019	0.0471	0.0019	0.0438	0.0025	0.0132	0.0013	0.0175	0.0008	0.0545	0.0012	0.0549	0.0020
Epha4	0.0917	0.0021	0.0902	0.0022	0.1258	0.0045	0.1241	0.0070	0.0648	0.0051	0.0736	0.0032	0.0304	0.0018	0.0328	0.0014
Egfl7	0.0582	0.0031	0.0544	0.0021	0.0515	0.0018	0.0490	0.0014	0.0256	0.0021	0.0346	0.0026	0.0186	0.0005	0.0204	0.0011
Igav	0.2505	0.0006	0.2592	0.0072	0.1370	0.0103	0.1377	0.0044	0.1593	0.0097	0.1693	0.0103	0.0876	0.0030	0.0838	0.0048
Inad1	0.2964	0.0133	0.2817	0.0098	0.1463	0.0087	0.1378	0.0046	0.6524	0.0226	0.6445	0.0237	0.0366	0.0026	0.0343	0.0021
I116	0.0136	0.0011	0.0100	0.0009	0.0104	0.0004	0.0004	0.0009	0.0007	0.0014	0.0008	0.0013	0.0014	0.0003	0.0014	0.0003
I110rb	0.0289	0.0019	0.0274	0.0018	0.0212	0.0007	0.0190	0.0009	0.0197	0.0016	0.0228	0.0019	0.0091	0.0003	0.0086	0.0004
Gria2	0.0729	0.0025	0.0662	0.0012	0.0929	0.0057	0.0955	0.0043	0.7745	0.0371	0.8087	0.0309	0.2860	0.0145	0.2885	0.0075
Gim4980	0.0967	0.0064	0.0738	0.0081	0.1157	0.0075	0.1080	0.0084	0.0332	0.0110	0.0335	0.0083	0.0208	0.0020	0.0217	0.0016
Ntn	0.5082	0.0165	0.4909	0.0179	0.5771	0.0308	0.5999	0.0272	1.4419	0.0622	1.5039	0.0424	0.7315	0.0433	0.6568	0.0147
Nrcam	0.9532	0.0427	0.9149	0.0397</												

Gpr88	0.0416	0.0082	0.0389	0.0065	0.0301	0.0035	0.0277	0.0019	0.0079	0.0068	0.0073	0.0044	0.0013	0.0004	0.0008	0.0001
Ifitm1	0.0309	0.0053	0.0326	0.0091	0.0199	0.0011	0.0177	0.0012	0.0546	0.0192	0.0455	0.0107	0.0126	0.0013	0.0100	0.0004
I117re	0.0007	0.0001	0.0007	0.0001	0.0007	0.0000	0.0007	0.0001	0.0105	0.0010	0.0117	0.0007	0.0015	0.0001	0.0013	0.0002
Lgals3	0.0019	0.0002	0.0024	0.0003	0.0004	0.0000	0.0006	0.0001	0.0013	0.0003	0.0012	0.0002	0.0011	0.0001	0.0011	0.0001
Mbl2	0.0000	0.0000	0.0000	0.0000	0.0000	0.0000	0.0000	0.0000	0.0000	0.0000	0.0000	0.0000	0.0001	0.0001	0.0000	0.0000
Nif3	0.0022	0.0003	0.0021	0.0002	0.0056	0.0003	0.0049	0.0005	0.1733	0.0150	0.1759	0.0054	0.1454	0.0027	0.1279	0.0100
Pcp4l1	1.1474	0.0275	1.0853	0.0308	0.4843	0.0227	0.5159	0.0136	0.2450	0.0090	0.2492	0.0090	0.0719	0.0030	0.0658	0.0035
Pex51	1.0980	0.0155	1.0164	0.0327	0.2207	0.0144	0.2112	0.0133	0.2557	0.0136	0.2567	0.0097	0.0124	0.0006	0.0112	0.0007
Pkib	0.0250	0.0008	0.0253	0.0010	0.0216	0.0007	0.0201	0.0007	0.2168	0.0108	0.2077	0.0088	0.0712	0.0033	0.0639	0.0040
S1pr3	0.0007	0.0001	0.0009	0.0001	0.0005	0.0001	0.0005	0.0001	0.0063	0.0049	0.0058	0.0032	0.0010	0.0004	0.0005	0.0001
Spin2	0.0378	0.0017	0.0398	0.0028	0.0526	0.0022	0.0539	0.0036	0.0957	0.0049	0.0950	0.0041	0.0486	0.0023	0.0506	0.0027
Tmem204	0.0721	0.0008	0.0741	0.0025	0.0457	0.0016	0.0499	0.0020	0.1318	0.0087	0.1320	0.0042	0.0507	0.0014	0.0463	0.0031
Wnt7a	0.0625	0.0029	0.0613	0.0041	0.0456	0.0017	0.0477	0.0017	0.2542	0.0157	0.2689	0.0103	0.0589	0.0021	0.0521	0.0031
I1810041L13Rik	0.0582	0.0025	0.0594	0.0012	0.0872	0.0032	0.0878	0.0040	0.0225	0.0008	0.0218	0.0012	0.0477	0.0006	0.0447	0.0020
Tmem248	0.1781	0.0027	0.1770	0.0038	0.1649	0.0026	0.1523	0.0102	0.1608	0.0097	0.1618	0.0064	0.0781	0.0025	0.0787	0.0038
Mgp	0.1456	0.0366	0.1623	0.0546	0.0812	0.0027	0.0847	0.0045	0.1721	0.0193	0.1648	0.0119	0.0311	0.0026	0.0320	0.0037
Mfsd6	0.2817	0.0032	0.2936	0.0061	0.1480	0.0059	0.1437	0.0089	0.1521	0.0101	0.1616	0.0080	0.0532	0.0019	0.0466	0.0025
Mboat7	0.1822	0.0048	0.1890	0.0088	0.1585	0.0044	0.1583	0.0090	0.1179	0.0069	0.1204	0.0044	0.0499	0.0005	0.0483	0.0023
March11	0.0093	0.0006	0.0098	0.0006	0.0099	0.0006	0.0095	0.0005	0.0233	0.0028	0.0263	0.0014	0.0155	0.0005	0.0145	0.0011
Ache	1.1979	0.0352	1.1597	0.0215	1.1431	0.0368	1.1641	0.0855	0.3992	0.0158	0.3986	0.0217	0.1054	0.0037	0.0978	0.0063
Ndnf	0.1591	0.0071	0.1626	0.0043	0.1825	0.0089	0.1862	0.0138	0.0536	0.0037	0.0513	0.0031	0.0247	0.0002	0.0235	0.0007
A730017C20Rik	0.2991	0.0047	0.2800	0.0071	0.2798	0.0033	0.2800	0.0175	0.0347	0.0018	0.0380	0.0031	0.0284	0.0008	0.0264	0.0013
6430571L13Rik	0.0237	0.0013	0.0221	0.0013	0.0207	0.0008	0.0215	0.0011	0.1373	0.0071	0.1272	0.0057	0.0459	0.0018	0.0425	0.0024
Vstm5	0.0408	0.0009	0.0414	0.0009	0.0393	0.0010	0.0413	0.0020	0.0047	0.0003	0.0053	0.0003	0.0029	0.0001	0.0028	0.0002
fam210b	0.1361	0.0063	0.1171	0.0050	0.0998	0.0041	0.0996	0.0021	0.1050	0.0037	0.0981	0.0028	0.1038	0.0060	0.1087	0.0037
Aqp6	0.0069	0.0002	0.0080	0.0004	0.0022	0.0001	0.0028	0.0002	0.0950	0.0062	0.1000	0.0042	0.0087	0.0005	0.0077	0.0005
Anxa2	0.0729	0.0051	0.0749	0.0077	0.0849	0.0026	0.0755	0.0023	0.0370	0.0031	0.0368	0.0024	0.0238	0.0012	0.0222	0.0011
Amhr2	0.0035	0.0003	0.0044	0.0002	0.0016	0.0001	0.0013	0.0001	0.0025	0.0002	0.0033	0.0001	0.0006	0.0001	0.0003	0.0000
Alox5ap	0.0371	0.0012	0.0368	0.0017	0.0254	0.0015	0.0233	0.0006	0.0298	0.0017	0.0316	0.0006	0.0162	0.0003	0.0143	0.0013
Adeyap1	0.2488	0.0082	0.2405	0.0123	0.2520	0.0093	0.2557	0.0105	0.0448	0.0030	0.0549	0.0045	0.0194	0.0003	0.0166	0.0010
Adey2	0.0775	0.0023	0.0717	0.0020	0.0802	0.0038	0.0843	0.0056	0.0475	0.0033	0.0453	0.0017	0.0138	0.0005	0.0131	0.0012
Atp1b1	5.7814	0.1110	5.8126	0.1214	4.1146	0.1137	3.8870	0.2802	5.3704	0.2797	5.6608	0.1751	1.4281	0.0482	1.3005	0.0712
Atp13a2	0.4431	0.0064	0.4317	0.0187	0.4977	0.0127	0.4977	0.0245	0.3275	0.0182	0.3257	0.0080	0.1660	0.0040	0.1639	0.0091
Asph	0.3244	0.0078	0.3258	0.0111	0.2059	0.0048	0.2010	0.0054	2.1263	0.0956	2.1205	0.0284	0.3611	0.0073	0.3146	0.0142
asap1	0.0948	0.0014	0.1000	0.0027	0.0847	0.0023	0.0860	0.0046	0.0622	0.0047	0.0637	0.0025	0.0258	0.0007	0.0246	0.0013
Armxc2	0.5570	0.0038	0.5403	0.0170	0.4601	0.0199	0.4641	0.0217	0.3390	0.0203	0.3469	0.0170	0.2950	0.0065	0.2630	0.0120
Arhgap15	0.0007	0.0001	0.0007	0.0001	0.0007	0.0001	0.0006	0.0001	0.0006	0.0001	0.0005	0.0001	0.0000	0.0000	0.0000	0.0000
Cartpt	0.2435	0.0063	0.2824	0.0118	0.2348	0.0085	0.2604	0.0073	0.0011	0.0001	0.0025	0.0010	0.0021	0.0002	0.0031	0.0008
Cacng5	0.0335	0.0007	0.0396	0.0027	0.0655	0.0010	0.0718	0.0031	0.1516	0.0115	0.1554	0.0050	0.0565	0.0012	0.0481	0.0020
Cacna1g	0.1160	0.0082	0.1129	0.0030	0.1492	0.0050	0.1438	0.0072	0.8811	0.0502	0.8972	0.0168	0.3763	0.0169	0.3356	0.0230
Bthd11	0.1513	0.0019	0.1479	0.0036	0.1796	0.0054	0.1863	0.0105	0.1077	0.0062	0.1129	0.0049	0.0540	0.0006	0.0457	0.0035
Bgn	0.1158	0.0096	0.1199	0.0237	0.1664	0.0029	0.1457	0.0089	0.1460	0.0115	0.1437	0.0068	0.1552	0.0095	0.1424	0.0038
BC048546	0.0001	0.0000	0.0001	0.0000	0.0001	0.0001	0.0001	0.0001	0.0000	0.0000	0.0000	0.0000	0.0000	0.0000	0.0000	0.0000
Cdon	0.0236	0.0017	0.0250	0.0014	0.0176	0.0009	0.0200	0.0011	0.0967	0.0105	0.0947	0.0069	0.0158	0.0005	0.0109	0.0006
Cdh15	0.0143	0.0006	0.0144	0.0015	0.0142	0.0010	0.0148	0.0005	0.2628	0.0124	0.2620	0.0185	0.0477	0.0022	0.0368	0.0040
Cd302	0.0480	0.0028	0.0466	0.0027	0.0416	0.0033	0.0518	0.0019	0.0374	0.0019	0.0452	0.0024	0.0248	0.0009	0.0175	0.0011
Cd24a	0.2190	0.0128	0.2272	0.0158	0.2020	0.0032	0.2406	0.0136	0.0894	0.0198	0.0981	0.0116	1.1487	0.0355	1.0983	0.0257
Cd11642	0.0323	0.0010	0.0310	0.0012	0.0218	0.0006	0.0247	0.0017	0.0232	0.0111	0.0210	0.0055	0.0060	0.0009	0.0053	0.0005
Case4	0.2991	0.0139	0.2824	0.0145	0.2916	0.0186	0.3421	0.0333	0.3960	0.0280	0.3525	0.0239	0.1984	0.0061	0.2315	0.0264
Cgref1	0.0686	0.0011	0.0668	0.0012	0.1285	0.0052	0.1292	0.0123	0.0298	0.0014	0.0289	0.0015	0.0263	0.0014	0.0279	0.0007
Chid1	0.1358	0.0049	0.1306	0.0038	0.1639	0.0102	0.1530	0.0113	0.1728	0.0062	0.1399	0.0097	0.0662	0.0020	0.0694	0.0030
Ckif	0.0217	0.0008	0.0216	0.0011	0.0194	0.0009	0.0199	0.0007	0.0175	0.0009	0.0152	0.0013	0.0234	0.0011	0.0253	0.0008
Clec10a	0.0024	0.0004	0.0022	0.0003	0.0015	0.0002	0.0013	0.0002	0.0035	0.0005	0.0036	0.0007	0.0017	0.0001	0.0016	0.0004
Clu	2.1128	0.0390	1.9602	0.0866	1.3006	0.0968	1.1704	0.0831	2.2744	0.1131	1.7798	0.1840	0.2583	0.0087	0.2620	0.0117
Cnksr2	0.0969	0.0022	0.0952	0.0036	0.0567	0.0044	0.0512	0.0042	0.5632	0.0280	0.4856	0.0462	0.0962	0.0061	0.0867	0.0027
Cnr1	0.5960	0.0234	0.5862	0.0164	0.6305	0.0518	0.6044	0.0552	6.6804	0.4642	5.5241	0.3256	1.3729	0.0448	1.5510	0.0308
Copz2	0.0247	0.0004	0.0246	0.0025	0.0166	0.0004	0.0161	0.0006	0.0334	0.0026	0.0284	0.0024	0.0131	0.0002	0.0136	0.0004
Crlf2	0.0064	0.0005	0.0068	0.0005	0.0078	0.0005	0.0077	0.0006	0.0077	0.0008	0.0057	0.0015	0.0027	0.0001	0.0034	0.0002
Crtap	0.0611	0.0025	0.0582	0.0033	0.0756	0.0032	0.0716	0.0053	0.0841	0.0068	0.0697	0.0059	0.0512	0.0026	0.0546	0.0013
Ctcf	0.0168	0.0015	0.0199	0.0035	0.0109	0.0005	0.0111	0.0013	0.0163	0.0036	0.0135	0.0011	0.0021	0.0002	0.0104	0.0011
Ctla2a	0.0294	0.0006	0.0337	0.0023	0.0418	0.0010	0.0446	0.0029	0.0459	0.0029	0.0433	0.0026	0.0236	0.0007	0.0261	0.0011
Ctla2b	0.0083	0.0007	0.0104	0.0010	0.0076	0.0002	0.0083	0.0007	0.0244	0.0114	0.0209	0.0055	0.0060	0.0006	0.0058	0.0003
Ctln1	0.2598	0.0115	0.2348	0.0152	0.2893	0.0290	0.2738	0.0192	0.0477	0.0041	0.0468	0.0044	0.3887	0.0115	0.4088	0.0116
Ctln2	0.0357	0.0016	0.0351	0.0015	0.0538	0.0031	0.0489	0.0038	0.0099	0.0009	0.0095	0.0011	0.0067	0.0003	0.0072	0.0003
Cyb561d	0.2479	0.0073	0.2384	0.0105	0.1778	0.0109	0.1563	0.0145	0.1317	0.0105	0.1069	0.0110	0.0402	0.0015	0.0399	0.0021
Dias2	0.0539	0.0013														

Igfbp3	0.1452	0.0227	0.1669	0.0505	0.1852	0.0119	0.1907	0.0143	0.2989	0.0386	0.2573	0.0203	0.0832	0.0032	0.0839	0.0013
Igf1	0.0281	0.0006	0.0335	0.0079	0.0656	0.0050	0.0694	0.0041	0.0357	0.0039	0.0338	0.0025	0.0397	0.0016	0.0413	0.0021
Hf27	0.2854	0.0080	0.2596	0.0100	0.0803	0.0043	0.0715	0.0072	0.2491	0.0156	0.1921	0.0168	0.0266	0.0006	0.0289	0.0018
Ier3	0.0934	0.0047	0.0918	0.0035	0.0562	0.0016	0.0565	0.0039	0.1612	0.0121	0.1466	0.0132	0.0445	0.0016	0.0571	0.0009
H2-T10_H2-T22_H2-T9	0.0053	0.0002	0.0054	0.0003	0.0017	0.0001	0.0018	0.0004	0.0047	0.0004	0.0040	0.0004	0.0012	0.0001	0.0011	0.0001
H2-Aa	0.0184	0.0049	0.0107	0.0010	0.0095	0.0005	0.0089	0.0011	0.0237	0.0060	0.0145	0.0020	0.0022	0.0006	0.0022	0.0003
Jup	0.2313	0.0072	0.2240	0.0073	0.1002	0.0056	0.0898	0.0070	1.1059	0.0927	0.9576	0.1073	0.1855	0.0067	0.1863	0.0082
Jakmp1	0.0903	0.0042	0.0936	0.0032	0.1055	0.0032	0.1018	0.0081	0.0622	0.0070	0.0623	0.0046	0.0329	0.0011	0.0333	0.0010
Im2a	0.5097	0.0192	0.5087	0.0246	0.3575	0.0227	0.3014	0.0195	0.6441	0.0285	0.5351	0.0545	0.1954	0.0073	0.1906	0.0013
Ipcfl1	0.0283	0.0022	0.0282	0.0032	0.0468	0.0020	0.0517	0.0028	0.2233	0.0186	0.2041	0.0113	0.0261	0.0014	0.0242	0.0016
Isgf3	0.2611	0.0074	0.2541	0.0141	0.3491	0.0214	0.3434	0.0277	0.2417	0.0198	0.2036	0.0183	0.6944	0.0144	0.8353	0.0375
Igfbp5	0.2849	0.0120	0.2738	0.0462	0.3168	0.0252	0.2908	0.0219	1.1161	0.0768	1.0501	0.1000	0.3709	0.0079	0.4165	0.0058
Kcnp2	0.0456	0.0038	0.0424	0.0032	0.0607	0.0021	0.0625	0.0034	0.0016	0.0008	0.0107	0.0010	0.0219	0.0016	0.0243	0.0020
Kcnp2	0.3646	0.0152	0.3635	0.0090	0.2240	0.0156	0.1820	0.0195	0.1409	0.0096	0.1244	0.0082	0.0428	0.0017	0.0473	0.0022
Kcng1	0.0953	0.0118	0.0770	0.0090	0.0599	0.0041	0.0526	0.0072	0.0016	0.0003	0.0022	0.0002	0.0010	0.0002	0.0010	0.0001
Kcnd2	0.6094	0.0157	0.5862	0.0197	0.9575	0.0606	0.8619	0.0746	3.5739	0.2776	3.1732	0.2841	0.8483	0.0411	0.8179	0.2220
Kcnc1	2.8279	0.1161	2.5901	0.1267	1.3595	0.1197	1.2077	0.1151	8.4846	0.8016	6.3946	0.4368	1.0941	0.0719	1.0615	0.8608
Kcna6	0.4800	0.0131	0.4595	0.0130	0.3892	0.0202	0.3545	0.0344	0.4192	0.0235	0.3579	0.0234	0.1468	0.0051	0.1475	0.0067
Leprt	0.1388	0.0045	0.1336	0.0053	0.1084	0.0058	0.1056	0.0073	0.1029	0.0087	0.0961	0.0093	0.0691	0.0038	0.0710	0.0111
Lcn2	0.0018	0.0006	0.0020	0.0002	0.0014	0.0001	0.0018	0.0002	0.0113	0.0090	0.0028	0.0003	0.0009	0.0001	0.0011	0.0002
Lapin4b	1.6732	0.0650	1.7094	0.0593	0.8868	0.0436	0.7830	0.0661	1.4768	0.0985	1.2679	0.1093	0.3405	0.0114	0.3320	0.0108
Kcng5	0.0518	0.0034	0.0475	0.0053	0.0823	0.0112	0.0920	0.0109	0.0078	0.0008	0.0097	0.0005	0.0640	0.0034	0.0600	0.0024
Kcng2	0.5978	0.0246	0.5485	0.0273	0.3816	0.0088	0.3647	0.0364	0.5194	0.0656	0.4908	0.0509	0.1429	0.0052	0.1443	0.0025
Kcng12	0.0581	0.0041	0.0614	0.0048	0.0340	0.0006	0.0324	0.0014	0.2294	0.0147	0.2639	0.0159	0.0489	0.0022	0.0388	0.0068
Lypd6b	0.0871	0.0051	0.0788	0.0082	0.0990	0.0050	0.1237	0.0113	0.0063	0.0002	0.0065	0.0003	0.0041	0.0003	0.0032	0.0002
Ly6h	1.2844	0.0650	1.2069	0.0895	2.3836	0.1064	2.5473	0.1386	0.3155	0.0244	0.3331	0.0087	0.6578	0.0256	0.8788	0.0261
Lypd6	0.0536	0.0027	0.0523	0.0030	0.0973	0.0047	0.1099	0.0059	0.1455	0.0087	0.1516	0.0062	0.0270	0.0019	0.0236	0.0012
Lpl	0.0368	0.0019	0.0333	0.0018	0.0383	0.0019	0.0385	0.0027	0.0137	0.0020	0.0081	0.0011	0.0241	0.0018	0.0230	0.0005
Adgr1	0.1762	0.0091	0.1787	0.0086	0.3079	0.0167	0.3340	0.0222	0.1606	0.0127	0.1274	0.0124	0.0944	0.0034	0.0915	0.0007
Lhfp15	0.1180	0.0062	0.1078	0.0047	0.1387	0.0105	0.1387	0.0164	0.0397	0.0032	0.0341	0.0027	0.0164	0.0005	0.0180	0.0006
Mmp15	0.2340	0.0079	0.2451	0.0138	0.2347	0.0103	0.2492	0.0127	0.1224	0.0119	0.1071	0.0052	0.0966	0.0042	0.0968	0.0030
Mrv1	0.0072	0.0004	0.0076	0.0006	0.0026	0.0001	0.0027	0.0003	0.0043	0.0004	0.0050	0.0004	0.0016	0.0002	0.0013	0.0002
Nat8l	2.3722	0.1463	2.4146	0.1526	0.7953	0.0409	0.7313	0.0494	1.0263	0.1065	0.9745	0.0698	0.2082	0.0095	0.1897	0.0300
Ninj1	0.0841	0.0006	0.0903	0.0038	0.1035	0.0048	0.0961	0.0028	0.0822	0.0075	0.0773	0.0061	0.0365	0.0011	0.0413	0.0019
Npe2	1.0460	0.0367	1.1224	0.0540	0.7448	0.0325	0.7459	0.0296	0.7726	0.0853	0.6257	0.0466	0.4457	0.0102	0.4237	0.0168
Npat	0.0257	0.0009	0.0253	0.0011	0.0777	0.0019	0.0794	0.0056	0.0231	0.0034	0.0189	0.0011	0.0180	0.0011	0.0200	0.0005
Nptx2	0.0346	0.0015	0.0360	0.0022	0.0754	0.0032	0.0811	0.0075	0.0140	0.0020	0.0131	0.0011	0.0170	0.0004	0.0155	0.0009
Tenn2	0.1459	0.0045	0.1631	0.0053	0.1996	0.0062	0.1939	0.0148	0.1261	0.0155	0.1112	0.0078	0.1164	0.0031	0.1210	0.0034
Opr1	0.0743	0.0020	0.0874	0.0038	0.1031	0.0030	0.0896	0.0080	0.0184	0.0028	0.0165	0.0011	0.0384	0.0025	0.0273	0.0010
Oscp1	0.0613	0.0014	0.0645	0.0029	0.0586	0.0025	0.0598	0.0041	0.0374	0.0036	0.0303	0.0018	0.0226	0.0005	0.0249	0.0012
Panx1	0.1005	0.0025	0.1082	0.0022	0.1726	0.0058	0.1807	0.0144	0.0507	0.0054	0.0438	0.0026	0.1898	0.0042	0.1851	0.0047
Pard6b	0.0124	0.0006	0.0138	0.0006	0.0142	0.0007	0.0129	0.0012	0.0481	0.0053	0.0438	0.0036	0.0163	0.0011	0.0129	0.0006
Pecde	0.0752	0.0023	0.0865	0.0050	0.1088	0.0008	0.0187	0.0009	0.0386	0.0043	0.0344	0.0055	0.0116	0.0005	0.0110	0.0008
Pes45	0.0162	0.0011	0.0199	0.0015	0.0357	0.0008	0.0367	0.0033	0.0084	0.0011	0.0070	0.0006	0.0069	0.0005	0.0072	0.0002
Pde2a	0.0303	0.0016	0.0306	0.0017	0.0256	0.0010	0.0238	0.0013	0.0380	0.0041	0.0322	0.0013	0.0132	0.0007	0.0127	0.0006
Plp2	0.0077	0.0004	0.0095	0.0008	0.0162	0.0011	0.0152	0.0009	0.0255	0.0048	0.0201	0.0038	0.0529	0.0017	0.0505	0.0017
Plxdc1	0.0602	0.0042	0.0639	0.0035	0.0428	0.0022	0.0391	0.0025	0.3806	0.0420	0.3322	0.0109	0.1524	0.0072	0.1372	0.0062
Pmepa1	0.3900	0.0128	0.4341	0.0195	0.3111	0.0161	0.2899	0.0181	0.1974	0.0225	0.1973	0.0253	0.1916	0.0072	0.1737	0.0056
Ponde3	0.0027	0.0002	0.0030	0.0002	0.0020	0.0002	0.0018	0.0001	0.0001	0.0000	0.0002	0.0000	0.0003	0.0001	0.0012	0.0001
Ppap2c	0.1221	0.0065	0.1406	0.0111	0.1206	0.0109	0.1385	0.0053	0.0548	0.0061	0.0502	0.0028	0.0307	0.0012	0.0317	0.0018
Prrm8	0.0900	0.0056	0.0942	0.0032	0.1310	0.0045	0.1352	0.0079	0.3807	0.0403	0.3463	0.0180	0.2022	0.0050	0.1919	0.0048
Prss23	0.0884	0.0038	0.1014	0.0088	0.0416	0.0015	0.0400	0.0016	0.1496	0.0103	0.1319	0.0037	0.0281	0.0008	0.0263	0.0013
Ptn	1.9527	0.0458	1.9822	0.1182	3.1878	0.0839	3.1688	0.0879	2.3589	0.2253	2.0436	0.1176	2.4613	0.0837	2.4283	0.0576
Hac44	0.0154	0.0007	0.0149	0.0015	0.0211	0.0007	0.0179	0.0005	0.0093	0.0013	0.0082	0.0005	0.0084	0.0005	0.0082	0.0002
Opc1	0.0523	0.0029	0.0526	0.0034	0.0510	0.0021	0.0507	0.0031	0.0509	0.0055	0.0452	0.0015	0.0299	0.0012	0.0311	0.0014
Rab6b	0.9809	0.0218	1.1649	0.0306	1.0846	0.0338	1.1152	0.0839	1.0599	0.1275	0.9073	0.0672	0.4622	0.0218	0.4397	0.0118
Rab29	0.0368	0.0013	0.0410	0.0021	0.0221	0.0011	0.0221	0.0016	0.0448	0.0051	0.0406	0.0015	0.0148	0.0002	0.0128	0.0001
Rasgrp2	0.3393	0.0131	0.3667	0.0207	0.4756	0.0108	0.4849	0.0417	0.0829	0.0087	0.0786	0.0065	0.0464	0.0018	0.0423	0.0014
Rel12	0.4327	0.0167	0.4126	0.0126	0.3272	0.0130	0.3217	0.0156	0.3377	0.0304	0.2792	0.0086	0.1246	0.0042	0.1236	0.0050
Resp18	1.2157	0.0430	1.3878	0.0507	1.0994	0.0345	1.0416	0.0649	0.1077	0.0143	0.1027	0.0107	0.0473	0.0020	0.0431	0.0019
Rgs19	0.0461	0.0010	0.0502	0.0025	0.0804	0.0029	0.0840	0.0055	0.0359	0.0052	0.0318	0.0019	0.0336	0.0014	0.0291	0.0013
Rhbdd2	0.4176	0.0196	0.4537	0.0109	0.3721	0.0134	0.3776	0.0242	0.2835	0.0291	0.2604	0.0134	0.1152	0.0027	0.1075	0.0030
Rnaset2a	0.0934	0.0037	0.1079	0.0085	0.0903	0.0031	0.0938	0.0031	0.1127	0.0103	0.1044	0.0087	0.0874	0.0024	0.0785	0.0026
Rnaset2b	0.0064	0.0003	0.0076	0.0003	0.0034	0.0002	0.0032	0.0002	0.0033	0.0004	0.0031	0.0002	0.0054	0.0002	0.0053	0.0004
Rnf19b	0.0979	0.0037	0.1083	0.0031	0.1163	0.0018	0.1158	0.0061	0.6018	0.0529	0.5418	0.0287	0.1918	0.0053	0.1706	0.0034
Rock2	0.1576	0.0060	0.1738	0.0090	0.0881											

Tspan6	0.0504	0.0024	0.0563	0.0056	0.1323	0.0029	0.1377	0.0035	0.0337	0.0026	0.0379	0.0022	0.0863	0.0023	0.0811	0.0030
Trhde	0.0252	0.0007	0.0297	0.0026	0.0455	0.0033	0.0481	0.0051	0.1993	0.0249	0.2250	0.0119	0.0396	0.0023	0.0359	0.0019
Tnfsf9	0.0022	0.0003	0.0030	0.0003	0.0032	0.0002	0.0031	0.0004	0.0142	0.0014	0.0140	0.0006	0.0066	0.0003	0.0053	0.0002
Tnfrsf11b	0.0133	0.0010	0.0162	0.0032	0.0109	0.0009	0.0106	0.0006	0.0155	0.0015	0.0174	0.0014	0.0042	0.0002	0.0034	0.0002
Tmie	0.0571	0.0029	0.0618	0.0046	0.0419	0.0030	0.0485	0.0028	0.0172	0.0023	0.0166	0.0006	0.0072	0.0002	0.0066	0.0004
Znrf2	0.0951	0.0024	0.1203	0.0092	0.1291	0.0064	0.1394	0.0066	0.1286	0.0124	0.1367	0.0061	0.1964	0.0048	0.1952	0.0070
Znrf1	0.1245	0.0043	0.1454	0.0145	0.1624	0.0057	0.1746	0.0072	0.1301	0.0142	0.1407	0.0065	0.0950	0.0060	0.1020	0.0067
Zdhc22	0.1848	0.0059	0.1963	0.0108	0.1930	0.0077	0.1967	0.0192	0.0285	0.0042	0.0272	0.0021	0.0687	0.0053	0.0582	0.0042
Vstm2l	0.3257	0.0236	0.3862	0.0596	0.5045	0.0389	0.5281	0.0468	0.0625	0.0065	0.0707	0.0028	0.0224	0.0009	0.0218	0.0004
Vstm2a	0.2005	0.0132	0.2586	0.0249	0.2609	0.0192	0.2868	0.0188	0.0557	0.0054	0.0471	0.0044	0.2549	0.0323	0.3536	0.0138

Supplementary table 3 : R script for gene expression analysis

```
cbd <- read.csv2("Delta_CT_IOP11_Final.csv", sep=";", row.names=1)
#Charger les groupes
PCP <- c("BS_PCP1_P11","BS_PCP2_P11","BS_PCP3_P11","BS_PCP4_P11")
Veh <- c("BS_Veh1_P11","BS_Veh2_P11","BS_Veh3_P11","BS_Veh4_P11")
y <- data.frame(cbd)
frame <- data.matrix(cbd, rownames=TRUE)

# Creation des deux groupes de moyennes, et calcul du fold_change

Mean_PCP <- apply(frame[,PCP],1,mean)
Mean_Veh <- apply(frame[,Veh],1,mean)
cbd$gene_name <- rownames(cbd)
Fold_change <- Mean_PCP/Mean_Veh
#T test systematique
pvalue <- sapply(1:nrow(frame), function(i){
  t.test(as.numeric(frame[i,Veh]), as.numeric(frame[i,PCP]), exact=FALSE, var.equal=TRUE)
}$p.value})
pvalue <- data.matrix(pvalue)
rownames(pvalue) <- rownames(frame)
t_pvalue_corrected <- as.matrix(p.adjust(pvalue, method = "BH"))
rownames(t_pvalue_corrected) <- rownames(frame)
Significant_qvalue_ttest <- subset(t_pvalue_corrected, t_pvalue_corrected < 0.05)
# volcano plot sans correction
library(ggrepel) # pour que le texte s'affiche proprement
# pour créer le groupe de gènes "différentiellement exprimé (avec critère fold change > 10%)"
cbd$diffexpressed <- "NO"
cbd$diffexpressed[log2(Fold_change) > 0.1375 & t_pvalue < 0.05] <- "UP"
cbd$diffexpressed[log2(Fold_change) < -0.152003 & t_pvalue < 0.05] <- "DOWN"
# pour créer tous les labels des gènes changés significativement
```

```

cbd$changed_gene_label <- NA cbd$changed_gene_label[cbd$diffexpressed != "NO"] <-
cbd$gene_name[cbd$diffexpressed != "NO"]

#Et le plot...

volcanoplot_not_corrected <- ggplot(data=cbd, aes(x=log2(Fold_change), y=-log10(t_pvalue),
col=diffexpressed, label=changed_gene_label)) + ggtitle("Brainstem_P11") + geom_point() +
theme_minimal() + xlim(-2,4) + ylim(0,5) + geom_text_repel() + theme(plot.title = element_text(hjust
= 0.5))

volcanoplot_not_corrected2 <- volcanoplot_not_corrected+ geom_vline(xintercept = c(-
0.152003,0.1375), col="blue")+ geom_hline(yintercept = -log10(0.05), col="red")

volcanoplot_not_corrected3 <- volcanoplot_not_corrected2
+scale_color_manual(values=c("blue","black","red"))

volcanoplot_not_corrected3

# volcano plot après correction

# pour créer le groupe de gènes "différentiellement exprimé après correction (avec critère fold change
> 10%)"

cbd$diffexpressed_corrected <- "NO"

cbd$diffexpressed_corrected[log2(Fold_change) > 0.152003 & t_pvalue_corrected < 0.05] <- "UP"
cbd$diffexpressed_corrected[log2(Fold_change) < -0.1375 & t_pvalue_corrected < 0.05] <- "DOWN"

cbd$changed_gene_label_corrected <- NA

cbd$changed_gene_label_corrected[cbd$diffexpressed_corrected != "NO"] <-
cbd$gene_name[cbd$diffexpressed_corrected != "NO"]

volcanoplot_corrected <- ggplot(data=cbd, aes(x=log2(Fold_change), y=-log10(t_pvalue_corrected),
col=diffexpressed_corrected, label=changed_gene_label_corrected)) +
ggtitle("Cerebellum_P11_corrected") + geom_point(shape=16, size=2) + theme_classic() + ylab("T-
test p-value(-log10)") + xlab("Fold-change PCP/Vehicle(Log2)") + geom_text_repel() + xlim(-2,2.5)
+ ylim(0,3) + theme(plot.title = element_text(hjust = 0.5))

volcanoplot_corrected2 <- volcanoplot_corrected+ geom_vline(xintercept = c(0.152003,-0.1375),
col="blue")+ geom_hline(yintercept = -log10(0.05), col="black") + geom_hline(yintercept = -
log10(0.1), col="black", linetype="dotted")

volcanoplot_corrected3 <- volcanoplot_corrected2
+scale_color_manual(values=c("blue","grey","red"))

volcanoplot_corrected3

ggsave("CBP11.eps", width = 6.17, heigh= 3.33)

```

Part 2: No deficits in cerebellar synapses in a genetic model of schizophrenia.

Article in preparation.

The LgDel genetic mouse model of schizophrenia has a normal development of the olivo-cerebellar synaptic network.

Veleanu M.¹, Selimi F.^{1*}

Affiliations:

¹ Center for Interdisciplinary Research in Biology (CIRB), College de France, CNRS, INSERM, PSL Research University, Paris, France

*Corresponding author: fekrije.selimi@college-de-france.fr

Abstract

Schizophrenia is one of the most severe debilitating neurodevelopmental disorders. While its symptomatology has been widely described, understanding the causal physiopathological mechanisms remains challenging. Postmortem and genetic studies suggest that schizophrenia is a “synaptopathy,” a disease of the synapse. Moreover, while most schizophrenia studies focus on the prefrontal cortex or hippocampus, there is now compelling evidence that the cerebellum could play a role in schizophrenia. The 22q11.2 human deletion is one of the highest risk factors for developing schizophrenia. We analyzed the neuronal network in the cerebellar cortex of the LgDel +/- mouse that models the 22q11.2 deletion and found that the cerebellar cytoarchitecture, Purkinje cell spontaneous activity, and the morphology of Purkinje cell synapses are normal in juvenile mice. These results suggest that the postnatal development of the synaptic circuitry is not impaired in the LgDel +/- cerebellum.

Introduction

The genetic origin of schizophrenia is now well established, since studies on twins have revealed a very high concordance rate of illness in monozygotic and dizygotic twins, respectively around 40% and 17% (Gottesman, 1991). Recent large-scale Genome Wide Association Studies allowed the identification of more than one hundred frequent (>1% population) loci that were significantly associated with schizophrenia (Fromer et al., 2014), but with a very low penetrance (Odds Ratio <1.4). On the contrary, a few rare but penetrant genetic alterations have been identified in several genetic pedigree, such as DISC1 (Disrupted in Schizophrenia 1), a balanced reciprocal translocation found in a Scottish family with schizophrenia and other psychiatric disorders, or the 22q11.2 deletion, a large genetic deletion known to induce the Velo Cardio Facial Syndrome (VCFS) (Shprintzen et al., 1978).

Despite being quite rare (prevalence of 1/4000 birth), the 22q11.2 deletion is responsible for a 25 to 30-fold increased risk of developing schizophrenia (Gur et al., 2017; Murphy et al., 1999), and is frequently associated with cognitive deficits (Philip and Bassett, 2011). Moreover, the 22q11.2 deletion accounts for 1 to 2% of sporadic cases of schizophrenia. This deletion covers 3 megabases of the chromosome 22, and spans around 60 known genes (Karayiorgou et al., 2010). These include synaptic genes previously linked with schizophrenia, such as the one coding for Catechol-O-methyl transferase (COMT) responsible for the degradation of dopamine and other catecholamines in the synaptic cleft (Egan et al., 2001; Gupta et al., 2009; Wonodi et al., 2005), and SNAP29 (Saito et al., 2001), a presynaptic protein important for synapse function (Osimo et al., 2018; Owen et al., 2005; Pocklington et al., 2014). Genetically modified mouse models have been generated to understand the biological mechanisms responsible for the increased pathological risk: the mouse model LgDel (for Large deletion) (Merscher et al., 2001), or the similar Df(16)A(+/-) (Stark et al., 2008), both mimicking the 22q11.2 human mutation. Those mice present several alterations relevant to schizophrenia: an alteration of prepulse inhibition and of social recognition of a novel mouse (Piskorowski et al., 2016; Saito et al., 2020), a decreased density of Parvalbumin (PV) inhibitory neurons and impaired inhibitory synapses function and plasticity in the hippocampus (Piskorowski et al., 2016) and the prefrontal cortex (Mukherjee et al., 2019a).

While studies on schizophrenia predominantly focus on the prefrontal cortex or the hippocampus, we decided to study the cerebellum, which is increasingly considered as an interesting structure to study in the context of neuropsychiatric disorders. Its implication in

cognitive processes has been suggested by several studies in humans (Guell et al., 2015; Schmahmann, 2019) and in animal models (Carta et al., 2019; Sendhilnathan et al., 2020; Wagner et al., 2017), and neuroimaging studies in humans have linked schizophrenia to the cerebellum (Andreasen et al., 1998). In particular a decreased cerebellar volume is found in patients and is recapitulated in the Df16 model (Ellegood et al., 2014). However, contrary to other psychiatric diseases such as Autism Spectrum Disorder, to our knowledge, there are no studies on animal models of schizophrenia focusing on the cerebellum and the synaptic connectivity of Purkinje cells. We thus decided to analyze the synaptic properties of cerebellar Purkinje cells in the LgDel mouse model.

Results

Global cerebellar cytoarchitecture and spontaneous firing properties of Purkinje cells are normal in the LgDel Model

The cerebellar cortex is organized in 4 layers, the white matter, the granular layer containing the soma of the granule cells, the Purkinje layer containing the soma of Purkinje Cells, the only output of the cerebellar cortex, and the molecular layer containing interneurons, the dendritic tree of the Purkinje Cells and all the afferent synapses. Previous studies have shown a decreased cerebellar volume in Df16 model (Ellegood et al., 2014). To assess whether global cerebellar cytoarchitecture is impaired in LgDel +/- mice, cerebellar sections from the vermis of mice at P30, an age corresponding to the early adolescence, were immunostained for calbindin, a marker that allows the visualization of the entire Purkinje cell, soma, dendritic tree, spines and axon. The mean area of a vermal section (**Figure 1A and 1B**) and the thickness of the molecular layer in lobules VI and VIII (**Figure 1C**) were not different between LgDel +/- and control mice, suggesting that the cytoarchitecture of the cerebellum is normal in early adolescence in LgDel +/- mice.

Purkinje cells have a tonic electrophysiological activity constituted of simple spikes, that is modulated by Purkinje cells' afferents. To determine whether this tonic activity is affected in the LgDel +/- mice, we recorded spontaneous electrophysiological activity *ex vivo* in cerebellar slices using high density extracellular recordings (**Figure 2A**). Simple spikes from Purkinje cells were sorted (**Figure 2B**) based on the shape of their action potential for further analysis (**Figure 2B**). We found no difference between LgDel +/- and control mice in the mean

firing rate, the Coefficient of Variation (CV) measuring the mean variance of Inter Spike Intervals (ISI) during the whole recording, and in the CV2, a measure of the variability of spiking between two adjacent intervals (Holt et al., 1996). Altogether, these results suggest that LgDel +/- mice have normal cerebellar morphology, cytoarchitecture, and global PC spontaneous activity at P30.

There are no alterations of the morphology of presynaptic boutons in LgDel +/- Purkinje cells.

The Purkinje cell, the sole output of the cerebellar cortex, receives four different afferents: two excitatory, the parallel fibers originating from the granule cells and the climbing fibers (CF), which are the axons of the Inferior olivary neurons in the brainstem, and two inhibitory, originating from the stellate cells and basket cells located in the molecular layer of the cerebellar cortex. To verify if LgDel +/- mice have a normal cerebellar synaptic organization, we performed a systematic afferent specific analysis of Purkinje cells presynaptic boutons morphology. All the measurements were been done in two different lobules of the cerebellar cortex: the lobule VI (engaged in language tasks, working memory paradigms, and spatial navigation) and lobule VIII (engaged in sensorimotor tasks), in order to verify if the eventual deficits are present across several lobules, or on the contrary are lobule specific.

During cerebellar development, climbing fibers translocate along the dendritic tree of the Purkinje cells, and form synapses that can be labeled using an anti-VGLUT2 antibody, a presynaptic marker. These synapses extend up to approximately 80% of the molecular layer height, defining the extension of CF synaptic territory. We found no difference in the extension of CF synaptic territory in any of the lobules analyzed in the LgDel +/- mice (**Figure 3A and 3B**). We also quantified the mean volume and density of VGLUT2 clusters and found no change (**Figure 3C and 3D**).

Presynaptic boutons from the second excitatory afferent, the parallel fibers, can be labeled using the VGLUT1 marker. Their mean intensity in the molecular layer was measured instead of the quantification of presynaptic boutons, since the puncta are too small and too dense to be segmented and quantified adequately. No difference in the mean VGLUT1 labeling intensity was found in the molecular layer of LgDel +/- mice compared to controls, suggesting that LgDel +/- mice have no deficits in parallel fiber /Purkinje cells synapse formation (**Figure 4**).

Using GAD65 immunolabeling, we assessed the density (**Figure 5A and 5B**) and volume (**Figure 5C and 5D**) of inhibitory pre-synaptic boutons in the molecular layer of LgDel +/- mice versus controls, and found no differences.

Altogether, these results show no major change in the organization, morphology, and subcellular localization of synapses on Purkinje cell dendrites in LgDel +/- mice, showing that this large genetic deletion does not induce major impairments of synaptic development in cerebellar Purkinje cells.

Discussion

This study focused on developmental deficits of cerebellar synapses in a genetic model of schizophrenia. Our results show that LgDel +/- mice have a normal cerebellar cytoarchitecture, a normal spontaneous activity of Purkinje cells, and that cerebellar synaptic morphology is unaffected by the deletion at P30, suggesting that there are no deficits of postnatal cerebellar synapses development.

While previous studies noticed a reduced cerebellar volume in the Df(16)A(+/-) mouse model (Ellegood et al., 2014), we didn't find any changes in the LgDel mouse. However, Ellegood et al. performed a high-resolution MRI analysis that allows quantification of the volume in three dimensions and detected small volume changes. Their most consistent morphological deficits were restricted to some substructures of the cerebellum: the anterior lobules IV/V, vermis lobule IX/X, crus 1, paraflocculus and flocculus. In our analysis, we only quantified the area of sections in the vermis, and thus might have missed specific and small volume decreases in specific lobules.

Recent papers using the LgDel model have noticed deficits of PV inhibitory interneurons density in the hippocampus, but also a reduced expression level of PV and GAD67 protein in the neocortex, hippocampus, and the dorsal striatum (Mukherjee et al., 2019). However, it is noteworthy that their results were most marked at late adolescence (P60) and adult age, while at early adolescence (P40) the differences seem restricted to the hippocampal CA1 and subiculum. This suggests that inhibitory deficits take place around late adolescence (P60), correlating with the critical period of psychotic transition in humans.

In our case, we were focusing on the morphology and organization of the synaptic network of the cerebellar cortex, and didn't find any differences in P30 LgDel +/- mice, suggesting that deficits in synaptic formation and early maturation may not be a primary feature of this model. However, to exclude that cerebellar synapses are impaired in adult LgDel +/- mice, functional analysis of Purkinje cell synapses in the LgDel model is warranted. It might show differences that are not detectable by morphological analysis, such as deficits of synaptic transmission or plasticity.

Finally, while the 22q11.2 deletion has a relatively high penetrance, it may not reflect exhaustively the physiopathology. Schizophrenia is a very heterogenous disease, as shown by the heterogeneity of symptoms and neurobiological alterations seen in patients. Our results don't exclude that deficits in cerebellar postnatal development and refinement of synaptic network could be a part of schizophrenia. The study of other models of schizophrenia, in particular dual hit models combining a genetic predisposition with environmental prenatal insult, might detect deficits that are not found in the LgDel model.

Material and methods

Antibodies

The following primary antibodies were used: mouse monoclonal anti-CABP (1:1000; swant, Switzerland, #300), rabbit polyclonal anti-CABP (1:1000; swant, #9.03), guinea pig polyclonal anti VGLUT1 (1:5000; Millipore, Massachusetts, USA, #AB5905), guinea pig polyclonal anti-VGLUT2 (1:5000; Millipore, #AB2251), mouse anti-Parvalbumin (1:1000: swant, #PV235) and mouse anti-GAD65 (1:500, abcam, Cambridge, United Kingdom, #ab26113)

The following secondary antibodies were used: donkey polyclonal anti-guinea pig Alexa Fluor 594 (1:1000; Invitrogen, California, USA, #A11076), donkey anti-mouse Alexa Fluor 488 (1:1000; invitrogen, #R37114), donkey polyclonal anti-Mouse Alexa Fluor 568 (1:1000; invitrogen, #A10037), donkey polyclonal anti-Rabbit Alexa Fluor 488 (1:1000; invitrogen, #A21206).

Immunohistochemistry

Mice brains were extracted after intracardiac perfusion with 4% Paraformaldehyde (PFA) in Phosphate-buffered saline (PBS) solution. After dissection, the brain was stored in the 4% PFA

in PBS 1X solution for one hour at 4°C, and then cryoprotected for 48h into a 30% sucrose in PBS solution at 4°C. After sectioning with a freezing microtome, brain slices were washed three times for five minutes in PBS, then blocked with 4% donkey serum in PBS for 30 minutes at room temperature. The primary antibodies were diluted in PBS, 1% triton X-100, 1% donkey serum, at their respective concentration, and incubated overnight at 4°C under agitation. The sections were then washed three times for five minutes in PBS 1% triton X-100 and incubated for one hour at room temperature in the secondary antibody, diluted in PBS, 1% triton X-100, 1% donkey serum. The sections were then incubated for 15 minutes at room temperature with the nuclear marker Hoechst 33342 (0,2 mg/mL; Sigma, Gothenburg, Sweden, Cat#H6024) in PBS 0.2% triton. The sections were then washed three times for five minutes in PBS 1% triton and recovered in PBS. The sections were finally mounted with Prolong Gold between microscope slides and coverslips.

Image acquisition and quantification

Images for global cerebellar morphology were taken using a Zeiss Axiozoom V16 macroscope, equipped with a digital camera (AxioCam HRm) using a 10x objective (pixel size 0,650x0,650 μ m).

Images for synaptic quantifications were taken using a Zeiss Axioobserver Z1 inverted spinning disk microscope with a CSUW11 scan head with a 63x objective (1.4NA, WD:0.1mm, pixel size 103x103nm)

All the quantifications have been done, in a blind condition, with Fiji software.

First, for VGLUT2 and GAD65 quantifications, all the images were normalized using quantile-based normalization plugin of ImageJ.

Then, then synaptic boutons were extracted from the background using the 3D Weka Segmentation plugin (https://imagej.net/Trainable_Weka_Segmentation) after manual selection of signal and background samples. The plugin extracts the signal from background and produces a binary image. The Fiji built-in plugin 3D object counter was then used in order to count and measure every object (cluster of VGLUT2 or GAD65 positive signal).

For VGLUT1 quantification, the background of the whole image was artificially subtracted using the Fiji built-in subtract background plugin. The signal measured was the raw integrated density (the sum of the values of the pixels in the selection) divided by the area in μ m², thus providing a measure of the mean intensity per μ m².

High density microelectrode array (MEA) analysis of Purkinje cell spiking in acute cerebellar slices

Experiments were performed on acute cerebellar slices obtained from 1 month old mice in artificial cerebrospinal fluid (ACSF) containing (in mM): NaCl 125, KCl 2.5, D(+)Glucose 25, NaHCO₃ 25, NaH₂PO₄ 1.25, CaCl₂ 2, and MgCl₂ 1, gassed with 5% CO₂/95% O₂. Parasagittal slices (320 μm) were cut at 30°C with a Campden Ci 7000 smz microtome at an advance speed of 0.03 mm/s and vertical vibration set to 0.1–0.3 μm. Slices were then transferred to a chamber filled with oxygenated ACSF at 37°C and allowed to recover for 1 h before recordings.

For recording, the slices were placed over a high-density micro electrode array of 4096 electrodes (electrode size, 21 × 21 μm; pitch, 42 μm; 64 × 64 matrix; Biocam X, 3Brain, Wädenswil, Switzerland), and constantly perfused with oxygenated ACSF at 37°C. Extracellular activity was digitized at 17 kHz and data were analyzed with the Brainwave software from 3Brain. The signal was filtered with a butterworth high-pass filter at 200 Hz, spikes were detected with a hard threshold set at -100 μV, and unsupervised spike sorting was done by the software. We selected units with a firing rate between 15 and 100 spikes per second and we excluded units presenting more than 5% of refractory period violation (set to 3 ms). Firing pattern variability, or regularity, is defined as a measure of the consistency of time intervals between spikes (interspike interval (ISI) = seconds). To quantify the average variability in firing pattern, the coefficient of variance of the ISI (CV) was calculated as the ratio of the standard deviation (SD) of ISIs to the mean ISI of a given cell. To measure rhythmicity of cells, CV2 was calculated. CV2 measures firing pattern variability within a short period of two ISIs [$CV2 = 2|ISI_{n+1} - ISI_n| / (ISI_{n+1} + ISI_n)$] (Holt and Douglas, 1996).

Statistical Analysis

Data were analyzed using GraphPad Prism for statistics. Values were given as mean ± SEM. Normality was estimated using d'Agostino Pearson normality test. The means between two conditions were compared using unpaired Student t test when both data sets follow a normal law, otherwise, they were compared using a Mann-Whitney nonparametric test.

Acknowledgments: Rebecca Piskorowski for providing the LgDel mice, Marco Aquila and Alessandro Maccione for technical help with the MEA and the spike sorting, respectively We acknowledge the Orion imaging facility, CIRB, and also the personnel from the CIRB Animal facility. This work was supported by funding from: ATIP-AVENIR program (RSE11005JSA to FS), Fondation pour la Recherche Médicale Equipe FRM DEQ20150331748 (FS), and European Research Council ERC consolidator grant SynID 724601 (to FS).

Contributions: F.S. and M.V. designed the study and the experiments. M.V. performed the experiments and collected the data; M.V. wrote the first draft of the manuscript, and F.S. revised the manuscript.

Competing interests: Authors declare no competing interests.

References

- Andreasen, N.C., Paradiso, S., O'Leary, D.S., 1998. "Cognitive dysmetria" as an integrative theory of schizophrenia: a dysfunction in cortical-subcortical-cerebellar circuitry? *Schizophr. Bull.* 24, 203–218. <https://doi.org/10.1093/oxfordjournals.schbul.a033321>
- Carta, I., Chen, C.H., Schott, A.L., Dorizan, S., Khodakhah, K., 2019. Cerebellar modulation of the reward circuitry and social behavior. *Science* 363, eaav0581. <https://doi.org/10.1126/science.aav0581>
- Egan, M.F., Goldberg, T.E., Kolachana, B.S., Callicott, J.H., Mazzanti, C.M., Straub, R.E., Goldman, D., Weinberger, D.R., 2001. Effect of COMT Val108/158 Met genotype on frontal lobe function and risk for schizophrenia. *Proc. Natl. Acad. Sci.* 98, 6917–6922. <https://doi.org/10.1073/pnas.111134598>
- Ellegood, J., Markx, S., Lerch, J.P., Steadman, P.E., Genç, C., Provenzano, F., Kushner, S.A., Henkelman, R.M., Karayiorgou, M., Gogos, J.A., 2014. Neuroanatomical phenotypes in a mouse model of the 22q11.2 microdeletion. *Mol. Psychiatry* 19, 99–107. <https://doi.org/10.1038/mp.2013.112>
- Fromer, M., Pocklington, A.J., Kavanagh, D.H., Williams, H.J., Dwyer, S., Gormley, P., Georgieva, L., Rees, E., Palta, P., Ruderfer, D.M., Carrera, N., Humphreys, I., Johnson, J.S., Roussos, P., Barker, D.D., Banks, E., Milanova, V., Grant, S.G., Hannon, E., Rose, S.A., Chambert, K., Mahajan, M., Scolnick, E.M., Moran, J.L., Kirov, G., Palotie, A., McCarroll, S.A., Holmans, P., Sklar, P., Owen, M.J., Purcell, S.M., O'Donovan, M.C., 2014. De novo mutations in schizophrenia implicate synaptic networks. *Nature* 506, 179–184. <https://doi.org/10.1038/nature12929>
- Gottesman, I.I., 1991. *Schizophrenia genesis: The origins of madness*, Schizophrenia genesis: The origins of madness. W H Freeman/Times Books/ Henry Holt & Co, New York, NY, US.
- Guell, X., Hoche, F., Schmahmann, J.D., 2015. Metalinguistic deficits in patients with cerebellar dysfunction: empirical support for the dysmetria of thought theory. *Cerebellum Lond. Engl.* 14, 50–58. <https://doi.org/10.1007/s12311-014-0630-z>
- Gupta, M., Bhatnagar, P., Grover, S., Kaur, H., Baghel, R., Bhasin, Y., Chauhan, C., Verma, B., Manduva, V., Mukherjee, O., Purushottam, M., Sharma, A., Jain, S., Brahmachari, S.K., Kukreti, R., 2009. Association studies of catechol-O-methyltransferase (COMT) gene with schizophrenia and response to antipsychotic treatment. *Pharmacogenomics* 10, 385–397. <https://doi.org/10.2217/14622416.10.3.385>
- Gur, R., Bassett, A., McDonald-McGinn, D., Bearden, C., Chow, E., Emanuel, B., Owen, M., Swillen, A., Van den Bree, M., Vermeesch, J., Vorstman, J., Warren, S., Lehner, T., Morrow, B., 2017. A neurogenetic model for the study of schizophrenia spectrum disorders: the International 22q11.2 Deletion Syndrome Brain Behavior Consortium. *Mol. Psychiatry* 22, 1664–1672. <https://doi.org/10.1038/mp.2017.161>
- Holt, G.R., Douglas, J., 1996. Comparison of Discharge Variability Visual Cortex Neurons. *J. Neurophysiol.* 75, 1806–1814.
- Holt, G.R., Softky, W.R., Koch, C., Douglas, R.J., 1996. Comparison of discharge variability in vitro and in vivo in cat visual cortex neurons. *J. Neurophysiol.* 75, 1806–1814. <https://doi.org/10.1152/jn.1996.75.5.1806>
- Karayiorgou, M., Simon, T.J., Gogos, J.A., 2010. 2q11.2 microdeletions: linking DNA structural variation to brain dysfunction and schizophrenia. *Nat. Rev. Neurosci.* 11, 402–416. <https://doi.org/10.1038/nrn2841>
- Merscher, S., Funke, B., Epstein, J.A., Heyer, J., Puech, A., Lu, M.M., Xavier, R.J., Demay, M.B., Russell, R.G., Factor, S., Tokooya, K., Jore, B.St., Lopez, M., Pandita, R.K.,

- Lia, M., Carrion, D., Xu, H., Schorle, H., Kobler, J.B., Scambler, P., Wynshaw-Boris, A., Skoultschi, A.I., Morrow, B.E., Kucherlapati, R., 2001. TBX1 Is Responsible for Cardiovascular Defects in Velo-Cardio-Facial/DiGeorge Syndrome. *Cell* 104, 619–629. [https://doi.org/10.1016/S0092-8674\(01\)00247-1](https://doi.org/10.1016/S0092-8674(01)00247-1)
- Mukherjee, A., Carvalho, F., Eliez, S., Caroni, P., 2019. Long-Lasting Rescue of Network and Cognitive Dysfunction in a Genetic Schizophrenia Model. *Cell* 178, 1387-1402.e14. <https://doi.org/10.1016/j.cell.2019.07.023>
- Murphy, K.C., Jones, L.A., Owen, M.J., 1999. High rates of schizophrenia in adults with velo-cardio-facial syndrome. *Arch. Gen. Psychiatry* 56, 940–945. <https://doi.org/10.1001/archpsyc.56.10.940>
- Osimo, E.F., Beck, K., Reis Marques, T., Howes, O.D., 2018. Synaptic loss in schizophrenia: a meta-analysis and systematic review of synaptic protein and mRNA measures. *Mol. Psychiatry*. <https://doi.org/10.1038/s41380-018-0041-5>
- Owen, M.J., O'Donovan, M.C., Harrison, P.J., 2005. Schizophrenia: a genetic disorder of the synapse? *BMJ* 330, 158–159.
- Philip, N., Bassett, A., 2011. Cognitive, Behavioural and Psychiatric Phenotype in 22q11.2 Deletion Syndrome. *Behav. Genet.* 41, 403–412. <https://doi.org/10.1007/s10519-011-9468-z>
- Piskorowski, R.A., Nasrallah, K., Diamantopoulou, A., Mukai, J., Hassan, S.I., Siegelbaum, S.A., Gogos, J.A., Chevalleyre, V., 2016. Age-Dependent Specific Changes in Area CA2 of the Hippocampus and Social Memory Deficit in a Mouse Model of the 22q11.2 Deletion Syndrome. *Neuron* 89, 163–176. <https://doi.org/10.1016/j.neuron.2015.11.036>
- Pocklington, A.J., O'Donovan, M., Owen, M.J., 2014. The synapse in schizophrenia. *Eur. J. Neurosci.* 39, 1059–1067. <https://doi.org/10.1111/ejn.12489>
- Saito, R., Koebis, M., Nagai, T., Shimizu, K., Liao, J., Wulaer, B., Sugaya, Y., Nagahama, K., Uesaka, N., Kushima, I., Mori, D., Maruyama, K., Nakao, K., Kurihara, H., Yamada, K., Kano, M., Fukada, Y., Ozaki, N., Aiba, A., 2020. Comprehensive analysis of a novel mouse model of the 22q11.2 deletion syndrome: a model with the most common 3.0-Mb deletion at the human 22q11.2 locus. *Transl. Psychiatry* 10, 35. <https://doi.org/10.1038/s41398-020-0723-z>
- Saito, T., Guan, F., Papolos, D.F., Rajouria, N., Fann, C.S.J., Lachman, H.M., 2001. Polymorphism in SNAP29 gene promoter region associated with schizophrenia. *Mol. Psychiatry* 6, 193–201. <https://doi.org/10.1038/sj.mp.4000825>
- Schmahmann, J.D., 2019. The cerebellum and cognition. *Neurosci. Lett.* 688, 62–75. <https://doi.org/10.1016/j.neulet.2018.07.005>
- Sendhilnathan, N., Ipata, A.E., Goldberg, M.E., 2020. Neural Correlates of Reinforcement Learning in Mid-lateral Cerebellum. *Neuron* 106, 188-198.e5. <https://doi.org/10.1016/j.neuron.2019.12.032>
- Shprintzen, R.J., Goldberg, R.B., Lewin, M.L., Sidoti, E.J., Berkman, M.D., Argamaso, R.V., Young, D., 1978. A new syndrome involving cleft palate, cardiac anomalies, typical facies, and learning disabilities: velo-cardio-facial syndrome. *Cleft Palate J.* 15, 56–62.
- Stark, K.L., Xu, B., Bagchi, A., Lai, W.-S., Liu, H., Hsu, R., Wan, X., Pavlidis, P., Mills, A.A., Karayiorgou, M., Gogos, J.A., 2008. Altered brain microRNA biogenesis contributes to phenotypic deficits in a 22q11-deletion mouse model. *Nat. Genet.* 40, 751–760. <https://doi.org/10.1038/ng.138>
- Wagner, M.J., Kim, T.H., Savall, J., Schnitzer, M.J., Luo, L., 2017. Cerebellar granule cells encode the expectation of reward. *Nature* 544, 96–100. <https://doi.org/10.1038/nature21726>

Wonodi, I., Hong, L.E., Avila, M.T., Buchanan, R.W., Carpenter, W.T., Stine, O.C., Mitchell, B.D., Thaker, G.K., 2005. Association between polymorphism of the SNAP29 gene promoter region and schizophrenia. *Schizophr. Res.* 78, 339–341.
<https://doi.org/10.1016/j.schres.2005.03.023>

Figures

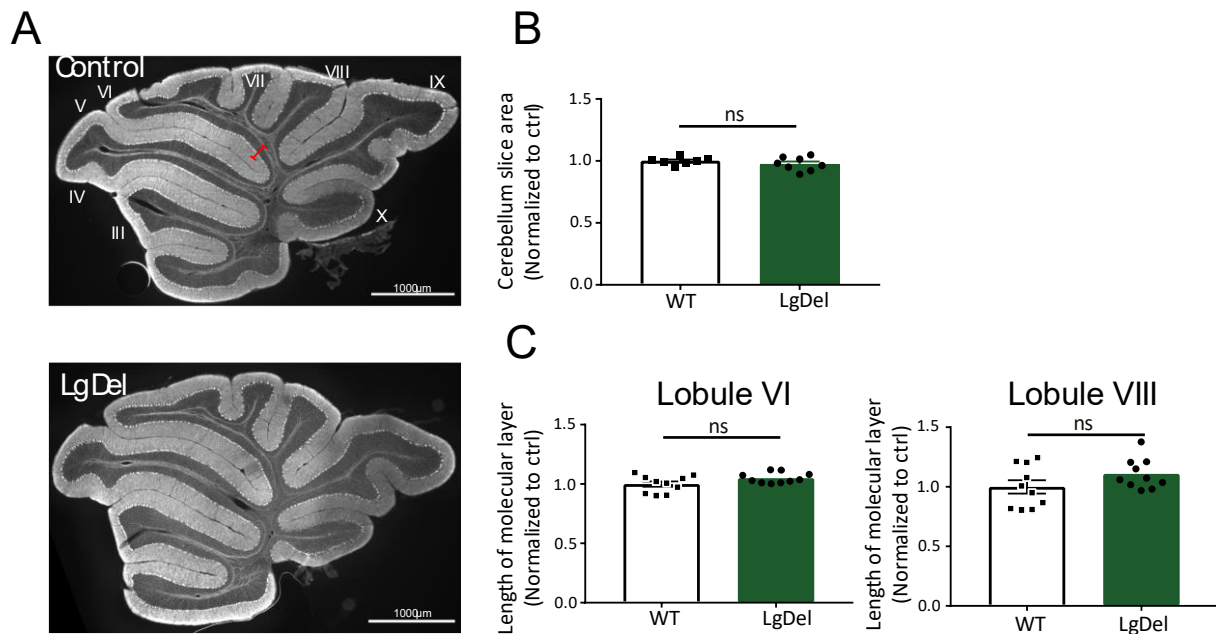


Figure 1. Normal global cerebellar morphology in P30 LgDel mice.

- (A) Sagittal cerebellar slices from P30 WT (top) and LgDel (right) animals were immunostained with an anti-calbindin antibody that specifically stains Purkinje cells. Scale bar: 1000 μ m.
- (B) Quantification of the main area of the cerebellar slices show no significant differences between the two conditions in the vermal area. Mean \pm SEM. WT: n=7, LgDel: n=8, Unpaired Student's test, n.s.= not significant.
- (C) Thickness of the molecular layer has been measured from the Purkinje cell's beginning of primary dendrite to the upper extremity of the molecular layer. No significant differences in the thickness of the molecular layer are found between Vehicle- and LgDel animals. Mean \pm SEM. Vehicle: n=10, LgDel: n=10, Unpaired Student's test, ns. = not significant.

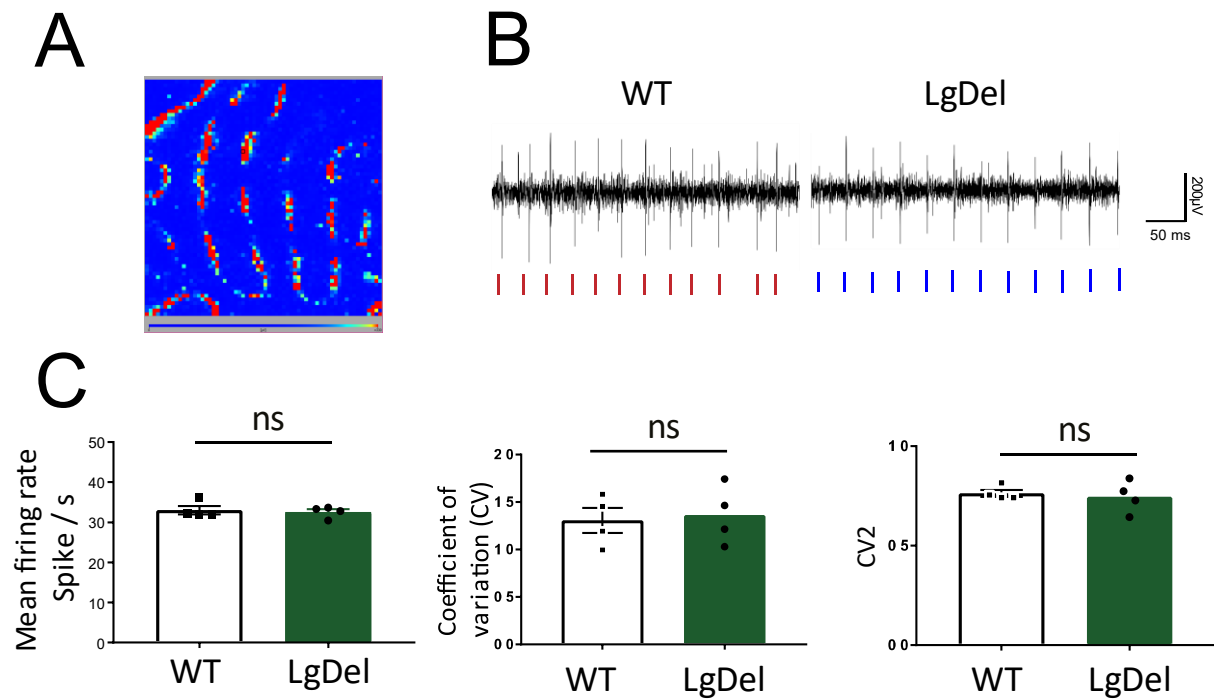


Figure 2. Normal spontaneous electrophysiological activity of Purkinje Cells in the cerebellar cortex of LgDel +/- mice

High density microelectrode array (MEA) analysis of Purkinje cell spiking in acute cerebellar slices from WT and LgDel mice.

- (A) Example representation of the recorded electrical activity in a cerebellar slice of a WT mouse. Each pixel represents one channel, where units showing high activity in red, and low activity in blue.
- (B) Representative traces of electrical activity recorded in one channel for each type of animal. Each colored vertical bar represents an action potential detected by the Brainwave software after spike detection.
- (C) Histograms of mean firing rate, coefficient of variation of Inter Spike Intervals (CV1) and CV2. Recordings have been done on two slices per animal, each slice containing between 20 and 200 active neurons. The software sorted all the detected spike into clusters called “unit”, based on the similarity of their shapes and their spatial localization. All the units (supposed to represent spiking neurons) from two slices of a same animal are pooled together. Mean \pm SEM. WT n=4 mice and LgDel n=4 mice, Unpaired Student’s test, ns. = not significant.

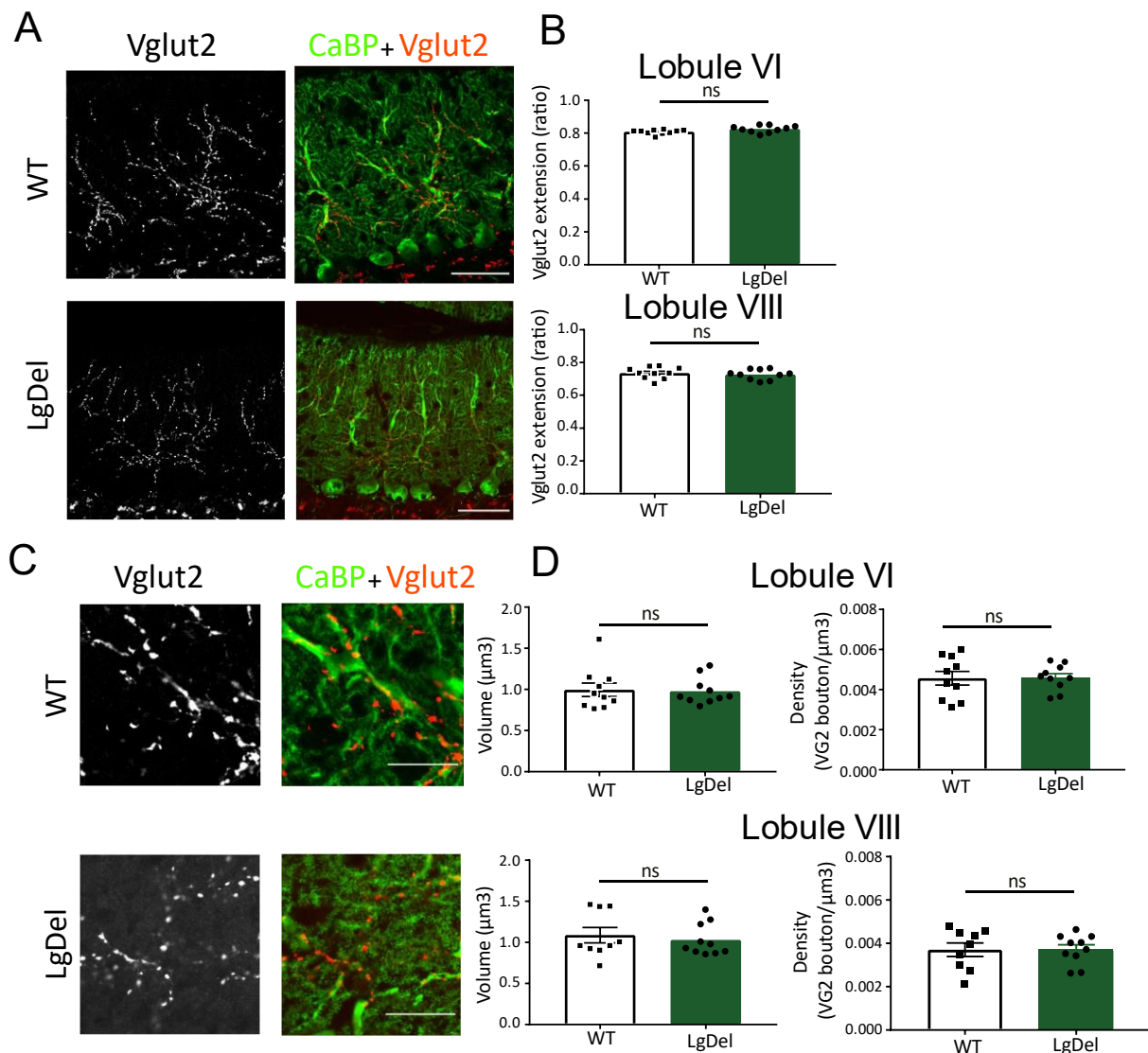


Figure 3. Normal climbing fiber presynaptic boutons morphology in LgDel mice

- (A) Climbing fiber presynaptic boutons were immunostained with an anti-VGLUT2 antibody (red), and Purkinje cells and their dendritic tree with an anti-calbindin antibody (green), in sagittal cerebellar sections from P30 WT and LgDel mice. Scale bar: 50 μm .
- (B) The extension of Climbing fiber synaptic territory has been calculated by quantifying the extent of VGLUT2 labelling relative to the height of the Purkinje cell dendritic tree. Climbing fiber extension is normal in both lobules VI and lobule VIII of LgDel mice. WT n = 10, LgDel: n = 10. Mean \pm SEM, unpaired student t test.
- (C) High magnification image of VGLUT2 clusters (red) and Purkinje cell dendrites (green) in sagittal cerebellar sections from P30 WT and LgDel mice labeled as in (A). Scale bar: 20 μm .

(D) Left: Quantification of the mean density of VGLUT2 puncta in lobule VI and lobule VIII, right: quantification of VGLUT2 puncta mean volume in lobule VI and lobule VIII. VGLUT2 puncta density and volume are normal in LgDel mice. Mean \pm SEM. WT: n=10, LgDel n=10. Unpaired Student t-test, ns. = not significant.

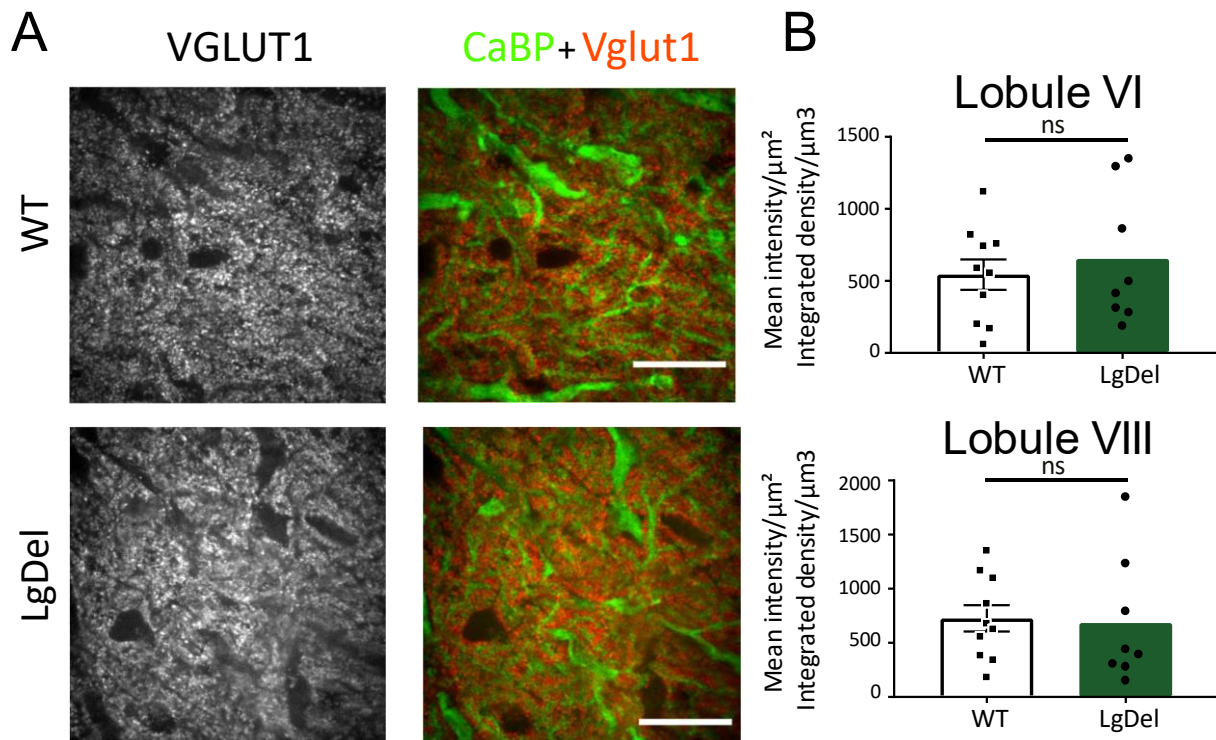


Figure 4. Normal parallel fiber synaptic density in LgDel mice.

- (A) Parallel fiber presynaptic boutons were immunostained with an anti-VGLUT1 antibody (red), and an anti-calbindin antibody (green) has been used to stain Purkinje cells and its dendritic tree in sagittal cerebellar sections from P30 WT and LgDel mice. Scale bar: 50 μm .
- (B) Quantification of mean intensity of VGLUT1 staining in the molecular layer using ImageJ software found no change in the LgDel model Mean \pm SEM. WT: n=10, LgDel n=10. Unpaired Student t-test, ns. = not significant.

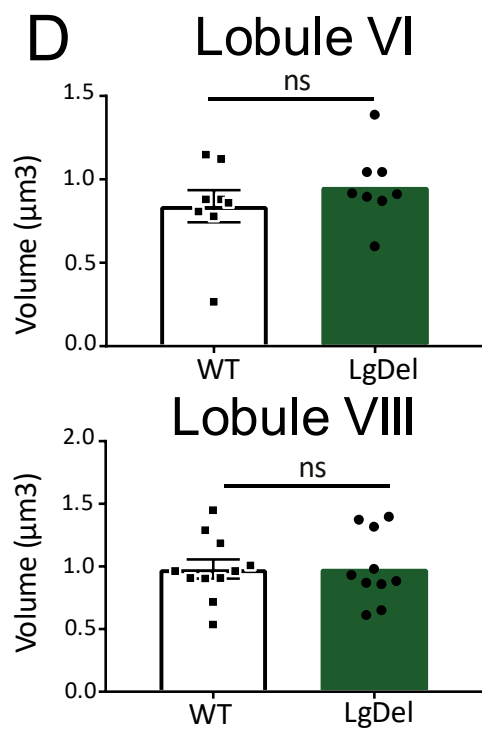
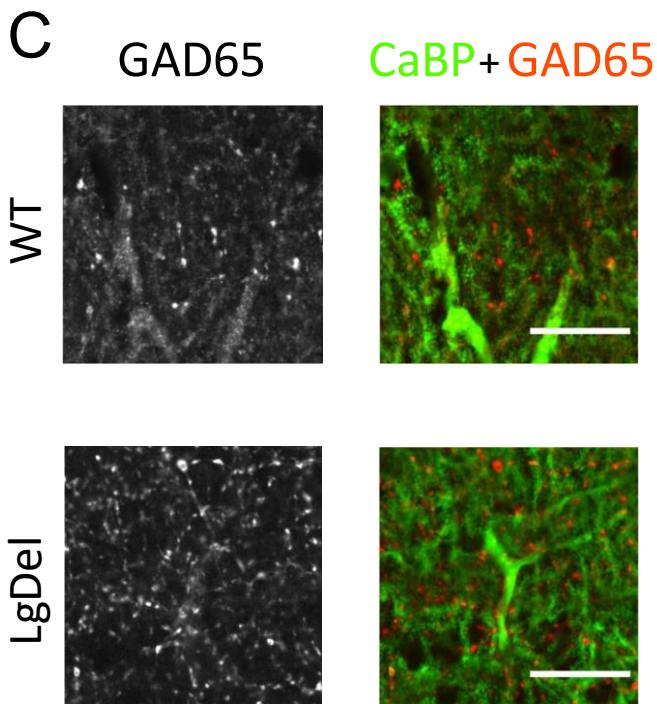
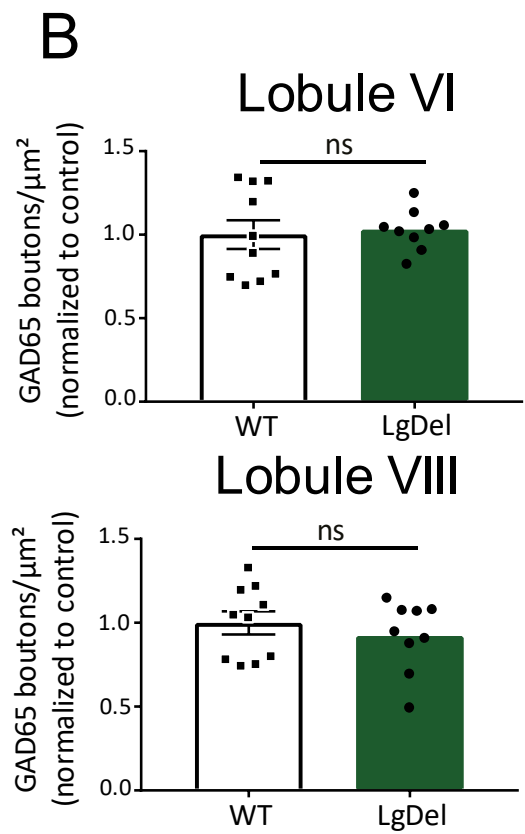
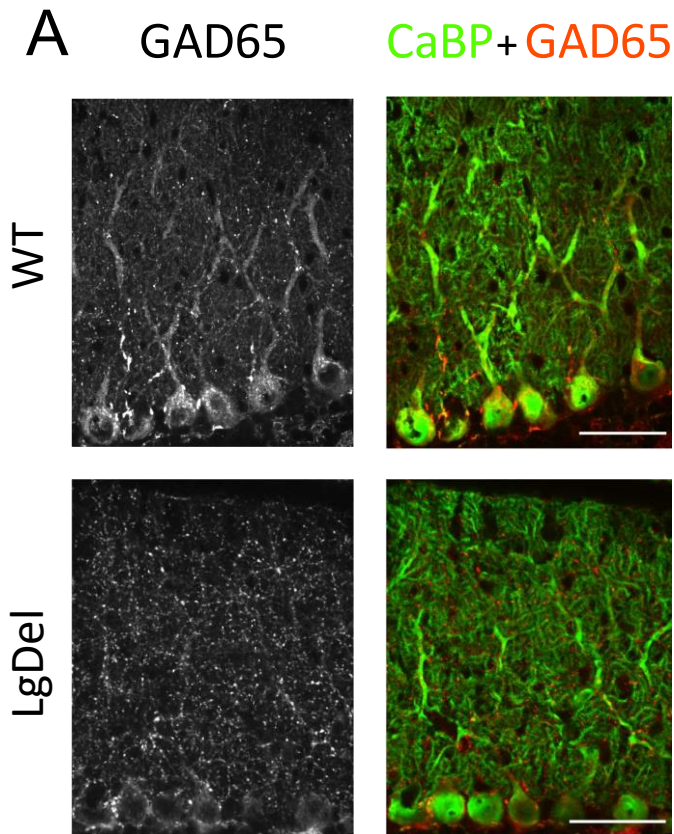


Figure 5. Normal Molecular Layer Interneurons presynaptic boutons morphology in LgDel mice.

- (A) Molecular Layer Interneurons presynaptic boutons were immunostained with an anti-GAD65 antibody (red), and an anti-calbindin antibody (green) has been used to stain Purkinje cells and its dendritic tree in sagittal cerebellar sections from P30 WT and LgDel mice. Scale bar: 50 μ m.
- (B) Quantification of GAD65 puncta revealed normal presynaptic inhibitory boutons density in the molecular layer of lobules VI and VIII in LgDel mice. Mean \pm SEM. WT: n=10, LgDel n=10. Unpaired Student t-test, ns. = not significant.
- (C) High magnification image of GAD65 clusters (red) and Purkinje cell dendrites (green) in sagittal cerebellar sections from P30 vehicle and PCP mice labeled as in (A). Scalebar: 20 μ m.
- (D) Quantification of GAD65 puncta revealed normal presynaptic inhibitory boutons volume in lobules VI and VIII in LgDel mice. Mean \pm SEM. WT: n=10, LgDel n=10. Unpaired Student t-test, ns. = not significant.

General discussion

The goal of my PhD work was to study cerebellar deficits at the synapse-specific level in mice models of schizophrenia, and to decipher the molecular mechanisms underlying these deficits.

My first aim was to bring physiopathological insight concerning schizophrenia. Notably, while there is genetic and postmortem evidence for synaptic deficits in schizophrenia, little is known about synapse-specific alterations that could lead to abnormal network function. We studied this issue in the olivo-cerebellar network, but our results could eventually be transposed to other structures.

The second goal, following the recent work of the lab, was to identify potential new actors of the establishment and regulation of the precise connectivity of the cerebellar Purkinje cell. Using pathological models such as a pharmacological or genetic perturbation of the synaptic development, we can deduct potential mechanisms and molecular pathways that play a role in the development of Purkinje cell connectivity.

Summary of the main results

Using the same systematic descriptive approach on two different developmental models of schizophrenia, we were able to find lasting synaptic deficits in the environmental neonatal phencyclidine (PCP) model, but not in the genetic LgDel model. In the PCP model, we found morphological deficits specific of the climbing fiber/Purkinje cell synapses, while synapses of the other excitatory afferent, the parallel fibers, and the inhibitory afferents were unaffected. In particular, we have detected a decrease in the volume of the climbing fiber presynaptic boutons in the neonatal PCP model, suggesting a deficit of climbing fiber synaptic maturation. We also found an increased density of climbing fiber presynaptic boutons in one of the two lobules analyzed, suggesting a region-specific effect of the treatment on either synapse formation or synapse elimination.

Furthermore, to decipher the molecular alterations responsible for these deficits and to identify potential new pathways implicated in the regulation of the olivo-cerebellar synaptic network, we performed a high throughput expression analysis on a selection of genes coding for membrane and secreted proteins. These genes were preselected from a previous work of the laboratory (Keerthana Iyer thesis), which aimed to identify new genes that are potentially playing a role in the development of the Purkinje cell excitatory synaptic network and its precise

pattern of connectivity. This preselection was based on two criteria: these genes should code for membrane and secreted proteins, the major class of molecules that regulates directly the formation of synaptic connectivity, and they should be enriched specifically in each excitatory afferent of the Purkinje cell: the inferior olivary neurons and the granule cells.

We found that the PCP treatment induces transient perturbation in the expression of 30 such genes in the cerebellum, and 2 genes in the brainstem. Several of these genes were associated with molecular pathways implicated in synapse formation, maturation and elimination, suggesting a causal link between the synaptic deficits and the transient molecular changes. We identified one particular candidate gene, *Ctgf*, which shows the highest perturbation following PCP treatment, and whose molecular functions are compatible with a role in synapse development.

What is the effect of PCP subchronic injections during development on climbing fiber/Purkinje cell synapses?

We found a decrease in the volume of VGLUT2 presynaptic clusters on Purkinje cells, in the two lobules we analyzed in the PCP model. This morphological deficit suggests that climbing fiber / Purkinje cell synaptic function might be altered in a long-lasting manner by PCP injections during the second postnatal week.

An atrophy of climbing fiber presynaptic boutons has been found in several non-physiological conditions, such as in conditional knock-out mice for neuroligins in Purkinje cells (Zhang et al., 2015), in the G protein subunit G α knock-out mouse (Cha et al., 2019), in a knock-down of postsynaptic protein BAI3 (Sigoillot et al., 2015), or in a mouse model of early neonatal alcohol exposure (Pierce et al., 2011). Interestingly, in the neuroligin conditional knock-out, and in the BAI3 knock-down, the authors found that the climbing fiber boutons atrophy is associated with a decrease of CF-EPSC amplitude, suggesting that climbing fiber synapse function is impaired in this model. To test whether synaptic transmission is deficient in the neonatal PCP model, we are currently doing patch-clamp analysis of cerebellar Purkinje cells, to measure the amplitude and kinetics of the excitatory Post Synaptic Currents (EPSCs) elicited in PCs by CF stimulation. PCP-induced deficits of synaptic transmission have been described in the mPFC and the hippocampus (Arvanov and Wang, 1999; Ninan, 2003; Raja and Guyenet, 1982), strengthening the hypothesis that synaptic function may be altered by PCP.

Our results also show that there is an increase of climbing fiber presynaptic bouton density in lobule VI of the PCP model. This increase could arise from two sources: either an increase of synapse formation, or a deficit of synapse elimination. As discussed in part 3.2.2 of the introduction, cerebellar Purkinje cells are innervated by up to five climbing fibers at birth, and the supernumerary climbing fibers are progressively eliminated during the second and third postnatal weeks to reach a ratio of one climbing fiber per Purkinje cell (Li et al., 2015; Schwarz et al., 2010). In our results in the PCP model, we found an increase of the climbing fiber / Purkinje cell boutons density at P30. This deficit could be explained by a deficit of synapse elimination. It has been previously shown that the local *in vivo* application of AP-5, an NMDA antagonist, in the surface of rat cerebellum from P4 to P16, induces the persistence of multi-innervation of Purkinje cells by several climbing fibers (Rabacchi et al., 1992). To test whether

PCP injections have the same effect, we are currently analyzing the multi-innervation of Purkinje cells in PCP-treated mice using patch-clamp recordings.

Our deficit in synaptic density was region specific: we only found an increased density in lobule VI, not in lobule VIII. This specificity could be caused by the asynchronous development of the cerebellar cortex combined with the relatively short (35 minutes) half-life of PCP (Nabeshima et al., 1987). This suggests that PCP is likely to act during a relatively short time-window and might not affect synapse elimination in Purkinje cells similarly depending on the developmental stage. However, we cannot exclude an eventual regional specificity, since the cerebellar cortex is not physiologically homogenous. For example, the simple and complex spike activity of Purkinje cells differs between different cerebellar subregions characterized by the presence or absence of the glycolytic enzyme Aldolase C (or zebrin (Zhou et al., 2014)), and we cannot exclude that our measurement in lobule VI and in lobule VIII were done in different subpopulations of Purkinje cells. Thus, if some zones show molecular specificity, such as, for example different NMDA subunit receptors, it could change the sensitivity to PCP. Further characterization of the presence or absence of zebrin in the studied areas could eventually clarify this point.

Does *Ctgf* overexpression cause synaptic alterations in the neonatal PCP model?

Our results in the PCP model have found that *Ctgf* is significantly overexpressed in the cerebellum and brainstem at P11, right after the last PCP injection. *Ctgf* is particularly interesting, because the amplitude of gene expression change is the highest amongst all the genes analyzed (close to a five-fold increase in the cerebellum) but also because of the predicted functions of this gene. This secreted protein is a member of the CCN protein family (acronym for Connective tissue growth factor (CTGF), Cystein rich protein (Cyr61), and Nephroblastoma Overexpressed Genes (NOV) (Bork, 1993)), that are known to be implicated in various functions, such as cell adhesion, migration, proliferation, or neuronal development. CCN proteins all have four conserved protein domains: an insulin-like growth factor-binding protein (IGFBP), a von Willebrand factor type C (VWC), a thrombospondin type-1 (TSP1) and a C-terminal cystine knot-like (CT) domain (Takigawa, 2017). The role of CTGF in synaptogenesis has been recently highlighted by a study at the neuromuscular junction (Ohkawara et al., 2020). The authors have shown that CTGF interacts through its CT domain with LRP4, a cell adhesion protein implicated in post-synaptic function in the neuromuscular junction, and that loss of

CTGF affects the maturation and function of the presynaptic nerve terminal (Ohkawara et al., 2020).

Ctgf interacts with several other proteins and pathways implicated in synaptic development, maturation, and cerebellar synapse elimination, such as TGF β , BMP4, or IGF1 (Abreu et al., 2002; Araujo et al., 2016; Bialas and Stevens, 2013; Kakizawa et al., 2003; Kalinovsky et al., 2011; Stevens et al., 2007). This suggests that the misregulation of the *Ctgf* gene induced by PCP in the cerebellum could perturb several signaling pathways that could control the development and maturation of the climbing fiber synapses on Purkinje cells.

Ctgf is known to activate TGF β signaling. In the visual system, TGF- β signaling is a regulator of the neuronal expression of the complement protein C1q, and activates the complement-dependent synaptic refinement (Bialas and Stevens, 2013). In the olfactory system, CTGF act as a potentiator of C1q protein through the TGF- β pathway, and thus plays a role in synaptic refinement.

CTGF also interacts with BMP4 through its CR domain, and blocks its activity by preventing its binding to BMP receptors (Abreu et al., 2002). The BMP pathway has been linked to synapse development. BMP4 is implicated in the elimination of inappropriate mossy fiber-Purkinje cell contacts during the development of the cerebellar cortex (Kalinowski et al., 2011). In the auditory system, conditional loss of BMP β 1a and 2b led to several synapse-morphological and functional abnormalities (Xiao et al., 2013). In the calyx of Held, this double deletion led to a decrease of the presynaptic nerve terminal volume measured by the immunohistochemical marker Synaptotagmin-2, and a deficit in synaptic transmission revealed by a reduced amplitude of EPSCs, suggesting a deficit of synapse maturation. Moreover, the authors found that the deletion of BMP receptors doesn't affect initial synapse formation, but rather would affect synapse elimination and synapse remodeling. In the calyx, the post-synaptic neurons in the medial nucleus of the trapezoid body (MNTB) are initially innervated by several calyx nerve terminals, and the supernumerary inputs are eliminated at P2-P4, to reach mono-innervation. This is similar to the development of climbing fiber innervation on Purkinje cells. In the BMP β 1a-2b double KO, multi-innervation is still present at P14, suggesting a deficit of synapse elimination. Thus, BMP4 loss in the auditory system results in the same deficits than those we observe for climbing fiber presynaptic boutons in the PCP cerebellum, namely the decrease of presynaptic boutons volume and their increased density in the lobule VI.

Finally, CTGF interacts with IGF-1, through its IGF-binding domain (Kim et al., 1997). IGF-1 function during synapse development has been described in the cerebellum: local application of IGF-1 at P8 in mouse cerebellum interferes with climbing fiber synapse elimination, by increasing the strength of developing climbing fibers, thus leading to an increased degree of multiple climbing fiber innervation (Kakizawa et al., 2003).

Altogether, CTGF roles in synaptic development in the neuromuscular junction, but also its functional interaction with several molecular pathways implicated in synapse formation, maturation and elimination, in the cerebellum but also in other structures, strongly suggests that CTGF could be an actor of synaptic development, and that its deregulation in the PCP model could explain both the decrease of climbing fiber synaptic bouton volumes, and the increased synaptic boutons we detected on lobule VI. We are currently testing this hypothesis by inducing an overexpression of *Ctgf* at P7, through intra-cerebellar injections of a lentiviral vector containing a cDNA coding for *Ctgf* under the control of the Phosphoglycerate kinase (PGK) promoter, and studying the morphological consequences at P30. In particular, we are measuring whether *Ctgf* overexpression reproduces the PCP induced climbing fiber decrease in presynaptic bouton volume and the increased density seen in the lobule VI. One alternative experiment could be to Knock-Down (KD) *Ctgf* expression in the cerebellum from P7 PCP-treated mice using intracerebellar injection of a lentiviral vector containing a shRNA, and to check whether it prevents the PCP-induced morphological deficits of climbing fibers synapses.

As suggested above, this potential effect of CTGF on cerebellar synaptic development could be either direct, or mediated through a molecular pathway, such as BMP, IGF1, or TGF β pathways. To check whether *Ctgf* acts through TGF β pathways, one possible method would be to knock-in *Ctgf* while knocking-down TGF β receptor (Khodosevich et al., 2013) at P7. Thus, if TGF β act as a downstream pathway of *Ctgf*, the effect of *Ctgf* overexpression may be abolished. Similarly, to test whether *Ctgf* acts on BMP pathways, one possibility would be to design a viral vector containing a CTGF cDNA lacking the CR domain, thus unable to fix BMP4, and overexpress this truncated *Ctgf* in the cerebellum during development from P7. If the hypothesis is true, the truncated *Ctgf* should not induce synaptic deficits. Another possible strategy would be to co-inject PCP with a BMP4 agonist passing the blood-brain barrier, such as Ventromorphins (Genthe et al., 2017). If PCP's effect on cerebellar synapses is mediated through a CTGF/ BMP4 cascade, a BMP4 agonist should prevent these deficits.

Hypothesis for the link between PCP, neuronal activity and synaptic alterations in cerebellar Purkinje cells

In addition to providing knowledge about synaptic deficits in the context of neurodevelopmental disorders, our results could also bring new clues to the understanding of mechanisms of synapse development in the olivo-cerebellar network.

Phencyclidine is an NMDA antagonist, thus expected to inhibit glutamate transmission through NMDA receptors. In the cerebellum, NMDA receptors are present at mossy fiber – granule cell synapses (Cathala et al., 2000), at climbing fiber- Purkinje cells synapses (Piochon et al., 2010), in molecular layer interneurons (Bidoret et al., 2015), and presynaptically at the parallel fiber / Purkinje cell synapses (Casado et al., 2000). Neuronal activity is known to play a major role in the development and refinement of synaptic networks, by regulating synaptic maturation and pruning (Tessier and Broadie, 2009; Zhang and Poo, 2001). In the cerebellum, climbing fiber synapse elimination is dependent on the activity of Purkinje cells (Lorenzetto et al., 2009) and climbing fibers (Andjus et al., 2003) for the early phase, and on granule cell activity for the late phase of climbing fiber synapse elimination (Kano and Hashimoto, 2012).

Hence, an NMDA antagonist could have different repercussions on neuronal activity in the olivo-cerebellar network. The first possibility would be that NMDA antagonism leads to an inhibition of neuronal activity. PCP could block post-synaptic NMDA receptors in the inferior olivary neurons, in granule cells, and in climbing fiber / Purkinje cells synapses, thus supposed to induce a decrease of Purkinje cells / granule cell activity. The second possibility would be a global increase of Purkinje or granule cell activity through the blockade of the inhibitory activity of molecular layer interneurons and / or the Golgi cells, thus disinhibiting Purkinje cells and granule cells, respectively. Several reports in the literature suggest that PCP may act preferentially in GABAergic interneurons. Indeed, NMDA receptors blockage usually causes excitation in the mPFC (Gratton et al., 1987; Jodo et al., 2005), and this effect is thought to act via disinhibition of inhibitory interneurons (Homayoun and Moghaddam, 2007; Jodo et al., 2005; Su et al., 2018). And in the cerebellum, PCP administration leads to marked increase of *c-fos* expression in granule cells revealed by immunostaining, suggesting that PCP increases granule cells activity (Näkki et al., 1996), but also of inhibition of inhibitory Golgi neurons (Bullock et al., 2009), thus expected to disinhibit granule cells.

We quantified the expression of *c-fos*, an immediate early gene used as a marker of neuronal activity (Bullitt, 1990), and found a significant increase in PCP-treated mice at P11

compared to saline, thus in favor of a global increase of cerebellar activity (**Figure S1A**). Hence, to test whether the effect of neonatal PCP treatment in cerebellar synaptic morphology and the transient molecular changes are caused by changes of neuronal activity, we are using a Designer Receptor Exclusively Activated by Designer Drugs (DREADDs) strategy to modulate granule cells activity (and thus, indirectly, Purkinje cells activity) during the same period of cerebellar development as PCP injections.

To test whether an increase of granule cell activity at the same period as PCP treatment is reproducing the synaptic alterations and molecular changes induced by PCP, we crossed mice expressing Hm3dq gene (excitatory DREADDs) in a CRE-dependent manner and mice expressing the CRE recombinase under the NeuroD1 promoter, allowing expression of CRE in granule cells specifically in the olivo-cerebellar network. We activated HM3Dq by injecting the mice with Clozapine-N-Oxide (CNO, concentration 30mg/kg) at P7, P9, and P11. RTqPCR suggests that expression of *c-fos* is increased in the cerebellar extracts of CNO injected mice compared to controls confirming the efficacy of the DREADDs strategy (**Figure S1B and S1C**). To check if cerebellar synaptic deficits in PCP-treated mice are also caused by neuronal activity changes, we are characterizing the cerebellar excitatory synapses morphology, using VGLU1 and VGLUT2 specific markers, in mice with subchronic increase of granule cells activity (Hm3dq tg/0 mice treated with CNO) versus controls (Hm3dq 0/0 treated with CNO). A second control using injection of physiological serum in both genotypes will also be done in order to check an eventual contribution of CNO itself to the results.

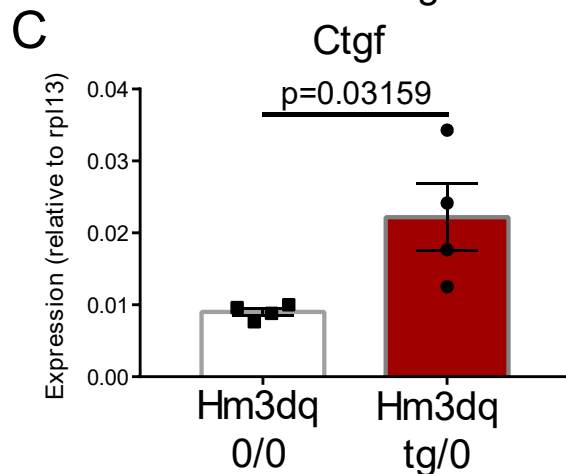
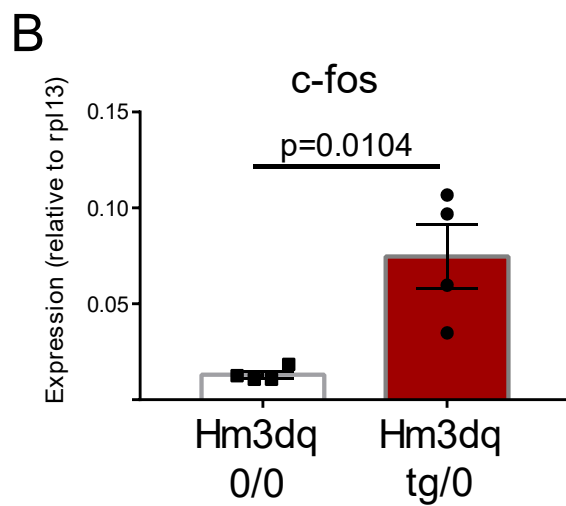
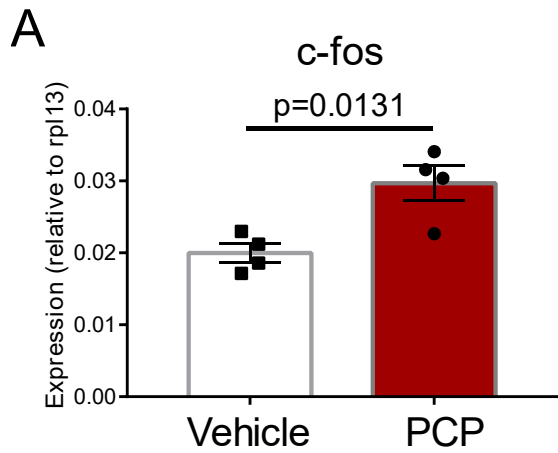


Figure S1 : Preliminary results for the role of activity in PCP-elicited deficits

- (A) Immediate early gene c-fos is overexpressed in the cerebellum of P11 PCP-treated mice versus saline. Vehicle: n=4, PCP: n=4. Mann-Whitney non-parametric test.
- (B) Expression of c-fos in NeuroD1cre - Hm3dq mice tg/0 – tg/0 versus tg/0 – 0/0 mice in cerebellum of P11 mice, after 3 injections of CNO (30mg/kg) at P7, P9 and P11. n=4 for Hm3dq 0/0, n=4 for Hm3dq tg/0.
- (C) Expression of Ctgf in NeuroD1cre - Hm3dq mice tg/0 – tg/0 versus tg/0 – 0/0 mice in cerebellum of P11 mice, after 3 injections of CNO (30mg/kg) at P7, P9 and P11 n=4 for Hm3dq 0/0, n=4 for Hm3dq tg/0.

Preliminary results also suggest that an increase of granule cells activity is sufficient to induce an overexpression of *Ctgf* in the cerebellum, and that *Ctgf* transient upregulation in PCP-treated mice is probably activity-dependent.

What could be the activity-dependent mechanism for a CTGF induced perturbation of climbing fiber synapses?

CTGF expression in the cerebellum low after birth, but increases from P7, and reach a peak at P21, before decreasing (Figure Supplementary 3 page 114). PCP neonatal treatment induces a massive activity-dependent overexpression of CTGF in the cerebellum at P11, superior to the peak in untreated mice. If *Ctgf* overexpression is responsible for PCP induced decrease of climbing fiber boutons and increase of boutons density, one possible hypothesis would be that *Ctgf* acts as an “end of maturation signal”. By provoking this *Ctgf* peak too early in the development, it could cause a precocial stop of climbing fiber presynaptic development, leading to immature climbing fiber synaptic boutons, that could explain the decreased volume in PCP model. This hypothesis could also explain the increased density that we observed in the lobule VI, if a *Ctgf* peak is associated to an “end of maturation” signal for synapse elimination (that would normally occur around the third postnatal week). Climbing fiber elimination is dependent on neuronal activity (Kano et al., 2018). In particular, the late phase of climbing fiber elimination (after P12) is dependent on granule cells activity. Parallel fiber and climbing fiber compete for the synaptic territory in the dendritic tree of the Purkinje cell (Bailly et al., 2018b; Ichikawa et al., 2016). One could imagine that activity-dependent secretion of *Ctgf* in the cerebellar cortex could be an actor of this heterosynaptic competition between parallel fiber and climbing fibers. For example, activity-dependent secretion of CTGF by parallel fibers could be a quantitative marker of parallel fiber activity, and could play a role in the regulation of the competition with climbing fibers, perhaps by stopping climbing fiber maturation and elimination when reaching a certain amount. Thus, according to this hypothesis, the precocial peak of CTGF induced by the PCP model, would stop climbing fiber maturation and elimination too early.

Finally, this hypothesis is proposing a molecular mechanism for explaining PCP induced perturbations of cerebellar synaptic development, which could eventually be transposed to other brain regions.

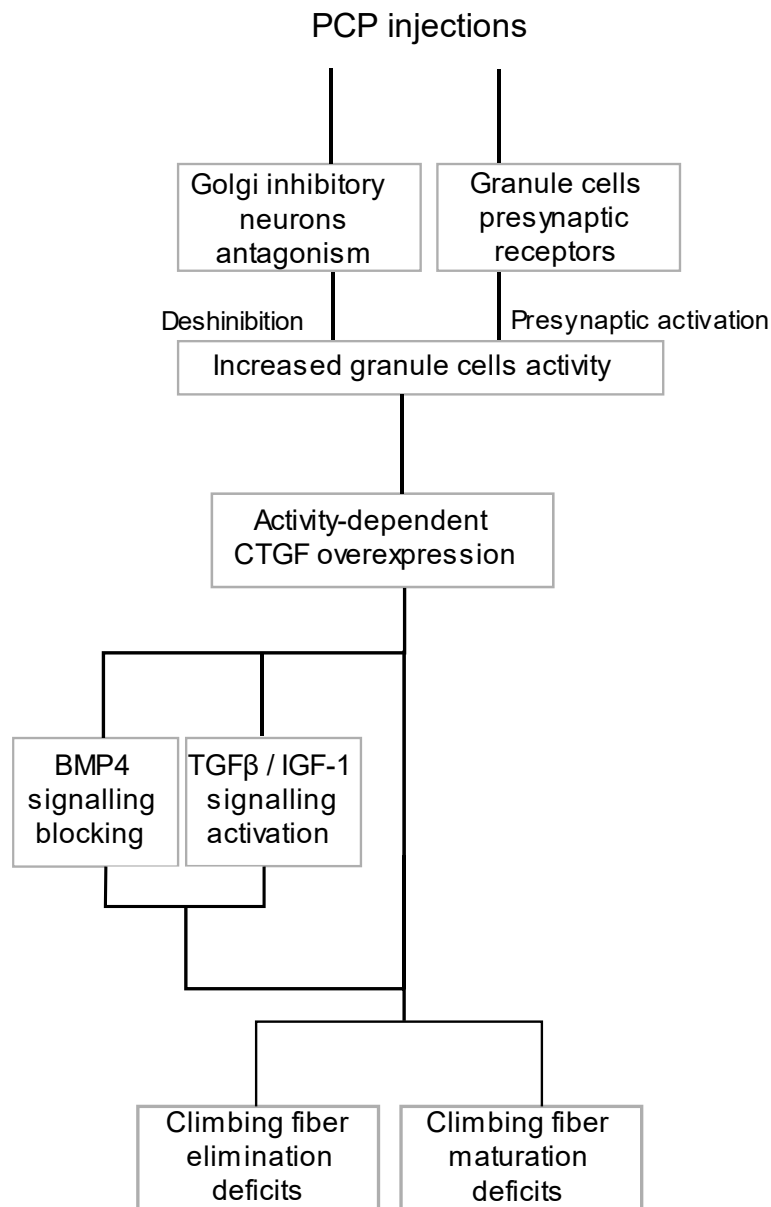


Figure S.2: Hypothesis for a potential mechanism for PCP induced cerebellar synaptic deficits.

PCP injections, as an NMDA antagonist, are blocking the activity of cerebellar Golgi Interneurons, in turn disinhibiting granule cells. Increased granule cells activity will then increase Purkinje cells activity. Additionally, presynaptic parallel fibers / Purkinje cells NMDA receptors could also participate to an increased Purkinje cell activity. Several activity dependent genes are overexpressed following neuronal hyperactivity, comprising *Ctgf*.

Ctgf could either act directly on climbing fiber synapses maturation and elimination, or indirectly through activation of TGFβ or IGF1 pathways, or inhibition of BMP4 pathway.

Neuronal activity, a potential actor of neurodevelopmental and synaptic disorders?

The hypothesis mentioned above suggests that PCP-induced disruption of the cerebellar synaptic development is caused by a deregulation of neuronal activity during the development. How could neuronal activity play a role in neurodevelopmental disorders?

During early brain development, sensory experience modifies synaptic maturation and elimination through neuronal activity and is necessary to shape a normal and efficient synaptic network (Wiesel, 1982). Indeed, neuronal activity regulates several signaling pathways implicated in synapse development, the synthesis of proteins at the synapse, regulating their function and strength in reaction to experience (Ebert and Greenberg, 2013; Kandel, 2001). Thus, early alterations of genes and proteins regulating neuronal activity, such as excitatory or inhibitory neurotransmitters and receptors could lead to an impairment of the establishment of a normal synaptic network. Several activity-dependent molecular pathways are regulating synapse formation, maturation, elimination and plasticity, such as the post-synaptic Arc, mTOR or BDNF pathways. The fact that many mutations impact activity-dependent signaling networks raise the hypothesis that impairment of activity-dependent pathways could be a feature of neurodevelopmental disorders such as Autism Spectrum Disorders (Chubykin et al., 2007; Morrow et al., 2008; Walsh et al., 2008), and that it may affect sensory experience dependent development of synaptic networks.

In the case of schizophrenia, many synaptic genes and pathways highlighted by genetic studies, such as Arc, BDNF, PSD95, or the NMDA receptor subunits, are both regulated by and regulating activity. Moreover, studies on schizophrenia human-induced pluripotent stem cells neurons (hiPSC) revealed that neurons from schizophrenic patients have a significant dysregulation of activity-dependent genes. In this study, the authors also studied the response of hiPSC from schizophrenic patients to neuronal depolarization, as a way to study activity-dependent responses, and also found differential regulation of gene expression in schizophrenia derived compared to controls-derived hiPSC (Roussos et al., 2016).

Hence, similarly to ASD, schizophrenia could also implicate activity-dependent mechanisms. This hypothesis also correlates well with the history of the disease: usually, schizophrenia onset occurs during adolescence, after a period of synaptic development and maturation during childhood. It is plausible that genetic predisposition factors leading to impairment of activity-related pathways integrate improperly sensory experience during

childhood, thus leading to an abnormal synaptic network at adolescence, favoring schizophrenia onset.

Furthermore, it could also be an explanation for the burden of the environmental factors in schizophrenia, as suggested by twin studies showing a concordance rate of only 33% in monozygotic twins (Hilker et al., 2018). Moreover, it could be hypothesized that a strong environmental stimulation leading to an increased risk of developing schizophrenia could act through chronic excessive modulation of neuronal activity. Several environmental risk factors have been linked with schizophrenia, comprising child sexual abuse, victimization, urban living or migration, factors that could leave to excessive emotional or sensorial elicited neuronal activity. While there is up to now no proven evidence that environmental factors may be sufficient for inducing schizophrenia, it is plausible that these mechanisms could have an impact in schizophrenia together with genetic susceptibility.

Identifying how neuronal activity could impact the development of synaptic circuit, and linking these mechanisms to neurodevelopmental disorders such as schizophrenia could have important clinical repercussions, for finding potential drug targets regulating neuronal activity, but also for finding potential environmental prevention or precocial psychotherapy, a link between environmental therapy and neuronal activity could be found.

How this study could contribute to the understanding of schizophrenia physiopathology?

In this project, we used two developmental models commonly used to mimic schizophrenia physiopathology. While both models are obviously not perfect, they allow to describe several physiopathological abnormalities that could arise from such developmental perturbation. Moreover, schizophrenia is a very heterogenous disease, and while dissociation and loss of contact with reality are commonly shared by most of the patients, the diversity of symptoms and the diversity of genes linked to schizophrenia suggests that this pathology could come from different origins.

In our results, we found that the neonatal PCP model induces afferent specific alterations of cerebellar synaptic development. While it remains controversial whether injecting PCP at such early stages of the development is a realistic way of inducing schizophrenia, the fact that

rodents display long term behavioral and neuropathological deficits, is encouraging. Nevertheless, our results suggest that precocial perturbation of synaptic development could lead to long-term deficits in synaptic network, which could eventually be linked to a schizophrenia-related symptomatology. Moreover, we have hypothesized that neuronal activity could play a role in these deficits. If that hypothesis is verified, it will suggest that neuronal activity during the early development could play a role in the normal synaptic development – which could reflect the importance of environmental factors that could leave to abnormal sensorimotor or emotional stimulation, such as chronic stress, migration, social isolation...

In the genetic LgDel model, we didn't find any differences in the cerebellar synaptic network organization. However, we didn't check if there were any molecular or synaptic electrophysiological abnormalities in the LgDel model. Since this genetic deletion is supposed to bring a higher risk to develop schizophrenia, but is not sufficient to induce the pathology by its own, it is possible that LgDel mice have an increased sensibility to environmental influence. It is also possible that the LgDel model induces other kinds of deficits that would occur later in the development. In a recent article, Mukherjee et al. have shown that LgDel mice have several network dysfunction in the hippocampus and mPFC, associated with cognitive deficits, and that these deficits likely take place from adolescence (P60) to adulthood (P120) (Mukherjee et al., 2019). Indeed, the authors found deficits in parvalbumin (PV) expression, and in PV neuron plasticity mostly after P60, while at P40 deficits were restricted to a few areas. Moreover, they were able to rescue adult connectivity deficits (increased high-gamma power in the mPFC) and cognitive deficits by modulating the activity of PV interneurons during a short time window at P60 – P70. This article suggests that developmental alteration of neuronal network in the mPFC would impact more late adolescence mechanisms than early postnatal. Hence, while our results suggest that LgDel mice don't have deficits of early cerebellar synaptic development, we cannot exclude that LgDel mice show cerebellar synaptic deficits in later stages, for example synaptic plasticity deficits.

Moreover, the polygenic hypothesis of schizophrenia implicates that the combination of several mutations brings a higher susceptibility to develop schizophrenia, and many results converge on synaptic genes, suggesting that synaptic network may be more “sensitive” to disruptions. To test this hypothesis, combining the LgDel model to an environmental stressor might be an option.

Relevance of cerebellar synaptic deficits in schizophrenia?

While not all schizophrenic patients have cerebellar deficits, there is a high prevalence of numerous motor symptoms in which the cerebellum plays a role: neurological soft signs (a set of motor coordination, equilibrium and sensory integration deficits), dyscoordination, or impaired eyeblink conditioning (Picard et al., 2008). Moreover, they are often associated with poor outcome, and greater negative and cognitive symptoms (Picard et al., 2008; Prikryl et al., 2007; Wassink et al., 1999). Our results suggest that PCP mice have impaired integration of climbing fiber signal in Purkinje cell. Amongst other roles, climbing fiber is often considered as an “error signal”, bringing sensorimotor information to correct the movement, and allowing motor learning (De Zeeuw et al., 1998, Ito, 2013). Moreover, impairment in climbing fiber input generally leads to motor learning or motor coordination deficits, such as ataxia (Horn et al., 2013; Llinás et al., 1975). However, except a long-term increase of motor locomotion in neonatal PCP mice, to our knowledge, motor deficits, neurological soft signs, and motor coordination hasn't been studied yet. Linking motor behavior deficits to the synaptic alterations we detected on the PCP model would help to understand the mechanisms leading to schizophrenia motor endophenotypes.

Finally, a recent hypothesis about the role of the cerebellum in schizophrenia suggests that cerebellar deficits could lead to “cognitive dysmetria”, a general dyscoordination of sensorimotor and mental processes, extrapolated from cerebellum's role in motor coordination (Andreasen and Pierson, 2008). In this hypothesis, the cerebellum would play a role in the integration and sorting of internal representation and external “reality” (for example, the wrong perception of an imaginary voice when no one is around in auditory hallucinations). Then, impairment of climbing fiber input as an error signal could disrupt the ability of the cerebellum to sort these internal versus external information, leading to an aberrant output.

Encouragingly, several recent papers have succeeded to induce cognitive and social deficits in animals by cerebellar specific modulations (Badura et al., 2018; Deverett et al., 2019; Rochefort et al., 2011). It would be worth to determine whether developmental modulation of granule cells activity using DREADDs in a way that recapitulates the PCP neonatal model is able to induce relevant behavioral cognitive alterations.

Bibliography

- Abreu, J.G., Ketpura, N.I., Reversade, B., De Robertis, E.M., 2002. Connective-tissue growth factor (CTGF) modulates cell signaling by BMP and TGF- β . *Nat. Cell Biol.* 4, 599–604. <https://doi.org/10.1038/ncb826>
- Akbarian, S., Sucher, N., Bradley, D., Tafazzoli, A., Trinh, D., Hetrick, W., Potkin, S., Sandman, C., Bunney, W., Jones, E., 1996a. Selective alterations in gene expression for NMDA receptor subunits in prefrontal cortex of schizophrenics. *J. Neurosci.* 16, 19–30. <https://doi.org/10.1523/JNEUROSCI.16-01-00019.1996>
- Akbarian, S., Sucher, N., Bradley, D., Tafazzoli, A., Trinh, D., Hetrick, W., Potkin, S., Sandman, C., Bunney, W., Jones, E., 1996b. Selective alterations in gene expression for NMDA receptor subunits in prefrontal cortex of schizophrenics. *J. Neurosci.* 16, 19–30. <https://doi.org/10.1523/JNEUROSCI.16-01-00019.1996>
- Andjus, P.R., Zhu, L., Cesa, R., Carulli, D., Strata, P., 2003. A change in the pattern of activity affects the developmental regression of the purkinje cell polyinnervation by climbing fibers in the rat cerebellum. *Neuroscience* 121, 563–572. [https://doi.org/10.1016/S0306-4522\(03\)00556-6](https://doi.org/10.1016/S0306-4522(03)00556-6)
- Andreasen, N.C., Nopoulos, P., Magnotta, V., Pierson, R., Ziebell, S., Ho, B.-C., 2011. Progressive brain change in schizophrenia: a prospective longitudinal study of first-episode schizophrenia. *Biol. Psychiatry* 70, 672–679. <https://doi.org/10.1016/j.biopsych.2011.05.017>
- Andreasen, N.C., Nopoulos, P., O’Leary, D.S., Miller, D.D., Wassink, T., Flaum, M., 1999. Defining the phenotype of schizophrenia: cognitive dysmetria and its neural mechanisms. *Biol. Psychiatry* 46, 908–920. [https://doi.org/10.1016/S0006-3223\(99\)00152-3](https://doi.org/10.1016/S0006-3223(99)00152-3)
- Andreasen, N.C., O’Leary, D.S., Cizadlo, T., Arndt, S., Rezai, K., Ponto, L.L., Watkins, G.L., Hichwa, R.D., 1996. Schizophrenia and cognitive dysmetria: a positron-emission tomography study of dysfunctional prefrontal-thalamic-cerebellar circuitry. *Proc. Natl. Acad. Sci.* 93, 9985–9990.
- Andreasen, N.C., Paradiso, S., O’Leary, D.S., 1998. “Cognitive dysmetria” as an integrative theory of schizophrenia: a dysfunction in cortical-subcortical-cerebellar circuitry? *Schizophr. Bull.* 24, 203–218. <https://doi.org/10.1093/oxfordjournals.schbul.a033321>
- Andreasen, N.C., Pierson, R., 2008. The Role of the Cerebellum in Schizophrenia. *Biol. Psychiatry* 64, 81–88. <https://doi.org/10.1016/j.biopsych.2008.01.003>
- Apps, R., Garwicz, M., 2005. Anatomical and physiological foundations of cerebellar information processing. *Nat. Rev. Neurosci.* 6, 297–311. <https://doi.org/10.1038/nrn1646>
- Araujo, A.P.B., Diniz, L.P., Eller, C.M., de Matos, B.G., Martinez, R., Gomes, F.C.A., 2016. Effects of Transforming Growth Factor Beta 1 in Cerebellar Development: Role in Synapse Formation. *Front. Cell. Neurosci.* 10. <https://doi.org/10.3389/fncel.2016.00104>
- Arvanov, V.L., Wang, R.Y., 1999. Clozapine, But Not Haloperidol, Prevents the Functional Hyperactivity of N-Methyl-d-Aspartate Receptors in Rat Cortical Neurons Induced by Subchronic Administration of Phencyclidine. *J. Pharmacol. Exp. Ther.* 289, 1000–1006.
- Ba, W., Yan, Y., Reijnders, M.R.F., Schuurs-Hoeijmakers, J.H.M., Feenstra, I., Bongers, E.M.H.F., Bosch, D.G.M., De Leeuw, N., Pfundt, R., Gilissen, C., De Vries, P.F., Veltman, J.A., Hoischen, A., Mefford, H.C., Eichler, E.E., Vissers, L.E.L.M., Nadif Kasri, N., De Vries, B.B.A., 2016. TRIO loss of function is associated with mild intellectual disability and affects dendritic branching and synapse function. *Hum. Mol. Genet.* 25, 892–902. <https://doi.org/10.1093/hmg/ddv618>

- Badura, A., Verpeut, J.L., Metzger, J.W., Pereira, T.D., Pisano, T.J., Deverett, B., Bakshinskaya, D.E., Wang, S.S.-H., 2018. Normal cognitive and social development require posterior cerebellar activity. *eLife* 7, e36401. <https://doi.org/10.7554/eLife.36401>
- Bailly, Y., Rabacchi, S., Sherrard, R.M., Rodeau, J.-L., Demais, V., Lohof, A.M., Mariani, J., 2018a. Elimination of all redundant climbing fiber synapses requires granule cells in the postnatal cerebellum. *Sci. Rep.* 8, 10017. <https://doi.org/10.1038/s41598-018-28398-7>
- Bailly, Y., Rabacchi, S., Sherrard, R.M., Rodeau, J.-L., Demais, V., Lohof, A.M., Mariani, J., 2018b. Elimination of all redundant climbing fiber synapses requires granule cells in the postnatal cerebellum. *Sci. Rep.* 8, 10017. <https://doi.org/10.1038/s41598-018-28398-7>
- Baldeweg, T., Klugman, A., Gruzelier, J., Hirsch, S.R., 2004. Mismatch negativity potentials and cognitive impairment in schizophrenia. *Schizophr. Res.* 69, 203–217. <https://doi.org/10.1016/j.schres.2003.09.009>
- Barbour, B., 1993. Synaptic currents evoked in purkinje cells by stimulating individual granule cells [WWW Document]. *Neuron*. [https://doi.org/10.1016/0896-6273\(93\)90085-6](https://doi.org/10.1016/0896-6273(93)90085-6)
- Bartos, M., Vida, I., Jonas, P., 2007. Synaptic mechanisms of synchronized gamma oscillations in inhibitory interneuron networks. *Nat. Rev. Neurosci.* 8, 45–56. <https://doi.org/10.1038/nrn2044>
- Benes, F.M., Sorensen, I., Bird, E.D., 1991. Reduced Neuronal Size in Posterior Hippocampus of Schizophrenic Patients. *Schizophr. Bull.* 17, 597–608. <https://doi.org/10.1093/schbul/17.4.597>
- Benes, F.M., Vincent, S.L., Marie, A., Khan, Y., 1996. Up-regulation of GABAA receptor binding on neurons of the prefrontal cortex in schizophrenic subjects [WWW Document]. *Neuroscience*. [https://doi.org/10.1016/0306-4522\(96\)00328-4](https://doi.org/10.1016/0306-4522(96)00328-4)
- Beneyto, M., Meador-Woodruff, J.H., 2008. Lamina-Specific Abnormalities of NMDA Receptor-Associated Postsynaptic Protein Transcripts in the Prefrontal Cortex in Schizophrenia and Bipolar Disorder [WWW Document]. *Neuropsychopharmacology*. <https://doi.org/10.1038/sj.npp.1301604>
- Bialas, A.R., Stevens, B., 2013. TGF- β signaling regulates neuronal C1q expression and developmental synaptic refinement. *Nat. Neurosci.* 16, 1773–1782. <https://doi.org/10.1038/nn.3560>
- Bidoret, C., Bouvier, G., Ayon, A., Szapiro, G., Casado, M., 2015. Properties and molecular identity of NMDA receptors at synaptic and non-synaptic inputs in cerebellar molecular layer interneurons. *Front. Synaptic Neurosci.* 7. <https://doi.org/10.3389/fnsyn.2015.00001>
- Bielawski, M., Bondurant, H., 2015. Psychosis following a stroke to the cerebellum and midbrain: a case report. *Cerebellum Ataxias* 2, 17. <https://doi.org/10.1186/s40673-015-0037-8>
- Bleuler, E., 1950. *Dementia praecox or the group of schizophrenias*, Dementia praecox or the group of schizophrenias. International Universities Press, Oxford, England.
- Bork, P., 1993. The modular architecture of a new family of growth regulators related to connective tissue growth factor. *FEBS Lett.* 327, 125–130. [https://doi.org/10.1016/0014-5793\(93\)80155-n](https://doi.org/10.1016/0014-5793(93)80155-n)
- Bosch, C., Masachs, N., Exposito-Alonso, D., Martínez, A., Teixeira, C.M., Feraud, I., Pujadas, L., Ulloa, F., Comella, J.X., DeFelipe, J., Merchán-Pérez, A., Soriano, E., 2016. Reelin Regulates the Maturation of Dendritic Spines, Synaptogenesis and Glial

- Ensheathment of Newborn Granule Cells. *Cereb. Cortex* 26, 4282–4298.
<https://doi.org/10.1093/cercor/bhw216>
- Brady, R.O., Gonsalvez, I., Lee, I., Öngür, D., Seidman, L.J., Schmahmann, J.D., Eack, S.M., Keshavan, M.S., Pascual-Leone, A., Halko, M.A., 2019. Cerebellar-Prefrontal Network Connectivity and Negative Symptoms in Schizophrenia. *Am. J. Psychiatry* 176, 512–520. <https://doi.org/10.1176/appi.ajp.2018.18040429>
- Brown, A.M., Arancillo, M., Lin, T., Catt, D.R., Zhou, J., Lackey, E.P., Stay, T.L., Zuo, Z., White, J.J., Sillitoe, R.V., 2019. Molecular layer interneurons shape the spike activity of cerebellar Purkinje cells [WWW Document]. *Sci. Rep.*
<https://doi.org/10.1038/s41598-018-38264-1>
- Brown, A.S., Susser, E.S., 2008. Prenatal Nutritional Deficiency and Risk of Adult Schizophrenia. *Schizophr. Bull.* 34, 1054–1063. <https://doi.org/10.1093/schbul/sbn096>
- Brown, K.M., Sugihara, I., Shinoda, Y., Ascoli, G.A., 2012. Digital Morphometry of Rat Cerebellar Climbing Fibers Reveals Distinct Branch and Bouton Types. *J. Neurosci.* 32, 14670–14684. <https://doi.org/10.1523/JNEUROSCI.2018-12.2012>
- Browning, M.D., Dudek, E.M., Rapier, J.L., Leonard, S., Freedman, R., 1993. Significant reductions in synapsin but not synaptophysin specific activity in the brains of some schizophrenics. *Biol. Psychiatry* 34, 529–535. [https://doi.org/10.1016/0006-3223\(93\)90195-J](https://doi.org/10.1016/0006-3223(93)90195-J)
- Bullitt, E., 1990. Expression of C-fos-like protein as a marker for neuronal activity following noxious stimulation in the rat. *J. Comp. Neurol.* 296, 517–530.
<https://doi.org/10.1002/cne.902960402>
- Bullock, W.M., Bolognani, F., Botta, P., Valenzuela, C.F., Perrone-Bizzozero, N.I., 2009. Schizophrenia-like GABAergic gene expression deficits in cerebellar Golgi cells from rats chronically exposed to low-dose phencyclidine. *Neurochem. Int.* 55, 775–782.
<https://doi.org/10.1016/j.neuint.2009.07.010>
- Buzsáki, G., Draguhn, A., 2004. Neuronal oscillations in cortical networks. *Science* 304, 1926–1929. <https://doi.org/10.1126/science.1099745>
- Cajal, R., 1888. Estructura del cerebelo. *Gac Med Catalana*.
- Cambon, K., Hansen, S.M., Venero, C., Herrero, A.I., Skibo, G., Berezin, V., Bock, E., Sandi, C., 2004. A Synthetic Neural Cell Adhesion Molecule Mimetic Peptide Promotes Synaptogenesis, Enhances Presynaptic Function, and Facilitates Memory Consolidation. *J. Neurosci.* 24, 4197–4204.
<https://doi.org/10.1523/JNEUROSCI.0436-04.2004>
- Carlsson, A., Lindqvist, M., 1963. Effect of Chlorpromazine or Haloperidol on Formation of 3-Methoxytyramine and Normetanephrine in Mouse Brain. *Acta Pharmacol. Toxicol. (Copenh.)* 20, 140–144. <https://doi.org/10.1111/j.1600-0773.1963.tb01730.x>
- Carlsson, M., Carlsson, A., 1990. Schizophrenia: a subcortical neurotransmitter imbalance syndrome? *Schizophr. Bull.* 16, 425–432. <https://doi.org/10.1093/schbul/16.3.425>
- Carta, I., Chen, C.H., Schott, A.L., Dorizan, S., Khodakhah, K., 2019. Cerebellar modulation of the reward circuitry and social behavior. *Science* 363, eaav0581.
<https://doi.org/10.1126/science.aav0581>
- Casado, M., Dieudonné, S., Ascher, P., 2000. Presynaptic N-methyl-d-aspartate receptors at the parallel fiber–Purkinje cell synapse. *Proc. Natl. Acad. Sci.* 97, 11593–11597.
<https://doi.org/10.1073/pnas.200354297>
- Castejon, O.J., Sims, P., 2006. Three-dimensional morphology of cerebellar climbing fibers. A study by means of confocal laser scanning microscopy and scanning electron microscopy. *Scanning* 22, 211–217. <https://doi.org/10.1002/sca.4950220309>
- Castillo, M.A., Ghose, S., Tamminga, C.A., Ulery-Reynolds, P.G., 2010. Deficits in Syntaxin 1 Phosphorylation in Schizophrenia Prefrontal Cortex. *Biol. Psychiatry, Synaptic*

- Plasticity Deficits in Schizophrenia 67, 208–216.
<https://doi.org/10.1016/j.biopsych.2009.07.029>
- Cathala, L., Misra, C., Cull-Candy, S., 2000. Developmental Profile of the Changing Properties of NMDA Receptors at Cerebellar Mossy Fiber–Granule Cell Synapses. *J. Neurosci.* 20, 5899–5905. <https://doi.org/10.1523/JNEUROSCI.20-16-05899.2000>
- Cha, H.L., Choi, J.-M., Oh, H.-H., Bashyal, N., Kim, S.-S., Birnbaumer, L., Suh-Kim, H., 2019. Deletion of the α subunit of the heterotrimeric Go protein impairs cerebellar cortical development in mice. *Mol. Brain* 12, 57. <https://doi.org/10.1186/s13041-019-0477-9>
- Chedotal, A., Sotelo, C., 1993. The “creeper stage” in cerebellar climbing fiber synaptogenesis precedes the ‘pericellular nest’--ultrastructural evidence with parvalbumin immunocytochemistry. *Brain Res. Dev. Brain Res.* 76, 207–220. [https://doi.org/10.1016/0165-3806\(93\)90209-s](https://doi.org/10.1016/0165-3806(93)90209-s)
- Chen, X.-W., Feng, Y.-Q., Hao, C.-J., Guo, X.-L., He, X., Zhou, Z.-Y., Guo, N., Huang, H.-P., Xiong, W., Zheng, H., Zuo, P.-L., Zhang, C.X., Li, W., Zhou, Z., 2008. DTNBP1, a schizophrenia susceptibility gene, affects kinetics of transmitter release [WWW Document]. *J. Cell Biol.* <https://doi.org/10.1083/jcb.200711021>
- Chubykin, A.A., Atasoy, D., Etherton, M.R., Brose, N., Kavalali, E.T., Gibson, J.R., Südhof, T.C., 2007. Activity-Dependent Validation of Excitatory versus Inhibitory Synapses by Neuroligin-1 versus Neuroligin-2. *Neuron* 54, 919–931. <https://doi.org/10.1016/j.neuron.2007.05.029>
- Colantuoni, C., Lipska, B.K., Ye, T., Hyde, T.M., Tao, R., Leek, J.T., Colantuoni, E.A., Elkhouloun, A.G., Herman, M.M., Weinberger, D.R., Kleinman, J.E., 2011. Temporal dynamics and genetic control of transcription in the human prefrontal cortex. *Nature* 478, 519–523. <https://doi.org/10.1038/nature10524>
- Cole, M.W., Anticevic, A., Repovs, G., Barch, D., 2011. Variable Global Dysconnectivity and Individual Differences in Schizophrenia. *Biol. Psychiatry* 70, 43–50. <https://doi.org/10.1016/j.biopsych.2011.02.010>
- Corti, C., Xuereb, J.H., Crepaldi, L., Corsi, M., Michielin, F., Ferraguti, F., 2011. Altered levels of glutamatergic receptors and Na⁺/K⁺ ATPase- α 1 in the prefrontal cortex of subjects with schizophrenia. *Schizophr. Res.* 128, 7–14. <https://doi.org/10.1016/j.schres.2011.01.021>
- Crabtree, G.W., Gogos, J.A., 2014. Synaptic plasticity, neural circuits, and the emerging role of altered short-term information processing in schizophrenia. *Front. Synaptic Neurosci.* 6. <https://doi.org/10.3389/fnsyn.2014.00028>
- Crepel, F., 1971. Maturation of climbing fiber responses in the rat. *Brain Res.* 35, 272–276. [https://doi.org/10.1016/0006-8993\(71\)90617-2](https://doi.org/10.1016/0006-8993(71)90617-2)
- Crepel, F., Delhay-Bouchaud, N., Dupont, J.L., 1981. Fate of the multiple innervation of cerebellar Purkinje cells by climbing fibers in immature control, X-irradiated and hypothyroid rats. *Dev. Brain Res.* 1, 59–71. [https://doi.org/10.1016/0165-3806\(81\)90094-8](https://doi.org/10.1016/0165-3806(81)90094-8)
- Crespo-Facorro, B., Wiser, A.K., Andreasen, N.C., O’Leary, D.S., Watkins, G.L., Ponto, L.L.B., Hichwa, R.D., 2001. Neural basis of novel and well-learned recognition memory in schizophrenia: A positron emission tomography study. *Hum. Brain Mapp.* 12, 219–231. [https://doi.org/10.1002/1097-0193\(200104\)12:4<219::AID-HBM1017>3.0.CO;2-L](https://doi.org/10.1002/1097-0193(200104)12:4<219::AID-HBM1017>3.0.CO;2-L)
- Cross-Disorder Group of the Psychiatric Genomics Consortium, Lee, S.H., Ripke, S., Neale, B.M., Faraone, S.V., Purcell, S.M., Perlis, R.H., Mowry, B.J., Thapar, A., Goddard, M.E., Witte, J.S., Absher, D., Agartz, I., Akil, H., Amin, F., Andreassen, O.A., Anjorin, A., Anney, R., Anttila, V., Arking, D.E., Asherson, P., Azevedo, M.H.,

Backlund, L., Badner, J.A., Bailey, A.J., Banaschewski, T., Barchas, J.D., Barnes, M.R., Barrett, T.B., Bass, N., Battaglia, A., Bauer, M., Bayés, M., Bellivier, F., Bergen, S.E., Berrettini, W., Betancur, C., Bettecken, T., Biederman, J., Binder, E.B., Black, D.W., Blackwood, D.H.R., Bloss, C.S., Boehnke, M., Boomsma, D.I., Breen, G., Breuer, R., Bruggeman, R., Cormican, P., Buccola, N.G., Buitelaar, J.K., Bunney, W.E., Buxbaum, J.D., Byerley, W.F., Byrne, E.M., Caesar, S., Cahn, W., Cantor, R.M., Casas, M., Chakravarti, A., Chambert, K., Choudhury, K., Cichon, S., Cloninger, C.R., Collier, D.A., Cook, E.H., Coon, H., Cormand, B., Corvin, A., Coryell, W.H., Craig, D.W., Craig, I.W., Crosbie, J., Cuccaro, M.L., Curtis, D., Czamara, D., Datta, S., Dawson, G., Day, R., De Geus, E.J., Degenhardt, F., Djurovic, S., Donohoe, G.J., Doyle, A.E., Duan, J., Dudbridge, F., Duketis, E., Ebstein, R.P., Edenberg, H.J., Elia, J., Ennis, S., Etain, B., Fanous, A., Farmer, A.E., Ferrier, I.N., Flickinger, M., Fombonne, E., Foroud, T., Frank, J., Franke, B., Fraser, C., Freedman, R., Freimer, N.B., Freitag, C.M., Friedl, M., Frisé, L., Gallagher, L., Gejman, P.V., Georgieva, L., Gershon, E.S., Geschwind, D.H., Giegling, I., Gill, M., Gordon, S.D., Gordon-Smith, K., Green, E.K., Greenwood, T.A., Grice, D.E., Gross, M., Grozeva, D., Guan, W., Gurling, H., De Haan, L., Haines, J.L., Hakonarson, H., Hallmayer, J., Hamilton, S.P., Hamshere, M.L., Hansen, T.F., Hartmann, A.M., Hautzinger, M., Heath, A.C., Henders, A.K., Herms, S., Hickie, I.B., Hipolito, M., Hoefels, S., Holmans, P.A., Holsboer, F., Hoogendijk, W.J., Hottenga, J.-J., Hultman, C.M., Hus, V., Ingason, A., Ising, M., Jamain, S., Jones, E.G., Jones, I., Jones, L., Tzeng, J.-Y., Kähler, A.K., Kahn, R.S., Kandaswamy, R., Keller, M.C., Kennedy, J.L., Kenny, E., Kent, L., Kim, Y., Kirov, G.K., Klauck, S.M., Klei, L., Knowles, J.A., Kohli, M.A., Koller, D.L., Konte, B., Korszun, A., Krabbendam, L., Krasucki, R., Kuntsi, J., Kwan, P., Landén, M., Långström, N., Lathrop, M., Lawrence, J., Lawson, W.B., Leboyer, M., Ledbetter, D.H., Lee, P.H., Lencz, T., Lesch, K.-P., Levinson, D.F., Lewis, C.M., Li, J., Lichtenstein, P., Lieberman, J.A., Lin, D.-Y., Linszen, D.H., Liu, C., Lohoff, F.W., Loo, S.K., Lord, C., Lowe, J.K., Lucae, S., MacIntyre, D.J., Madden, P.A.F., Maestrini, E., Magnusson, P.K.E., Mahon, P.B., Maier, W., Malhotra, A.K., Mane, S.M., Martin, C.L., Martin, N.G., Mattheisen, M., Matthews, K., Mattingsdal, M., McCarroll, S.A., McGhee, K.A., McGough, J.J., McGrath, P.J., McGuffin, P., McInnis, M.G., McIntosh, A., McKinney, R., McLean, A.W., McMahan, F.J., McMahan, W.M., McQuillin, A., Medeiros, H., Medland, S.E., Meier, S., Melle, I., Meng, F., Meyer, J., Middeldorp, C.M., Middleton, L., Milanova, V., Miranda, A., Monaco, A.P., Montgomery, G.W., Moran, J.L., Moreno-De-Luca, D., Morken, G., Morris, D.W., Morrow, E.M., Moskvina, V., Muglia, P., Mühleisen, T.W., Muir, W.J., Müller-Myhsok, B., Murtha, M., Myers, R.M., Myin-Germeys, I., Neale, M.C., Nelson, S.F., Nievergelt, C.M., Nikolov, I., Nimgaonkar, V., Nolen, W.A., Nöthen, M.M., Nurnberger, J.I., Nwulia, E.A., Nyholt, D.R., O'Dushlaine, C., Oades, R.D., Olincy, A., Oliveira, G., Olsen, L., Ophoff, R.A., Osby, U., Owen, M.J., Palotie, A., Parr, J.R., Paterson, A.D., Pato, C.N., Pato, M.T., Penninx, B.W., Pergadia, M.L., Pericak-Vance, M.A., Pickard, B.S., Pimm, J., Piven, J., Posthuma, D., Potash, J.B., Poustka, F., Propping, P., Puri, V., Quedsted, D.J., Quinn, E.M., Ramos-Quiroga, J.A., Rasmussen, H.B., Raychaudhuri, S., Rehnström, K., Reif, A., Ribasés, M., Rice, J.P., Rietschel, M., Roeder, K., Roeyers, H., Rossin, L., Rothenberger, A., Rouleau, G., Ruderfer, D., Rujescu, D., Sanders, A.R., Sanders, S.J., Santangelo, S.L., Sergeant, J.A., Schachar, R., Schalling, M., Schatzberg, A.F., Scheftner, W.A., Schellenberg, G.D., Scherer, S.W., Schork, N.J., Schulze, T.G., Schumacher, J., Schwarz, M., Scolnick, E., Scott, L.J., Shi, J., Shilling, P.D., Shyn, S.I., Silverman, J.M., Slager, S.L., Smalley, S.L., Smit, J.H., Smith, E.N., Sonuga-Barke, E.J.S., St Clair, D., State,

- M., Steffens, M., Steinhausen, H.-C., Strauss, J.S., Strohmaier, J., Stroup, T.S., Sutcliffe, J.S., Szatmari, P., Szelinger, S., Thirumalai, S., Thompson, R.C., Todorov, A.A., Tozzi, F., Treutlein, J., Uhr, M., van den Oord, E.J.C.G., Van Grootheest, G., Van Os, J., Vicente, A.M., Vieland, V.J., Vincent, J.B., Visscher, P.M., Walsh, C.A., Wassink, T.H., Watson, S.J., Weissman, M.M., Werge, T., Wienker, T.F., Wijsman, E.M., Willemsen, G., Williams, N., Willsey, A.J., Witt, S.H., Xu, W., Young, A.H., Yu, T.W., Zammit, S., Zandi, P.P., Zhang, P., Zitman, F.G., Zöllner, S., Devlin, B., Kelsoe, J.R., Sklar, P., Daly, M.J., O'Donovan, M.C., Craddock, N., Sullivan, P.F., Smoller, J.W., Kendler, K.S., Wray, N.R., International Inflammatory Bowel Disease Genetics Consortium (IIBDGC), 2013. Genetic relationship between five psychiatric disorders estimated from genome-wide SNPs. *Nat. Genet.* 45, 984–994. <https://doi.org/10.1038/ng.2711>
- de Jonge, J.C., Vinkers, C.H., Hulshoff Pol, H.E., Marsman, A., 2017. GABAergic Mechanisms in Schizophrenia: Linking Postmortem and In Vivo Studies. *Front. Psychiatry* 8. <https://doi.org/10.3389/fpsyt.2017.00118>
- Deverett, B., Kislin, M., Tank, D.W., Wang, S.S.-H., 2019. Cerebellar disruption impairs working memory during evidence accumulation. *Nat. Commun.* 10, 3128. <https://doi.org/10.1038/s41467-019-11050-x>
- Ding, M., Chao, D., Wang, G., Shen, K., 2007. Spatial regulation of an E3 ubiquitin ligase directs selective synapse elimination. *Science* 317, 947–951. <https://doi.org/10.1126/science.1145727>
- Diño, M.R., Willard, F.H., Mugnaini, E., 1999. [No title found]. *J. Neurocytol.* 28, 99–123. <https://doi.org/10.1023/A:1007072105919>
- Dracheva, S., McGurk, S.R., Haroutunian, V., 2005. mRNA expression of AMPA receptors and AMPA receptor binding proteins in the cerebral cortex of elderly schizophrenics. *J. Neurosci. Res.* 79, 868–878. <https://doi.org/10.1002/jnr.20423>
- Eastwood, S.L., Cotter, D., Harrison, P.J., 2001. Cerebellar synaptic protein expression in schizophrenia. *Neuroscience* 105, 219–229. [https://doi.org/10.1016/S0306-4522\(01\)00141-5](https://doi.org/10.1016/S0306-4522(01)00141-5)
- Eastwood, S.L., Harrison, P.J., 2005. Decreased expression of vesicular glutamate transporter 1 and complexin II mRNAs in schizophrenia: further evidence for a synaptic pathology affecting glutamate neurons. *Schizophr. Res.* 73, 159–172. <https://doi.org/10.1016/j.schres.2004.05.010>
- Eastwood, S.L., Kerwin, R.W., Harrison, P.J., 1997. Immunoautoradiographic evidence for a loss of alpha-amino-3-hydroxy-5-methyl-4-isoxazole propionate-preferring non-N-methyl-D-aspartate glutamate receptors within the medial temporal lobe in schizophrenia. *Biol. Psychiatry* 41, 636–643. [https://doi.org/10.1016/S0006-3223\(96\)00220-X](https://doi.org/10.1016/S0006-3223(96)00220-X)
- Eastwood, S.L., McDonald, B., Burnet, P.W., Beckwith, J.P., Kerwin, R.W., Harrison, P.J., 1995. Decreased expression of mRNAs encoding non-NMDA glutamate receptors GluR1 and GluR2 in medial temporal lobe neurons in schizophrenia. *Brain Res. Mol. Brain Res.* 29, 211–223. [https://doi.org/10.1016/0169-328x\(94\)00247-c](https://doi.org/10.1016/0169-328x(94)00247-c)
- Ebert, D.H., Greenberg, M.E., 2013. Activity-dependent neuronal signaling and autism spectrum disorder. *Nature* 493, 327–337. <https://doi.org/10.1038/nature11860>
- Ehrlichman, R.S., Gandal, M.J., Maxwell, C.R., Lazarewicz, M.T., Finkel, L.H., Contreras, D., Turetsky, B.I., Siegel, S.J., 2009. N-methyl-d-aspartic acid receptor antagonist-induced frequency oscillations in mice recreate pattern of electrophysiological deficits in schizophrenia. *Neuroscience* 158, 705–712. <https://doi.org/10.1016/j.neuroscience.2008.10.031>

- Fanous, A.H., Zhou, B., Aggen, S.H., Bergen, S.E., Amdur, R.L., Duan, J., Sanders, A.R., Shi, J., Mowry, B.J., Olincy, A., Amin, F., Cloninger, C.R., Silverman, J.M., Buccola, N.G., Byerley, W.F., Black, D.W., Freedman, R., Dudbridge, F., Holmans, P.A., Ripke, S., Gejman, P.V., Kendler, K.S., Levinson, D.F., Schizophrenia Psychiatric Genome-Wide Association Study (GWAS) Consortium, 2012. Genome-wide association study of clinical dimensions of schizophrenia: polygenic effect on disorganized symptoms. *Am. J. Psychiatry* 169, 1309–1317. <https://doi.org/10.1176/appi.ajp.2012.12020218>
- Faulkner, H.J., Traub, R.D., Whittington, M.A., 1999. Anaesthetic/amnesic agents disrupt beta frequency oscillations associated with potentiation of excitatory synaptic potentials in the rat hippocampal slice. *Br. J. Pharmacol.* 128, 1813–1825. <https://doi.org/10.1038/sj.bjp.0702948>
- Ferreira, A., Rapoport, M., 2002. The synapsins: beyond the regulation of neurotransmitter release. *Cell. Mol. Life Sci. CMLS* 59, 589–595. <https://doi.org/10.1007/s00018-002-8451-5>
- Flores, C., Wen, X., Labelle-Dumais, C., Kolb, B., 2007. Chronic phencyclidine treatment increases dendritic spine density in prefrontal cortex and nucleus accumbens neurons. *Synapse* 61, 978–984. <https://doi.org/10.1002/syn.20452>
- Forlim, C.G., Klock, L., Bächle, J., Stoll, L., Giemsa, P., Fuchs, M., Schoofs, N., Montag, C., Gallinat, J., Kühn, S., 2020. Reduced Resting-State Connectivity in the Precuneus is correlated with Apathy in Patients with Schizophrenia. *Sci. Rep.* 10, 1–8. <https://doi.org/10.1038/s41598-020-59393-6>
- Fornito, A., Harrison, B.J., Zalesky, A., Simons, J.S., 2012. Competitive and cooperative dynamics of large-scale brain functional networks supporting recollection. *Proc. Natl. Acad. Sci.* 109, 12788–12793. <https://doi.org/10.1073/pnas.1204185109>
- Freedman, R., Leonard, S., Gault, J.M., Hopkins, J., Cloninger, C.R., Kaufmann, C.A., Tsuang, M.T., Farone, S.V., Malaspina, D., Svrakic, D.M., Sanders, A., Gejman, P., 2001. Linkage disequilibrium for schizophrenia at the chromosome 15q13-14 locus of the alpha7-nicotinic acetylcholine receptor subunit gene (CHRNA7). *Am. J. Med. Genet.* 105, 20–22.
- Fromer, M., Pocklington, A.J., Kavanagh, D.H., Williams, H.J., Dwyer, S., Gormley, P., Georgieva, L., Rees, E., Palta, P., Ruderfer, D.M., Carrera, N., Humphreys, I., Johnson, J.S., Roussos, P., Barker, D.D., Banks, E., Milanova, V., Grant, S.G., Hannon, E., Rose, S.A., Chambert, K., Mahajan, M., Scolnick, E.M., Moran, J.L., Kirov, G., Palotie, A., McCarroll, S.A., Holmans, P., Sklar, P., Owen, M.J., Purcell, S.M., O'Donovan, M.C., 2014. De novo mutations in schizophrenia implicate synaptic networks. *Nature* 506, 179–184. <https://doi.org/10.1038/nature12929>
- Funk, A.J., Rumbaugh, G., Haroutunian, V., McCullumsmith, R.E., Meador-Woodruff, J.H., 2009. Decreased expression of NMDA receptor-associated proteins in frontal cortex of elderly patients with schizophrenia. *Neuroreport* 20, 1019–1022. <https://doi.org/10.1097/WNR.0b013e32832d30d9>
- Gabriel, S.M., Haroutunian, V., Powchik, P., Honer, W.G., Davidson, M., Davies, P., Davis, K.L., 1997. Increased concentrations of presynaptic proteins in the cingulate cortex of subjects with schizophrenia. *Arch. Gen. Psychiatry* 54, 559–566. <https://doi.org/10.1001/archpsyc.1997.01830180077010>
- Gao, X.M., Sakai, K., Roberts, R.C., Conley, R.R., Dean, B., Tamminga, C.A., 2000. Ionotropic glutamate receptors and expression of N-methyl-D-aspartate receptor subunits in subregions of human hippocampus: effects of schizophrenia. *Am. J. Psychiatry* 157, 1141–1149. <https://doi.org/10.1176/appi.ajp.157.7.1141>

- Garey, L., Ong, W., Patel, T., Kanani, M., Davis, A., Mortimer, A., Barnes, T., Hirsch, S., 1998. Reduced dendritic spine density on cerebral cortical pyramidal neurons in schizophrenia. *J. Neurol. Neurosurg. Psychiatry* 65, 446–453.
- Gaspar, H.A., Breen, G., 2017. Drug enrichment and discovery from schizophrenia genome-wide association results: an analysis and visualisation approach. *Sci. Rep.* 7, 1–9. <https://doi.org/10.1038/s41598-017-12325-3>
- Genovese, G., Fromer, M., Stahl, E.A., Ruderfer, D.M., Chambert, K., Landén, M., Moran, J.L., Purcell, S.M., Sklar, P., Sullivan, P.F., Hultman, C.M., McCarroll, S.A., 2016. Increased burden of ultra-rare protein-altering variants among 4,877 individuals with schizophrenia [WWW Document]. *Nat. Neurosci.* <https://doi.org/10.1038/nn.4402>
- Genthe, J.R., Min, J., Farmer, D.M., Shelat, A.A., Grenet, J.A., Lin, W., Finkelstein, D., Vrijens, K., Chen, T., Guy, R.K., Clements, W.K., Roussel, M.F., 2017. Ventromorphins: A New Class of Small Molecule Activators of the Canonical BMP Signaling Pathway. *ACS Chem. Biol.* 12, 2436–2447. <https://doi.org/10.1021/acscchembio.7b00527>
- George, M., Maheshwari, S., Chandran, S., Manohar, J.S., Rao, T.S.S., 2017. Understanding the schizophrenia prodrome. *Indian J. Psychiatry* 59, 505–505. https://doi.org/10.4103/psychiatry.IndianJPsychiatry_464_17
- Ghose, S., Gleason, K.A., Potts, B.W., Lewis-Amezcu, K., Tamminga, C.A., 2009. Differential expression of metabotropic glutamate receptors 2 and 3 in schizophrenia: a mechanism for antipsychotic drug action? *Am. J. Psychiatry* 166, 812–820. <https://doi.org/10.1176/appi.ajp.2009.08091445>
- Gilbert, P.L., Harris, M.J., McAdams, L.A., Jeste, D.V., 1995. Neuroleptic Withdrawal in Schizophrenic Patients: A Review of the Literature. *Arch. Gen. Psychiatry* 52, 173–188. <https://doi.org/10.1001/archpsyc.1995.03950150005001>
- Glantz, L.A., Lewis, D.A., 2000. Decreased Dendritic Spine Density on Prefrontal Cortical Pyramidal Neurons in Schizophrenia. *Arch. Gen. Psychiatry* 57, 65–73. <https://doi.org/10.1001/archpsyc.57.1.65>
- Glantz, L.A., Lewis, D.A., 1997. Reduction of Synaptophysin Immunoreactivity in the Prefrontal Cortex of Subjects With Schizophrenia: Regional and Diagnostic Specificity. *Arch. Gen. Psychiatry* 54, 660–669. <https://doi.org/10.1001/archpsyc.1997.01830190088009>
- Glausier, J.R., Lewis, D.A., 2013. Dendritic Spine Pathology in Schizophrenia. *Neuroscience* 251, 90–107. <https://doi.org/10.1016/j.neuroscience.2012.04.044>
- Glickstein, M., Strata, P., Voogd, J., 2009. Cerebellum: history. *Neuroscience* 162, 549–559. <https://doi.org/10.1016/j.neuroscience.2009.02.054>
- Godwin, D., Ji, A., Kandala, S., Mamah, D., 2017. Functional Connectivity of Cognitive Brain Networks in Schizophrenia during a Working Memory Task. *Front. Psychiatry* 8. <https://doi.org/10.3389/fpsy.2017.00294>
- Goldstein, J.M., Goodman, J.M., Seidman, L.J., Kennedy, D.N., Makris, N., Lee, H., Tourville, J., Verne S. Caviness, J., Faraone, S.V., Tsuang, M.T., 1999. Cortical Abnormalities in Schizophrenia Identified by Structural Magnetic Resonance Imaging. *Arch. Gen. Psychiatry* 56, 537–547.
- Gómez-Sintes, R., Kvajo, M., Gogos, J.A., Lucas, J.J., 2014. Mice with a naturally occurring DISC1 mutation display a broad spectrum of behaviors associated to psychiatric disorders. *Front. Behav. Neurosci.* 8. <https://doi.org/10.3389/fnbeh.2014.00253>
- Gonzalez-Burgos, G., Hashimoto, T., Lewis, D.A., 2010. Alterations of Cortical GABA Neurons and Network Oscillations in Schizophrenia. *Curr. Psychiatry Rep.* 12, 335–344. <https://doi.org/10.1007/s11920-010-0124-8>

- Gottesman, I.I., 1991. Schizophrenia genesis: The origins of madness, Schizophrenia genesis: The origins of madness. W H Freeman/Times Books/ Henry Holt & Co, New York, NY, US.
- Gouder, L., Vitrac, A., Goubran-Botros, H., Danckaert, A., Tinevez, J.-Y., André-Leroux, G., Atanasova, E., Lemièrre, N., Biton, A., Leblond, C.S., Poulet, A., Boland, A., Deleuze, J.-F., Benchoua, A., Delorme, R., Bourgeron, T., Cloëz-Tayarani, I., 2019. Altered spinogenesis in iPSC-derived cortical neurons from patients with autism carrying de novo SHANK3 mutations. *Sci. Rep.* 9, 94. <https://doi.org/10.1038/s41598-018-36993-x>
- Gratton, A., Hoffer, B.J., Freedman, R., 1987. Electrophysiological effects of phencyclidine in the medial prefrontal cortex of the rat. *Neuropharmacology* 26, 1275–1283. [https://doi.org/10.1016/0028-3908\(87\)90087-6](https://doi.org/10.1016/0028-3908(87)90087-6)
- Gray, L.J., Dean, B., Kronsbein, H.C., Robinson, P.J., Scarr, E., 2010. Region and diagnosis-specific changes in synaptic proteins in schizophrenia and bipolar I disorder. *Psychiatry Res.* 178, 374–380. <https://doi.org/10.1016/j.psychres.2008.07.012>
- Guell, X., Hoche, F., Schmahmann, J.D., 2015. Metalinguistic deficits in patients with cerebellar dysfunction: empirical support for the dysmetria of thought theory. *Cerebellum Lond. Engl.* 14, 50–58. <https://doi.org/10.1007/s12311-014-0630-z>
- Guell, X., Schmahmann, J.D., Gabrieli, J.D., Ghosh, S.S., 2018. Functional gradients of the cerebellum. *eLife* 7, e36652. <https://doi.org/10.7554/eLife.36652>
- Gulsuner, S., Walsh, T., Watts, A.C., Lee, M.K., Thornton, A.M., Casadei, S., Rippey, C., Shahin, H., Consortium on the Genetics of Schizophrenia (COGS), PAARTNERS Study Group, Nimgaonkar, V.L., Go, R.C.P., Savage, R.M., Swerdlow, N.R., Gur, R.E., Braff, D.L., King, M.-C., McClellan, J.M., 2013. Spatial and temporal mapping of de novo mutations in schizophrenia to a fetal prefrontal cortical network. *Cell* 154, 518–529. <https://doi.org/10.1016/j.cell.2013.06.049>
- Gupta, D.S., McCullumsmith, R.E., Beneyto, M., Haroutunian, V., Davis, K.L., Meador-Woodruff, J.H., 2005. Metabotropic glutamate receptor protein expression in the prefrontal cortex and striatum in schizophrenia. *Synap. N. Y. N* 57, 123–131. <https://doi.org/10.1002/syn.20164>
- Gur, R., Bassett, A., McDonald-McGinn, D., Bearden, C., Chow, E., Emanuel, B., Owen, M., Swillen, A., Van den Bree, M., Vermeesch, J., Vorstman, J., Warren, S., Lehner, T., Morrow, B., 2017. A neurogenetic model for the study of schizophrenia spectrum disorders: the International 22q11.2 Deletion Syndrome Brain Behavior Consortium. *Mol. Psychiatry* 22, 1664–1672. <https://doi.org/10.1038/mp.2017.161>
- Gutierrez-Castellanos, N., Da Silva-Matos, C.M., Zhou, K., Canto, C.B., Renner, M.C., Koene, L.M.C., Ozyildirim, O., Sprengel, R., Kessels, H.W., De Zeeuw, C.I., 2017. Motor Learning Requires Purkinje Cell Synaptic Potentiation through Activation of AMPA-Receptor Subunit GluA3. *Neuron* 93, 409–424. <https://doi.org/10.1016/j.neuron.2016.11.046>
- Haijma, S.V., Van Haren, N., Cahn, W., Koolschijn, P.C.M.P., Hulshoff Pol, H.E., Kahn, R.S., 2013. Brain Volumes in Schizophrenia: A Meta-Analysis in Over 18 000 Subjects. *Schizophr. Bull.* 39, 1129–1138. <https://doi.org/10.1093/schbul/sbs118>
- Hamm, J.P., Peterka, D.S., Gogos, J.A., Yuste, R., 2017. Altered Cortical Ensembles in Mouse Models of Schizophrenia. *Neuron* 94, 153-167.e8. <https://doi.org/10.1016/j.neuron.2017.03.019>
- Hansel, C., Linden, D.J., 2000. Long-term depression of the cerebellar climbing fiber--Purkinje neuron synapse. *Neuron* 26, 473–482. [https://doi.org/10.1016/s0896-6273\(00\)81179-4](https://doi.org/10.1016/s0896-6273(00)81179-4)

- Hardingham, N., Dachtler, J., Fox, K., 2013. The role of nitric oxide in pre-synaptic plasticity and homeostasis. *Front. Cell. Neurosci.* 7. <https://doi.org/10.3389/fncel.2013.00190>
- Harms, L., Parras, G.G., Michie, P.T., Malmierca, M.S., 2020. The Role of Glutamate Neurotransmission in Mismatch Negativity (MMN), A Measure of Auditory Synaptic Plasticity and Change-detection. *Neuroscience*. <https://doi.org/10.1016/j.neuroscience.2020.01.046>
- Harrison, P.J., McLaughlin, D., Kerwin, R.W., 1991. Decreased hippocampal expression of a glutamate receptor gene in schizophrenia. *Lancet Lond. Engl.* 337, 450–452. [https://doi.org/10.1016/0140-6736\(91\)93392-m](https://doi.org/10.1016/0140-6736(91)93392-m)
- Harvey, R.J., Napper, R.M., 1991. Quantitative studies on the mammalian cerebellum. *Prog. Neurobiol.* 36, 437–463. [https://doi.org/10.1016/0301-0082\(91\)90012-p](https://doi.org/10.1016/0301-0082(91)90012-p)
- Hashimoto, K., Kano, M., 2013. Synapse elimination in the developing cerebellum. *Cell. Mol. Life Sci.* 70, 4667–4680. <https://doi.org/10.1007/s00018-013-1405-2>
- Hashimoto, K., Watanabe, M., Kurihara, H., Offermanns, S., Jiang, H., Wu, Y., Jun, K., Shin, H.-S., Inoue, Y., Wu, D., Simon, M.I., Kano, M., 2000. Climbing fiber synapse elimination during postnatal cerebellar development requires signal transduction involving Gαq and phospholipase Cβ4, in: *Progress in Brain Research, Cerebellar Modules: Molecules, Morphology and Function*. Elsevier, pp. 31–48. [https://doi.org/10.1016/S0079-6123\(00\)24006-5](https://doi.org/10.1016/S0079-6123(00)24006-5)
- Hashimoto, K., Yoshida, T., Sakimura, K., Mishina, M., Watanabe, M., Kano, M., 2009. Influence of parallel fiber-Purkinje cell synapse formation on postnatal development of climbing fiber-Purkinje cell synapses in the cerebellum. *Neuroscience* 162, 601–611. <https://doi.org/10.1016/j.neuroscience.2008.12.037>
- Hashimoto, T., Arion, D., Unger, T., Maldonado-Avilés, J.G., Morris, H.M., Volk, D.W., Mirnics, K., Lewis, D.A., 2008. Alterations in GABA-related transcriptome in the dorsolateral prefrontal cortex of subjects with schizophrenia. *Mol. Psychiatry* 13, 147–161. <https://doi.org/10.1038/sj.mp.4002011>
- Hashimoto, T., Volk, D.W., Eggan, S.M., Mirnics, K., Pierri, J.N., Sun, Z., Sampson, A.R., Lewis, D.A., 2003. Gene expression deficits in a subclass of GABA neurons in the prefrontal cortex of subjects with schizophrenia. *J. Neurosci. Off. J. Soc. Neurosci.* 23, 6315–6326.
- Heckers, S., Heinsen, H., Heinsen, Y., Beckmann, H., 1991. Cortex, white matter, and basal ganglia in schizophrenia: A volumetric postmortem study. *Biol. Psychiatry* 29, 556–566. [https://doi.org/10.1016/0006-3223\(91\)90091-Y](https://doi.org/10.1016/0006-3223(91)90091-Y)
- Hilker, R., Helenius, D., Fagerlund, B., Skytthe, A., Christensen, K., Werge, T.M., Nordentoft, M., Glenthøj, B., 2018. Heritability of Schizophrenia and Schizophrenia Spectrum Based on the Nationwide Danish Twin Register. *Biol. Psychiatry* 83, 492–498. <https://doi.org/10.1016/j.biopsych.2017.08.017>
- Hirai, H., Pang, Z., Bao, D., Miyazaki, T., Li, L., Miura, E., Parris, J., Rong, Y., Watanabe, M., Yuzaki, M., Morgan, J.I., 2005. Cbln1 is essential for synaptic integrity and plasticity in the cerebellum. *Nat. Neurosci.* 8, 1534–1541. <https://doi.org/10.1038/nn1576>
- Homayoun, H., Moghaddam, B., 2007. NMDA Receptor Hypofunction Produces Opposite Effects on Prefrontal Cortex Interneurons and Pyramidal Neurons. *J. Neurosci.* 27, 11496–11500. <https://doi.org/10.1523/JNEUROSCI.2213-07.2007>
- Horn, K.M., Deep, A., Gibson, A.R., 2013. Progressive limb ataxia following inferior olive lesions. *J. Physiol.* 591, 5475–5489. <https://doi.org/10.1113/jphysiol.2012.234898>
- Hossein Fatemi, S., Sary, J.M., Earle, J.A., Araghi-Niknam, M., Eagan, E., 2005. GABAergic dysfunction in schizophrenia and mood disorders as reflected by

- decreased levels of glutamic acid decarboxylase 65 and 67 kDa and Reelin proteins in cerebellum. *Schizophr. Res.* 72, 109–122. <https://doi.org/10.1016/j.schres.2004.02.017>
- Hou, X.-Y., Zhang, G.-Y., Yan, J.-Z., Chen, M., Liu, Y., 2002. Activation of NMDA receptors and L-type voltage-gated calcium channels mediates enhanced formation of Fyn-PSD95-NR2A complex after transient brain ischemia. *Brain Res.* 955, 123–132. [https://doi.org/10.1016/s0006-8993\(02\)03376-0](https://doi.org/10.1016/s0006-8993(02)03376-0)
- Hoxha, E., Tempia, F., Lippiello, P., Miniaci, M.C., 2016. Modulation, Plasticity and Pathophysiology of the Parallel Fiber-Purkinje Cell Synapse. *Front. Synaptic Neurosci.* 8. <https://doi.org/10.3389/fnsyn.2016.00035>
- Huttenlocher, P.R., Dabholkar, A.S., 1997. Regional differences in synaptogenesis in human cerebral cortex [WWW Document]. *J. Comp. Neurol.* [https://doi.org/10.1002/\(SICI\)1096-9861\(19971020\)387:2<167::AID-CNE1>3.0.CO;2-Z](https://doi.org/10.1002/(SICI)1096-9861(19971020)387:2<167::AID-CNE1>3.0.CO;2-Z)
- Ichikawa, R., Hashimoto, K., Miyazaki, T., Uchigashima, M., Yamasaki, M., Aiba, A., Kano, M., Watanabe, M., 2016. Territories of heterologous inputs onto Purkinje cell dendrites are segregated by mGluR1-dependent parallel fiber synapse elimination. *Proc. Natl. Acad. Sci.* 113, 2282–2287. <https://doi.org/10.1073/pnas.1511513113>
- Ichikawa, R., Miyazaki, T., Kano, M., Hashikawa, T., Tatsumi, H., Sakimura, K., Mishina, M., Inoue, Y., Watanabe, M., 2002. Distal Extension of Climbing Fiber Territory and Multiple Innervation Caused by Aberrant Wiring to Adjacent Spiny Branchlets in Cerebellar Purkinje Cells Lacking Glutamate Receptor $\delta 2$. *J. Neurosci.* 22, 8487–8503. <https://doi.org/10.1523/JNEUROSCI.22-19-08487.2002>
- Ilzarbe, D., de la Serna, E., Baeza, I., Rosa, M., Puig, O., Calvo, A., Masias, M., Borrás, R., Pariente, J.C., Castro-Fornieles, J., Sugranyes, G., 2019. The relationship between performance in a theory of mind task and intrinsic functional connectivity in youth with early onset psychosis. *Dev. Cogn. Neurosci.* 40, 100726. <https://doi.org/10.1016/j.dcn.2019.100726>
- Ito, M., 2008. Control of mental activities by internal models in the cerebellum. *Nat. Rev. Neurosci.* 9, 304–313. <https://doi.org/10.1038/nrn2332>
- Ito, M., 1972. Neural design of the cerebellar motor control system. *Brain Res.* 40, 81–84. [https://doi.org/10.1016/0006-8993\(72\)90110-2](https://doi.org/10.1016/0006-8993(72)90110-2)
- Ito, M., Itō, M., 1984. *The Cerebellum and Neural Control*. Raven Press.
- Ito, M., Kano, M., 1982. Long-lasting depression of parallel fiber-Purkinje cell transmission induced by conjunctive stimulation of parallel fibers and climbing fibers in the cerebellar cortex. *Neurosci. Lett.* 33, 253–258. [https://doi.org/10.1016/0304-3940\(82\)90380-9](https://doi.org/10.1016/0304-3940(82)90380-9)
- Ito-Ishida, A., Miura, E., Emi, K., Matsuda, K., Iijima, T., Kondo, T., Kohda, K., Watanabe, M., Yuzaki, M., 2008. Cbln1 Regulates Rapid Formation and Maintenance of Excitatory Synapses in Mature Cerebellar Purkinje Cells In Vitro and In Vivo [WWW Document]. *J. Neurosci.* <https://doi.org/10.1523/JNEUROSCI.1030-08.2008>
- Jacobsen, L.K., Giedd, J.N., Castellanos, F.X., Vaituzis, A.C., Hamburger, S.D., Kumra, S., Lenane, M.C., Rapoport, J.L., 1998. Progressive reduction of temporal lobe structures in childhood-onset schizophrenia. *Am. J. Psychiatry* 155, 678–685. <https://doi.org/10.1176/ajp.155.5.678>
- Javitt, D.C., Steinschneider, M., Schroeder, C.E., Arezzo, J.C., 1996. Role of cortical N-methyl-D-aspartate receptors in auditory sensory memory and mismatch negativity generation: implications for schizophrenia. *Proc. Natl. Acad. Sci.* 93, 11962–11967. <https://doi.org/10.1073/pnas.93.21.11962>
- Jenkins, T.A., Harte, M.K., McKibben, C.E., Elliott, J.J., Reynolds, G.P., 2008. Disturbances in social interaction occur along with pathophysiological deficits following sub-

- chronic phencyclidine administration in the rat. *Behav. Brain Res.* 194, 230–235. <https://doi.org/10.1016/j.bbr.2008.07.020>
- Jentsch, J., 1999. The Neuropsychopharmacology of Phencyclidine From NMDA Receptor Hypofunction to the Dopamine Hypothesis of Schizophrenia. *Neuropsychopharmacology* 20, 201–225. [https://doi.org/10.1016/S0893-133X\(98\)00060-8](https://doi.org/10.1016/S0893-133X(98)00060-8)
- Jodo, E., Suzuki, Y., Katayama, T., Hoshino, K.-Y., Takeuchi, S., Niwa, S.-I., Kayama, Y., 2005. Activation of Medial Prefrontal Cortex by Phencyclidine is Mediated via a Hippocampo-prefrontal Pathway. *Cereb. Cortex* 15, 663–669. <https://doi.org/10.1093/cercor/bhh168>
- Johannessen, J.O., Larsen, T.K., Joa, I., Melle, I., Friis, S., Opjordsmoen, S., Rund, B.R., Simonsen, E., Vaglum, P., Mcglashan, T.H., 2005. Pathways to care for first-episode psychosis in an early detection healthcare sector: Part of the Scandinavian TIPS study. *Br. J. Psychiatry* 187, s24–s28. <https://doi.org/10.1192/bjp.187.48.s24>
- Jones, C., Watson, D., Fone, K., 2011. Animal models of schizophrenia: Animal models of schizophrenia. *Br. J. Pharmacol.* 164, 1162–1194. <https://doi.org/10.1111/j.1476-5381.2011.01386.x>
- Kakegawa, W., Mitakidis, N., Miura, E., Abe, M., Matsuda, K., Takeo, Y.H., Kohda, K., Motohashi, J., Takahashi, A., Nagao, S., Muramatsu, S., Watanabe, M., Sakimura, K., Aricescu, A.R., Yuzaki, M., 2015. Anterograde C1ql1 signaling is required in order to determine and maintain a single-winner climbing fiber in the mouse cerebellum. *Neuron* 85, 316–329. <https://doi.org/10.1016/j.neuron.2014.12.020>
- Kakizawa, S., Yamada, K., Iino, M., Watanabe, M., Kano, M., 2003. Effects of insulin-like growth factor I on climbing fibre synapse elimination during cerebellar development. *Eur. J. Neurosci.* 17, 545–554. <https://doi.org/10.1046/j.1460-9568.2003.02486.x>
- Kalinovsky, A., Boukhtouche, F., Blazeski, R., Bornmann, C., Suzuki, N., Mason, C.A., Scheiffele, P., 2011. Development of Axon-Target Specificity of Ponto-Cerebellar Afferents. *PLOS Biol.* 9, e1001013. <https://doi.org/10.1371/journal.pbio.1001013>
- Kallmann, F.J., 1938. The genetics of schizophrenia, The genetics of schizophrenia. J. J. Augustin, Oxford, England.
- Kandel, E.R., 2001. The Molecular Biology of Memory Storage: A Dialogue Between Genes and Synapses. *Science* 294, 1030–1038. <https://doi.org/10.1126/science.1067020>
- Kano, M., Hashimoto, K., 2012. Activity-Dependent Maturation of Climbing Fiber to Purkinje Cell Synapses during Postnatal Cerebellar Development. *The Cerebellum* 11, 449–450. <https://doi.org/10.1007/s12311-011-0337-3>
- Kano, M., Hashimoto, K., Chen, C., Abeliovich, A., Aiba, A., Kurihara, H., Watanabe, M., Inoue, Y., Tonegawa, S., 1995. Impaired synapse elimination during cerebellar development in PKC gamma mutant mice. *Cell* 83, 1223–1231. [https://doi.org/10.1016/0092-8674\(95\)90147-7](https://doi.org/10.1016/0092-8674(95)90147-7)
- Kano, M., Watanabe, T., Uesaka, N., Watanabe, M., 2018. Multiple Phases of Climbing Fiber Synapse Elimination in the Developing Cerebellum. *The Cerebellum* 17, 722–734. <https://doi.org/10.1007/s12311-018-0964-z>
- Karayorgou, M., Simon, T.J., Gogos, J.A., 2010. 2q11.2 microdeletions: linking DNA structural variation to brain dysfunction and schizophrenia. *Nat. Rev. Neurosci.* 11, 402–416. <https://doi.org/10.1038/nrn2841>
- Karson, C.N., Mrazek, R.E., Schluterman, K.O., Sturmer, W.Q., Sheng, J.G., Griffin, W.S.T., 1999. Alterations in synaptic proteins and their encoding mRNAs in prefrontal cortex in schizophrenia: a possible neurochemical basis for ‘hypofrontality.’ *Mol. Psychiatry* 4, 39–45. <https://doi.org/10.1038/sj.mp.4000459>

- Kasai, K., Shenton, M.E., Salisbury, D.F., Onitsuka, T., Toner, S.K., Yurgelun-Todd, D., Kikinis, R., Jolesz, F.A., McCarley, R.W., 2003. Differences and similarities in insular and temporal pole MRI gray matter volume abnormalities in first-episode schizophrenia and affective psychosis. *Arch. Gen. Psychiatry* 60, 1069–1077. <https://doi.org/10.1001/archpsyc.60.11.1069>
- Kasperek, T., Reholova, J., Kerkovsky, M., Sprlakova, A., Mechl, M., Mikl, M., 2012. Cortico-cerebellar functional connectivity and sequencing of movements in schizophrenia. *BMC Psychiatry* 12, 17. <https://doi.org/10.1186/1471-244X-12-17>
- Kattenstroth, G., Tantalaki, E., Südhof, T.C., Gottmann, K., Missler, M., 2004. Postsynaptic N-methyl-d-aspartate receptor function requires α -neurexins. *Proc. Natl. Acad. Sci. U. S. A.* 101, 2607–2612. <https://doi.org/10.1073/pnas.0308626100>
- Keller, A., Castellanos, F.X., Vaituzis, A.C., Jeffries, N.O., Giedd, J.N., Rapoport, J.L., 2003. Progressive loss of cerebellar volume in childhood-onset schizophrenia. *Am. J. Psychiatry* 160, 128–133. <https://doi.org/10.1176/appi.ajp.160.1.128>
- Khodosevich, K., Lazarini, F., von Engelhardt, J., Kaneko, H., Lledo, P.-M., Monyer, H., 2013. Connective Tissue Growth Factor Regulates Interneuron Survival and Information Processing in the Olfactory Bulb. *Neuron* 79, 1136–1151. <https://doi.org/10.1016/j.neuron.2013.07.011>
- Kim, H.-S., Nagalla, S.R., Oh, Y., Wilson, E., Roberts, C.T., Rosenfeld, R.G., 1997. Identification of a family of low-affinity insulin-like growth factor binding proteins (IGFBPs): Characterization of connective tissue growth factor as a member of the IGFBP superfamily. *Proc. Natl. Acad. Sci.* 94, 12981–12986. <https://doi.org/10.1073/pnas.94.24.12981>
- Kirov, G., Grozeva, D., Norton, N., Ivanov, D., Mantripragada, K.K., Holmans, P., International Schizophrenia Consortium, Wellcome Trust Case Control Consortium, Craddock, N., Owen, M.J., O'Donovan, M.C., 2009. Support for the involvement of large copy number variants in the pathogenesis of schizophrenia. *Hum. Mol. Genet.* 18, 1497–1503. <https://doi.org/10.1093/hmg/ddp043>
- Kissler, J., Müller, M.M., Fehr, T., Rockstroh, B., Elbert, T., 2000. MEG gamma band activity in schizophrenia patients and healthy subjects in a mental arithmetic task and at rest. *Clin. Neurophysiol.* 111, 2079–2087. [https://doi.org/10.1016/S1388-2457\(00\)00425-9](https://doi.org/10.1016/S1388-2457(00)00425-9)
- Knable, M.B., Barci, B.M., Bartko, J.J., Webster, M.J., Torrey, E.F., 2002. Molecular abnormalities in the major psychiatric illnesses: Classification and Regression Tree (CRT) analysis of post-mortem prefrontal markers [WWW Document]. *Mol. Psychiatry*. <https://doi.org/10.1038/sj.mp.4001034>
- Koh, P.O., Undie, A.S., Kabbani, N., Levenson, R., Goldman-Rakic, P.S., Lidow, M.S., 2003. Up-regulation of neuronal calcium sensor-1 (NCS-1) in the prefrontal cortex of schizophrenic and bipolar patients. *Proc. Natl. Acad. Sci. U. S. A.* 100, 313–317. <https://doi.org/10.1073/pnas.232693499>
- Komuro, H., Yacubova, Ellada, Yacubova, Elina, Rakic, P., 2001. Mode and Tempo of Tangential Cell Migration in the Cerebellar External Granular Layer [WWW Document]. *J. Neurosci.* <https://doi.org/10.1523/JNEUROSCI.21-02-00527.2001>
- Konnerth, A., Llano, I., Armstrong, C.M., 1990. Synaptic currents in cerebellar Purkinje cells. [WWW Document]. *Proc. Natl. Acad. Sci.* <https://doi.org/10.1073/pnas.87.7.2662>
- Krystal, J.H., Anticevic, A., 2015. Toward illness phase-specific pharmacotherapy for schizophrenia. *Biol. Psychiatry* 78, 738–740. <https://doi.org/10.1016/j.biopsych.2015.08.017>
- Krystal, J.H., Anticevic, A., Yang, G.J., Dragoi, G., Driesen, N.R., Wang, X.-J., Murray, J.D., 2017. Impaired tuning of neural ensembles and the pathophysiology of schizophrenia:

- a translational and computational neuroscience perspective. *Biol. Psychiatry* 81, 874–885. <https://doi.org/10.1016/j.biopsych.2017.01.004>
- Kuroda, K., Yamada, S., Tanaka, M., Iizuka, M., Yano, H., Mori, D., Tsuboi, D., Nishioka, T., Namba, T., Iizuka, Y., Kubota, S., Nagai, T., Ibi, D., Wang, R., Enomoto, A., Isotani-Sakakibara, M., Asai, N., Kimura, K., Kiyonari, H., Abe, T., Mizoguchi, A., Sokabe, M., Takahashi, M., Yamada, K., Kaibuchi, K., 2011. Behavioral alterations associated with targeted disruption of exons 2 and 3 of the *Disc1* gene in the mouse. *Hum. Mol. Genet.* 20, 4666–4683. <https://doi.org/10.1093/hmg/ddr400>
- Kvajo, M., McKellar, H., Arguello, P.A., Drew, L.J., Moore, H., MacDermott, A.B., Karayiorgou, M., Gogos, J.A., 2008a. A mutation in mouse *Disc1* that models a schizophrenia risk allele leads to specific alterations in neuronal architecture and cognition. *Proc. Natl. Acad. Sci.* 105, 7076–7081. <https://doi.org/10.1073/pnas.0802615105>
- Kvajo, M., McKellar, H., Arguello, P.A., Drew, L.J., Moore, H., MacDermott, A.B., Karayiorgou, M., Gogos, J.A., 2008b. A mutation in mouse *Disc1* that models a schizophrenia risk allele leads to specific alterations in neuronal architecture and cognition. *Proc. Natl. Acad. Sci.* 105, 7076–7081. <https://doi.org/10.1073/pnas.0802615105>
- Laborit, H., Huguenard, P., Alluaume, R., 1952. [A new vegetative stabilizer; 4560 R.P.]. *Presse Med.* 60, 206–208.
- Labouesse, M.A., Dong, E., Grayson, D.R., Guidotti, A., Meyer, U., 2015. Maternal immune activation induces *GAD1* and *GAD2* promoter remodeling in the offspring prefrontal cortex. *Epigenetics* 10, 1143–1155. <https://doi.org/10.1080/15592294.2015.1114202>
- Lawrie, S.M., 2018. Are structural brain changes in schizophrenia related to antipsychotic medication? A narrative review of the evidence from a clinical perspective. *Ther. Adv. Psychopharmacol.* 8, 319–326. <https://doi.org/10.1177/2045125318782306>
- Lee, S.H., DeCandia, T.R., Ripke, S., Yang, J., Sullivan, P.F., Goddard, M.E., Keller, M.C., Visscher, P.M., Wray, N.R., 2012. Estimating the proportion of variation in susceptibility to schizophrenia captured by common SNPs. *Nat. Genet.* 44, 247–250. <https://doi.org/10.1038/ng.1108>
- Letellier, M., Wehrlé, R., Mariani, J., Lohof, A.M., 2009. Synapse elimination in olivocerebellar explants occurs during a critical period and leaves an indelible trace in Purkinje cells. *Proc. Natl. Acad. Sci.* 106, 14102–14107. <https://doi.org/10.1073/pnas.0902820106>
- Levenes, C., Daniel, H., Jaillard, D., Conquet, F., Crépel, F., 1997. Incomplete regression of multiple climbing fibre innervation of cerebellar Purkinje cells in mGluR1 mutant mice. *Neuroreport* 8, 571–574. <https://doi.org/10.1097/00001756-199701200-00038>
- Levinson, D.F., Shi, J., Wang, K., Oh, S., Riley, B., Pulver, A.E., Wildenauer, D.B., Laurent, C., Mowry, B.J., Gejman, P.V., Owen, M.J., Kendler, K.S., Nestadt, G., Schwab, S.G., Mallet, J., Nertney, D., Sanders, A.R., Williams, N.M., Wormley, B., Lasseter, V.K., Albus, M., Godard-Bauché, S., Alexander, M., Duan, J., O'Donovan, M.C., Walsh, D., O'Neill, A., Papadimitriou, G.N., Dikeos, D., Maier, W., Lerer, B., Campion, D., Cohen, D., Jay, M., Fanous, A., Eichhammer, P., Silverman, J.M., Norton, N., Zhang, N., Hakonarson, H., Gao, C., Citri, A., Hansen, M., Ripke, S., Schizophrenia Psychiatric GWAS Consortium, Dudbridge, F., Holmans, P.A., 2012. Genome-wide association study of multiplex schizophrenia pedigrees. *Am. J. Psychiatry* 169, 963–973. <https://doi.org/10.1176/appi.ajp.2012.11091423>
- Lewis, D.A., González-Burgos, G., 2008. Neuroplasticity of Neocortical Circuits in Schizophrenia. *Neuropsychopharmacology* 33, 141–165. <https://doi.org/10.1038/sj.npp.1301563>

- Li, Y., Yolken, R., Cowan, D.N., Boivin, M.R., Liu, T., Niebuhr, D.W., 2015. Biomarker Identification and Effect Estimation on Schizophrenia – A High Dimensional Data Analysis. *Front. Public Health* 3. <https://doi.org/10.3389/fpubh.2015.00075>
- Lieberman, J.A., Kane, J.M., Alvir, J., 1987. Provocative tests with psychostimulant drugs in schizophrenia. *Psychopharmacology (Berl.)* 91, 415–433. <https://doi.org/10.1007/bf00216006>
- Llinás, R., Walton, K., Hillman, D.E., Sotelo, C., 1975. Inferior olive: its role in motor learning. *Science* 190, 1230–1231. <https://doi.org/10.1126/science.128123>
- Lodge, D.J., 2013. The MAM rodent model of schizophrenia. *Curr. Protoc. Neurosci.* Editor. Board Jacqueline N Crawley AI 0 9, Unit9.43. <https://doi.org/10.1002/0471142301.ns0943s63>
- Lohmueller, K.E., Pearce, C.L., Pike, M., Lander, E.S., Hirschhorn, J.N., 2003. Meta-analysis of genetic association studies supports a contribution of common variants to susceptibility to common disease. *Nat. Genet.* 33, 177–182. <https://doi.org/10.1038/ng1071>
- Lorenzetto, E., Caselli, L., Feng, G., Yuan, W., Nerbonne, J.M., Sanes, J.R., Buffelli, M., 2009. Genetic perturbation of postsynaptic activity regulates synapse elimination in developing cerebellum. *Proc. Natl. Acad. Sci.* 106, 16475–16480. <https://doi.org/10.1073/pnas.0907298106>
- Lucas, F.R., Salinas, P.C., 1997. WNT-7a induces axonal remodeling and increases synapsin I levels in cerebellar neurons. *Dev. Biol.* 192, 31–44. <https://doi.org/10.1006/dbio.1997.8734>
- Ma, C., Gu, C., Huo, Y., Li, X., Luo, X.-J., 2018. The integrated landscape of causal genes and pathways in schizophrenia. *Transl. Psychiatry* 8, 1–14. <https://doi.org/10.1038/s41398-018-0114-x>
- Ma, J., Leung, L.S., 2000. Relation between hippocampal gamma waves and behavioral disturbances induced by phencyclidine and methamphetamine. *Behav. Brain Res.* 111, 1–11. [https://doi.org/10.1016/s0166-4328\(00\)00138-8](https://doi.org/10.1016/s0166-4328(00)00138-8)
- Macêdo, D.S., Araújo, D.P., Sampaio, L.R.L., Vasconcelos, S.M.M., Sales, P.M.G., Sousa, F.C.F., Hallak, J.E., Crippa, J.A., Carvalho, A.F., 2012. Animal models of prenatal immune challenge and their contribution to the study of schizophrenia: a systematic review. *Braz. J. Med. Biol. Res.* 45, 179–186. <https://doi.org/10.1590/S0100-879X2012007500031>
- Madhusoodanan, S., Ting, M.B., Farah, T., Ugur, U., 2015. Psychiatric aspects of brain tumors: A review [WWW Document]. *World J. Psychiatry*. <https://doi.org/10.5498/wjp.v5.i3.273>
- Maher, B.J., LoTurco, J.J., Tell, F., 2012. Disrupted-in-Schizophrenia (DISC1) Functions Presynaptically at Glutamatergic Synapses [WWW Document]. *PLoS ONE*. <https://doi.org/10.1371/journal.pone.0034053>
- Malavasi, E.L.V., Economides, K.D., Grünewald, E., Makedonopoulou, P., Gautier, P., Mackie, S., Murphy, L.C., Murdoch, H., Crummie, D., Ogawa, F., McCartney, D.L., O’Sullivan, S.T., Burr, K., Torrance, H.S., Phillips, J., Bonneau, M., Anderson, S.M., Perry, P., Pearson, M., Constantinides, C., Davidson-Smith, H., Kabiri, M., Duff, B., Johnstone, M., Polites, H.G., Lawrie, S.M., Blackwood, D.H., Semple, C.A., Evans, K.L., Didier, M., Chandran, S., McIntosh, A.M., Price, D.J., Houslay, M.D., Porteous, D.J., Millar, J.K., 2018. DISC1 regulates N-methyl-D-aspartate receptor dynamics: abnormalities induced by a Disc1 mutation modelling a translocation linked to major mental illness [WWW Document]. *Transl. Psychiatry*. <https://doi.org/10.1038/s41398-018-0228-1>

- Manahan-Vaughan, D., von Haebler, D., Winter, C., Juckel, G., Heinemann, U., 2008. A single application of MK801 causes symptoms of acute psychosis, deficits in spatial memory, and impairment of synaptic plasticity in rats. *Hippocampus* 18, 125–134. <https://doi.org/10.1002/hipo.20367>
- Manto, M., Bower, J.M., Conforto, A.B., Delgado-García, J.M., da Guarda, S.N.F., Gerwig, M., Habas, C., Hagura, N., Ivry, R.B., Mariën, P., Molinari, M., Naito, E., Nowak, D.A., Ben Taib, N.O., Pelisson, D., Tesche, C.D., Tilikete, C., Timmann, D., 2012. Consensus Paper: Roles of the Cerebellum in Motor Control—The Diversity of Ideas on Cerebellar Involvement in Movement. *Cerebellum Lond. Engl.* 11, 457–487. <https://doi.org/10.1007/s12311-011-0331-9>
- Mariani, J., Crepel, F., Mikoshiba, K., Changeux, J.P., Sotelo, C., Boycott, B.B., 1977. Anatomical, Physiological and biochemical studies of the cerebellum from reeler mutant mouse. *Philos. Trans. R. Soc. Lond. B Biol. Sci.* 281, 1–28. <https://doi.org/10.1098/rstb.1977.0121>
- Matosin, N., Fernandez-Enright, F., Lum, J.S., Engel, M., Andrews, J.L., Gassen, N.C., Wagner, K.V., Schmidt, M.V., Newell, K.A., 2016. Molecular evidence of synaptic pathology in the CA1 region in schizophrenia. *Npj Schizophr.* 2, 1–8. <https://doi.org/10.1038/npjSchz.2016.22>
- Matsuda, K., Miura, E., Miyazaki, T., Kakegawa, W., Emi, K., Narumi, S., Fukazawa, Y., Ito-Ishida, A., Kondo, T., Shigemoto, R., Watanabe, M., Yuzaki, M., 2010. Cbln1 Is a Ligand for an Orphan Glutamate Receptor 2, a Bidirectional Synapse Organizer. *Science* 328, 363–368. <https://doi.org/10.1126/science.1185152>
- Maussion, G., Carayol, J., Lepagnol-Bestel, A.-M., Tores, F., Loe-Mie, Y., Milbreta, U., Rousseau, F., Fontaine, K., Renaud, J., Moalic, J.-M., Philippi, A., Chedotal, A., Gorwood, P., Ramoz, N., Hager, J., Simonneau, M., 2008. Convergent evidence identifying MAP/microtubule affinity-regulating kinase 1 (MARK1) as a susceptibility gene for autism. *Hum. Mol. Genet.* 17, 2541–2551. <https://doi.org/10.1093/hmg/ddn154>
- Meador-Woodruff, J.H., Hogg, A.J., Smith, R.E., 2001. Striatal ionotropic glutamate receptor expression in schizophrenia, bipolar disorder, and major depressive disorder. *Brain Res. Bull., Neuropathology of Severe Mental Illness: Studies from the Stanley Foundation Neuropathology Consortium* 55, 631–640. [https://doi.org/10.1016/S0361-9230\(01\)00523-8](https://doi.org/10.1016/S0361-9230(01)00523-8)
- Mednick, S.A., Machon, R.A., Huttunen, M.O., Bonett, D., 1988. Adult schizophrenia following prenatal exposure to an influenza epidemic. *Arch. Gen. Psychiatry* 45, 189–192. <https://doi.org/10.1001/archpsyc.1988.01800260109013>
- Miall, R.C., Antony, J., Goldsmith-Sumner, A., Harding, S.R., McGovern, C., Winter, J.L., 2016. Modulation of linguistic prediction by TDCS of the right lateral cerebellum [WWW Document]. *Neuropsychologia*. <https://doi.org/10.1016/j.neuropsychologia.2016.04.022>
- Millar, J.K., Wilson-Annan, J.C., Anderson, S., Christie, S., Taylor, M.S., Semple, C.A., Devon, R.S., St Clair, D.M., Muir, W.J., Blackwood, D.H., Porteous, D.J., 2000. Disruption of two novel genes by a translocation co-segregating with schizophrenia. *Hum. Mol. Genet.* 9, 1415–1423. <https://doi.org/10.1093/hmg/9.9.1415>
- Moberget, T., Alnæs, D., Kaufmann, T., Doan, N.T., Córdova-Palomera, A., Norbom, L.B., Rokicki, J., van der Meer, D., Andreassen, O.A., Westlye, L.T., 2019. Cerebellar Gray Matter Volume Is Associated With Cognitive Function and Psychopathology in Adolescence [WWW Document]. *Biol. Psychiatry*. <https://doi.org/10.1016/j.biopsych.2019.01.019>

- Moberget, T., Doan, N.T., Alnæs, D., Kaufmann, T., Córdova-Palomera, A., Lagerberg, T.V., Diedrichsen, J., Schwarz, E., Zink, M., Eisenacher, S., Kirsch, P., Jönsson, E.G., Fatouros-Bergman, H., Flyckt, L., Pergola, G., Quarto, T., Bertolino, A., Barch, D., Meyer-Lindenberg, A., Agartz, I., Andreassen, O.A., Westlye, L.T., 2018. Cerebellar volume and cerebellocerebral structural covariance in schizophrenia: a multisite mega-analysis of 983 patients and 1349 healthy controls. *Mol. Psychiatry* 23, 1512–1520. <https://doi.org/10.1038/mp.2017.106>
- Morrow, E.M., Yoo, S.-Y., Flavell, S.W., Kim, T.-K., Lin, Y., Hill, R.S., Mukaddes, N.M., Balkhy, S., Gascon, G., Hashmi, A., Al-Saad, S., Ware, J., Joseph, R.M., Greenblatt, R., Gleason, D., Ertelt, J.A., Apse, K.A., Bodell, A., Partlow, J.N., Barry, B., Yao, H., Markianos, K., Ferland, R.J., Greenberg, M.E., Walsh, C.A., 2008. Identifying autism loci and genes by tracing recent shared ancestry. *Science* 321, 218–223. <https://doi.org/10.1126/science.1157657>
- Mukai, J., Cannavò, E., Crabtree, G.W., Sun, Z., Diamantopoulou, A., Thakur, P., Chang, C.-Y., Cai, Y., Lomvardas, S., Takata, A., Xu, B., Gogos, J.A., 2019. Recapitulation and Reversal of Schizophrenia-Related Phenotypes in Setd1a-Deficient Mice. *Neuron* 104, 471–487.e12. <https://doi.org/10.1016/j.neuron.2019.09.014>
- Mukai, J., Dhillia, A., Drew, L.J., Stark, K.L., Cao, L., MacDermott, A.B., Karayiorgou, M., Gogos, J.A., 2008. Palmitoylation-dependent neurodevelopmental deficits in a mouse model of the 22q11 microdeletion. *Nat. Neurosci.* 11, 1302–1310. <https://doi.org/10.1038/nn.2204>
- Mukherjee, A., Carvalho, F., Eliez, S., Caroni, P., 2019. Long-Lasting Rescue of Network and Cognitive Dysfunction in a Genetic Schizophrenia Model. *Cell* 178, 1387–1402.e14. <https://doi.org/10.1016/j.cell.2019.07.023>
- Murphy, K.C., Jones, L.A., Owen, M.J., 1999. High rates of schizophrenia in adults with velo-cardio-facial syndrome. *Arch. Gen. Psychiatry* 56, 940–945. <https://doi.org/10.1001/archpsyc.56.10.940>
- Murray, R.M., Lewis, S.W., 1987. Is schizophrenia a neurodevelopmental disorder? *Br. Med. J. Clin. Res. Ed* 295, 681–682.
- Nabeshima, T., Fukaya, H., Yamaguchi, K., Ishikawa, K., Furukawa, H., Kameyama, T., 1987. Development of tolerance and supersensitivity to phencyclidine in rats after repeated administration of phencyclidine. *Eur. J. Pharmacol.* 135, 23–33. [https://doi.org/10.1016/0014-2999\(87\)90753-9](https://doi.org/10.1016/0014-2999(87)90753-9)
- Näkki, R., Sharp, F.R., Sagar, S.M., 1996. FOS expression in the brainstem and cerebellum following phencyclidine and MK801. *J. Neurosci. Res.* 43, 203–212. [https://doi.org/10.1002/\(SICI\)1097-4547\(19960115\)43:2<203::AID-JNR8>3.0.CO;2-K](https://doi.org/10.1002/(SICI)1097-4547(19960115)43:2<203::AID-JNR8>3.0.CO;2-K)
- Napper, R.M.A., Harvey, R.J., 1988. Number of parallel fiber synapses on an individual Purkinje cell in the cerebellum of the rat. *J. Comp. Neurol.* 274, 168–177. <https://doi.org/10.1002/cne.902740204>
- Neufeld, N., Gallagher, D., Aviv, R., Feinstein, A., 2016. Remote Cerebellar Stroke Associated With Delusions and Disorganization. *J. Neuropsychiatry Clin. Neurosci.* 28, 335–337. <https://doi.org/10.1176/appi.neuropsych.15110398>
- Nilsson, S.R.O., Heath, C.J., Takillah, S., Didienne, S., Fejgin, K., Nielsen, V., Nielsen, J., Saksida, L.M., Mariani, J., Faure, P., Didriksen, M., Robbins, T.W., Bussey, T.J., Mar, A.C., 2018. Continuous performance test impairment in a 22q11.2 microdeletion mouse model: improvement by amphetamine. *Transl. Psychiatry* 8, 1–14. <https://doi.org/10.1038/s41398-018-0295-3>
- Ninan, I., 2003. Olanzapine and clozapine but not haloperidol reverse subchronic phencyclidine-induced functional hyperactivity of N-methyl-D-aspartate receptors in

- pyramidal cells of the rat medial prefrontal cortex. *Neuropharmacology* 44, 462–472. [https://doi.org/10.1016/S0028-3908\(03\)00033-9](https://doi.org/10.1016/S0028-3908(03)00033-9)
- Nomura, T., Oyamada, Y., Fernandes, H.B., Remmers, C., Xu, J., Meltzer, H., Contractor, A., 2016. Subchronic phencyclidine treatment in adult mice increases GABAergic transmission and LTP threshold in the hippocampus. *Neuropharmacology* 100, 90–97. <https://doi.org/10.1016/j.neuropharm.2015.04.012>
- Nopoulos, P.C., Ceilley, J.W., Gailis, E.A., Andreasen, N.C., 1999. An MRI study of cerebellar vermis morphology in patients with schizophrenia: evidence in support of the cognitive dysmetria concept. *Biol. Psychiatry* 46, 703–711. [https://doi.org/10.1016/S0006-3223\(99\)00093-1](https://doi.org/10.1016/S0006-3223(99)00093-1)
- Offermanns, S., Hashimoto, K., Watanabe, M., Sun, W., Kurihara, H., Thompson, R.F., Inoue, Y., Kano, M., Simon, M.I., 1997. Impaired motor coordination and persistent multiple climbing fiber innervation of cerebellar Purkinje cells in mice lacking *Gαq*. *Proc. Natl. Acad. Sci. U. S. A.* 94, 14089–14094.
- Ohkawara, B., Kobayakawa, A., Kanbara, S., Hattori, T., Kubota, S., Ito, M., Masuda, A., Takigawa, M., Lyons, K.M., Ishiguro, N., Ohno, K., 2020. CTGF/CCN2 facilitates LRP4-mediated formation of the embryonic neuromuscular junction. *EMBO Rep.* n/a, e48462. <https://doi.org/10.15252/embr.201948462>
- Ohnuma, T., Augood, S.J., Arai, H., McKenna, P.J., Emson, P.C., 1998. Expression of the human excitatory amino acid transporter 2 and metabotropic glutamate receptors 3 and 5 in the prefrontal cortex from normal individuals and patients with schizophrenia. *Brain Res. Mol. Brain Res.* 56, 207–217. [https://doi.org/10.1016/s0169-328x\(98\)00063-1](https://doi.org/10.1016/s0169-328x(98)00063-1)
- Olfson, M., Gerhard, T., Huang, C., Crystal, S., Stroup, T.S., 2015. Premature Mortality Among Adults With Schizophrenia in the United States. *JAMA Psychiatry* 72, 1172–1181. <https://doi.org/10.1001/jamapsychiatry.2015.1737>
- Onay, H., Kacamak, D., Kavasoglu, A., Akgun, B., Yalcinli, M., Kose, S., Ozbaran, B., 2016. Mutation analysis of the *NRXN1* gene in autism spectrum disorders [WWW Document]. *Balk. J. Med. Genet.* <https://doi.org/10.1515/bjmg-2016-0031>
- Onwordi, E.C., Halff, E.F., Whitehurst, T., Mansur, A., Cotel, M.-C., Wells, L., Creaney, H., Bonsall, D., Rogdaki, M., Shatalina, E., Reis Marques, T., Rabiner, E.A., Gunn, R.N., Natesan, S., Vernon, A.C., Howes, O.D., 2020. Synaptic density marker SV2A is reduced in schizophrenia patients and unaffected by antipsychotics in rats. *Nat. Commun.* 11, 246. <https://doi.org/10.1038/s41467-019-14122-0>
- Osimo, E.F., Beck, K., Marques, T.R., Howes, O.D., 2019. Synaptic loss in schizophrenia: a meta-analysis and systematic review of synaptic protein and mRNA measures. *Mol. Psychiatry* 24, 549–561. <https://doi.org/10.1038/s41380-018-0041-5>
- Pakkenberg, B., 1993. Total nerve cell number in neocortex in chronic schizophrenics and controls estimated using optical disectors. *Biol. Psychiatry* 34, 768–772. [https://doi.org/10.1016/0006-3223\(93\)90065-L](https://doi.org/10.1016/0006-3223(93)90065-L)
- Pakkenberg, B., 1987. Post-mortem Study of Chronic Schizophrenic Brains. *Br. J. Psychiatry* 151, 744–752. <https://doi.org/10.1192/bjp.151.6.744>
- Palaniyappan, L., Simmonite, M., White, T.P., Liddle, E.B., Liddle, P.F., 2013. Neural Primacy of the Salience Processing System in Schizophrenia. *Neuron* 79, 814–828. <https://doi.org/10.1016/j.neuron.2013.06.027>
- Palay, S.L., Chan-Palay, V., 2012. *Cerebellar Cortex: Cytology and Organization*. Springer Science & Business Media.
- Palkovits, M., Magyar, P., Szentágothai, J., 1972. Quantitative histological analysis of the cerebellar cortex in the cat. IV. Mossy fiber-purkinje cell numerical transfer. *Brain Res.* 45, 15–29. [https://doi.org/10.1016/0006-8993\(72\)90213-2](https://doi.org/10.1016/0006-8993(72)90213-2)

- Pätz, C., Brachtendorf, S., Eilers, J., 2018. The transgenic mouse line Igsf9-eGFP allows targeted stimulation of inferior olive efferents. *J. Neurosci. Methods* 296, 84–92. <https://doi.org/10.1016/j.jneumeth.2017.12.024>
- Pérez-Villegas, E.M., Negrete-Díaz, J.V., Porrás-García, M.E., Ruiz, R., Carrión, A.M., Rodríguez-Moreno, A., Armengol, J.A., 2018. Mutation of the HERC 1 Ubiquitin Ligase Impairs Associative Learning in the Lateral Amygdala. *Mol. Neurobiol.* 55, 1157–1168. <https://doi.org/10.1007/s12035-016-0371-8>
- Philip, N., Bassett, A., 2011. Cognitive, Behavioural and Psychiatric Phenotype in 22q11.2 Deletion Syndrome. *Behav. Genet.* 41, 403–412. <https://doi.org/10.1007/s10519-011-9468-z>
- Picard, H., Amado, I., Mouchet-Mages, S., Olié, J.-P., Krebs, M.-O., 2008. The Role of the Cerebellum in Schizophrenia: an Update of Clinical, Cognitive, and Functional Evidences. *Schizophr. Bull.* 34, 155–172. <https://doi.org/10.1093/schbul/sbm049>
- Pierce, D.R., Hayar, A., Williams, D.K., Light, K.E., 2011. Olivary Climbing Fiber Alterations in PN40 Rat Cerebellum Following Postnatal Ethanol Exposure. *Brain Res.* 1378, 54–65. <https://doi.org/10.1016/j.brainres.2011.01.028>
- Piochon, C., Levenes, C., Ohtsuki, G., Hansel, C., 2010. Purkinje Cell NMDA Receptors Assume a Key Role in Synaptic Gain Control in the Mature Cerebellum. *J. Neurosci.* 30, 15330–15335. <https://doi.org/10.1523/JNEUROSCI.4344-10.2010>
- Piskorowski, R.A., Nasrallah, K., Diamantopoulou, A., Mukai, J., Hassan, S.I., Siegelbaum, S.A., Gogos, J.A., Chevalleyre, V., 2016. Age-Dependent Specific Changes in Area CA2 of the Hippocampus and Social Memory Deficit in a Mouse Model of the 22q11.2 Deletion Syndrome. *Neuron* 89, 163–176. <https://doi.org/10.1016/j.neuron.2015.11.036>
- Porter, R.H., Eastwood, S.L., Harrison, P.J., 1997. Distribution of kainate receptor subunit mRNAs in human hippocampus, neocortex and cerebellum, and bilateral reduction of hippocampal GluR6 and KA2 transcripts in schizophrenia. *Brain Res.* 751, 217–231. [https://doi.org/10.1016/s0006-8993\(96\)01404-7](https://doi.org/10.1016/s0006-8993(96)01404-7)
- Pradhan, S.N., 1984. Phencyclidine (PCP): some human studies. *Neurosci. Biobehav. Rev.* 8, 493–501. [https://doi.org/10.1016/0149-7634\(84\)90006-x](https://doi.org/10.1016/0149-7634(84)90006-x)
- Prikryl, R., Ceskova, E., Kasperek, T., Kucerova, H., 2007. Neurological soft signs and their relationship to 1-year outcome in first-episode schizophrenia. *Eur. Psychiatry* 22, 499–504. <https://doi.org/10.1016/j.eurpsy.2007.03.012>
- Purcell, S.M., Moran, J.L., Fromer, M., Ruderfer, D., Solovieff, N., Roussos, P., O’Dushlaine, C., Chambert, K., Bergen, S.E., Kähler, A., Duncan, L., Stahl, E., Genovese, G., Fernández, E., Collins, M.O., Komiyama, N.H., Choudhary, J.S., Magnusson, P.K.E., Banks, E., Shakir, K., Garimella, K., Fennell, T., DePristo, M., Grant, S.G.N., Haggarty, S.J., Gabriel, S., Scolnick, E.M., Lander, E.S., Hultman, C.M., Sullivan, P.F., McCarroll, S.A., Sklar, P., 2014. A polygenic burden of rare disruptive mutations in schizophrenia. *Nature* 506, 185–190. <https://doi.org/10.1038/nature12975>
- Quinn, P.D., Rickert, M.E., Weibull, C.E., Johansson, A.L.V., Lichtenstein, P., Almqvist, C., Larsson, H., Iliadou, A.N., D’Onofrio, B.M., 2017. Association Between Maternal Smoking During Pregnancy and Severe Mental Illness in Offspring. *JAMA Psychiatry* 74, 589–596. <https://doi.org/10.1001/jamapsychiatry.2017.0456>
- Rabacchi, S., Bailly, Y., Delhayé-Bouchaud, N., Mariani, J., 1992. Involvement of the N-methyl D-aspartate (NMDA) receptor in synapse elimination during cerebellar development. *Science* 256, 1823–1825. <https://doi.org/10.1126/science.1352066>
- Raja, S.N., Guyenet, P.G., 1982. Action of phencyclidine on synaptic transmission in the hippocampus. *Brain Res.* 236, 289–304. [https://doi.org/10.1016/0006-8993\(82\)90715-6](https://doi.org/10.1016/0006-8993(82)90715-6)

- Rajkowska, G., Selemon, L.D., Goldman-Rakic, P.S., 1998. Neuronal and glial somal size in the prefrontal cortex: a postmortem morphometric study of schizophrenia and Huntington disease. *Arch. Gen. Psychiatry* 55, 215–224. <https://doi.org/10.1001/archpsyc.55.3.215>
- Raman, I.M., Bean, B.P., 1999. Ionic Currents Underlying Spontaneous Action Potentials in Isolated Cerebellar Purkinje Neurons [WWW Document]. *J. Neurosci.* <https://doi.org/10.1523/JNEUROSCI.19-05-01663.1999>
- Ramos, B., Gaudillière, B., Bonni, A., Gill, G., 2007. Transcription factor Sp4 regulates dendritic patterning during cerebellar maturation. *Proc. Natl. Acad. Sci. U. S. A.* 104, 9882–9887. <https://doi.org/10.1073/pnas.0701946104>
- Reeber, S.L., White, J.J., George-Jones, N.A., Sillitoe, R.V., 2013. Architecture and development of olivocerebellar circuit topography. *Front. Neural Circuits* 6. <https://doi.org/10.3389/fncir.2012.00115>
- Rees, E., O'Donovan, M.C., Owen, M.J., 2015. Genetics of schizophrenia. *Curr. Opin. Behav. Sci., Behavioral genetics* 2, 8–14. <https://doi.org/10.1016/j.cobeha.2014.07.001>
- Reyes, M.G., Gordon, A., 1981. Cerebellar vermis in schizophrenia. *Lancet Lond. Engl.* 2, 700–701.
- Reynolds, G.P., Abdul-Monim, Z., Neill, J.C., Zhang, Z.-J., 2004. Calcium binding protein markers of GABA deficits in schizophrenia — post mortem studies and animal models [WWW Document]. *Neurotox. Res.* <https://doi.org/10.1007/BF03033297>
- Ripke, S., Neale, B.M., Corvin, A., Walters, J.T.R., Farh, K.-H., Holmans, P.A., Lee, P., Bulik-Sullivan, B., Collier, D.A., Huang, H., Pers, T.H., Agartz, I., Agerbo, E., Albus, M., Alexander, M., Amin, F., Bacanu, S.A., Begemann, M., Belliveau Jr, R.A., Bene, J., Bergen, S.E., Bevilacqua, E., Bigdeli, T.B., Black, D.W., Bruggeman, R., Buccola, N.G., Buckner, R.L., Byerley, W., Cahn, W., Cai, G., Champion, D., Cantor, R.M., Carr, V.J., Carrera, N., Catts, S.V., Chambert, K.D., Chan, R.C.K., Chen, R.Y.L., Chen, E.Y.H., Cheng, W., Cheung, E.F.C., Ann Chong, S., Robert Cloninger, C., Cohen, D., Cohen, N., Cormican, P., Craddock, N., Crowley, J.J., Curtis, D., Davidson, M., Davis, K.L., Degenhardt, F., Del Favero, J., Demontis, D., Dikeos, D., Dinan, T., Djurovic, S., Donohoe, G., Drapeau, E., Duan, J., Dudbridge, F., Durmishi, N., Eichhammer, P., Eriksson, J., Escott-Price, V., Essioux, L., Fanous, A.H., Farrell, M.S., Frank, J., Franke, L., Freedman, R., Freimer, N.B., Friedl, M., Friedman, J.I., Fromer, M., Genovese, G., Georgieva, L., Giegling, I., Giusti-Rodríguez, P., Godard, S., Goldstein, J.I., Golimbet, V., Gopal, S., Gratten, J., de Haan, L., Hammer, C., Hamshere, M.L., Hansen, M., Hansen, T., Haroutunian, V., Hartmann, A.M., Henskens, F.A., Herms, S., Hirschhorn, J.N., Hoffmann, P., Hofman, A., Hollegaard, M.V., Hougaard, D.M., Ikeda, M., Joa, I., Julià, A., Kahn, R.S., Kalaydjieva, L., Karachanak-Yankova, S., Karjalainen, J., Kavanagh, D., Keller, M.C., Kennedy, J.L., Khrunin, A., Kim, Y., Klovins, J., Knowles, J.A., Konte, B., Kucinskas, V., Ausrele Kucinskiene, Z., Kuzelova-Ptackova, H., Kähler, A.K., Laurent, C., Lee Chee Keong, J., Hong Lee, S., Legge, S.E., Lerer, B., Li, M., Li, T., Liang, K.-Y., Lieberman, J., Limborska, S., Loughland, C.M., Lubinski, J., Lönnqvist, J., Macek Jr, M., Magnusson, P.K.E., Maher, B.S., Maier, W., Mallet, J., Marsal, S., Mattheisen, M., Mattingsdal, M., McCarley, R.W., McDonald, C., McIntosh, A.M., Meier, S., Meijer, C.J., Melegh, B., Melle, I., Meshulam-Gately, R.I., Metspalu, A., Michie, P.T., Milani, L., Milanova, V., Mokrab, Y., Morris, D.W., Mors, O., Murphy, K.C., Murray, R.M., Myin-Germeys, I., Müller-Myhsok, B., Nelis, M., Nenadic, I., Nertney, D.A., Nestadt, G., Nicodemus, K.K., Nikitina-Zake, L., Nisenbaum, L., Nordin, A., O'Callaghan, E., O'Dushlaine, C., O'Neill, F.A., Oh, S.-Y., Olincy, A., Olsen, L., Van Os, J., Pantelis, C., Papadimitriou, G.N., Papiol, S., Parkhomenko, E., Pato, M.T., Paunio, T., Pejovic-

- Milovancevic, M., Perkins, D.O., Pietiläinen, O., Pimm, J., Pocklington, A.J., Powell, J., Price, A., Pulver, A.E., Purcell, S.M., Queded, D., Rasmussen, H.B., Reichenberg, A., Reimers, M.A., Richards, A.L., Roffman, J.L., Roussos, P., Ruderfer, D.M., Salomaa, V., Sanders, A.R., Schall, U., Schubert, C.R., Schulze, T.G., Schwab, S.G., Scolnick, E.M., Scott, R.J., Seidman, L.J., Shi, J., Sigurdsson, E., Silagadze, T., Silverman, J.M., Sim, K., Slominsky, P., Smoller, J.W., So, H.-C., Spencer, C.A., Stahl, E.A., Stefansson, H., Steinberg, S., Stogmann, E., Straub, R.E., Strengman, E., Strohmaier, J., Scott Stroup, T., Subramaniam, M., Suvisaari, J., Svrakic, D.M., Szatkiewicz, J.P., Söderman, E., Thirumalai, S., Toncheva, D., Tosato, S., Veijola, J., Waddington, J., Walsh, D., Wang, D., Wang, Q., Webb, B.T., Weiser, M., Wildenauer, D.B., Williams, N.M., Williams, S., Witt, S.H., Wolen, A.R., Wong, E.H.M., Wormley, B.K., Simon Xi, H., Zai, C.C., Zheng, X., Zimprich, F., Wray, N.R., Stefansson, K., Visscher, P.M., Trust Case-Control Consortium, W., Adolfsson, R., Andreassen, O.A., Blackwood, D.H.R., Bramon, E., Buxbaum, J.D., Børglum, A.D., Cichon, S., Darvasi, A., Domenici, E., Ehrenreich, H., Esko, T., Gejman, P.V., Gill, M., Gurling, H., Hultman, C.M., Iwata, N., Jablensky, A.V., Jönsson, E.G., Kendler, K.S., Kirov, G., Knight, J., Lencz, T., Levinson, D.F., Li, Q.S., Liu, J., Malhotra, A.K., McCarroll, S.A., McQuillin, A., Moran, J.L., Mortensen, P.B., Mowry, B.J., Nöthen, M.M., Ophoff, R.A., Owen, M.J., Palotie, A., Pato, C.N., Petryshen, T.L., Posthuma, D., Rietschel, M., Riley, B.P., Rujescu, D., Sham, P.C., Sklar, P., St Clair, D., Weinberger, D.R., Wendland, J.R., Werge, T., Schizophrenia Working Group of the Psychiatric Genomics Consortium, Psychosis Endophenotypes International Consortium, 2014. Biological insights from 108 schizophrenia-associated genetic loci. *Nature* 511, 421–427. <https://doi.org/10.1038/nature13595>
- Roberts, R., Barksdale, K., Roche, J., Lahti, A., 2015. Decreased synaptic and mitochondrial density in the postmortem anterior cingulate cortex in schizophrenia. *Schizophr. Res.* 168, 543–553. <https://doi.org/10.1016/j.schres.2015.07.016>
- Roberts, R.C., Gaither, L.A., Peretti, F.J., Lapidus, B., Chute, D.J., 1996. Synaptic organization of the human striatum: A postmortem ultrastructural study. *J. Comp. Neurol.* 374, 523–534. [https://doi.org/10.1002/\(SICI\)1096-9861\(19961028\)374:4<523::AID-CNE4>3.0.CO;2-3](https://doi.org/10.1002/(SICI)1096-9861(19961028)374:4<523::AID-CNE4>3.0.CO;2-3)
- Roberts, R.C., McCollum, L.A., Schoonover, K.E., Mabry, S.J., Roche, J.K., Lahti, A.C., 2020. Ultrastructural evidence for glutamatergic dysregulation in schizophrenia. *Schizophr. Res.* <https://doi.org/10.1016/j.schres.2020.01.016>
- Rochefort, C., Arabo, A., Andre, M., Poucet, B., Save, E., Rondi-Reig, L., 2011. Cerebellum Shapes Hippocampal Spatial Code. *Science* 334, 385–389. <https://doi.org/10.1126/science.1207403>
- Rondi-Reig, L., Paradis, A.-L., Lefort, J.M., Babayan, B.M., Tobin, C., 2014. How the cerebellum may monitor sensory information for spatial representation. *Front. Syst. Neurosci.* 8. <https://doi.org/10.3389/fnsys.2014.00205>
- Rosoklija, G., Toomayan, G., Ellis, S.P., Keilp, J., Mann, J.J., Latov, N., Hays, A.P., Dwork, A.J., 2000. Structural Abnormalities of Subicular Dendrites in Subjects With Schizophrenia and Mood Disorders: Preliminary Findings. *Arch. Gen. Psychiatry* 57, 349–356. <https://doi.org/10.1001/archpsyc.57.4.349>
- Roussos, P., Guennewig, B., Kaczorowski, D.C., Barry, G., Brennand, K.J., 2016. Activity-Dependent Changes in Gene Expression in Schizophrenia Human-Induced Pluripotent Stem Cell Neurons. *JAMA Psychiatry* 73, 1180–1188. <https://doi.org/10.1001/jamapsychiatry.2016.2575>
- Rujescu, D., Ingason, A., Cichon, S., Pietiläinen, O.P.H., Barnes, M.R., Touloupoulou, T., Picchioni, M., Vassos, E., Ettinger, U., Bramon, E., Murray, R., Ruggeri, M., Tosato,

- S., Bonetto, C., Steinberg, S., Sigurdsson, E., Sigmundsson, T., Petursson, H., Gylfason, A., Olason, P.I., Hardarsson, G., Jonsdottir, G.A., Gustafsson, O., Fossdal, R., Giegling, I., Möller, H.-J., Hartmann, A.M., Hoffmann, P., Crombie, C., Fraser, G., Walker, N., Lonnqvist, J., Suvisaari, J., Tuulio-Henriksson, A., Djurovic, S., Melle, I., Andreassen, O.A., Hansen, T., Werge, T., Kiemenev, L.A., Franke, B., Veltman, J., Buizer-Voskamp, J.E., GROUP Investigators, Sabatti, C., Ophoff, R.A., Rietschel, M., Nöthen, M.M., Stefansson, K., Peltonen, L., St Clair, D., Stefansson, H., Collier, D.A., 2009. Disruption of the neurexin 1 gene is associated with schizophrenia. *Hum. Mol. Genet.* 18, 988–996. <https://doi.org/10.1093/hmg/ddn351>
- Rutter, L., Carver, F.W., Holroyd, T., Rajamoni Nadar, S., Mitchell-Francis, J., Apud, J., Weinberger, D.R., Coppola, R., 2009. Magnetoencephalographic Gamma Power Reduction in Patients with Schizophrenia during Resting Condition. *Hum. Brain Mapp.* 30, 3254–3264. <https://doi.org/10.1002/hbm.20746>
- Sachs, N.A., Sawa, A., Holmes, S.E., Ross, C.A., DeLisi, L.E., Margolis, R.L., 2005. A frameshift mutation in Disrupted in Schizophrenia 1 in an American family with schizophrenia and schizoaffective disorder. *Mol. Psychiatry* 10, 758–764. <https://doi.org/10.1038/sj.mp.4001667>
- Saha, S., Chant, D., Welham, J., McGrath, J., 2005. A Systematic Review of the Prevalence of Schizophrenia. *PLoS Med.* 2, e141–e141. <https://doi.org/10.1371/journal.pmed.0020141>
- Saito, T., Guan, F., Papolos, D.F., Rajouria, N., Fann, C.S.J., Lachman, H.M., 2001. Polymorphism in SNAP29 gene promoter region associated with schizophrenia. *Mol. Psychiatry* 6, 193–201. <https://doi.org/10.1038/sj.mp.4000825>
- Scarr, E., Gray, L., Keriakous, D., Robinson, P.J., Dean, B., 2006. Increased levels of SNAP-25 and synaptophysin in the dorsolateral prefrontal cortex in bipolar I disorder. *Bipolar Disord.* 8, 133–143. <https://doi.org/10.1111/j.1399-5618.2006.00300.x>
- Schijven, D., Kofink, D., Tragante, V., Verkerke, M., Pulit, S.L., Kahn, R.S., Veldink, J.H., Vinkers, C.H., Boks, M.P., Luykx, J.J., 2018. Comprehensive pathway analyses of schizophrenia risk loci point to dysfunctional postsynaptic signaling. *Schizophr. Res.* 199, 195–202. <https://doi.org/10.1016/j.schres.2018.03.032>
- Schmahmann, J.D., 2019. The cerebellum and cognition. *Neurosci. Lett.* 688, 62–75. <https://doi.org/10.1016/j.neulet.2018.07.005>
- Schmahmann, J.D., 1991. An Emerging Concept: The Cerebellar Contribution to Higher Function. *Arch. Neurol.* 48, 1178–1187. <https://doi.org/10.1001/archneur.1991.00530230086029>
- Schmahmann, J.D., MacMore, J., Vangel, M., 2009. Cerebellar stroke without motor deficit: clinical evidence for motor and non-motor domains within the human cerebellum. *Neuroscience, New Insights in Cerebellar Function* 162, 852–861. <https://doi.org/10.1016/j.neuroscience.2009.06.023>
- Schmahmann, J.D., Sherman, J.C., 1998. The cerebellar cognitive affective syndrome. *Brain J. Neurol.* 121 (Pt 4), 561–579. <https://doi.org/10.1093/brain/121.4.561>
- Schulz, B., 1933. Zur Erbpathologie der Schizophrenie. *Z. Für Gesamte Neurol. Psychiatr.* 143, 175–293. <https://doi.org/10.1007/BF02866172>
- Schwab, S.G., Knapp, M., Mondabon, S., Hallmayer, J., Borrmann-Hassenbach, M., Albus, M., Lerer, B., Rietschel, M., Trixler, M., Maier, W., Wildenauer, D.B., 2003. Support for Association of Schizophrenia with Genetic Variation in the 6p22.3 Gene, Dysbindin, in Sib-Pair Families with Linkage and in an Additional Sample of Triad Families. *Am. J. Hum. Genet.* 72, 185–190. <https://doi.org/10.1086/345463>
- Schwarz, E., Izmailov, R., Spain, M., Barnes, A., Mapes, J.P., Guest, P.C., Rahmoune, H., Pietsch, S., Leweke, F.M., Rothermundt, M., Steiner, J., Koethe, D., Kranaster, L.,

- Ohrmann, P., Suslow, T., Levin, Y., Bogerts, B., van Beveren, N.J., McAllister, G., Weber, N., Niebuhr, D., Cowan, D., Yolken, R.H., Bahn, S., 2010. Validation of a blood-based laboratory test to aid in the confirmation of a diagnosis of schizophrenia. *Biomark. Insights* 5, 39–47. <https://doi.org/10.4137/bmi.s4877>
- Sekar, A., Bialas, A.R., de Rivera, H., Davis, A., Hammond, T.R., Kamitaki, N., Tooley, K., Presumey, J., Baum, M., Van Doren, V., Genovese, G., Rose, S.A., Handsaker, R.E., Schizophrenia Working Group of the Psychiatric Genomics Consortium, Daly, M.J., Carroll, M.C., Stevens, B., McCarroll, S.A., 2016. Schizophrenia risk from complex variation of complement component 4. *Nature* 530, 177–183. <https://doi.org/10.1038/nature16549>
- Selemon, L.D., Rajkowska, G., Goldman-Rakic, P.S., 1998. Elevated neuronal density in prefrontal area 46 in brains from schizophrenic patients: Application of a three-dimensional, stereologic counting method. *J. Comp. Neurol.* 392, 402–412. [https://doi.org/10.1002/\(SICI\)1096-9861\(19980316\)392:3<402::AID-CNE9>3.0.CO;2-5](https://doi.org/10.1002/(SICI)1096-9861(19980316)392:3<402::AID-CNE9>3.0.CO;2-5)
- Selemon, L.D., Rajkowska, G., Goldman-Rakic, P.S., 1995. Abnormally High Neuronal Density in the Schizophrenic Cortex: A Morphometric Analysis of Prefrontal Area 9 and Occipital Area 17. *Arch. Gen. Psychiatry* 52, 805–818. <https://doi.org/10.1001/archpsyc.1995.03950220015005>
- Sellgren, C.M., Gracias, J., Watmuff, B., Biag, J.D., Thanos, J.M., Whittredge, P.B., Fu, T., Worringer, K., Brown, H.E., Wang, J., Kaykas, A., Karmacharya, R., Goold, C.P., Sheridan, S.D., Perlis, R.H., 2019. Increased synapse elimination by microglia in schizophrenia patient-derived models of synaptic pruning. *Nat. Neurosci.* 22, 374–385. <https://doi.org/10.1038/s41593-018-0334-7>
- Sendhilnathan, N., Ipata, A.E., Goldberg, M.E., 2020. Neural Correlates of Reinforcement Learning in Mid-lateral Cerebellum. *Neuron* 106, 188-198.e5. <https://doi.org/10.1016/j.neuron.2019.12.032>
- Shepherd, G.M.G., Raastad, M., Andersen, P., 2002. General and variable features of varicosity spacing along unmyelinated axons in the hippocampus and cerebellum. *Proc. Natl. Acad. Sci. U. S. A.* 99, 6340–6345. <https://doi.org/10.1073/pnas.052151299>
- Sigoillot, S.M., Iyer, K., Binda, F., González-Calvo, I., Talleur, M., Vodjdani, G., Isope, P., Selimi, F., 2015. The Secreted Protein C1QL1 and Its Receptor BAI3 Control the Synaptic Connectivity of Excitatory Inputs Converging on Cerebellar Purkinje Cells. *Cell Rep.* 10, 820–832. <https://doi.org/10.1016/j.celrep.2015.01.034>
- Sigurdsson, T., Stark, K.L., Karayiorgou, M., Gogos, J.A., Gordon, J.A., 2010. Impaired hippocampal-prefrontal synchrony in a genetic mouse model of schizophrenia. *Nature* 464, 763–767. <https://doi.org/10.1038/nature08855>
- Singer, W., 1999. Neuronal synchrony: a versatile code for the definition of relations? *Neuron* 24, 49–65, 111–125. [https://doi.org/10.1016/s0896-6273\(00\)80821-1](https://doi.org/10.1016/s0896-6273(00)80821-1)
- Skene, N.G., Roy, M., Grant, S.G., 2017. A genomic lifespan program that reorganises the young adult brain is targeted in schizophrenia. *eLife* 6, e17915. <https://doi.org/10.7554/eLife.17915>
- Sokolov, B.P., Tcherepanov, A.A., Haroutunian, V., Davis, K.L., 2000. Levels of mRNAs encoding synaptic vesicle and synaptic plasma membrane proteins in the temporal cortex of elderly schizophrenic patients. *Biol. Psychiatry* 48, 184–196. [https://doi.org/10.1016/S0006-3223\(00\)00875-1](https://doi.org/10.1016/S0006-3223(00)00875-1)
- Sotelo, C., 1978. Purkinje Cell Ontogeny: Formation and Maintenance of Spines [WWW Document]. *Prog. Brain Res.* [https://doi.org/10.1016/S0079-6123\(08\)61021-3](https://doi.org/10.1016/S0079-6123(08)61021-3)

- Sporn, A.L., Greenstein, D.K., Gogtay, N., Jeffries, N.O., Lenane, M., Gochman, P., Clasen, L.S., Blumenthal, J., Giedd, J.N., Rapoport, J.L., 2003. Progressive brain volume loss during adolescence in childhood-onset schizophrenia. *Am. J. Psychiatry* 160, 2181–2189. <https://doi.org/10.1176/appi.ajp.160.12.2181>
- St Clair, D., Blackwood, D., Muir, W., Carothers, A., Walker, M., Spowart, G., Gosden, C., Evans, H.J., 1990. Association within a family of a balanced autosomal translocation with major mental illness. *Lancet Lond. Engl.* 336, 13–16. [https://doi.org/10.1016/0140-6736\(90\)91520-k](https://doi.org/10.1016/0140-6736(90)91520-k)
- Stefansson, H., Petursson, H., Sigurdsson, E., Steinthorsdottir, V., Bjornsdottir, S., Sigmundsson, T., Ghosh, S., Brynjolfsson, J., Gunnarsdottir, S., Ivarsson, O., Chou, T.T., Hjaltason, O., Birgisdottir, B., Jonsson, H., Gudnadottir, V.G., Gudmundsdottir, E., Bjornsson, A., Ingvarsson, B., Ingason, A., Sigfusson, S., Hardardottir, H., Harvey, R.P., Lai, D., Zhou, M., Brunner, D., Mutel, V., Gonzalo, A., Lemke, G., Sainz, J., Johannesson, G., Andresson, T., Gudbjartsson, D., Manolescu, A., Frigge, M.L., Gurney, M.E., Kong, A., Gulcher, J.R., Stefansson, K., 2002. Neuregulin 1 and Susceptibility to Schizophrenia [WWW Document]. *Am. J. Hum. Genet.* <https://doi.org/10.1086/342734>
- Stephan, K.E., Baldeweg, T., Friston, K.J., 2006. Synaptic Plasticity and Dysconnection in Schizophrenia. *Biol. Psychiatry* 59, 929–939. <https://doi.org/10.1016/j.biopsych.2005.10.005>
- Stephan, K.E., Friston, K.J., Frith, C.D., 2009. Dysconnection in Schizophrenia: From Abnormal Synaptic Plasticity to Failures of Self-monitoring. *Schizophr. Bull.* 35, 509–527. <https://doi.org/10.1093/schbul/sbn176>
- Stevens, B., Allen, N.J., Vazquez, L.E., Howell, G.R., Christopherson, K.S., Nouri, N., Micheva, K.D., Mehalow, A.K., Huberman, A.D., Stafford, B., Sher, A., Litke, A.M., Lambris, J.D., Smith, S.J., John, S.W.M., Barres, B.A., 2007. The Classical Complement Cascade Mediates CNS Synapse Elimination. *Cell* 131, 1164–1178. <https://doi.org/10.1016/j.cell.2007.10.036>
- Stilo, S.A., Murray, R.M., 2019. Non-Genetic Factors in Schizophrenia. *Curr. Psychiatry Rep.* 21, 100. <https://doi.org/10.1007/s11920-019-1091-3>
- Stoodley, C.J., Schmahmann, J.D., 2010. Evidence for topographic organization in the cerebellum of motor control versus cognitive and affective processing. *Cortex J. Devoted Study Nerv. Syst. Behav.* 46, 831–844. <https://doi.org/10.1016/j.cortex.2009.11.008>
- Stoodley, C.J., Schmahmann, J.D., 2009. Functional topography in the human cerebellum: a meta-analysis of neuroimaging studies. *NeuroImage* 44, 489–501. <https://doi.org/10.1016/j.neuroimage.2008.08.039>
- Straub, R.E., Jiang, Y., MacLean, C.J., Ma, Y., Webb, B.T., Myakishev, M.V., Harris-Kerr, C., Wormley, B., Sadek, H., Kadambi, B., Cesare, A.J., Gibberman, A., Wang, X., O’Neill, F.A., Walsh, D., Kendler, K.S., 2002. Genetic Variation in the 6p22.3 Gene DTNBP1, the Human Ortholog of the Mouse Dysbindin Gene, Is Associated with Schizophrenia. *Am. J. Hum. Genet.* 71, 337–348.
- Su, T., Lu, Y., Geng, Y., Lu, W., Chen, Y., 2018. How could N-Methyl-D-Aspartate Receptor Antagonists Lead to Excitation Instead of Inhibition? *Brain Sci. Adv.* 4, 73–98. <https://doi.org/10.26599/BSA.2018.2018.9050009>
- Südhof, T.C., 2018. Towards an Understanding of Synapse Formation. *Neuron* 100, 276–293. <https://doi.org/10.1016/j.neuron.2018.09.040>
- Südhof, T.C., 2008. Neuroligins and neurexins link synaptic function to cognitive disease. *Nature* 455, 903–911. <https://doi.org/10.1038/nature07456>

- Sugihara, I., Bailly, Y., Mariani, J., 2000. Olivocerebellar Climbing Fibers in the Granuloprival Cerebellum: Morphological Study of Individual Axonal Projections in the X-Irradiated Rat. *J. Neurosci.* 20, 3745–3760. <https://doi.org/10.1523/JNEUROSCI.20-10-03745.2000>
- Sugihara, I., Shinoda, Y., 2004. Molecular, Topographic, and Functional Organization of the Cerebellar Cortex: A Study with Combined Aldolase C and Olivocerebellar Labeling. *J. Neurosci.* 24, 8771–8785. <https://doi.org/10.1523/JNEUROSCI.1961-04.2004>
- Sun, Y., Farzan, F., Barr, M.S., Kirihara, K., Fitzgerald, P.B., Light, G.A., Daskalakis, Z.J., 2011. Gamma oscillations in schizophrenia: Mechanisms and clinical significance. *Brain Res.* 1413, 98–114. <https://doi.org/10.1016/j.brainres.2011.06.065>
- Sweet, R.A., Henteleff, R.A., Zhang, W., Sampson, A.R., Lewis, D.A., 2009. Reduced dendritic spine density in auditory cortex of subjects with schizophrenia. *Neuropsychopharmacol. Off. Publ. Am. Coll. Neuropsychopharmacol.* 34, 374–389. <https://doi.org/10.1038/npp.2008.67>
- Takahashi, T., Suzuki, M., Zhou, S.-Y., Tanino, R., Nakamura, K., Kawasaki, Y., Seto, H., Kurachi, M., 2010. A follow-up MRI study of the superior temporal subregions in schizotypal disorder and first-episode schizophrenia. *Schizophr. Res.* 119, 65–74. <https://doi.org/10.1016/j.schres.2009.12.006>
- Takigawa, M., 2017. The CCN Proteins: An Overview. *Methods Mol. Biol. Clifton NJ* 1489, 1–8. https://doi.org/10.1007/978-1-4939-6430-7_1
- Talbot, K., Eidem, W.L., Tinsley, C.L., Benson, M.A., Thompson, E.W., Smith, R.J., Hahn, C.-G., Siegel, S.J., Trojanowski, J.Q., Gur, R.E., Blake, D.J., Arnold, S.E., 2004. Dysbindin-1 is reduced in intrinsic, glutamatergic terminals of the hippocampal formation in schizophrenia [WWW Document]. *J. Clin. Invest.* <https://doi.org/10.1172/JCI20425>
- Taylor, S.C., Ferri, S.L., Grewal, M., Smernoff, Z., Bucan, M., Weiner, J.A., Abel, T., Brodtkin, E.S., 2020. The Role of Synaptic Cell Adhesion Molecules and Associated Scaffolding Proteins in Social Affiliative Behaviors. *Biol. Psychiatry.* <https://doi.org/10.1016/j.biopsych.2020.02.012>
- Tessier, C.R., Broadie, K., 2009. Activity-dependent modulation of neural circuit synaptic connectivity. *Front. Mol. Neurosci.* 2. <https://doi.org/10.3389/neuro.02.008.2009>
- Toulopoulou, T., Grech, A., Morris, R.G., Schulze, K., McDonald, C., Chapple, B., Rabe-Hesketh, S., Murray, R.M., 2004. The relationship between volumetric brain changes and cognitive function: A family study on schizophrenia [WWW Document]. *Biol. Psychiatry.* <https://doi.org/10.1016/j.biopsych.2004.06.026>
- Tran, K.D., Smutzer, G.S., Doty, R.L., Arnold, S.E., 1998. Reduced Purkinje cell size in the cerebellar vermis of elderly patients with schizophrenia. *Am. J. Psychiatry* 155, 1288–1290. <https://doi.org/10.1176/ajp.155.9.1288>
- Uemura, T., Lee, S.-J., Yasumura, M., Takeuchi, T., Yoshida, T., Ra, M., Taguchi, R., Sakimura, K., Mishina, M., 2010. Trans-synaptic interaction of GluRdelta2 and Neurexin through Cbln1 mediates synapse formation in the cerebellum. *Cell* 141, 1068–1079. <https://doi.org/10.1016/j.cell.2010.04.035>
- Uesaka, N., Uchigashima, M., Mikuni, T., Nakazawa, T., Nakao, H., Hirai, H., Aiba, A., Watanabe, M., Kano, M., 2014. Retrograde semaphorin signaling regulates synapse elimination in the developing mouse brain. *Science* 344, 1020–1023. <https://doi.org/10.1126/science.1252514>
- Uhlhaas, P., 2018. 3.4 NEURAL OSCILLATIONS AND EXCITATION/INHIBITION BALANCE IN SCHIZOPHRENIA: A DEVELOPMENTAL PERSPECTIVE. *Schizophr. Bull.* 44, S2–S3. <https://doi.org/10.1093/schbul/sby014.006>

- Umbricht, D., Schmid, L., Koller, R., Vollenweider, F.X., Hell, D., Javitt, D.C., 2000. Ketamine-Induced Deficits in Auditory and Visual Context-Dependent Processing in Healthy Volunteers: Implications for Models of Cognitive Deficits in Schizophrenia. *Arch. Gen. Psychiatry* 57, 1139–1147. <https://doi.org/10.1001/archpsyc.57.12.1139>
- van Haren, N.E.M., Hulshoff Pol, H.E., Schnack, H.G., Cahn, W., Brans, R., Carati, I., Rais, M., Kahn, R.S., 2008. Progressive brain volume loss in schizophrenia over the course of the illness: evidence of maturational abnormalities in early adulthood. *Biol. Psychiatry* 63, 106–113. <https://doi.org/10.1016/j.biopsych.2007.01.004>
- Venables, N.C., Bernat, E.M., Sponheim, S.R., 2009. Genetic and Disorder-Specific Aspects of Resting State EEG Abnormalities in Schizophrenia. *Schizophr. Bull.* 35, 826–839. <https://doi.org/10.1093/schbul/sbn021>
- Volkow, N.D., Fowler, J.S., 1992. Neuropsychiatric disorders: Investigation of schizophrenia and substance abuse. *Semin. Nucl. Med., Positron Emission Tomography: Part II* 22, 254–267. [https://doi.org/10.1016/S0001-2998\(05\)80120-5](https://doi.org/10.1016/S0001-2998(05)80120-5)
- Vos, T., Abajobir, A.A., Abate, K.H., Abbafati, C., Abbas, K.M., Abd-Allah, F., Abdulkader, R.S., Abdulle, A.M., Abebo, T.A., Abera, S.F., Aboyans, V., Abu-Raddad, L.J., Ackerman, I.N., Adamu, A.A., Adetokunboh, O., Afarideh, M., Afshin, A., Agarwal, S.K., Aggarwal, R., Agrawal, A., Agrawal, S., Ahmadi, H., Ahmed, M.B., Aichour, M.T.E., Aichour, A.N., Aichour, I., Aiyar, S., Akinyemi, R.O., Akseer, N., Lami, F.H.A., Alahdab, F., Al-Aly, Z., Alam, K., Alam, N., Alam, T., Alasfoor, D., Alene, K.A., Ali, R., Alizadeh-Navaei, R., Alkerwi, A., Alla, F., Allebeck, P., Allen, C., Al-Maskari, F., Al-Raddadi, R., Alsharif, U., Alsowaidi, S., Altirkawi, K.A., Amare, A.T., Amini, E., Ammar, W., Amoako, Y.A., Andersen, H.H., Antonio, C.A.T., Anwari, P., Ärnlöv, J., Artaman, A., Aryal, K.K., Asayesh, H., Asgedom, S.W., Assadi, R., Atey, T.M., Atnafu, N.T., Atre, S.R., Avila-Burgos, L., Avokphako, E.F.G.A., Awasthi, A., Bacha, U., Badawi, A., Balakrishnan, K., Banerjee, A., Bannick, M.S., Barac, A., Barber, R.M., Barker-Collo, S.L., Bärnighausen, T., Barquera, S., Barregard, L., Barrero, L.H., Basu, S., Battista, B., Battle, K.E., Baune, B.T., Bazargan-Hejazi, S., Beardsley, J., Bedi, N., Beghi, E., Béjot, Y., Bekele, B.B., Bell, M.L., Bennett, D.A., Bensenor, I.M., Benson, J., Berhane, A., Berhe, D.F., Bernabé, E., Betsu, B.D., Beuran, M., Beyene, A.S., Bhala, N., Bhansali, A., Bhatt, S., Bhutta, Z.A., Biadgilign, S., Bicer, B.K., Bienhoff, K., Bikbov, B., Birungi, C., Biryukov, S., Bisanzio, D., Bizuayehu, H.M., Boneya, D.J., Boufous, S., Bourne, R.R.A., Brazinova, A., Brugha, T.S., Buchbinder, R., Bulto, L.N.B., Bumgarner, B.R., Butt, Z.A., Cahuana-Hurtado, L., Cameron, E., Car, M., Carabin, H., Carapetis, J.R., Cárdenas, R., Carpenter, D.O., Carrero, J.J., Carter, A., Carvalho, F., Casey, D.C., Caso, V., Castañeda-Orjuela, C.A., Castle, C.D., Catalá-López, F., Chang, H.-Y., Chang, J.-C., Charlson, F.J., Chen, H., Chibalabala, M., Chibueze, C.E., Chisumpa, V.H., Chitheer, A.A., Christopher, D.J., Ciobanu, L.G., Cirillo, M., Colombara, D., Cooper, C., Cortesi, P.A., Criqui, M.H., Crump, J.A., Dadi, A.F., Dalal, K., Dandona, L., Dandona, R., Neves, J. das, Davitoiu, D.V., Courten, B. de, Leo, D.D.D., Defo, B.K., Degenhardt, L., Deiparine, S., Dellavalle, R.P., Deribe, K., Jarlais, D.C.D., Dey, S., Dharmaratne, S.D., Dhillon, P.K., Dicker, D., Ding, E.L., Djalalinia, S., Do, H.P., Dorsey, E.R., Santos, K.P.B. dos, Douwes-Schultz, D., Doyle, K.E., Driscoll, T.R., Dubey, M., Duncan, B.B., El-Khatib, Z.Z., Ellerstrand, J., Enayati, A., Endries, A.Y., Ermakov, S.P., Erskine, H.E., Eshrati, B., Eskandarieh, S., Esteghamati, A., Estep, K., Fanuel, F.B.B., Farinha, C.S.E.S., Faro, A., Farzadfar, F., Fazeli, M.S., Feigin, V.L., Fereshtehnejad, S.-M., Fernandes, J.C., Ferrari, A.J., Feyissa, T.R., Filip, I., Fischer, F., Fitzmaurice, C., Flaxman, A.D., Flor, L.S., Foigt, N., Foreman, K.J., Franklin, R.C., Fullman, N., Fürst, T., Furtado, J.M., Futran, N.D., Gakidou, E., Ganji, M.,

Garcia-Basteiro, A.L., Gebre, T., Gebrehiwot, T.T., Geleto, A., Gemechu, B.L., Gesesew, H.A., Gething, P.W., Ghajar, A., Gibney, K.B., Gill, P.S., Gillum, R.F., Ginawi, I.A.M., Giref, A.Z., Gishu, M.D., Giussani, G., Godwin, W.W., Gold, A.L., Goldberg, E.M., Gona, P.N., Goodridge, A., Gopalani, S.V., Goto, A., Goulart, A.C., Griswold, M., Gughani, H.C., Gupta, Rahul, Gupta, Rajeev, Gupta, T., Gupta, V., Hafezi-Nejad, N., Hailu, G.B., Hailu, A.D., Hamadeh, R.R., Hamidi, S., Handal, A.J., Hankey, G.J., Hanson, S.W., Hao, Y., Harb, H.L., Hareri, H.A., Haro, J.M., Harvey, J., Hassanvand, M.S., Havmoeller, R., Hawley, C., Hay, S.I., Hay, R.J., Henry, N.J., Heredia-Pi, I.B., Hernandez, J.M., Heydarpour, P., Hoek, H.W., Hoffman, H.J., Horita, N., Hosgood, H.D., Hostiuc, S., Hotez, P.J., Hoy, D.G., Htet, A.S., Hu, G., Huang, H., Huynh, C., Iburg, K.M., Igumbor, E.U., Ikeda, C., Irvine, C.M.S., Jacobsen, K.H., Jahanmehr, N., Jakovljevic, M.B., Jassal, S.K., Javanbakht, M., Jayaraman, S.P., Jeemon, P., Jensen, P.N., Jha, V., Jiang, G., John, D., Johnson, S.C., Johnson, C.O., Jonas, J.B., Jürisson, M., Kabir, Z., Kadel, R., Kahsay, A., Kamal, R., Kan, H., Karam, N.E., Karch, A., Karema, C.K., Kasaeian, A., Kassa, G.M., Kassaw, N.A., Kassebaum, N.J., Kastor, A., Katikireddi, S.V., Kaul, A., Kawakami, N., Keiyoro, P.N., Kengne, A.P., Keren, A., Khader, Y.S., Khalil, I.A., Khan, E.A., Khang, Y.-H., Khosravi, A., Khubchandani, J., Kiadaliri, A.A., Kieling, C., Kim, Y.J., Kim, D., Kim, P., Kimokoti, R.W., Kinfu, Y., Kisa, A., Kissimova-Skarbek, K.A., Kivimaki, M., Knudsen, A.K., Kokubo, Y., Kolte, D., Kopec, J.A., Kosen, S., Koul, P.A., Koyanagi, A., Kravchenko, M., Krishnaswami, S., Krohn, K.J., Kumar, G.A., Kumar, P., Kumar, S., Kyu, H.H., Lal, D.K., Laloo, R., Lambert, N., Lan, Q., Larsson, A., Lavados, P.M., Leasher, J.L., Lee, P.H., Lee, J.-T., Leigh, J., Leshargie, C.T., Leung, J., Leung, R., Levi, M., Li, Yichong, Li, Yongmei, Kappe, D.L., Liang, X., Liben, M.L., Lim, S.S., Linn, S., Liu, P.Y., Liu, A., Liu, S., Liu, Y., Lodha, R., Logroscino, G., London, S.J., Looker, K.J., Lopez, A.D., Lorkowski, S., Lotufo, P.A., Low, N., Lozano, R., Lucas, T.C.D., Macarayan, E.R.K., Razek, H.M.A.E., Razek, M.M.A.E., Mahdavi, M., Majdan, M., Majdzadeh, R., Majeed, A., Malekzadeh, R., Malhotra, R., Malta, D.C., Mamun, A.A., Manguerra, H., Manhertz, T., Mantilla, A., Mantovani, L.G., Mapoma, C.C., Marczak, L.B., Martinez-Raga, J., Martins-Melo, F.R., Martopullo, I., März, W., Mathur, M.R., Mazidi, M., McAlinden, C., McGaughey, M., McGrath, J.J., McKee, M., McNellan, C., Mehata, S., Mehndiratta, M.M., Mekonnen, T.C., Memiah, P., Memish, Z.A., Mendoza, W., Mengistie, M.A., Mengistu, D.T., Mensah, G.A., Meretoja, T.J., Meretoja, A., Mezgebe, H.B., Micha, R., Millier, A., Miller, T.R., Mills, E.J., Mirarefin, M., Mirrahimov, E.M., Misganaw, A., Mishra, S.R., Mitchell, P.B., Mohammad, K.A., Mohammadi, A., Mohammed, K.E., Mohammed, S., Mohanty, S.K., Mokdad, A.H., Mollenkopf, S.K., Monasta, L., Montico, M., Moradi-Lakeh, M., Moraga, P., Mori, R., Morozoff, C., Morrison, S.D., Moses, M., Mountjoy-Venning, C., Mruts, K.B., Mueller, U.O., Muller, K., Murdoch, M.E., Murthy, G.V.S., Musa, K.I., Nachega, J.B., Nagel, G., Naghavi, M., Naheed, A., Naidoo, K.S., Naldi, L., Nangia, V., Natarajan, G., Negasa, D.E., Negoi, R.I., Negoi, I., Newton, C.R., Ngunjiri, J.W., Nguyen, T.H., Nguyen, Q.L., Nguyen, C.T., Nguyen, G., Nguyen, M., Nichols, E., Ningrum, D.N.A., Nolte, S., Nong, V.M., Norrving, B., Noubiap, J.J.N., O'Donnell, M.J., Ogbo, F.A., Oh, I.-H., Okoro, A., Oladimeji, O., Olagunju, T.O., Olagunju, A.T., Olsen, H.E., Olusanya, B.O., Olusanya, J.O., Ong, K., Opio, J.N., Oren, E., Ortiz, A., Osgood-Zimmerman, A., Osman, M., Owolabi, M.O., Pa, M., Pacella, R.E., Pana, A., Panda, B.K., Papachristou, C., Park, E.-K., Parry, C.D., Parsaeian, M., Patten, S.B., Patton, G.C., Paulson, K., Pearce, N., Pereira, D.M., Perico, N., Pesudovs, K., Peterson, C.B., Petzold, M., Phillips, M.R., Pigott, D.M., Pillay, J.D., Pinho, C., Plass, D., Pletcher,

- M.A., Popova, S., Poulton, R.G., Pourmalek, F., Prabhakaran, D., Prasad, N.M., Prasad, N., Purcell, C., Qorbani, M., Quansah, R., Quintanilla, B.P.A., Rabiee, R.H.S., Radfar, A., Rafay, A., Rahimi, K., Rahimi-Movaghar, A., Rahimi-Movaghar, V., Rahman, M.H.U., Rahman, M., Rai, R.K., Rajsic, S., Ram, U., Ranabhat, C.L., Rankin, Z., Rao, P.C., Rao, P.V., Rawaf, S., Ray, S.E., Reiner, R.C., Reinig, N., Reitsma, M.B., Remuzzi, G., Renzaho, A.M.N., Resnikoff, S., Rezaei, S., Ribeiro, A.L., Ronfani, L., Roshandel, G., Roth, G.A., Roy, A., Rubagotti, E., Ruhago, G.M., Saadat, S., Sadat, N., Safdarian, M., Safi, S., Safiri, S., Sagar, R., Sahathevan, R., Salama, J., Saleem, H.O.B., Salomon, J.A., Salvi, S.S., Samy, A.M., Sanabria, J.R., Santomauro, D., Santos, I.S., Santos, J.V., Milicevic, M.M.S., Sartorius, B., Satpathy, M., Sawhney, M., Saxena, S., Schmidt, M.I., Schneider, I.J.C., Schöttker, B., Schwebel, D.C., Schwendicke, F., Seedat, S., Sepanlou, S.G., Servan-Mori, E.E., Setegn, T., Shackelford, K.A., Shaheen, A., Shaikh, M.A., Shamsipour, M., Islam, S.M.S., Sharma, J., Sharma, R., She, J., Shi, P., Shields, C., Shifa, G.T., Shigematsu, M., Shinohara, Y., Shiri, R., Shirkoohi, R., Shirude, S., Shishani, K., Shrimme, M.G., Sibai, A.M., Sigfusdottir, I.D., Silva, D.A.S., Silva, J.P., Silveira, D.G.A., Singh, J.A., Singh, N.P., Sinha, D.N., Skiadaresi, E., Skirbekk, V., Slepak, E.L., Sligar, A., Smith, D.L., Smith, M., Sobaih, B.H.A., Sobngwi, E., Sorensen, R.J.D., Sousa, T.C.M., Sposato, L.A., Sreeramareddy, C.T., Srinivasan, V., Stanaway, J.D., Stathopoulou, V., Steel, N., Stein, M.B., Stein, D.J., Steiner, T.J., Steiner, C., Steinke, S., Stokes, M.A., Stovner, L.J., Strub, B., Subart, M., Sufiyan, M.B., Sunguya, B.F., Sur, P.J., Swaminathan, S., Sykes, B.L., Sylte, D.O., Tabarés-Seisdedos, R., Taffere, G.R., Takala, J.S., Tandon, N., Tavakkoli, M., Taveira, N., Taylor, H.R., Tehrani-Banihashemi, A., Tekelab, T., Terkawi, A.S., Tesfaye, D.J., Tessema, B., Thamsuwan, O., Thomas, K.E., Thrift, A.G., Tiruye, T.Y., Tobe-Gai, R., Tollanes, M.C., Tonelli, M., Topor-Madry, R., Tortajada, M., Touvier, M., Tran, B.X., Tripathi, S., Troeger, C., Truelsen, T., Tsoi, D., Tuem, K.B., Tuzcu, E.M., Tyrovolas, S., Ukwaja, K.N., Undurraga, E.A., Uneke, C.J., Updike, R., Uthman, O.A., Uzochukwu, B.S.C., Boven, J.F.M. van, Varughese, S., Vasankari, T., Venkatesh, S., Venketasubramanian, N., Vidavalur, R., Violante, F.S., Vladimirov, S.K., Vlassov, V.V., Vollset, S.E., Wadilo, F., Wakayo, T., Wang, Y.-P., Weaver, M., Weichenthal, S., Weiderpass, E., Weintraub, R.G., Werdecker, A., Westerman, R., Whiteford, H.A., Wijeratne, T., Wiysonge, C.S., Wolfe, C.D.A., Woodbrook, R., Woolf, A.D., Workicho, A., Xavier, D., Xu, G., Yadgir, S., Yaghoubi, M., Yakob, B., Yan, L.L., Yano, Y., Ye, P., Yimam, H.H., Yip, P., Yonemoto, N., Yoon, S.-J., Yotebieng, M., Younis, M.Z., Zaidi, Z., Zaki, M.E.S., Zegeye, E.A., Zenebe, Z.M., Zhang, X., Zhou, M., Zipkin, B., Zodpey, S., Zuhlke, L.J., Murray, C.J.L., 2017. Global, regional, and national incidence, prevalence, and years lived with disability for 328 diseases and injuries for 195 countries, 1990–2016: a systematic analysis for the Global Burden of Disease Study 2016. *The Lancet* 390, 1211–1259. [https://doi.org/10.1016/S0140-6736\(17\)32154-2](https://doi.org/10.1016/S0140-6736(17)32154-2)
- Vrijenhoek, T., Buizer-Voskamp, J.E., van der Stelt, I., Strengman, E., Sabatti, C., Geurts van Kessel, A., Brunner, H.G., Ophoff, R.A., Veltman, J.A., 2008. Recurrent CNVs Disrupt Three Candidate Genes in Schizophrenia Patients. *Am. J. Hum. Genet.* 83, 504–510. <https://doi.org/10.1016/j.ajhg.2008.09.011>
- Wagner, M.J., Kim, T.H., Savall, J., Schnitzer, M.J., Luo, L., 2017. Cerebellar granule cells encode the expectation of reward. *Nature* 544, 96–100. <https://doi.org/10.1038/nature21726>
- Walsh, C.A., Morrow, E.M., Rubenstein, J.L.R., 2008. Autism and Brain Development. *Cell* 135, 396–400. <https://doi.org/10.1016/j.cell.2008.10.015>

- Walsh, T., McClellan, J.M., McCarthy, S.E., Addington, A.M., Pierce, S.B., Cooper, G.M., Nord, A.S., Kusenda, M., Malhotra, D., Bhandari, A., Stray, S.M., Rippey, C.F., Roccanova, P., Makarov, V., Lakshmi, B., Findling, R.L., Sikich, L., Stromberg, T., Merriman, B., Gogtay, N., Butler, P., Eckstrand, K., Noory, L., Gochman, P., Long, R., Chen, Z., Davis, S., Baker, C., Eichler, E.E., Meltzer, P.S., Nelson, S.F., Singleton, A.B., Lee, M.K., Rapoport, J.L., King, M.-C., Sebat, J., 2008. Rare structural variants disrupt multiple genes in neurodevelopmental pathways in schizophrenia. *Science* 320, 539–543. <https://doi.org/10.1126/science.1155174>
- Wassink, T.H., Andreasen, N.C., Nopoulos, P., Flaum, M., 1999. Cerebellar morphology as a predictor of symptom and psychosocial outcome in schizophrenia. *Biol. Psychiatry* 45, 41–48. [https://doi.org/10.1016/S0006-3223\(98\)00175-9](https://doi.org/10.1016/S0006-3223(98)00175-9)
- Weinberger, D.R., 1987. Implications of normal brain development for the pathogenesis of schizophrenia. *Arch. Gen. Psychiatry* 44, 660–669. <https://doi.org/10.1001/archpsyc.1987.01800190080012>
- Weinberger, D.R., Kleinman, J.E., Luchins, D.J., Bigelow, L.B., Wyatt, R.J., 1980. Cerebellar pathology in schizophrenia: a controlled postmortem study. *Am. J. Psychiatry* 137, 359–361. <https://doi.org/10.1176/ajp.137.3.359>
- Wernicke, C., 1906. *Grundriss der Psychiatrie in klinischen Vorlesungen*. Thieme.
- Whitfield-Gabrieli, S., Thermenos, H.W., Milanovic, S., Tsuang, M.T., Faraone, S.V., McCarley, R.W., Shenton, M.E., Green, A.I., Nieto-Castanon, A., LaViolette, P., Wojcik, J., Gabrieli, J.D.E., Seidman, L.J., 2009. Hyperactivity and hyperconnectivity of the default network in schizophrenia and in first-degree relatives of persons with schizophrenia. *Proc. Natl. Acad. Sci. U. S. A.* 106, 1279–1284. <https://doi.org/10.1073/pnas.0809141106>
- Whittington, M.A., Traub, R.D., Jefferys, J.G.R., 1995. Synchronized oscillations in interneuron networks driven by metabotropic glutamate receptor activation. *Nature* 373, 612–615. <https://doi.org/10.1038/373612a0>
- Wiescholleck, V., Manahan-Vaughan, D., 2013. Persistent deficits in hippocampal synaptic plasticity accompany losses of hippocampus-dependent memory in a rodent model of psychosis. *Front. Integr. Neurosci.* 7. <https://doi.org/10.3389/fnint.2013.00012>
- Wiesel, T.N., 1982. Postnatal development of the visual cortex and the influence of environment. *Nature* 299, 583–591. <https://doi.org/10.1038/299583a0>
- Wolpert, D.M., Miall, R.C., Kawato, M., 1998. Internal models in the cerebellum. *Trends Cogn. Sci.* 2, 338–347. [https://doi.org/10.1016/S1364-6613\(98\)01221-2](https://doi.org/10.1016/S1364-6613(98)01221-2)
- Wright, I.C., Rabe-Hesketh, S., Woodruff, P.W.R., David, A.S., Murray, R.M., Bullmore, E.T., 2000. Meta-Analysis of Regional Brain Volumes in Schizophrenia. *Am. J. Psychiatry* 157, 16–25. <https://doi.org/10.1176/ajp.157.1.16>
- Wu, G.-Y., Liu, S.-L., Yao, J., Sun, L., Wu, B., Yang, Y., Li, X., Sun, Q.-Q., Feng, H., Sui, J.-F., 2018. Medial Prefrontal Cortex–Pontine Nuclei Projections Modulate Suboptimal Cue-Induced Associative Motor Learning. *Cereb. Cortex* 28, 880–893. <https://doi.org/10.1093/cercor/bhw410>
- Wulff, P., Schonewille, M., Renzi, M., Viltono, L., Sassoè-Pognetto, M., Badura, A., Gao, Z., Hoebeek, F.E., van Dorp, S., Wisden, W., Farrant, M., De Zeeuw, C.I., 2009. Synaptic inhibition of Purkinje cells mediates consolidation of vestibulo-cerebellar motor learning. *Nat. Neurosci.* 12, 1042–1049. <https://doi.org/10.1038/nn.2348>
- Xiao, L., Michalski, N., Kronander, E., Gjoni, E., Genoud, C., Knott, G., Schneggenburger, R., 2013. BMP signaling specifies the development of a large and fast CNS synapse. *Nat. Neurosci.* 16, 856–864. <https://doi.org/10.1038/nn.3414>

- Yang, Y., Ju, W., Zhang, H., Sun, L., 2018. Effect of Ketamine on LTP and NMDAR EPSC in Hippocampus of the Chronic Social Defeat Stress Mice Model of Depression. *Front. Behav. Neurosci.* 12. <https://doi.org/10.3389/fnbeh.2018.00229>
- Young, A.M.J., Stubbendorff, C., Valencia, M., Gerdjikov, T.V., 2015. Disruption of medial prefrontal synchrony in the subchronic phencyclidine model of schizophrenia in rats. *Neuroscience* 287, 157–163. <https://doi.org/10.1016/j.neuroscience.2014.12.014>
- Young, C.E., Arima, K., Xie, J., Hu, L., Beach, T.G., Falkai, P., Honer, W.G., 1998. SNAP-25 deficit and hippocampal connectivity in schizophrenia. *Cereb. Cortex N. Y. N* 1991 8, 261–268. <https://doi.org/10.1093/cercor/8.3.261>
- Yu, B., Wang, C., Liu, J., Johnson, K.M., Gallagher, J.P., 2002. Adaptation to chronic PCP results in hyperfunctional NMDA and hypofunctional GABAA synaptic receptors. *Neuroscience* 113, 1–10. [https://doi.org/10.1016/S0306-4522\(02\)00163-X](https://doi.org/10.1016/S0306-4522(02)00163-X)
- Zaidel, D.W., Esiri, M.M., Harrison, P.J., 1997. The hippocampus in schizophrenia: lateralized increase in neuronal density and altered cytoarchitectural asymmetry. *Psychol. Med.* 27, 703–713. <https://doi.org/10.1017/S0033291796004618>
- Zee, D.S., Leigh, R.J., Mathieu-Millaire, F., 1980. Cerebellar control of ocular gaze stability. *Ann. Neurol.* 7, 37–40. <https://doi.org/10.1002/ana.410070108>
- Zhang, B., Chen, L.Y., Liu, X., Maxeiner, S., Lee, S.-J., Gokce, O., Südhof, T.C., 2015. Neuroligins Sculpt Cerebellar Purkinje-Cell Circuits by Differential Control of Distinct Classes of Synapses. *Neuron* 87, 781–796. <https://doi.org/10.1016/j.neuron.2015.07.020>
- Zhang, L.I., Poo, M., 2001. Electrical activity and development of neural circuits. *Nat. Neurosci.* 4, 1207–1214. <https://doi.org/10.1038/nn753>
- Zhou, H., Lin, Z., Voges, K., Ju, C., Gao, Z., Bosman, L.W., Ruigrok, T.J., Hoebeek, F.E., De Zeeuw, C.I., Schonewille, M., 2014. Cerebellar modules operate at different frequencies. *eLife* 3. <https://doi.org/10.7554/eLife.02536>

Annexe

SUSD4 Controls Activity-Dependent Degradation of AMPA Receptor GLUA2 and Synaptic Plasticity

I. González-Calvo^{1,2,†}, K. Iyer^{1,†}, M. Carquin¹, A. Khayachi¹, F.A. Giuliani², J. Vincent³, M. Séveno⁴, S.M. Sigoillot¹, M. Veleanu¹, S. Tahraoui¹, M. Albert¹, O. Vigy⁵, Y. Nadjar⁶, A. Dumoulin⁶, A. Triller⁶, J.-L. Bessereau⁷, L. Rondi-Reig³, P. Isope², F. Selimi^{1*}

Affiliations:

¹ Center for Interdisciplinary Research in Biology (CIRB), Collège de France, CNRS, INSERM, PSL Research University, Paris, France.

² Institut de Neurosciences Cellulaires et Intégratives (INCI), CNRS, Université de Strasbourg, Strasbourg, France.

³ Institut Biology Paris Seine (IBPS), Neuroscience Paris Seine (NPS), CeZaMe, CNRS, Sorbonne University, INSERM, Paris, France.

⁴ BioCampus Montpellier, CNRS, INSERM, Université de Montpellier, Montpellier, France.

⁵ Institut de Génomique Fonctionnelle, CNRS, INSERM, Université de Montpellier, Montpellier, France.

⁶ École Normale Supérieure, Institut de Biologie de l'ENS, INSERM, CNRS, PSL Research University, Paris, France.

⁷ Université de Lyon, Université Claude Bernard Lyon 1, CNRS UMR 5310, INSERM U 1217, Institut Neuromyogène, 69008, Lyon, France.

* Correspondence to: fekrije.selimi@college-de-france.fr

† Equal contribution.

SUSD4 Controls Activity-Dependent Degradation of AMPA Receptor GLUA2 and Synaptic Plasticity

I. González-Calvo^{1,2,†}, K. Iyer^{1,†}, M. Carquin¹, A. Khayachi¹, F.A. Giuliani², J. Vincent³, M. Séveno⁴, S.M. Sigoillot¹, M. Veleanu¹, S. Tahraoui¹, M. Albert¹, O. Vigy⁵, Y. Nadjar⁶, A. Dumoulin⁶, A. Triller⁶, J.-L. Bessereau⁷, L. Rondi-Reig³, P. Isope², F. Selimi^{1*}

Affiliations:

¹ Center for Interdisciplinary Research in Biology (CIRB), Collège de France, CNRS, INSERM, PSL Research University, Paris, France.

² Institut de Neurosciences Cellulaires et Intégratives (INCI), CNRS, Université de Strasbourg, , Strasbourg, France.

³ Institut Biology Paris Seine (IBPS), Neuroscience Paris Seine (NPS), CeZaMe, CNRS, Sorbonne University, INSERM, Paris, France.

⁴ BioCampus Montpellier, CNRS, INSERM, Université de Montpellier, Montpellier, France.

⁵ Institut de Génomique Fonctionnelle, CNRS, INSERM, Université de Montpellier, Montpellier, France.

⁶ École Normale Supérieure, Institut de Biologie de l'ENS, INSERM, CNRS, PSL Research University, Paris, France.

⁷ Université de Lyon, Université Claude Bernard Lyon 1, CNRS UMR 5310, INSERM U 1217, Institut Neuromyogène, 69008, Lyon, France.

* Correspondence to: fekrije.selimi@college-de-france.fr

† Equal contribution.

Summary

At excitatory synapses, the choice between recycling or degradation of glutamate AMPA receptors controls the direction of synaptic plasticity. In this context, how the degradation machinery is targeted to specific synaptic substrates in an activity-dependent manner is not understood. Here we show that SUSD4, a complement-related transmembrane protein, is a tether for HECT ubiquitin ligases of the NEDD4 subfamily, which promote the degradation of a large number of cellular substrates. SUSD4 is expressed by many neuronal populations starting at the time of synapse formation. Loss-of-function of *Susd4* in the mouse prevents activity-dependent degradation of the GLUA2 AMPA receptor subunit and long-term depression at cerebellar synapses, and leads to impairment in motor coordination adaptation and learning. SUSD4 could thus act as an adaptor targeting NEDD4 ubiquitin ligases to AMPA receptors during long-term synaptic plasticity. These findings shed light on the potential contribution of *SUSD4* mutations to the etiology of neurodevelopmental diseases.

Introduction

AMPA-type glutamate receptors are responsible for fast excitatory transmission in the central nervous system. Fine-tuning of their properties and their synaptic numbers underlies synapse maturation and synapse plasticity and is central to proper circuit function and behavior (Anggono and Huganir, 2012; Diering and Huganir, 2018; Kessels and Malinow, 2009). Long-term synaptic plasticity has been proposed to underlie learning and memory (Collingridge et al., 2010; Nicoll, 2017). Synaptic strength can be either decreased (long-term depression, LTD) or increased (long-term potentiation, LTP) depending on the timing and pattern of neuronal activity in a network. Defects in the regulation of long-term synaptic plasticity and AMPA receptors could contribute to a range of brain diseases such as epilepsy, intellectual deficiencies and autism spectrum disorders (ASDs). Long-term synaptic plasticity deficits are a common phenotype of many mice models for intellectual disabilities and ASDs (Baudouin et al., 2012; Piochon et al., 2014; Volk et al., 2015). Mutations in genes coding for AMPA receptor subunits (Davies et al., 2017; Martin et al., 2017; Salpietro et al., 2019; Satterstrom et al., 2018) or their regulatory subunits (Brechet et al., 2017; Chiu et al., 2017) have been found in patients with neurodevelopmental disorders.

The modification of AMPA receptor numbers at synapses is a highly dynamic process, involving regulation of receptor diffusion (Choquet and Triller, 2013; Penn et al., 2017), their insertion in the plasma membrane, anchoring at the postsynaptic density and endocytosis (Anggono and Huganir, 2012). After activity-dependent endocytosis, AMPA receptors are either recycled to the plasma membrane or targeted to the endolysosomal compartment for degradation (Ehlers, 2000; Lee et al., 2004; Park et al., 2004). The decision between these two fates regulates the direction of synaptic plasticity. Recycling promotes LTP and relies on many molecules, such as GRASP1, GRIP1, PICK1 and NSF (Anggono and Huganir, 2012). Targeting to the endolysosomal compartment and degradation promote LTD (Fernandez-Monreal et al., 2012; Kim et al., 2017; Matsuda et al., 2013), but the regulation of the targeting and degradation process remains poorly understood. One mechanism that regulates activity-dependent degradation of synaptic proteins is ubiquitination, a major post-translational modification (Cajigas et al., 2010). Both GLUA1 and GLUA2 AMPA receptor subunits have been shown to be ubiquitinated in an activity-dependent manner (Lussier et al., 2011; Schwarz et al., 2010; Widagdo et al., 2015). A major remaining question however is how AMPA receptor degradation is specifically controlled given the large number of substrates for E3 ubiquitin ligases in cells, and the spatio-temporal specificity required for proper synaptic plasticity in neurons.

The *SUSD4* gene is located in a genomic region deleted in patients with the 1q41q42 syndrome that includes developmental delays and intellectual deficiency (Rosenfeld et al., 2011). *SUSD4* has been identified recently as one of the 124 genes enriched in *de novo* missense mutations in a large cohort of individuals with ASDs or intellectual deficiencies (Coe et al., 2019). A copy number variation and several *de novo* mutations with a high CADD score, which indicates the deleteriousness of the mutations, have been described in the *SUSD4* gene in patients with ASDs ((Cuscó et al., 2009); denovo-db, Seattle, WA (denovo-db.gs.washington.edu) 10, 2019). The mammalian *Susd4* gene codes for a transmembrane protein with four extracellular CCP (complement control protein) domains (**Figure 1A**) and is highly expressed in the central nervous system (Holmquist et al., 2013). The CCP domain, also known as Sushi domain, is evolutionarily conserved and found in several proteins with synaptic function. Acetylcholine receptor clustering is regulated by CCP-containing proteins in *Caenorhabditis elegans* (Gendrel et al., 2009) and in *Drosophila melanogaster* (Nakayama et al., 2016). In humans, mutations in the CCP domain-

containing secreted protein SRPX2 are associated with epilepsy and speech dysfunction, and SRPX2 knockdown leads to decreased synapse number and vocalization in mice (Sia et al., 2013). Despite the increase in the diversity of CCP domain-containing proteins in evolution (18 in *C. elegans* and 198 in humans; smart.embl.de), the function of many of the CCP domain-containing proteins remains unknown. The only described role for the SUSD4 protein is its ability to regulate complement system activation in erythrocytes by binding the C1Q domain (Holmquist et al., 2013). Interestingly, the C1Q globular domain is found in major synaptic regulators such as C1QA (Stevens et al., 2007), CBLNs (Matsuda et al., 2010; Uemura et al., 2010) and C1Q-like proteins (Bolliger et al., 2011; Kakegawa et al., 2015; Sigoillot et al., 2015). Altogether these studies point to a potential role of SUSD4 in synapse formation and/or function and in the etiology of several neurodevelopmental disorders.

Proper development and function of the cerebellar circuitry is central for motor coordination and adaptation, and a range of cognitive tasks (Badura et al., 2018; Hirai et al., 2005; Ichise et al., 2000; Lefort et al., 2019; Rochefort et al., 2011; Tsai et al., 2012), and cerebellar dysfunction is associated with several neurodevelopmental disorders including ASDs (Stoodley, 2016; Stoodley et al., 2018; Wang et al., 2014). Cerebellar Purkinje cells (PCs) receive more than a hundred thousand parallel fiber (PF) synapses whose formation, maintenance and plasticity are essential for cerebellar-dependent learning (Gutierrez-Castellanos et al., 2017; Hirai et al., 2005; Ito, 2006; Kashiwabuchi et al., 1995). Postsynaptic LTD was first described at synapses between PFs and cerebellar PCs (Gao et al., 2012; Hirano, 2018; Ito, 2001; Ito and Kano, 1982), where it can be induced by conjunctive stimulation of PFs with the other excitatory input received by PCs, the climbing fiber (CF) (Coesmans et al., 2004; Ito, 2001; Suvrathan et al., 2016). The function of members of the C1Q family, such as CBLN1 and C1QL1, is essential for excitatory synapse formation and LTD in cerebellar PCs (Hirai et al., 2005; Kakegawa et al., 2015; Matsuda et al., 2010; Sigoillot et al., 2015; Uemura et al., 2010), suggesting that proteins, such as SUSD4, that interact with the C1Q globular domain could regulate these processes. PF LTD is dependent on AMPA receptor endocytosis, in particular the GLUA2 subunit (Chung et al., 2003; Xia et al., 2000), and their targeting to RAB7 compartments (Kim et al., 2017). However, the mechanism regulating AMPA receptor targeting to the endolysosomal compartment at PF synapses, as at other synapses, remains unknown.

To identify the role of SUSD4 in brain development and function, we thus analyzed the phenotype of a *Susd4* loss-of-function mouse model in the cerebellum. We found that knockout of the *Susd4* gene leads to impaired synaptic LTD in cerebellar PCs and deficits in motor coordination and adaptation learning. Using affinity-purification followed by proteomics analysis and biochemical assays, we show that the SUSD4 protein binds E3 ubiquitin ligases of the NEDD4 family and regulates activity-dependent degradation of GLUA2 receptors. Because of the domain structure of SUSD4, our results suggest a new regulatory mechanism that can bring spatio-temporal specificity to the degradation machinery in neurons, allowing proper synaptic plasticity and learning.

Results

***Susd4* is broadly expressed in neurons during postnatal development**

Given the potential synaptic role for SUSD4, its pattern of expression should correlate with the timing of synapse formation and/or maturation during postnatal development. *In situ* hybridization experiments using mouse brain sections showed high expression of *Susd4* mRNA in neurons in

many regions of the central nervous system, including the cerebral cortex, the hippocampus, the cerebellum and the brainstem (**Figure 1** and **S1**). *Susd4* expression was already detected by postnatal day 0 (P0) in some regions, but increased with brain maturation (**Figure S1**). In the cerebellum, a structure where the developmental sequence leading to circuit formation and maturation is well described (Sotelo, 2004), quantitative RT-PCR showed that *Susd4* mRNA levels start increasing at P7 and by P21 reach about 15 times the levels detected at birth (**Figure 1B**). At P7, a major increase in synaptogenesis is observed in the cerebellum, due to the formation of hundreds of thousands of PF excitatory synapses on the distal dendritic spines of each PC, and the translocation of a single CF arising from an inferior olivary neuron that forms about 300 excitatory synapses on proximal PC dendrites (Leto et al., 2016). In the brainstem, where cell bodies of inferior olivary neurons are located, the increase in *Susd4* mRNA occurs earlier, already by P3, in parallel with the rate of synaptogenesis increasing during the first postnatal week in the inferior olive (Gotow and Sotelo, 1987). To identify the subcellular localization of the SUSD4 protein and because of the lack of suitable antibodies for immunolabeling, viral particles enabling CRE-dependent coexpression of HA-tagged SUSD4 and GFP in neurons were injected in the cerebellum of adult mice expressing the CRE recombinase specifically in cerebellar PCs. Immunofluorescent labeling against the HA tag demonstrated the presence of tagged SUSD4 in dendrites and distal dendritic spines that are the postsynaptic compartments of PF synapses in PCs (**Figure 1C**). Thus, its timing of expression during postnatal development and its subcellular localization in cerebellar PCs support a role for SUSD4 in excitatory synapse formation and/or function.

***Susd4* loss-of-function leads to deficits in motor coordination and learning**

To determine the synaptic function of SUSD4, we analyzed the phenotype of constitutive knockout (KO) mice completely lacking expression of *Susd4* mRNA due to deletion of exon 1 (**Figure 1D, 1E** and **S2**). No obvious alterations of mouse development and behavior were detected in those mutants, an observation that was confirmed by assessment of their physical characteristics (weight, piloerection, cf. **Table S1**), basic behavioral abilities such as sensorimotor reflexes (whisker responses, eye blinking, cf. **Table S1**) and motor responses (open field locomotion, cf. **Table S1**). Because of the high *Susd4* expression in the olivocerebellar system (**Figure 1** and **S1**), we further assessed the behavior of *Susd4* KO mice for two abilities well known to depend on normal function of this network, motor coordination and motor learning (Kayakabe et al., 2014; Lalonde and Strazielle, 2001; Rondi-Reig et al., 1997). Using a footprint test, a slightly larger print separation of the front and hind paws in the *Susd4* KO mice was detected but no differences in the stride length and stance width were found (**Figure S3**). In the accelerated rotarod assay, a classical test of motor adaptation and learning (Buitrago et al., 2004), the mice were tested three times per day at one hour interval during five consecutive days. The *Susd4* KO mice performed as well as the wild-type (WT) controls on the first trial, indicating that there is no deficit in their balance function (**Figure 1F**), despite the slight change in fine motor coordination found in the footprint test. However, while the WT mice improved their performance as early as the third trial on the first day, and further improved with several days of training, no learning could be observed for the *Susd4* KO mice either during the first day, or in the following days. These results show that *Susd4* loss-of-function leads to impaired motor coordination and learning in adult mice.

***Susd4* loss-of-function prevents long-term depression at cerebellar parallel fiber/Purkinje cell synapses**

Motor coordination and learning are deficient when cerebellar development is impaired (Hirai et al., 2005; Ichise et al., 2000; Tsai et al., 2012; Zuo et al., 1997). No deficits in the global cytoarchitecture of the cerebellum and morphology of PCs were found in *Susd4* KO mice (**Figure S4**). Using high density microelectrode array, we assessed the spontaneous activity of PCs in acute cerebellar slices from *Susd4* KO compared to WT (**Figure S5**). No differences were detected in either the mean spiking frequency, the coefficient of variation of interspike intervals (CV) and the intrinsic variability of spike trains (CV₂, (Holt and Douglas, 1996) showing that the firing properties of PCs are not affected by *Susd4* loss-of-function.

Co-immunolabeling of parallel fiber presynaptic boutons using an anti-VGLUT1 antibody and PCs using an anti-calbindin antibody in cerebellar sections from juvenile WT mice revealed an extremely dense staining in the molecular layer corresponding to the highly numerous parallel fibers contacting PC distal dendritic spines (**Figure 2A**). The labeling pattern was similar in *Susd4* KO and high-resolution microscopy and quantitative analysis confirmed that there are no significant changes in the mean density and volume of VGLUT1 clusters following *Susd4* loss-of-function (**Figure 2A**). Electric stimulation of increasing intensity in the molecular layer allows the progressive recruitment of the PFs (Konnerth et al., 1990), and can be used to assess the number of synapses and the basic PF/PC transmission using whole-cell patch-clamp recordings of PCs on acute cerebellar slices (**Figure 2B**). No difference was observed in the amplitude and the kinetics of the responses to PF stimulation in PCs from *Susd4* KO and control mice (**Figure 2C** and **Figure S6**). Furthermore, the probability of vesicular release in the presynaptic PF bouton, as assessed by measurements of paired pulse facilitation (Atluri and Regehr, 1996; Konnerth et al., 1990; Valera et al., 2012), was not changed at PF/PC synapses (**Figure 2C**). Finally, no differences in the frequency and amplitude of evoked quantal events were detected (**Figure S6**). Thus, in accordance with the morphological analysis, there is no major effect of *Susd4* invalidation on the number and basal transmission of PF/PC synapses.

Long-term synaptic plasticity of PF/PC synapses is involved in proper motor coordination and adaptation learning (Gutierrez-Castellanos et al., 2017; Hirano, 2018; Kakegawa et al., 2018). We first assessed LTD in PF/PC synapses using conjunctive stimulation of PFs and CFs and whole-cell patch-clamp recordings of PCs in acute cerebellar slices from juvenile mice. Our protocol induced a 42% average decrease in the amplitude of PF excitatory postsynaptic currents (EPSCs) in PCs from WT mice while the paired pulse facilitation ratio was not changed during the course of our recordings (**Figure 2D** and **Figure S6**). In *Susd4* KO PCs, the same LTD induction protocol did not induce any significant change in PF EPSCs during the 30 minutes recording period, showing that LTD is greatly impaired in the absence of SUSD4 (**Figure 2D**). LTP can be induced by high frequency stimulation of parallel fibers only, and is also involved in cerebellar dependent-learning (Binda et al., 2016; Gutierrez-Castellanos et al., 2017). In control mice, tetanic stimulation during 5 minutes induced a transient increase in transmission of about 20% and the amplitude of the response returned to baseline after only 15 minutes (**Figure 2E** and **Figure S6**). However, in the case of *Susd4* KO PCs, the same protocol induced a 27% increase in transmission that was maintained after 35 minutes (**Figure 2E**), indicating a facilitation of LTP of PF/PC synapses in the absence of *Susd4* expression.

Lack of LTD of PF/PC synapses could arise from deficient CF transmission. To test this possibility, we first crossed the *Susd4* knockout mice with the Htr5b-GFP BAC transgenic line

(www.gensat.org) expressing soluble GFP specifically in inferior olivary neurons in the olivocerebellar system to visualize CFs. We found that CFs had a normal morphology and translocated along the proximal dendrites of their PC target in *Susd4* KO mice (**Figure 3A**). We then assessed whether developmental elimination of supernumerary CFs was affected by *Susd4* invalidation using whole-cell patch-clamp recordings of PCs on cerebellar acute slices (Crepel et al., 1976; Hashimoto and Kano, 2003). No difference was found in the percentage of remaining multiply-innervated PCs in the absence of *Susd4* (**Figure 3B**). We next used VGLUT2 immunostaining to label CF presynaptic boutons and analyze their morphology using high resolution confocal microscopy and quantitative image analysis. VGLUT2 immunostaining revealed the typical CF innervation territory on PC proximal dendrites, extending up to about 80% of the molecular layer height both in control and *Susd4* KO mice (**Figure 3C**). Furthermore, the number and density of VGLUT2 clusters were not significantly different between WT and *Susd4* KO mice. To test whether the lack of PF LTD was due to deficient CF transmission, we used whole-cell patch-clamp recordings of PCs in acute cerebellar slices. Contrary to what could have been expected, the typical all-or-none climbing fiber evoked EPSC was detected in PCs from *Susd4* KO mice with similar kinetics (**Figure S7**), but with increased amplitude when compared to WT PCs (**Figure 3D**). Thus, the lack of CF-dependent PF/PC synapse LTD in *Susd4* KO mice is not due to reduced CF/PC synapse formation or transmission. Measurements of evoked quantal events revealed an increase in the amplitude of the quantal EPSCs at CF/PC synapses from juvenile mice (**Figure 3E and S7**). In *Susd4* KO, paired-pulse facilitation and depression at PF/PC and CF/PC synapses, respectively, are normal both in basal conditions and after plasticity induction (**Figures 2C, 3D, S6D and S6F**) suggesting that the changes in PF/PC synaptic plasticity and in CF/PC transmission in *Susd4* KO PCs have a postsynaptic origin. Overall our results show that *Susd4* loss-of-function in mice leads to a highly specific phenotype characterized by lack of postsynaptic LTD in the absence of defects in synaptogenesis and in basal transmission in PCs.

SUSD4 binds to HECT E3 ubiquitin ligases

What are the mechanisms that could allow control of long-term synaptic plasticity by SUSD4? We searched for SUSD4 molecular partners by affinity-purification of cerebellar synaptosome extracts using GFP-tagged SUSD4 as a bait (**Figure 4A**), followed by proteomic identification of interacting partners by liquid chromatography with tandem mass spectrometry (LC-MS/MS; Savas et al., 2014). Twenty-eight candidates were identified, several of which were functionally linked to ubiquitin ligase activity by gene ontology term analysis (**Figure 4A and Table 1**). Immunoblot analysis of affinity-purified extracts confirmed the interaction of SUSD4 with several members of the HECT E3 ubiquitin ligases of the NEDD4 subfamily (**Figure 4C**). Removal of the intracellular domain of SUSD4 (SUSD4- ΔC_T mutant) prevented this interaction proving the specificity of SUSD4 binding (**Figure 4B and C**). Ubiquitin ligases of the NEDD4 family bind variants of PY motifs on target substrates and adaptors (Chen et al., 2017). Two potential PY binding sites are present in the intracellular tail of SUSD4 (**Figure 4B**). To test whether these sites mediate interaction between SUSD4 and NEDD4 ubiquitin ligases, we generated single- and double- point mutants of SUSD4 and tested their ability to interact with NEDD4 ligases in transfected HEK293 cells. While the mutation of the PPxY site (SUSD4- Δ PPY mutant) abrogated binding of SUSD4 only partially, mutation of only the LPxY site (SUSD4- Δ LPY mutant) or of both sites (SUSD4- Δ PPY/LY mutant) completely prevented the binding to NEDD4 ubiquitin ligases (**Figure 4D**). These mutations did not change the level of SUSD4 expression in transfected HEK293 cells

suggesting that SUSD4 itself is not a substrate for NEDD4 ubiquitin ligases. Interestingly, NEDD4 ubiquitin ligases are autoinhibited by binding of the HECT domain to their WW domains. Interaction of regulatory proteins with these WW domains has been shown to release autoinhibition and allow ubiquitination of substrates by the NEDD4 ubiquitin ligases (Wang et al., 2019). Thus, our results suggest that while the LPxY site in SUSD4 is essential for binding to NEDD4 ubiquitin ligases, the PPxY might have a regulatory role in controlling the ubiquitin ligase activity. A survey of the expression of HECT-ubiquitin ligases shows that different members of the NEDD4 subfamily are broadly expressed in the mouse brain, however with only partially overlapping patterns (**Figure S8**, <http://mouse.brain-map.org>, Allen Brain Atlas). *Nedd4* and *Wwp1* are the most broadly expressed and are found in neurons that also express *Susd4*, such as hippocampal neurons, inferior olivary neurons in the brainstem and cerebellar PCs. Thus, SUSD4 is a tether for ubiquitin ligases of the NEDD4 family and might modulate their activity in neurons.

SUSD4 regulates activity-dependent degradation of GLUA2

Ubiquitination is a post-translational modification essential for the regulation of protein turnover and trafficking in cells (Tai and Schuman, 2008). The NEDD4 family of ubiquitin ligases are known to ubiquitinate and target for degradation many key signaling molecules, including GLUA1- and GLUA2-containing AMPA receptors (Widagdo et al., 2017). SUSD4 binding to NEDD4 ubiquitin ligases, the lack of LTD at PF/PC synapses and our analysis of evoked quantal events thus suggested the involvement of SUSD4 in the regulation of postsynaptic receptor numbers, in particular, GLUA2-containing receptor numbers. Further evidence came from co-immunolabeling experiments using an anti-GLUA2 and an anti-VGLUT2 antibody on cerebellar sections followed by high-resolution microscopy. Several GLUA2 clusters of varying sizes were detected in close association with each VGLUT2 presynaptic bouton corresponding to CF synapses, while very small and dense GLUA2 clusters were found in the rest of the molecular layer corresponding mostly to GLUA2 clusters at the PF/PC synapses (**Figure 5A**). No obvious change in GLUA2 distribution in the molecular layer in *Susd4* KO mice was found when compared to WT controls, in accordance with normal basal transmission in PF/PC synapses. Quantitative analysis of the GLUA2 clusters associated with VGLUT2 labelled CF presynaptic boutons did not reveal a significant change in the total mean intensity of GLUA2 clusters per CF presynaptic bouton (**Figure 5A**). However, the proportion of CF presynaptic boutons with no GLUA2 cluster was smaller in juvenile *Susd4* KO mice than in WT mice (**Figure 5A**), partially explaining the increase in the amplitude of quantal EPSCs and CF transmission (**Figure 3E**).

Our model implied that a tripartite complex could be formed between SUSD4, NEDD4 ubiquitin ligases and GLUA2-containing AMPA receptors. To test this, we first co-expressed GLUA2 with various HA-tagged SUSD4 constructs (**Figure 5B**) in heterologous HEK293 cells and performed co-immunoprecipitation experiments (**Figure 5C**). GLUA2 and the ubiquitin ligase NEDD4 could both be found in extracts obtained after affinity-purification of the HA-tagged full length (FL-) SUSD4, while both were absent if HA-tagged FL-SUSD4 was replaced by a control transmembrane protein, PVRL3 α (**Figure 5C**). NEDD4 interaction was absent when the SUSD4 Δ C_T construct lacking the intracellular domain was used but not with the SUSD4 Δ N_T construct lacking the extracellular domain, further confirming the binding of NEDD4 ubiquitin ligases to the intracellular domain of SUSD4. Strong co-immunoprecipitation of GLUA2 was detected in affinity-purified extracts from cells expressing the HA-tagged extracellular domain of SUSD4 alone (SUSD4N_T construct), showing that this domain is sufficient for GLUA2 interaction.

Conversely, binding to GLUA2 of a SUSD4 construct lacking the extracellular domain (SUSD4 Δ N_T) was lower than the binding of the extracellular domain alone (SUSD4_{N_T}), but was not completely abrogated, showing the cooperation of several domains of SUSD4 for the binding to GLUA2 (**Figure 5C**). In transfected cultured hippocampal neurons, clusters of GFP-tagged SUSD4 partially colocalize with GLUA2 clusters in spines (**Figure 5D**). Altogether our results suggest that SUSD4 acts as an adaptor protein that targets NEDD4 ubiquitin ligases to GLUA2-containing AMPA receptors to regulate their synaptic numbers.

If SUSD4 is involved in the targeting of AMPA receptors to RAB7-containing endolysosomal compartments for degradation, then it should also be found in RAB7-containing endolysosomal compartments. Co-transfection experiments in HeLa cells followed by immunolabeling showed that indeed SUSD4 is found in several intracellular compartments including the RAB7-positive endolysosomal compartments. Mutation of the PY binding site in SUSD4 decreases the colocalization of SUSD4 with RAB7 further suggesting a link between binding to NEDD4 ubiquitin ligases and SUSD4 localization in the degradation compartments (**Figure S9**). Given the role of NEDD4 ubiquitin ligases in the regulation of substrate degradation, SUSD4 could thus regulate GLUA2-containing AMPA receptor degradation. Indeed, total levels of GLUA2 are greatly reduced in HEK293 cells overexpressing SUSD4 when compared to control cells overexpressing a control transmembrane protein PVRL3 α (**Figure 5** and **S10**). Lack of LTD in *Susd4* KO mice suggests that SUSD4 regulation of GLUA2 degradation is activity-dependent in neurons. To assess this, we set up a biochemical assay in which we induced chemical LTD (cLTD) in acute cerebellar slices (Kim et al., 2017) and measured total protein levels either in control conditions or with inhibitors of the proteasome and lysosomes (to estimate the GLUA2 degraded pool, **Figure 5E**). Total GLUA2 levels were not significantly different on average between WT and *Susd4* KO cerebellar slices in basal conditions, in accordance with our morphological and electrophysiological analysis of PF/PC synapses (**Figure S11**). In slices from WT mice, chemical induction of cLTD induced a significant reduction in total GLUA2 protein levels (**Figure 5E**). This reduction was prevented by incubation with the proteasome inhibitor MG132 and the lysosomal inhibitor leupeptin, showing that it corresponds to the pool of GLUA2 degraded in an activity-dependent manner (**Figure 5E**). In slices from *Susd4* KO mice, this activity-dependent degradation of GLUA2 was completely absent. Furthermore, the chemical induction of LTD did not change the total protein levels of another synaptic receptor highly present at PF/PC postsynaptic densities, GLUR δ 2 (GRID2), either in slices from WT or from *Susd4* mice (**Figure 5E** and **S11**). Thus, SUSD4 specifically controls the activity-dependent degradation of GLUA2 subunits during synaptic LTD.

Discussion

Our study shows that the CCP domain containing protein SUSD4 starts to be expressed in various neurons of the mammalian central nervous system when synapses are formed and mature. SUSD4 can bind both ubiquitin ligases of the NEDD4 family through its C-terminus domain and the GLUA2 AMPA receptor subunit, thus allowing the formation of a tripartite complex. *Susd4* loss-of-function in mice leads to deficient activity-dependent degradation of GLUA2 AMPA receptor subunits, lack of synaptic LTD in cerebellar PCs and impaired motor coordination and adaptation learning.

SUSD4 promotes long-term synaptic depression

The choice between recycling of AMPA receptors to the membrane or targeting to the endolysosomal compartment for degradation is key for the regulation of the number of AMPA receptors at synapses, as well as for the direction and degree of activity-dependent synaptic plasticity (Ehlers, 2000; Lee et al., 2002). Blocking trafficking of AMPA receptors through recycling endosomes, for example using a RAB11 mutant, prevents LTP in neurons (Park et al., 2004). Conversely, blocking the sorting of AMPA receptors to the endolysosomal compartment, for example using a RAB7 mutant, impairs LTD in hippocampal CA1 pyramidal neurons and cerebellar PCs (Fernandez-Monreal et al., 2012; Kim et al., 2017). Further support for the role of receptor degradation comes from mathematical modeling showing that in cerebellar PCs LTD depends on the regulation of the total pool of glutamate receptors (Kim et al., 2017). The GLUA2 AMPA receptor subunit, and its regulation, is of particular importance for LTD (Diering and Huganir, 2018). Phosphorylation in its C-terminal tail and the binding of molecular partners such as PICK1 and GRIP1/2 is known to regulate endocytosis and recycling (Bassani et al., 2012; Chiu et al., 2017; Fiuza et al., 2017), and mutations in some of the phosphorylation sites leads to impaired LTD (Chung et al., 2003). The molecular partners regulating the targeting for degradation of GLUA2 subunits in an activity-dependent manner during LTD remain to be identified. Our study shows that loss-of-function of *Susd4* leads both to loss of LTD and of activity-dependent degradation of GLUA2 subunits. Furthermore, loss-of-function of *Susd4* facilitates LTP of PF/PC synapses, and SUSD4 localization to RAB7 compartments is partly dependent on its binding to NEDD4 ubiquitin ligases. Overall our results support a model in which, during LTD, a specific molecular machinery containing SUSD4 promotes targeting of GLUA2-containing AMPA receptors to the degradation compartment in an activity-dependent manner, away from the recycling pathway that promotes LTP.

SUSD4 is a tether for NEDD4 E3 ubiquitin ligases

The degradation of specific targets such as neurotransmitter receptors must be regulated in a stimulus-dependent and synapse-specific manner in neurons, to ensure proper long-term synaptic plasticity, learning and memory (Tai and Schuman, 2008). How is this level of specificity achieved? Ubiquitination is a post-translational modification that has been shown to regulate protein degradation or signaling depending on the type of the ubiquitin chain added to lysines on the substrate protein. This modification is catalyzed by hundreds of different E3 ubiquitin ligases that belong to several families distinguished by their structure, mode of action and substrate selectivity (Zheng and Shabek, 2017). The family of HECT E3 ubiquitin ligases contains 28 enzymes including the NEDD4 subgroup that is characterized by an N-terminal C2 domain, several WW domains and the catalytic HECT domain. This subgroup of E3 ligases adds K63 ubiquitin chains to their substrate, a modification that promotes sorting to the endolysosomal compartment for degradation (Boase and Kumar, 2015). Our affinity-purification experiments identified SUSD4 as a binding partner for HECT ubiquitin ligases of the NEDD4 family and the mutation of the binding motifs in SUSD4 do not increase the amount of SUSD4 protein in cells suggesting that SUSD4 degradation itself is not regulated by NEDD4 ligases. Adaptor proteins that regulate both activation and substrate binding have been described for several E3 ligases. The activity of NEDD4 ligases depends on the opening of a closed conformation that can be controlled by the binding of several WW domains to PY motifs (Chen et al., 2017). Interestingly, mutation of only one of the two PY motifs of SUSD4 completely abrogates binding to NEDD4 while

mutation on the other one only partially impairs it. Thus, SUSD4 could act as an adaptor protein that regulates NEDD4 E3 ligases activity by changing their conformation.

Adaptor proteins can also regulate substrate binding and thus participate in the specificity of signaling through E3 ubiquitin ligases. NEDD4 E3 ligases are highly expressed in neurons in the mammalian brain and have many known substrates, including ion channels and the GLUA1 AMPA receptor subunit. Their activity and substrate selectivity thus need to be finely tuned. Both GLUA1 and GLUA2 AMPA receptor subunits are ubiquitinated on lysine residues in their intracellular tails in an activity-dependent manner (Lin et al., 2011; Lussier et al., 2011; Schwarz et al., 2010; Widagdo et al., 2015). Mutation of these lysine residues decreases localization of GLUA1 and GLUA2 AMPA receptor subunits in the endolysosomal compartment in neurons (Widagdo et al., 2015). On the contrary, GLUA1 and GLUA2 subunits lack any obvious intracellular direct binding motif to the WW domain of NEDD4 ubiquitin ligases and thus an adaptor molecule would be necessary for ubiquitination by these enzymes. SUSD4 could act as a chaperone for NEDD4 binding to the GLUA2 subunit, its ubiquitination and subsequent targeting to the endolysosomal compartment for degradation. While direct modulation of GLUA2 ubiquitination by SUSD4 remains to be demonstrated, the formation of this complex could provide a simple mechanism to regulate the specificity of action of NEDD4 ubiquitin ligases in neurons and proper control of LTD. Indeed, loss-of-function of *Susd4* leads to misregulation of GLUA2 activity-dependent degradation, but does not affect regulation of another postsynaptic receptor, GRID2. The SUSD4-dependent complex could be used to increase the efficiency of GLUA2 ubiquitination since it has been shown recently that membrane tethering and polymerization increases activity of NEDD4 ubiquitin ligases (Mund and Pelham, 2018). The presence of four CCP domains in the extracellular domain of SUSD4 also suggests that it could bind other proteins extracellularly. In particular, it was previously shown that SUSD4 can bind the C1Q globular domain of the complement protein C1 (Holmquist et al., 2013), a domain that is also found in presynaptic proteins of the C1Q family known for their role in synapse formation and function (Sigoillot et al., 2015; Südhof, 2018; Yuzaki, 2011). SUSD4 could thus enable fine spatiotemporal regulation of the activity of HECT ubiquitin ligases and the degradation of GLUA2-containing AMPA receptors in a trans-synaptic manner.

SUSD4 and neurodevelopmental disorders

The 1q41-42 deletion syndrome is characterized by many symptoms including intellectual deficiencies and seizures, and in a high majority of the cases the microdeletion encompasses the *Susd4* gene (Rosenfeld et al., 2011). A *Susd4* copy number variation has been identified in a patient with ASD (Cuscó et al., 2009). *Susd4* was recently identified amongst the 124 genes with genome wide significance for *de novo* mutations in a cohort of more than 10,000 patients with ASD or intellectual deficiencies (Coe et al., 2019). The *GRIA2* gene (coding for the GLUA2 subunit) has been found as an ASD susceptibility gene (Satterstrom et al., 2018) and mutations or misregulation of ubiquitin ligases have been found in many models of ASDs or intellectual deficiencies (Cheon et al., 2018; Lee et al., 2018; Satterstrom et al., 2018). For example, ubiquitination of GLUA1 by NEDD4-2 is impaired in neurons from a model of Fragile X syndrome (Lee et al., 2018). Understanding the precise molecular mechanisms underlying the activity-dependent degradation of GLUA2 by the SUSD4/NEDD4 complex will thus be of particular importance for our understanding of the etiology of these neurodevelopmental disorders.

Mutations in the *Susd4* gene could contribute to the etiology of neurodevelopmental disorders by impairing synaptic plasticity. Deficits in LTD such as the one found in the *Susd4* KO mice are a common feature of several mouse models of ASDs (Auerbach et al., 2011; Baudouin et al., 2012; Piochon et al., 2014). *Susd4* loss-of-function leads to motor impairments, a symptom that is also found in ASD patients (Fournier et al., 2010). Long-term synaptic plasticity has been proposed as a mechanism for learning and memory. While *in vivo* evidence for the role of LTP in these processes has accumulated, the role of LTD is still discussed (Andersen et al., 2017; Kakegawa et al., 2018; Raymond and Medina, 2018; Schonewille et al., 2011). Because of the broad expression of SUSD4 and of ubiquitin ligases of the NEDD4 subfamily in the mammalian central nervous system, this complex is likely to control LTD at many synapse types and its misregulation might lead to impairments in many learning and memory paradigms. Manipulation of SUSD4's function will thus now provide the means to test the relevance of LTD in many behavioral paradigms and its implication in the etiology of neurodevelopmental disorders.

Acknowledgments: The authors wish to thank all the personnel from the CIRB Imaging facility, in particular P. Mailly for help with the design of the macro for GLUA2 quantification and Estelle Anceaume for image acquisition (panel 1C). We also thank the personnel from the CIRB, INCI and chronobiotron CNRS UMS 3415, IBPS and IBENS animal facilities. We would like to thank Philippe Marin for advice on proteomics analysis. Mass spectrometry experiments were carried out using facilities of the Functional Proteomics Platform of Montpellier. **Funding:** This work was supported by funding from: ATIP-AVENIR program (RSE11005JSA to FS), Idex PSL ANR-10-IDEX-0001-02 PSL*(FS), ANR 9139SAMA90010901 (to FS and PI), ANR-15-CE37-0001-01 CeMod (to PI and FS), Fondation pour la Recherche Médicale Equipe FRM DEQ20150331748 (FS) and DEQ20140329514 (PI), and European Research Council ERC consolidator grant SynID 724601 (to FS). KI was supported by a PhD grant from the Ecole des Neurosciences de Paris (ENP) and the ENS Labex MemoLife (ANR-10-LABX-54 MEMO LIFE). JV and LR-R were supported by ANR-10-LABX-BioPsy (ANR-11-IDEX-0004-02) and ENP Foundation.

Contributions: FS, PI, LR-R, IG-C and KI designed the study and the experiments. IG-C, KI, MC, AK, FAG, JV, MS, ST, MA, OV, YN, AD, FS, SMS and MV performed the experiments, and collected the data; AT and J-LB provided the SUSD4 knockout mice and conceptual advice; FS and IG-C wrote the first draft of the manuscript; all authors read the manuscript and KI, MC, AK, MS, SMS, MV, AD, J-LB, PI and LR-R revised the manuscript.

Competing interests: Authors declare no competing interests.

Data and materials availability: All data is available in the main text or the supplementary materials.

Supplementary Information:

Materials and Methods

Figs. S1 to S11

Tables 1 and S1

References

- Andersen, N., Krauth, N., and Nabavi, S. (2017). Hebbian plasticity in vivo: relevance and induction. *Curr. Opin. Neurobiol.* *45*, 188–192.
- Anggono, V., and Huganir, R.L. (2012). Regulation of AMPA receptor trafficking and synaptic plasticity. *Curr. Opin. Neurobiol.* *22*, 461–469.
- Atluri, P.P., and Regehr, W.G. (1996). Determinants of the Time Course of Facilitation at the Granule Cell to Purkinje Cell Synapse. *J. Neurosci.* *16*, 5661–5671.
- Auerbach, B.D., Osterweil, E.K., and Bear, M.F. (2011). Mutations causing syndromic autism define an axis of synaptic pathophysiology. *Nature* *480*, 63–68.
- Badura, A., Verpeut, J.L., Metzger, J.W., Pereira, T.D., Pisano, T.J., Deverett, B., Bakshinskaya, D.E., and Wang, S.S.-H. (2018). Normal cognitive and social development require posterior cerebellar activity. *Elife* *7*, 1–36.
- Bassani, S., Cingolani, L.A., Valnegri, P., Folci, A., Zapata, J., Gianfelice, A., Sala, C., Goda, Y., and Passafaro, M. (2012). The X-Linked Intellectual Disability Protein TSPAN7 Regulates Excitatory Synapse Development and AMPAR Trafficking. *Neuron* *73*, 1143–1158.
- Baudouin, S.J., Gaudias, J., Gerharz, S., Hatstatt, L., Zhou, K., Punakkal, P., Tanaka, K.F., Spooren, W., Hen, R., De Zeeuw, C.I., et al. (2012). Shared synaptic pathophysiology in syndromic and nonsyndromic rodent models of autism. *Science* (80-).
- Binda, F., Dorgans, K., Reibel, S., Sakimura, K., Kano, M., Poulain, B., and Isope, P. (2016). Inhibition promotes long-Term potentiation at cerebellar excitatory synapses. *Sci. Rep.* *6*, 1–12.
- Boase, N.A., and Kumar, S. (2015). NEDD4: The founding member of a family of ubiquitin-protein ligases. *Gene* *557*, 113–122.
- Bolliger, M.F., Martinelli, D.C., and Sudhof, T.C. (2011). The cell-adhesion G protein-coupled receptor BAI3 is a high-affinity receptor for C1q-like proteins. *Proc. Natl. Acad. Sci.* *108*, 2534–2539.
- Brechet, A., Buchert, R., Schwenk, J., Boudkazi, S., Zolles, G., Siquier-Pernet, K., Schaber, I., Bildl, W., Saadi, A., Bole-Feysot, C., et al. (2017). AMPA-receptor specific biogenesis complexes control synaptic transmission and intellectual ability. *Nat. Commun.* *8*.
- Buitrago, M.M., Schulz, J.B., Dichgans, J., and Luft, A.R. (2004). Short and long-term motor skill learning in an accelerated rotarod training paradigm. *Neurobiol. Learn. Mem.* *81*, 211–216.
- Cajigas, J., Will, T., and Schuman, E.M. (2010). Protein homeostasis and synaptic plasticity. *EMBO J.* *29*, 2746–2752.
- Chen, Z., Jiang, H., Xu, W., Li, X., Dempsey, D.R., Zhang, X., Devreotes, P., Wolberger, C., Amzel, L.M., Gabelli, S.B., et al. (2017). A Tunable Brake for HECT Ubiquitin Ligases. *Mol. Cell* *66*, 345-357.e6.
- Cheon, S., Dean, M., and Chahrour, M. (2018). The ubiquitin proteasome pathway in neuropsychiatric disorders. *Neurobiol. Learn. Mem.* 106791.
- Chiu, S.L., Diering, G.H., Ye, B., Takamiya, K., Chen, C.M., Jiang, Y., Niranjana, T., Schwartz,

- C.E., Wang, T., and Huganir, R.L. (2017). GRASP1 Regulates Synaptic Plasticity and Learning through Endosomal Recycling of AMPA Receptors. *Neuron* *93*, 1405-1419.e8.
- Choquet, D., and Triller, A. (2013). The dynamic synapse. *Neuron* *80*, 691–703.
- Chung, H.J., Steinberg, J.P., Huganir, R.L., and Linden, D.J. (2003). Requirement of AMPA receptor GluR2 phosphorylation for cerebellar long-term depression. *Science* (80-), *300*, 1751–1755.
- Coe, B.P., Stessman, H.A.F., Sulovari, A., Geisheker, M.R., Bakken, T.E., Lake, A.M., Dougherty, J.D., Lein, E.S., Hormozdiari, F., Bernier, R.A., et al. (2019). Neurodevelopmental disease genes implicated by de novo mutation and copy number variation morbidity. *Nat. Genet.* *51*, 106–116.
- Coesmans, M., Weber, J.T., De Zeeuw, C.I., and Hansel, C. (2004). Bidirectional parallel fiber plasticity in the cerebellum under climbing fiber control. *Neuron* *44*, 691–700.
- Collingridge, G.L., Peineau, S., Howland, J.G., and Wang, Y.T. (2010). Long-term depression in the CNS. *Nat. Rev. Neurosci.* *11*, 459–473.
- Crepel, F., Mariani, J., and Delhaye-Bouchaud, N. (1976). Evidence for a multiple innervation of purkinje cells by climbing fibers in the immature rat cerebellum. *J. Neurobiol.* *7*, 567–578.
- Cuscó, I., Medrano, A., Gener, B., Vilardell, M., Gallastegui, F., Villa, O., González, E., Rodríguez-Santiago, B., Vilella, E., Del Campo, M., et al. (2009). Autism-specific copy number variants further implicate the phosphatidylinositol signaling pathway and the glutamatergic synapse in the etiology of the disorder. *Hum. Mol. Genet.* *18*, 1795–1804.
- Davies, B., Brown, L.A., Cais, O., Watson, J., Clayton, A.J., Chang, V.T., Biggs, D., Preece, C., Hernandez-Pliego, P., Krohn, J., et al. (2017). A point mutation in the ion conduction pore of AMPA receptor GRIA3 causes dramatically perturbed sleep patterns as well as intellectual disability. *Hum. Mol. Genet.* *26*, 3869–3882.
- Diering, G.H., and Huganir, R.L. (2018). The AMPA Receptor Code of Synaptic Plasticity. *Neuron* *100*, 314–329.
- Ehlers, M.D. (2000). Reinsertion or degradation of AMPA receptors determined by activity-dependent endocytic sorting. *Neuron* *28*, 511–525.
- Fernandez-Monreal, M., Brown, T.C., Royo, M., and Esteban, J.A. (2012). The Balance between Receptor Recycling and Trafficking toward Lysosomes Determines Synaptic Strength during Long-Term Depression. *J. Neurosci.* *32*, 13200–13205.
- Fiuza, M., Rostosky, C., Parkinson, G., Bygrave, A., Halemani, N., Baptista, M., Milosevic, I., and Hanley, J.G. (2017). PICK1 regulates AMP receptor endocytosis via direct interaction with AP2 a-appendage and dynamin. *Rockefeller Univ. Press J. Cell Biol* *216*, 3323–3338.
- Fournier, K.A., Hass, C.J., Naik, S.K., Lodha, N., and Cauraugh, J.H. (2010). Motor coordination in autism spectrum disorders: A synthesis and meta-analysis. *J. Autism Dev. Disord.* *40*, 1227–1240.
- Gao, Z., Van Beugen, B.J., and De Zeeuw, C.I. (2012). Distributed synergistic plasticity and cerebellar learning. *Nat. Rev. Neurosci.* *13*, 619–635.
- Gendrel, M., Rapti, G., Richmond, J.E., and Bessereau, J.-L. (2009). A secreted complement-

- control-related protein ensures acetylcholine receptor clustering. *Nature* *461*, 992–996.
- Gotow, T., and Sotelo, C. (1987). Postnatal development of the inferior olivary complex in the rat: IV. Synaptogenesis of GABAergic afferents, analyzed by glutamic acid decarboxylase immunocytochemistry. *J. Comp. Neurol.* *263*, 526–552.
- Gutierrez-Castellanos, N., Da Silva-Matos, C.M., Zhou, K., Canto, C.B., Renner, M.C., Koene, L.M.C., Ozyildirim, O., Sprengel, R., Kessels, H.W., and De Zeeuw, C.I. (2017). Motor Learning Requires Purkinje Cell Synaptic Potentiation through Activation of AMPA-Receptor Subunit GluA3. *Neuron* *93*, 409–424.
- Hashimoto, K., and Kano, M. (2003). Functional differentiation of multiple climbing fiber inputs during synapse elimination in the developing cerebellum. *Neuron* *38*, 785–796.
- Hirai, H., Pang, Z., Bao, D., Miyazaki, T., Li, L., Miura, E., Parris, J., Rong, Y., Watanabe, M., Yuzaki, M., et al. (2005). Cbln1 is essential for synaptic integrity and plasticity in the cerebellum. *Nat. Neurosci.* *8*, 1534–1541.
- Hirano, T. (2018). Regulation and Interaction of Multiple Types of Synaptic Plasticity in a Purkinje Neuron and Their Contribution to Motor Learning. *Cerebellum* *17*, 756–765.
- Holmquist, E., Okroj, M., Nodin, B., Jirstrom, K., and Blom, A.M. (2013). Sushi domain-containing protein 4 (SUSD4) inhibits complement by disrupting the formation of the classical C3 convertase. *FASEB J.* *27*, 2355–2366.
- Holt, G.R., and Douglas, J. (1996). Comparison of Discharge Variability Visual Cortex Neurons. *J. Neurophysiol.* *75*, 1806–1814.
- Ichise, T., Kano, M., Hashimoto, K., Yanagihara, D., Nakao, K., Shigemoto, R., Katsuki, M., and Aiba, M. (2000). mGluR1 in cerebellar Purkinje cells essential for long-term depression, synapse elimination, and motor coordination. *Science* *288*, 1832–1835.
- Ito, M. (2001). Cerebellar Long-Term Depression: Characterization, Signal Transduction, and Functional Roles. *Physiol. Rev.* *81*, 1143–1195.
- Ito, M. (2006). Cerebellar circuitry as a neuronal machine. *Prog. Neurobiol.* *78*, 272–303.
- Ito, M., and Kano, M. (1982). Long-lasting depression of parallel fiber-Purkinje cell transmission induced by conjunctive stimulation of parallel fibers and climbing fibers in the cerebellar cortex. *Neurosci. Lett.* *33*, 253–258.
- Kakegawa, W., Mitakidis, N., Miura, E., Abe, M., Matsuda, K., Takeo, Y.H., Kohda, K., Motohashi, J., Takahashi, A., Nagao, S., et al. (2015). Anterograde C1ql1 signaling is required in order to determine and maintain a single-winner climbing fiber in the mouse cerebellum. *Neuron* *85*, 316–330.
- Kakegawa, W., Katoh, A., Narumi, S., Miura, E., Motohashi, J., Takahashi, A., Kohda, K., Fukazawa, Y., Yuzaki, M., and Matsuda, S. (2018). Optogenetic Control of Synaptic AMPA Receptor Endocytosis Reveals Roles of LTD in Motor Learning. *Neuron* *99*, 985–998.e6.
- Kashiwabuchi, N., Ikeda, K., Araki, K., Hirano, T., Shibuki, K., Takayama, C., Inoue, Y., Kutsuwada, T., Yagi, T., Kang, Y., et al. (1995). Impairment of Motor Coordination, Purkinje Cell Synapse Formation, and Cerebellar Long-Term Depression in GluRd2 Mutant Mice. *Cell* *81*, 245–252.

- Kayakabe, M., Kakizaki, T., Kaneko, R., Sasaki, A., Nakazato, Y., Shibasaki, K., Ishizaki, Y., Saito, H., Suzuki, N., Furuya, N., et al. (2014). Motor dysfunction in cerebellar Purkinje cell-specific vesicular GABA transporter knockout mice. *Front. Cell. Neurosci.* *7*, 1–11.
- Kessels, H.W., and Malinow, R. (2009). Synaptic AMPA Receptor Plasticity and Behavior. *Neuron* *61*, 340–350.
- Kim, T., Yamamoto, Y., and Tanaka-Yamamoto, K. (2017). Timely regulated sorting from early to late endosomes is required to maintain cerebellar long-term depression. *Nat. Commun.* *8*.
- Konnerth, A., Llanot, I., and Armstrong, C.M. (1990). Synaptic currents in cerebellar Purkinje cells. *Neurobiology* *87*, 2662–2665.
- Lalonde, R., and Strazielle, C. (2001). Motor performance and regional brain metabolism of spontaneous murine mutations with cerebellar atrophy. *J. Neurosci.* *21*, 103–108.
- Lee, K.Y., Jewett, K.A., Chung, H.J., and Tsai, N.P. (2018). Loss of fragile X protein FMRP impairs homeostatic synaptic downscaling through tumor suppressor p53 and ubiquitin E3 ligase Nedd4-2. *Hum. Mol. Genet.* *27*, 2805–2816.
- Lee, S.H., Liu, L., Wang, Y.T., and Sheng, M. (2002). Clathrin adaptor AP2 and NSF interact with overlapping sites of GluR2 and play distinct roles in AMPA receptor trafficking and hippocampal LTD. *Neuron* *36*, 661–674.
- Lee, S.H., Simonetta, A., and Sheng, M. (2004). Subunit rules governing the sorting of internalized AMPA receptors in hippocampal neurons. *Neuron* *43*, 221–236.
- Lefort, J.M., Vincent, J., Tallot, L., Jarlier, F., De Zeeuw, C.I., Rondi-Reig, L., and Rochefort, C. (2019). Impaired cerebellar Purkinje cell potentiation generates unstable spatial map orientation and inaccurate navigation. *Nat. Commun.* *10*, 1–13.
- Leto, K., Arancillo, M., Becker, E.B.E., Buffo, A., Chiang, C., Ding, B., Dobyns, W.B., Dusart, I., Haldipur, P., Hatten, M.E., et al. (2016). Consensus Paper: Cerebellar Development. *The Cerebellum* *15*, 789–828.
- Lin, A., Hou, Q., Jarzylo, L., Amato, S., Gilbert, J., Shang, F., and Man, H.Y. (2011). Nedd4-mediated AMPA receptor ubiquitination regulates receptor turnover and trafficking. *J. Neurochem.* *119*, 27–39.
- Lussier, M.P., Nasu-Nishimura, Y., and Roche, K.W. (2011). Activity-dependent ubiquitination of the AMPA receptor subunit GluA2. *J. Neurosci.* *31*, 3077–3081.
- Martin, S., Chamberlin, A., Shinde, D.N., Hempel, M., Strom, T.M., Schreiber, A., Johansen, J., Ousager, L.B., Larsen, M.J., Hansen, L.K., et al. (2017). De Novo Variants in GRIA4 Lead to Intellectual Disability with or without Seizures and Gait Abnormalities. *Am. J. Hum. Genet.* *101*, 1013–1020.
- Matsuda, K., Miura, E., Miyazaki, T., Kakegawa, W., Emi, K., Narumi, S., Fukazawa, Y., Ito-Ishida, A., Kondo, T., Shigemoto, R., et al. (2010). Cbln1 is a ligand for an orphan glutamate receptor delta2, a bidirectional synapse organizer. *Science* *328*, 363–368.
- Matsuda, S., Kakegawa, W., Budisantoso, T., Nomura, T., Kohda, K., and Yuzaki, M. (2013). Stargazin regulates AMPA receptor trafficking through adaptor protein complexes during long-term depression. *Nat. Commun.* *4*, 1–15.

- Mund, T., and Pelham, H.R. (2018). Substrate clustering potently regulates the activity of WW-HECT domain–containing ubiquitin ligases. *J. Biol. Chem.* *293*, 5200–5209.
- Nakayama, M., Suzuki, E., Tsunoda, S. -i., and Hama, C. (2016). The Matrix Proteins Hasp and Hig Exhibit Segregated Distribution within Synaptic Clefts and Play Distinct Roles in Synaptogenesis. *J. Neurosci.* *36*, 590–606.
- Nicoll, R.A. (2017). A Brief History of Long-Term Potentiation. *Neuron* *93*, 281–290.
- Park, M., Penick, E., Edwards, J., Kauer, J., and Ehlers, M.D. (2004). Recycling Endosomes Supply AMPA Receptors for Long-term Potentiation. *Science* (80-.). *305*, 1972–1975.
- Penn, A.C., Zhang, C.L., Georges, F., Royer, L., Breillat, C., Hosy, E., Petersen, J.D., Humeau, Y., and Choquet, D. (2017). Hippocampal LTP and contextual learning require surface diffusion of AMPA receptors. *Nature* *549*, 384–388.
- Piochon, C., Kloth, A.D., Grasselli, G., Titley, H.K., Nakayama, H., Hashimoto, K., Wan, V., Simmons, D.H., Eissa, T., Nakatani, J., et al. (2014). Cerebellar plasticity and motor learning deficits in a copy-number variation mouse model of autism. *Nat. Commun.* *5*, 1–12.
- Raymond, J.L., and Medina, J.F. (2018). Computational Principles of Supervised Learning in the Cerebellum. *Annu. Rev. Neurosci.* *41*, 233–253.
- Rochefort, C., Arabo, A., Andre, M., Poucet, B., Save, E., and Rondi-Reig, L. (2011). Cerebellum Shapes Hippocampal Spatial Code. *Science* (80-.). *334*, 385–389.
- Rondi-Reig, L., Delhay-Bouchaud, N., Mariani, J., and Caston, J. (1997). Role of the inferior olivary complex in motor skills and motor learning in the adult rat. *Neuroscience* *77*, 955–963.
- Rosenfeld, J.A., Lacassie, Y., El-Khechen, D., Escobar, L.F., Reggin, J., Heuer, C., Chen, E., Jenkins, L.S., Collins, A.T., Zinner, S., et al. (2011). New cases and refinement of the critical region in the 1q41q42 microdeletion syndrome. *Eur. J. Med. Genet.* *54*, 42–49.
- Salpietro, V., Dixon, C.L., Guo, H., Bello, O.D., Vandrovcova, J., Efthymiou, S., Maroofian, R., Heimer, G., Burglen, L., Valence, S., et al. (2019). AMPA receptor GluA2 subunit defects are a cause of neurodevelopmental disorders. *Nat. Commun.* *10*.
- Satterstrom, F.K., Kosmicki, J.A., Wang, J., and Breen, M.S. (2018). Large-scale exome sequencing study implicates both developmental and functional changes in the neurobiology of autism. 1–43.
- Savas, J.N., De Wit, J., Comoletti, D., Zemla, R., Ghosh, A., and Yates, J.R. (2014). Ecto-Fc MS identifies ligand-receptor interactions through extracellular domain Fc fusion protein baits and shotgun proteomic analysis. *Nat. Protoc.* *9*, 2061–2074.
- Schonewille, M., Gao, Z., Boele, H.J., Vinueza Veloz, M.F., Amerika, W.E., Šimek, A.A.M., De Jeu, M.T., Steinberg, J.P., Takamiya, K., Hoebeek, F.E., et al. (2011). Reevaluating the Role of LTD in Cerebellar Motor Learning. *Neuron* *70*, 43–50.
- Schwarz, L.A., Hall, B.J., and Patrick, G.N. (2010). Activity-dependent ubiquitination of GluA1 mediates a distinct AMPA receptor endocytosis and sorting pathway. *J. Neurosci.* *30*, 16718–16729.
- Sia, G.M., Clem, R.L., and Haganir, R.L. (2013). The human language-associated gene SRPX2 regulates synapse formation and vocalization in mice. *Science* (80-.). *342*, 987–991.

- Sigoillot, S.M., Iyer, K., Binda, F., González-Calvo, I., Talleur, M., Vodjdani, G., Isope, P., and Selimi, F. (2015). The Secreted Protein C1QL1 and Its Receptor BAI3 Control the Synaptic Connectivity of Excitatory Inputs Converging on Cerebellar Purkinje Cells. *Cell Rep.* 820–832.
- Sotelo, C. (2004). Cellular and genetic regulation of the development of the cerebellar system. *Prog. Neurobiol.* 72, 295–339.
- Stevens, B., Allen, N.J., Vazquez, L.E., Howell, G.R., Christopherson, K.S., Nouri, N., Micheva, K.D., Mehalow, A.K., Huberman, A.D., Stafford, B., et al. (2007). The Classical Complement Cascade Mediates CNS Synapse Elimination. *Cell* 131, 1164–1178.
- Stoodley, C.J. (2016). The Cerebellum and Neurodevelopmental Disorders. *The Cerebellum* 15, 34–37.
- Stoodley, C.J., D’Mello, A.M., Ellegood, J., Jakkamsetti, V., Liu, P., Nebel, M.B., Gibson, J.M., Kelly, E., Meng, F., Cano, C.A., et al. (2018). Author Correction: Altered cerebellar connectivity in autism and cerebellar-mediated rescue of autism-related behaviors in mice (Nature Neuroscience DOI: 10.1038/s41593-017-0004-1). *Nat. Neurosci.* 21, 1016.
- Südhof, T.C. (2018). Towards an Understanding of Synapse Formation. *Neuron*.
- Suvrathan, A., Payne, H.L., and Raymond, J.L. (2016). Timing Rules for Synaptic Plasticity Matched to Behavioral Function. *Neuron* 92, 959–967.
- Tai, H., and Schuman, E.M. (2008). Ubiquitin, the proteasome and protein degradation in neuronal function and dysfunction. *Nat. Rev. Neurosci.* 9.
- Tsai, P.T., Hull, C., Chu, Y., Greene-Colozzi, E., Sadowski, A.R., Leech, J.M., Steinberg, J., Crawley, J.N., Regehr, W.G., and Sahin, M. (2012). Autistic-like behaviour and cerebellar dysfunction in Purkinje cell Tsc1 mutant mice. *Nature* 488, 647–651.
- Uemura, T., Lee, S.-J., Yasumura, M., Takeuchi, T., Yoshida, T., Ra, M., Taguchi, R., Sakimura, K., and Mishina, M. (2010). Trans-Synaptic Interaction of GluR δ 2 and Neurexin through Cbln1 Mediates Synapse Formation in the Cerebellum. *Cell* 141, 1068–1079.
- Valera, A.M., Doussau, F., Poulain, B., Barbour, B., and Isope, P. (2012). Adaptation of Granule Cell to Purkinje Cell Synapses to High-Frequency Transmission. *J. Neurosci.* 32, 3267–3280.
- Volk, L., Chiu, S.-L., Sharma, K., and Haganir, R.L. (2015). Glutamate Synapses in Human Cognitive Disorders. *Annu. Rev. Neurosci.* 38, 127–149.
- Wang, S.S.H., Kloth, A.D., and Badura, A. (2014). The Cerebellum, Sensitive Periods, and Autism. *Neuron* 83, 518–532.
- Wang, Z., Liu, Z., Chen, X., Li, J., Yao, W., Huang, S., Gu, A., Lei, Q.-Y., Mao, Y., and Wen, W. (2019). A multi-lock inhibitory mechanism for fine-tuning enzyme activities of the HECT family E3 ligases. *Nat. Commun.* 10.
- Widagdo, J., Chai, Y.J., Ridder, M.C., Chau, Y.Q., Johnson, R.C., Sah, P., Haganir, R.L., and Anggono, V. (2015). Activity-Dependent ubiquitination of GluA1 and GluA2 regulates AMPA receptor intracellular sorting and degradation. *Cell Rep.* 10, 783–795.
- Widagdo, J., Guntupalli, S., Jang, S.E., and Anggono, V. (2017). Regulation of AMPA Receptor Trafficking by Protein Ubiquitination. *Front. Mol. Neurosci.* 10, 1–10.
- Xia, J., Chung, H.J., Wihler, C., Haganir, R.L., and Linden, D.J. (2000). Cerebellar long-term

depression requires PKC-regulated interactions between GluR2/3 and PDZ domain-containing proteins. *Neuron* 28, 499–510.

Yuzaki, M. (2011). Cbln1 and its family proteins in synapse formation and maintenance. *Curr. Opin. Neurobiol.* 21, 215–220.

Zheng, N., and Shabek, N. (2017). Ubiquitin Ligases: Structure, Function, and Regulation. *Annu. Rev. Biochem.* 86, 129–157.

Zuo, J., De Jager, P.L., Takahashi, K.A., Jiang, W., Linden, D.J., and Heintz, N. (1997). Neurodegeneration in Lurcher mice caused by mutation in delta2 glutamate receptor gene [see comments]. *Nature* 388, 769–773.

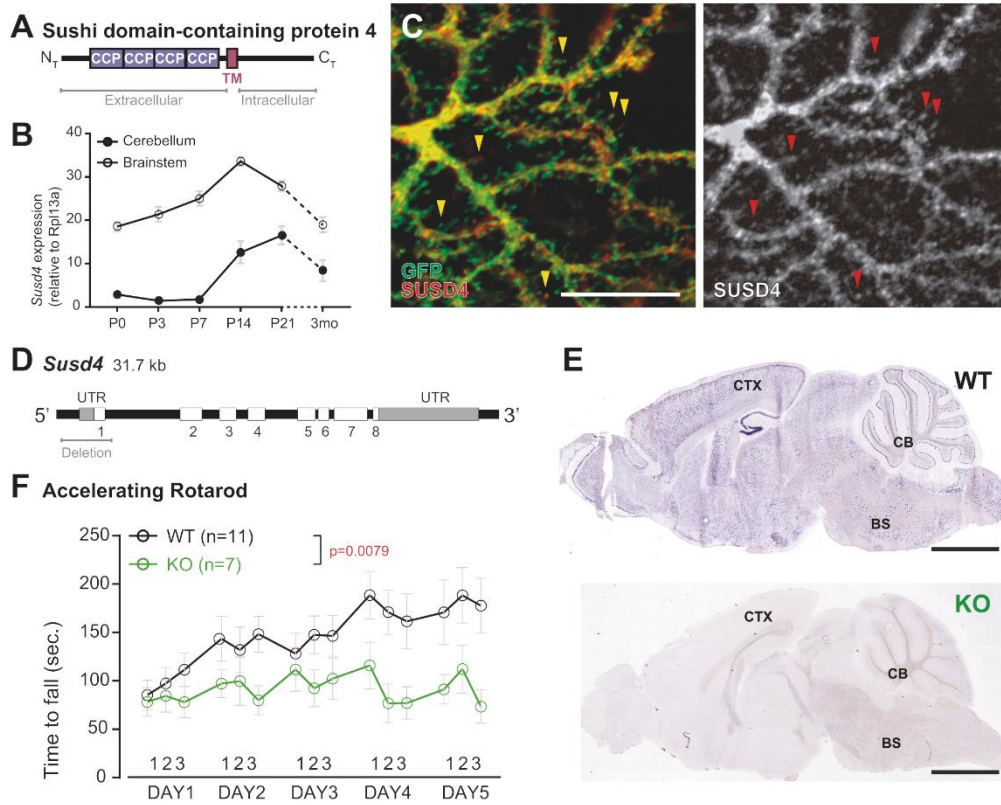


Figure 1. *Susd4* expression is necessary for motor coordination adaptation and learning.

- (A) Diagram of the protein SUSD4 showing its domain organization with four extracellular Complement Control Protein (CCP) domains, one transmembrane (TM) domain and a cytoplasmic domain (C₁).
- (B) Quantitative RT-PCR shows an increase in *Susd4* mRNA expression (relative to the housekeeping gene *Rpl13a*) during postnatal development in the cerebellum and in the brainstem. Mean \pm s.e.m. (n=3 independent experiments). Extracts were prepared from tissue samples of mice aged 0 to 21 days (P0-21) and three months (3mo).
- (C) HA-tagged SUSD4 is found in dendrites and distal dendritic spines in adult cerebellar Purkinje cells (arrowheads; anti-HA immunolabelling of parasagittal cerebellar sections obtained from adult mice after stereotaxic injection of AAV particles driving the expression of HA-SUSD4 and soluble GFP). Scale bar: 10 μ m.
- (D) Genomic structure of the *Susd4* gene. Labelled white boxes represent exons. Exon 1 is deleted in the *Susd4* loss-of-function mouse model.
- (E) *In situ* hybridization experiments were performed on brain sections from one month-old wild-type (WT) and *Susd4* knockout (KO) mice to detect *Susd4* mRNA. *Susd4* expression was found in many regions of the brain in WT mice (see also **Figure S1**) including the cerebral cortex (CTX), the cerebellum (CB), and the brainstem (BS). No labeling was found in the brain of *Susd4* KO mice. Scale bars: 500 μ m.
- (F) Motor coordination and learning is deficient in adult *Susd4* knockout (KO) mice compared to age-matched WT littermates. Each mouse was tested three times per day during five consecutive days on an accelerating rotarod (4 to 40 r.p.m. in 10 minutes) and the time spent on the rotarod measured. Mean \pm s.e.m. (WT n=11 and KO n=7, two-way ANOVA with repeated measures, Interaction (time and genotype): ** P=0.0079, F(14, 224) = 2.22; Time: **** P<0.0001, F(14, 224) = 3.469; Genotype: P=0.0553, F(1, 16) = 4.272).

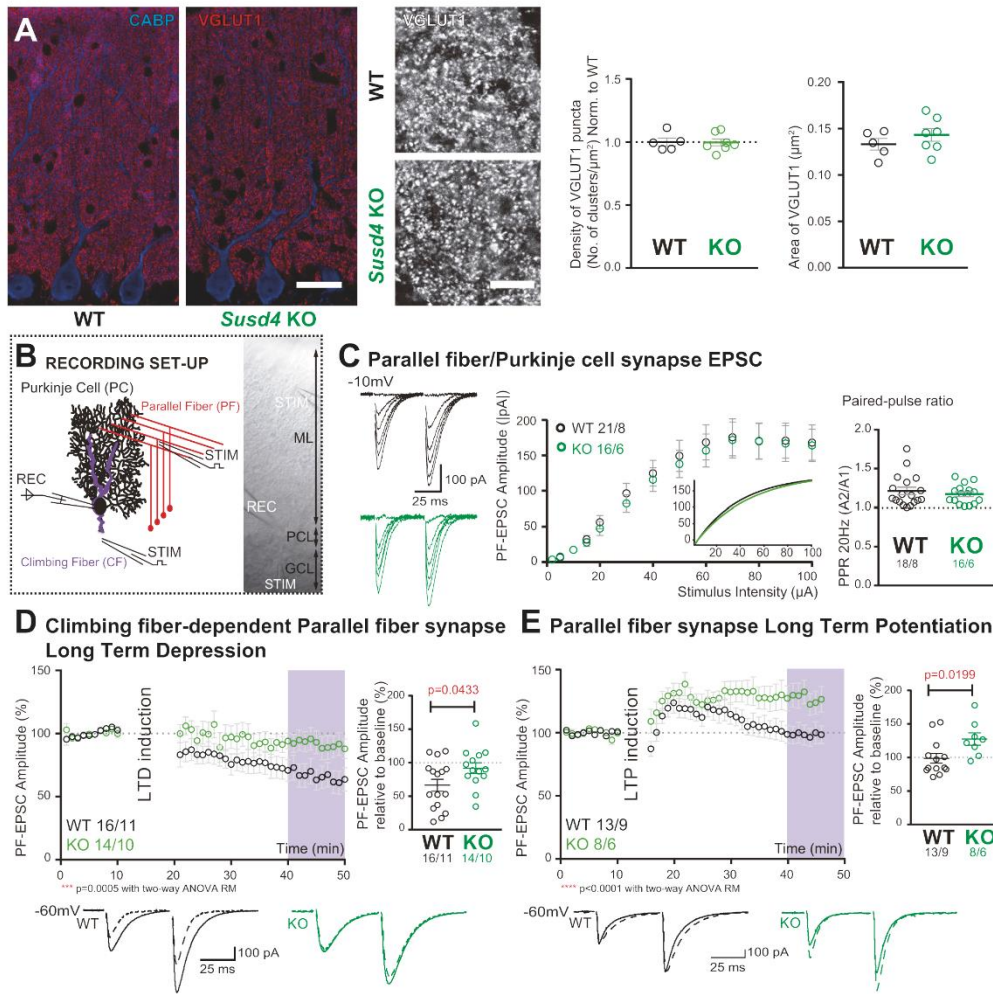


Figure 2. *Susd4* loss-of-function leads to deficient long-term depression and facilitated long-term potentiation of parallel fiber/Purkinje cell synapses.

- (A) Quantitative analysis of the morphology of parallel fiber presynaptic boutons immunolabeled by an anti-VGLUT1 antibody (red) in Purkinje cells (anti-CABP, blue). Quantifications of the density and the area of the VGLUT1 clusters did not reveal any difference between *Susd4* KO and WT mice. Mean \pm s.e.m. (WT n=5 and KO n=7; VGLUT1 clusters density: Mann-Whitney test, $P>0.9999$; area VGLUT1 clusters: Unpaired Student t-test, $P=0.3089$). Scale bars: 30 μ m (left) and 10 μ m (right).
- (B) Diagram of the setup for patch-clamp recordings (REC) of Purkinje cells in 300 μ m-thick parasagittal cerebellar slices. Parallel fiber and climbing fiber responses were elicited by electrical stimulation (STIM). ML: molecular layer; PCL: Purkinje cell layer; GCL: granule cell layer.
- (C) Input-output curve of the parallel fiber/Purkinje cell transmission. The amplitude of the elicited EPSCs increases with the intensity of the stimulus and is not significantly different between *Susd4* KO and WT littermates. The fitted curves for each genotype are presented in the inset. Mean \pm s.e.m. (WT n=21 cells, 8 mice and KO n=16 cells, 6 mice; Kolmogorov-Smirnov test, $P=0.8793$). Short-term plasticity of parallel fiber/Purkinje cell synapses is not affected by *Susd4* loss-of-function. Parallel fibers were stimulated twice at 50 ms interval and the paired-pulse ratio (PPR) was calculated by dividing the amplitude of the second peak divided by the amplitude of the first peak. Representative sample traces are presented. Mean \pm s.e.m. (Mann-Whitney test, $P=0.9052$).
- (D) Climbing fiber-dependent parallel fiber/Purkinje cell synapse long-term depression (LTD) is impaired in the absence of *Susd4* expression. LTD was induced by pairing stimulations of parallel fibers and climbing fibers at 100 milliseconds interval during 10 minutes at 0.5 Hz (**Figure S6C and D**). The amplitude of the PF EPSC was measured using two consecutive PF stimulation at 50 milliseconds interval. Representative sample traces are presented. Mean \pm s.e.m. (WT n=16 cells, 11 mice and KO n=14 cells, 10 mice). Right: EPSC amplitudes from the last 10 minutes (purple) of recordings were used to calculate the LTD ratio relative to baseline (Two-tailed Wilcoxon Signed Rank Test with null hypothesis of 100: WT ** $p=0.0063$; KO $p=0.2676$ Mann-Whitney test, WT vs KO * $p=0.0433$).
- (E) Loss-of-function of *Susd4* facilitates parallel fiber/Purkinje cell synapse long-term potentiation (LTP). Tetanic stimulation of only parallel fibers at 0.3 Hz for 100 times (**Figure S6E and F**) induced LTP in *Susd4* KO Purkinje cells while inducing only a transient increase in parallel fiber transmission in WT Purkinje cells. Representative sample traces are presented. Mean \pm s.e.m. (WT n=13 cells, 9 mice and KO n=8 cells, 6 mice). Right: EPSC amplitudes from the last 7 minutes (purple) were used to calculate the LTP ratio relative to baseline (Two-tailed Wilcoxon Signed Rank Test with null hypothesis of 100: WT $p=0.5879$; KO * $p=0.0234$; Mann-Whitney test, WT vs KO: * $p=0.0199$).

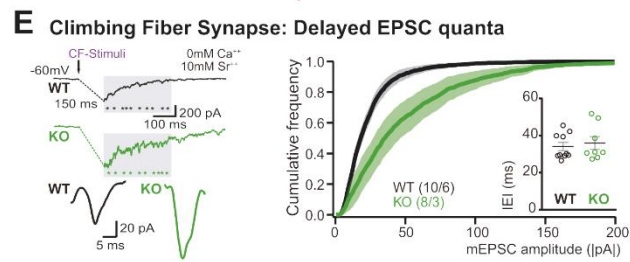
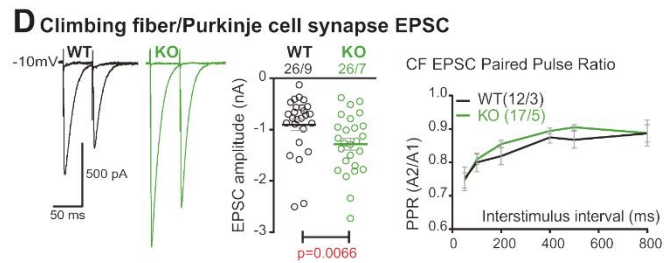
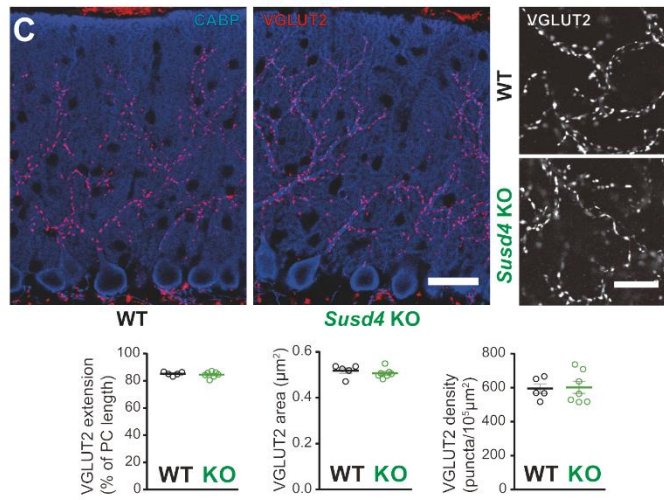
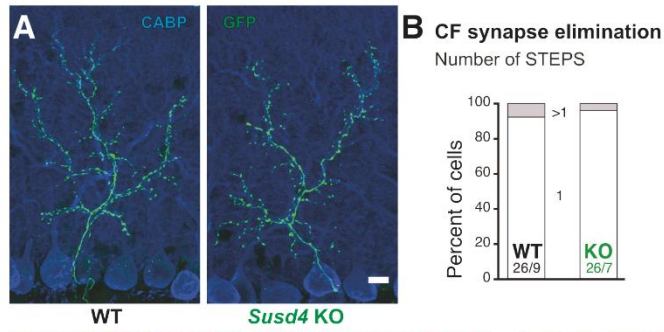


Figure 3. Transmission at the Climbing fiber/Purkinje cell synapses is increased in *Susd4* knockout mice.

- (A) Left: Climbing fibers were visualized in *Susd4* WT and KO mice crossed with Htr5b-eGFP reporter mice (www.gensat.org) expressing the green fluorescent protein specifically in inferior olivary neurons. Anti-GFP and anti-CABP immunofluorescence was performed on parasagittal sections of P30 mice, and showed no qualitative differences in the absence of *Susd4* expression. Scale bar: 10 μ m.
- (B) Patch-clamp recordings of Purkinje cells showed a similar percentage of mono- (1 climbing fiber) and multi-innervation (>1 climbing fibers) of Purkinje cells in P30 *Susd4* KO and WT mice, as measured by the number of steps elicited by electrical stimulation of the climbing fibers. WT n=26 cells from 9 mice and KO n=26 cells from 7 mice (Chi-square test, P=0.5520).
- (C) Climbing fiber presynaptic boutons were immunostained with an anti-VGLUT2 antibody in cerebellar sections from P30 WT and *Susd4* KO mice. The extension of the climbing fiber territory was calculated by measuring the extent of the VGLUT2 labeling relative to the height of the Purkinje cell dendritic tree (immunostained using an anti-CABP antibody, blue). Quantification of the mean density of VGLUT2 puncta and their mean area showed no differences between *Susd4* KO mice and their control littermates. Mean \pm s.e.m. (WT n=5 and KO n=7; VGLUT2 extension: Mann-Whitney test, P=0.6389; VGLUT2 area: Unpaired Student t-test, p=0.4311; VGLUT2 density: Unpaired Student t-test, p=0.8925). Scale bars: 30 μ m (left) and 10 μ m (right).
- (D) The amplitude of the climbing fiber elicited EPSC was increased in *Susd4* KO mice compared to WT littermates. (WT n=26 cells, 9 mice and KO n=26 cells, 7 mice, Mann-Whitney test, ** P=0.0066). Short-term synaptic plasticity of climbing fiber/Purkinje cell synapses was elicited by two consecutive stimulations at various intervals. No difference in the paired pulse ratios (PPR) was detected at any interval between *Susd4* KO mice and WT mice. Representative sample traces are presented. Mean \pm s.e.m. (WT n=12 cells, 3 mice and KO n=17 cells, 5 mice; Kolmogorov-Smirnov test, P=0.1666; see also **Figure S7**).
- (E) Delayed CF-EPSC quanta were evoked by CF stimulation in the presence of strontium instead of calcium to induce desynchronization of fusion events. Representative sample traces are presented. The cumulative probability for the amplitude of the events together with the individual amplitude values for each event show an increased amplitude associated with *Susd4* loss-of-function. Mean \pm s.e.m. (WT n=10 cells, 6 mice and KO n=8 cells, 3 mice; Kolmogorov-Smirnov distribution test, *** P<0.0001). The individual frequency values for each cell (measured as interevent interval, IEI) present no differences between the genotypes. Mean \pm s.e.m. (Mann-Whitney test, P=0.6334; see also **Figure S7**).

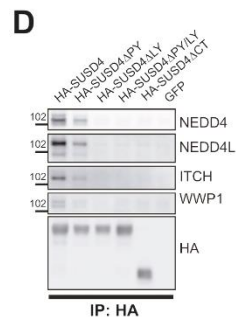
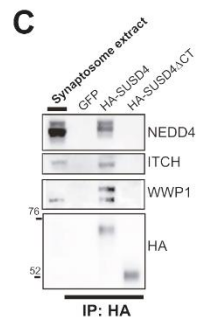
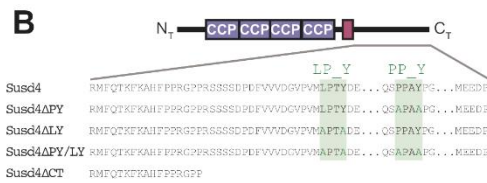
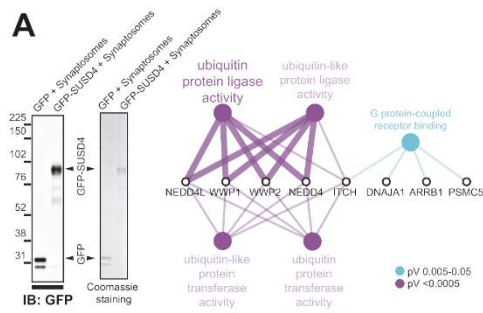


Figure 4. SUSD4 interacts with HECT E3 ubiquitin ligases.

- (A) Mass spectrometry identification of SUSD4 interactors. Left: Affinity-purification from cerebellar synaptosomes was performed using either GFP-SUSD4 as a bait or GFP as a control. Proteins were then resolved using SDS-PAGE followed by immunoblot for anti-GFP and coomassie staining of proteins. Right: Gene Ontology (GO) enrichment analysis network (Molecular Function category) of the 28 candidate proteins (Cytoscape plugin ClueGO) identified after affinity-purification of cerebellar synaptosomes using GFP-SUSD4 as a bait followed by LC MS/MS. The Ubiquitin ligase activity term is significantly enriched due in particular to the identification of several members of the NEDD4 family of HECT-ubiquitin ligase. See also **Table 1**.
- (B) Schematic representation of SUSD4 and different mutant constructs: SUSD4 Δ PY (point mutation of the PPxY site); SUSD4 Δ LY (point mutation of the LPxY); SUSD4 Δ PY/LY (double mutant at both PPxY and LPxY) and SUSD4 Δ C_r (lacking the cytoplasmic tail).
- (C) Affinity-purification experiments followed by western blot analysis confirm the interaction of full length SUSD4 (HA-tagged, HA-SUSD4) with members of the NEDD4 family. This interaction is lost when the C-terminal tail of SUSD4 is deleted (HA-SUSD4 Δ C_r) or when GFP is used instead of SUSD4 as a control.
- (D) HEK293 cells were transfected with HA-SUSD4 full length, HA-SUSD4 Δ PY, HA-SUSD4 Δ LY, HA-SUSD4 Δ PY/LY or HA-SUSD4 Δ C_r or control GFP. Immunoprecipitation was then performed with an anti-HA antibody and extracts were probed for co-immunoprecipitation of the HECT ubiquitin ligases NEDD4, NEDD4L, ITCH and WWP1.

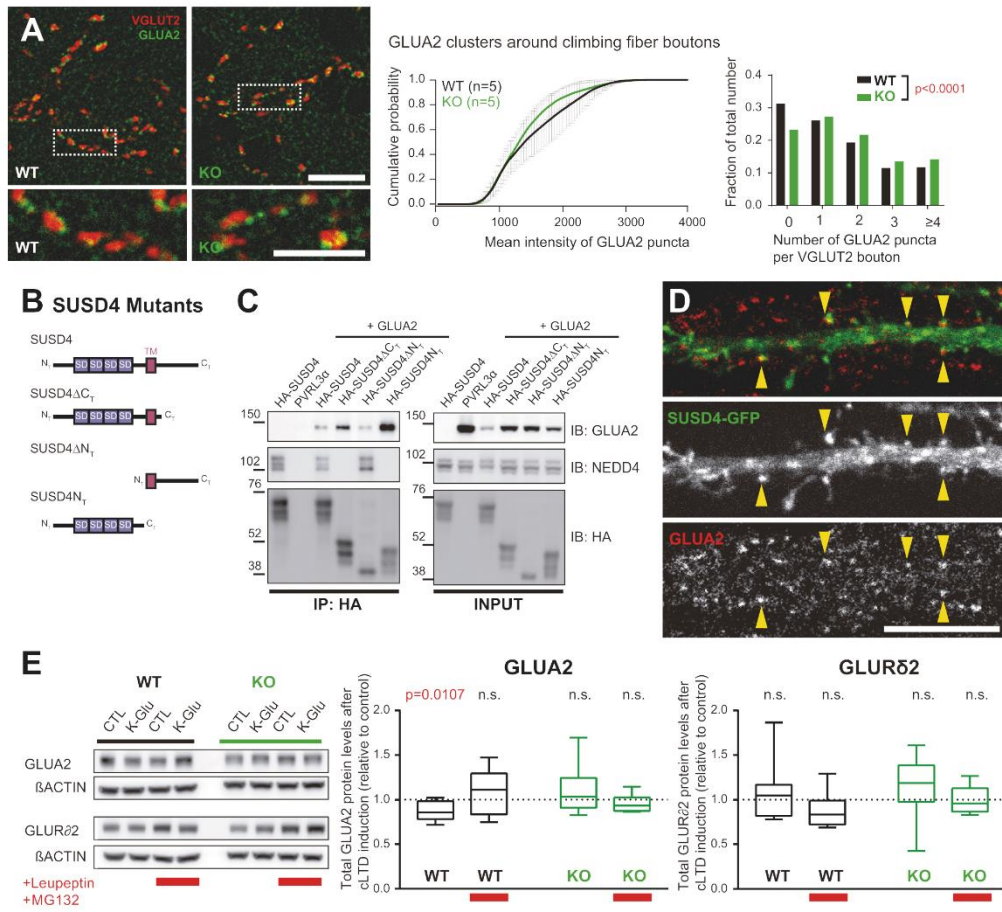


Figure 5. SUSD4 controls activity-dependent degradation of the AMPA receptor subunit GLUA2.

- (A) The number of GLUA2 clusters (anti-GLUA2 immunolabeling, green) per climbing fiber presynaptic bouton (anti-VGLUT2 immunolabeling, red) and their intensity was quantified in cerebellar sections of juvenile *Susd4* KO mice and WT littermates. Scale bars: 30 μm (top); 15 μm (bottom). Cumulative plot for the mean GLUA2 intensity per VGLUT2 bouton shows no significant change between WT and KO. Mean \pm s.e.m. (WT n= 5 and KO n= 5 mice. Kolmogorov-Smirnov test, $P=0.5009$). The distribution of the VGLUT2 boutons according to the number of associated GLUA2 clusters is significantly different between WT and KO (Chi-square contingency test, **** $P<0.0001$).
- (B) Schematic representation of SUSD4 and different mutant constructs: SUSD4 ΔC_7 (lacking the cytoplasmic tail), SUSD4 ΔN_7 (lacking the extracellular domains) and SUSD4 N_7 (lacking the transmembrane and intracellular domains).
- (C) SUSD4 interaction with GLUA2 and NEDD4. HEK293 cell extracts were transfected with HA-SUSD4 full length or HA-SUSD4 ΔC_7 , or SUSD4 ΔN_7 , or SUSD4 N_7 , or control PVRL3 α together with GLUA2. Immunoprecipitation was then performed with an anti-HA antibody and probed for co-immunoprecipitation of GLUA2 and the ubiquitin ligase NEDD4 (n=3 independent experiments).
- (D) Mouse hippocampal neurons were transfected at 13 days *in vitro* (DIV13) with a GFP-tagged SUSD4 construct and immunostained at DIV17 for green fluorescent protein (GFP, green) to localize SUSD4 and for the endogenous GLUA2 subunit (anti-GLUA2, red). The yellow arrowheads indicate the spines containing SUSD4 and GLUA2. Scale bar: 10 μm .
- (E) Activity-dependent degradation of GLUA2 was induced in cerebellar acute slices from *Susd4* WT mice using a protocol for chemical LTD (cLTD; K-Glu: K⁺ 50mM and glutamate 10 μM for 5 minutes followed by 30 minutes recovery). This degradation was absent when slices were incubated with 100 $\mu\text{g}/\text{mL}$ leupeptin and with 50 μM MG132 (to inhibit lysosomal and proteasome degradation, respectively), or when slices were obtained from *Susd4* KO mice. Band intensities of GLUA2 and GLUR δ 2 were normalized to β -ACTIN. The ratios between levels with cLTD induction (K-Glu) and without cLTD induction (CTL) are represented. Mean \pm s.e.m. Two-tailed Student's one sample t-test was performed on the ratios with a null hypothesis of 1, * $P=0.0107$, n.s.= not significant (n=8 independent experiments; see also **Figure S11**).

Supplementary Information

SUSD4 Controls Activity-Dependent Degradation of AMPA Receptor GLUA2 and Synaptic Plasticity

I. González-Calvo, K. Iyer, M. Carquin, A. Khayachi, F.A. Giuliani, J. Vincent, M. Séveno, S.M. Sigoillot, M. Veleanu, S. Tahraoui, M. Albert, O. Vigy, Y. Nadjar, A. Dumoulin, A. Triller, J.-L. Bessereau, L. Rondi-Reig, P. Isope, F. Selimi*

* Correspondence to: fekrije.selimi@college-de-france.fr

Supplementary Information:

Table S1

Figures S1 to S11

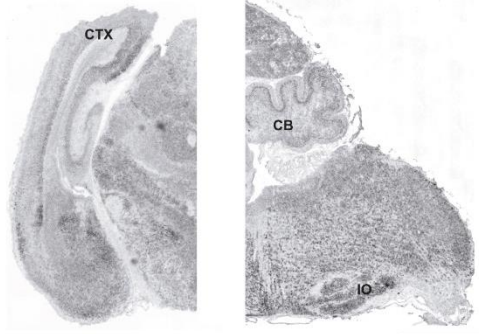
STAR Methods

Supplementary references

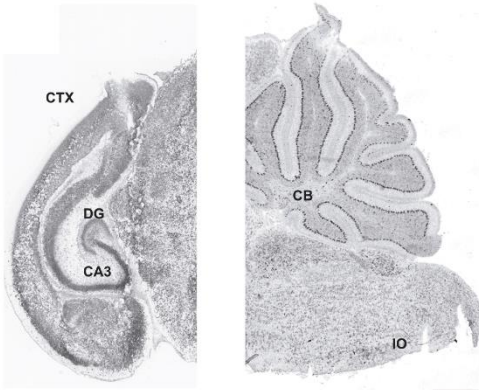
Table Supplementary 1. Behavioral characterization of *Susd4* KO mice. From three month-old *Susd4* KO and *wild type* mice.

	WT		<i>Susd4</i> KO	
<i>Physical Characteristics</i>				
Weight (g)	24,1	± 2,91	24,7	± 3,45
Whiskers (% with)	80	%	83,3	%
Palpebral Closure (% with)	0	%	0	%
Piloerection (% with)	20	%	25	%
<i>Sensorimotor Reflexes</i>				
<i>(% subjects displaying "normal response")</i>				
Cage movement	100	%	100	%
Whisker response	100	%	100	%
Eye Blink	100	%	100	%
Ear Twitch	100	%	100	%
<i>Motor Responses</i>				
Open Field Locomotion				
Improvement (number)	21,92	± 2,83	19,42	± 2,03
Distance (cm)	2653,84	± 230,25	2300,68	± 158,47
Speed (cm/s)	12,79	± 0,41	13,06	± 0,30
Time on Center (%)	12,76	± 1,30	11,18	± 1,26

A P0



B P7



C Adult

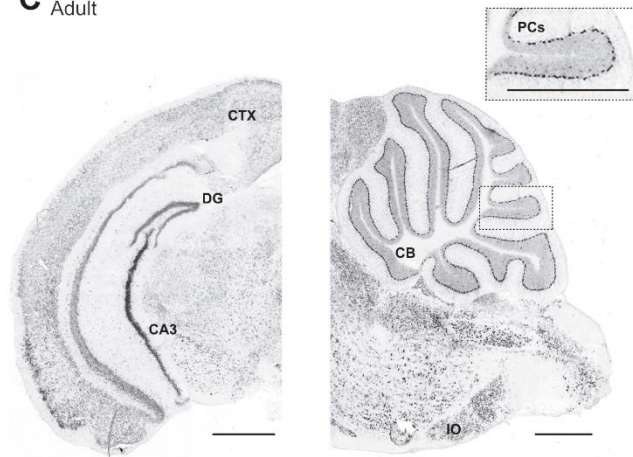


Figure Supplementary 1. *Susd4* mRNA expression in the developing mouse brain.

- (A) *Susd4* mRNA expression was visualized in the brain of wild-type mouse by *in situ* hybridization. Coronal (left) and sagittal (right) sections are presented at postnatal day 0,
- (B) postnatal day 7 and
- (C) postnatal day 30. *Susd4* expression was found in many regions including the cerebral cortex (CTX), the dentate gyrus (DG) and CA3 regions in the hippocampus (coronal section), the cerebellum (CB), in particular Purkinje cells (PCs), and the inferior olive (IO; sagittal section, right). Scale bars: 250 μ m (A, B) and 500 μ m (C).

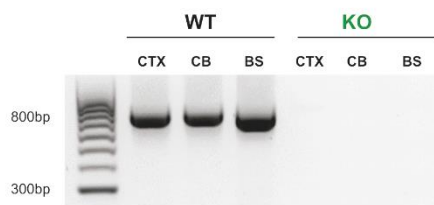
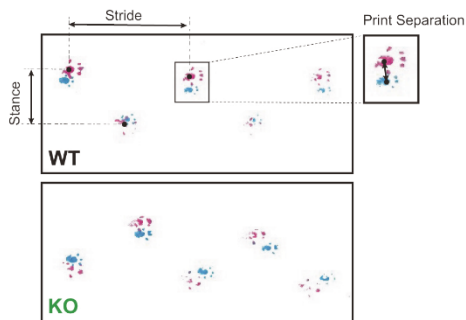


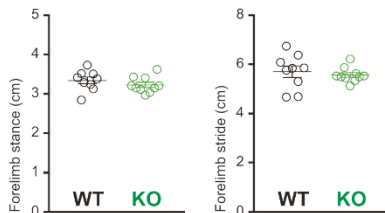
Figure Supplementary 2. Characterization of *Susd4* knockout mice.

Susd4 expression was assessed by RT-PCR in extracts from cortex (CTX), cerebellum (CB) and brainstem (BS) in control and *Susd4* KO mice.

Footprint Test



FORELIMB



HINDLIMB

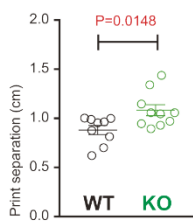
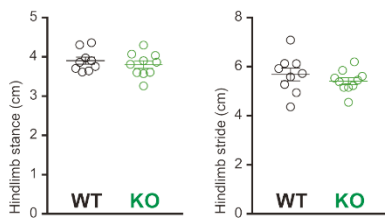


Figure Supplementary 3. Footprint analysis and motor correlations in *Susd4* KO mice.

Footprint patterns of P30 wild-type and KO mice were quantitatively analyzed by measuring stride length for the fore paws (pink) and hind paws (blue), stance length for the forelimbs and hindlimbs, and print separation. Mean \pm s.e.m. (WT n=9 and KO n=10 mice; Forelimb stance, unpaired Student's t-test, P=0.3059; Forelimb stride, P=0.5882; Hindlimb stance, P=0.4533; Hindlimb stride, P=0.3580; Print separation, * P=0.0148).

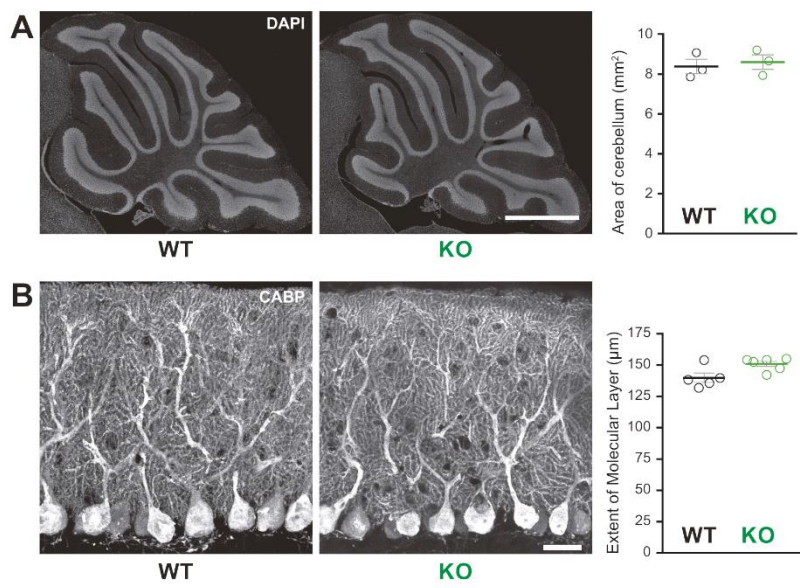


Figure Supplementary 4. Normal cerebellar cytoarchitecture in *Susd4* KO mice.

- (A) Parasagittal sections of P30 wild-type and KO cerebella were stained with Hoechst
(B) and calbindin protein (CABP) immunostaining and used for quantitative analysis of the mean area of the cerebellum. (Mean \pm s.e.m; WT n=3 and KO n=3 mice, unpaired Student's t-test, P=0,4932) and of the height of the molecular layer (Mean \pm s.e.m. WT n=5 and KO n=6 mice; unpaired Student's t-test, P=0,1157), respectively. Scale bars: 500 μ m (A) and 30 μ m (B).

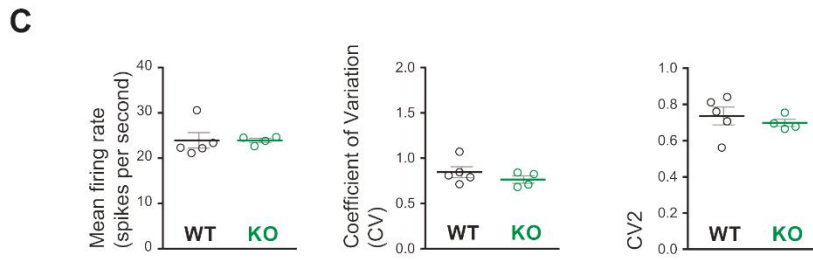
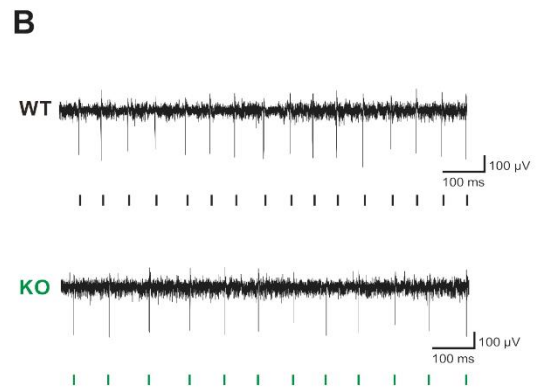
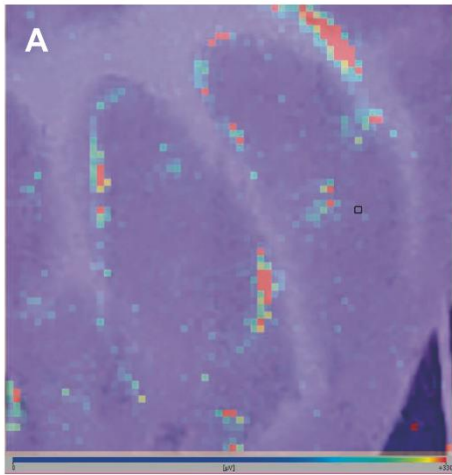


Figure Supplementary 5. High density microelectrode array (MEA) analysis of Purkinje cell spiking in acute cerebellar slices from *Susd4* KO compared to WT.

- (A) Image of the cerebellar acute slice overlapped with the image of the color map of the MEA recording. Each pixel represents one channel, where the active units are in red.
- (B) Representative traces of electrical activity recorded in one channel. Each tick represents one action potential that has been detected and sorted by the Brainwave software.
- (C) Histograms of the mean firing rate, coefficient of variation of Inter Spike Intervals (CV) and CV2. (Mean \pm s.e.m.; WT n=5 mice and KO n=4 mice; Mean Firing Rate: Mann Whitney test, P=0.2857; Coefficient of Variation: Mann Whitney test, P=0.4127; CV2: Mann Whitney test, P=0.5373).

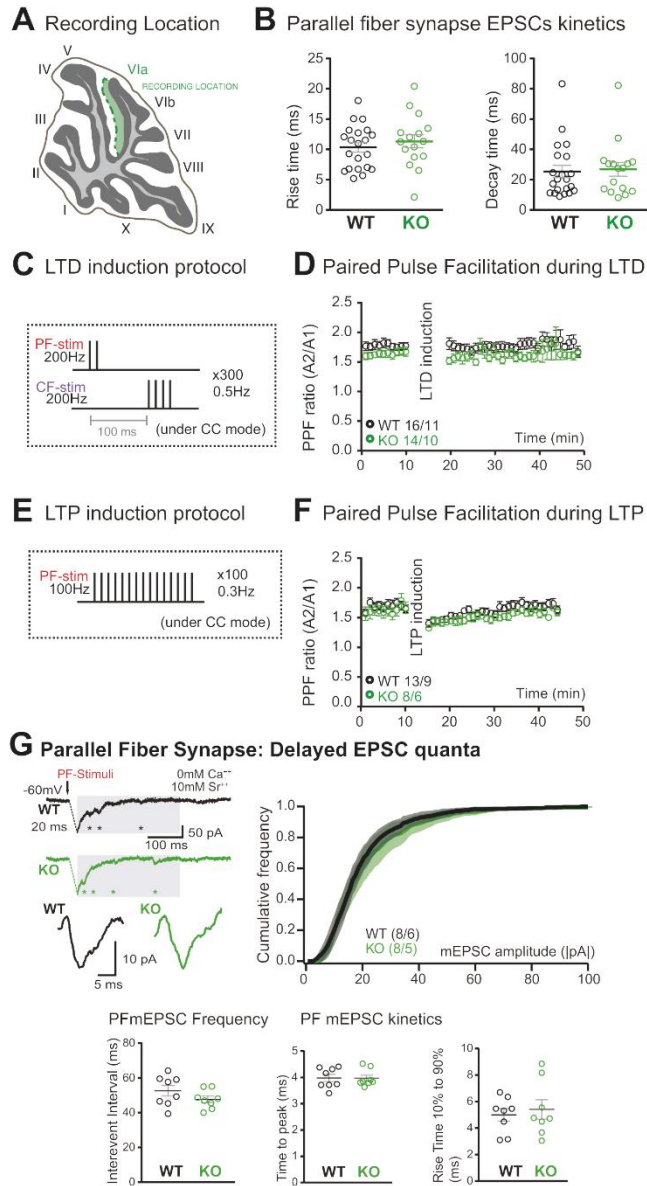
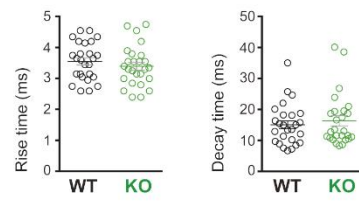


Figure Supplementary 6. Parallel fiber/Purkinje cell synapse EPSCs kinetics, long-term plasticity induction protocols, paired-pulse facilitation ratio and delayed EPSC quanta.

- (A) Schematic representation of the recording location, internal lobule VIa of the vermis.
- (B) No change in the decay and rise time of Parallel fiber/Purkinje cell synapse EPSCs was induced by *Susd4* deletion. (Mean \pm s.e.m.; WT n=21 cells/8 mice and KO n=16 cells/6 mice; Decay time: Mann Whitney test, P=0.7276; Rise time: unpaired Student's t-test, P=0.4570).
- (C) Parallel fiber long-term depression induction protocol.
- (D) Paired-pulse ratio (A2/A1) measured at 20 Hz (Mean \pm s.e.m. WT n=16 cells/11 mice and KO n=14 cells/10 mice, two-way ANOVA with repeated measures, Interaction (time and genotype): P=0.9935, F(39, 1092) = 0.5222).
- (E) Parallel fiber long-term potentiation induction protocol.
- (F) Paired-pulse ratio (A2/A1) measured at 20Hz (Mean \pm s.e.m. WT n=13 cells/9 mice and KO n=8 cells/6 mice, two-way ANOVA with repeated measures, Interaction (time and genotype): P=0.9366, F(39, 741) = 0.6745).
- (G) Delayed PF-EPSC quanta were evoked by PF stimulation in the presence of strontium instead of calcium to induce desynchronization of fusion events. Representative sample traces are presented. The cumulative probability for the amplitude shows no difference with *Susd4* loss-of-function. Mean \pm s.e.m. (WT n=8 cells, 6 mice and KO n=8 cells, 5 mice; Kolmogorov-Smirnov distribution test, P=0.1667). The individual frequency values for each cell (measured as interevent interval) present no differences between the genotypes. Mean \pm s.e.m. (Mann Whitney test, P=0.1913). No change in the time to peak and in the rise time of PF/PC synapse delayed EPSC quanta was induced by *Susd4* deletion. (Mean \pm s.e.m. WT n=8 cells/6 mice and KO n=8 cells/5 mice; Time to peak: Mann Whitney test, P=0.6454; Rise time 10% to 90%: unpaired Student's t-test, P=0.6486).

A Climbing fiber synapse EPSCs kinetics



B Climbing fiber synapse mEPSCs kinetics

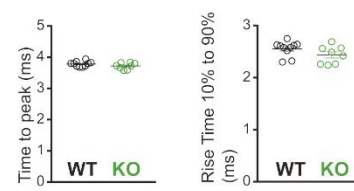


Figure Supplementary 7. Kinetics of the climbing fiber/Purkinje cell synapse EPSC.

- (A) No change in the rise and decay times of climbing fiber/Purkinje cell synapse EPSCs was induced by *Susd4* deletion. (Mean \pm s.e.m. WT n=26 cells/9 mice and KO n=26 cells/7 mice; Rise time: unpaired Student's t-test, P=0.3750; Decay time: Mann Whitney test, P=0.7133).
- (B) No change in the time to peak and in the rise time of CF/PC synapse delayed EPSC quanta was induced by *Susd4* deletion. (Mean \pm s.e.m. WT n=10 cells/6 mice and KO n=8 cells/3 mice; Time to peak: unpaired Student's t-test, P=0.1692; Rise time 10% to 90%: Mann Whitney test, P=0.0639).

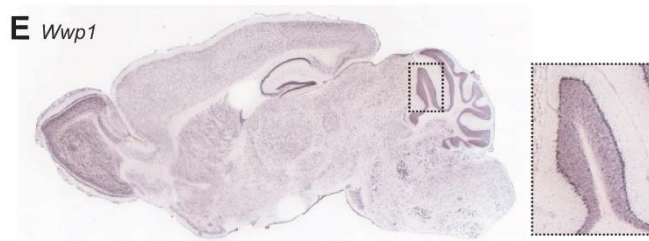
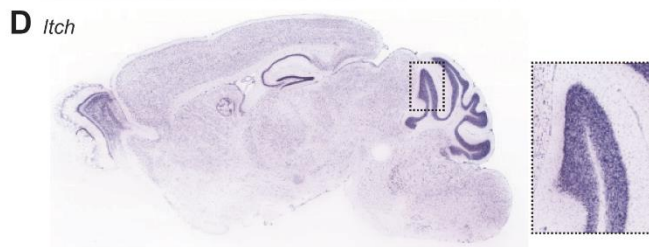
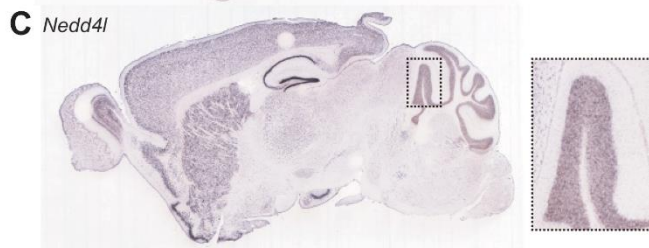
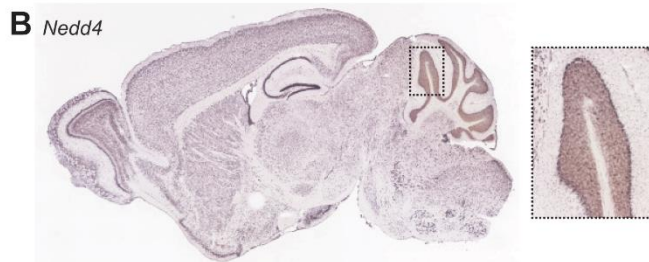
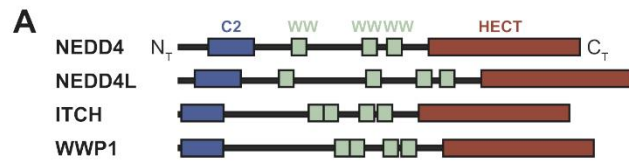


Figure Supplementary 8. Expression of HECT ubiquitin ligases in adult mouse brain.

- (A) Schematic representation of four SUSD4 interactors: NEDD4, NEDD4L, ITCH and WWP1. Legends: N, N-terminus; HECT, Homologous to the E6-AP C-terminus domain; C, C-terminus.
- (B) Pattern of expression of *Nedd4* (RP_050712_03_C08),
- (C) *Nedd4l* (RP_040625_01_G10),
- (D) *Itch* (RP_050222_01_H06) and
- (E) *Wwp1* (RP_050510_02_E12) mRNA in the adult mouse brain. From Allen Brain Atlas (www.brain-map.org).

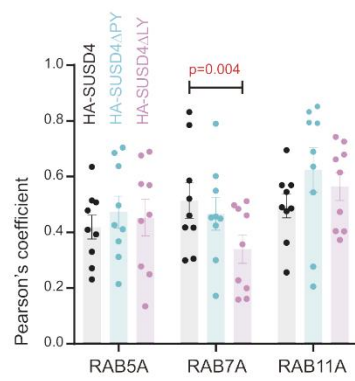
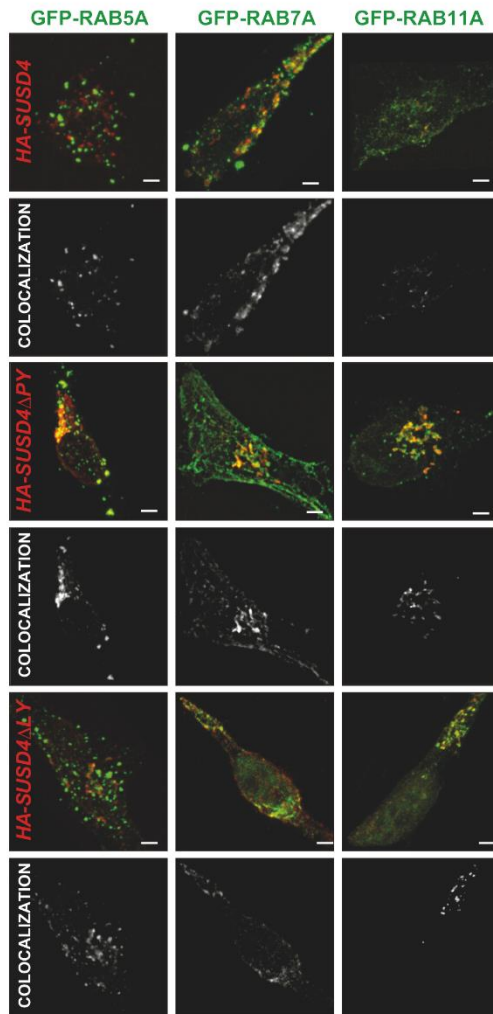


Figure Supplementary 9. SUSD4 *in vitro* localization in intracellular compartments.

Representative images of HeLA cells transfected with HA-SUSD4, HA-SUSD4 Δ PY or HA-SUSD4 Δ LY together with the early endosomal marker (RAB5a-GFP, clathrin coated pits), the late endosomal and lysosomal marker (RAB7a-GFP) or the recycling endosomal marker (RAB11a-GFP). Colocalization between SUSD4 constructs (red; anti-HA) and the endosomal compartment markers (green; anti-GFP) channels was measured using the Pearson's correlation coefficient. Mean \pm s.e.m. (n=9 cells from 3 independent experiments).

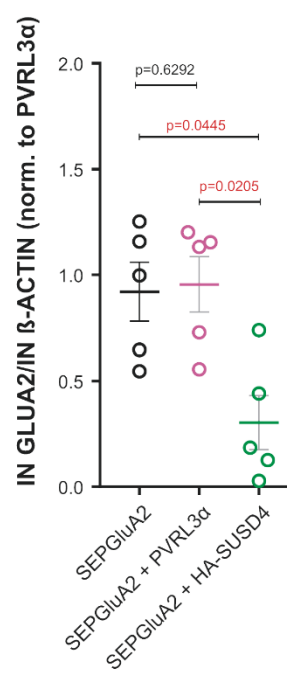


Figure Supplementary 10. SUSD4 overexpression in transfected cells reduces total GLUA2 levels.

HEK293 cells were transfected with SEPGLUA2 alone or with the control transmembrane protein PVRL3 or with HASUSD4. The levels of GLUA2 were quantified. Mean \pm s.e.m. (5 independent experiments).

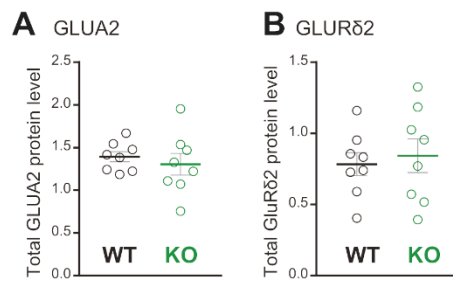


Figure Supplementary 11. Total GLUA2 levels after modulation of SUSD4 expression.

- (A) Mean total protein levels (normalized to β -Actin) of GLUA2 and
(B) GLUR δ 2 (GRID2) were not changed in cerebellar slices in basal conditions. Mean \pm s.e.m. (n=8; unpaired Student's t-test; GLUA2: P=0.5424; GLUR δ 2: P=0.6821).

STAR Methods

Animals

Susd4 knockout mice were generated and maintained on the C57BL/6J background (generated by Lexicon Genetics Incorporated, The Woodlands, USA). Out of the 8 *Susd4* exons, coding exon 1 (NCBI accession NM_144796.2) and the 5'UTR (NCBI accession BM944003) were targeted by homologous recombination. This resulted in the deletion of a 1.3kb sequence spanning the transcription initiation site and exon 1 (**Figure 1D**). Subsequent genotyping of mice was performed using PCR to detect the wild-type allele (Forward primer: 5' CTG TGG TTT CAA CTG GCG CTG TG 3'; reverse primer 5'GCT GCC GGT GGG TGT GCG AAC CTA 3') or the targeted allele (forward primer 5'TTG GCG GTT TCG CTA AAT AC 3'; reverse primer 5' GGA GCT CGT TAT CGC TAT GAC 3'). The Htr5b-GFP mouse line was used for labeling of climbing fibers (The Gene Expression Nervous System Atlas (GENSAT) Project, NINDS Contracts N01NS02331 & HHSN271200723701C to The Rockefeller University (New York, NY)). Genotyping was performed using the following primers: 5'-TTG GCG CGC CTC CAA CAG GAT GTT AAC AAC-3'; 5'-CGC CCT CGC CGG ACA CGC TGA AC-3'. The L7Cre mouse line was obtained from Jackson laboratories (B6.129-Tg(Pcp2-cre)2Mpin/J ; Stock Number: 004146) and genotyping was performed using the following primers: 5' GGT GAC GGT CAG TAA ATT GGA C 3'; 5' CAC TTC TGA CTT GCA CTT TCC TTG G 3'; 5' TTC TTC AAG CTG CCC AGC AGA GAG C 3'. All animal protocols were approved by the *Comité Régional d'Ethique en Experimentation Animale* (no. 00057.01) and animals were housed in authorized facilities of the CIRB (# C75 05 12).

Antibodies

The following primary antibodies were used: mouse monoclonal anti-CABP (1:1000; Swant, Switzerland, Cat#300), rabbit polyclonal anti-CABP (1:1000; Swant, Cat#CB38), mouse monoclonal anti-GFP (1:1000; Abcam, Cambridge, United Kingdom, Cat#ab1218), rabbit polyclonal anti-GFP (1:1000; Abcam, Cat#ab6556), mouse monoclonal anti-GluR2 (clone 6C4; 1:500; Millipore, Massachusetts, USA, Cat#MAB397 and BD, New Jersey, USA, Cat#556341), rabbit polyclonal anti-GLUR δ 1/2 (1:1000; Millipore, Cat#AB2285), rat monoclonal anti-HA (1:1000; Roche Life Science, Penzberg, Upper Bavaria, Germany, Cat#11867423001), rabbit monoclonal anti-ITCH (1:1000; Cell Signaling Technology, Massachusetts, USA, Cat#12117), rabbit polyclonal anti-NEDD4 (1:10000; Millipore, Cat#07-049), guinea pig polyclonal anti-VGLUT1 (1:5000; Millipore, Cat#AB5905), guinea pig polyclonal anti-VGLUT2 (1:5000; Millipore, Cat#AB2251) and rabbit polyclonal anti-WWP1 (1:2000; Proteintech, Chicago, USA, Cat#13587-1-AP).

The following secondary antibodies were used: donkey polyclonal anti-Goat Alexa Fluor 568 (1:1000; Invitrogen, California, USA, Cat#A11057), donkey anti-Mouse Alexa Fluor 488 (1:1000; Invitrogen, Cat#R37114), donkey polyclonal anti-Mouse Alexa Fluor 568 (1:1000; Invitrogen, #A10037), donkey polyclonal anti-Rabbit Alexa Fluor 488 (1:1000; Invitrogen, Cat#A21206), donkey polyclonal anti-Rat Alexa Fluor 594 (1:1000; Invitrogen, #A21209), donkey polyclonal anti-Rat Alexa Fluor 568 (1:1000; Abcam, Cat#175475), goat polyclonal anti-Guinea Pig Alexa Fluor 488 (1:1000; Invitrogen, Cat#A110-73), goat polyclonal anti-Guinea Pig Alexa Fluor 647 (1:1000; Invitrogen, Cat#A21450), goat polyclonal anti-Mouse HRP (1:20000; Jackson Immune Research Laboratories, Pennsylvania, USA, Cat#115-035-174), goat polyclonal

anti-rat HRP (1:20000; Jackson Immune Research Laboratories, #112-035-175) and mouse polyclonal anti-rabbit HRP (1:20000; Jackson Immune Research Laboratories, #211-032-171).

The following conjugated antibodies were used: sheep polyclonal anti-digoxigenin alkaline phosphatase (1:2000 - 1:5000; Roche, Cat#11093274910), mouse monoclonal anti-βactin (clone AC-15) HRP (1:25000; Abcam, Cat#ab49900), rabbit polyclonal anti-GFP Alexa Fluor 647 (1:1000; Invitrogen, Cat#A31852), mouse monoclonal anti-GluR2 (clone 6C4) Alexa Fluor 488 (1:1000; Millipore, Cat#MAB397A4) and mouse monoclonal anti-HA (clone 2-2.2.14) DyLight 650 (1:1000; Thermo Fisher Scientific, Cat#26183-D650).

Plasmids

Full-length *Susd4* was cloned into the mammalian expression vector pEGFP-N1 (Addgene, Massachusetts, USA, Cat#6085-1) to express a SUSD4-GFP fusion construct under the control of the CMV promoter (pSUSD44-GFP). An N-terminal HA tag was inserted just after the signal peptide (pHA-Susd4-GFP). pHA-SUSD4 was obtained by removal of the C terminal GFP of pHA-SUSD4-GFP. A truncated form of *Susd4*, HA-SUSD4-ΔC_T, was obtained by inserting a stop codon downstream of the sixth exon, 39bp after the transmembrane domain using PCR on the pHA-SUSD4-GFP plasmid and the following primers: forward primer 5' GCG CTA GCG ATG TAT CCT TAT GAT GTT CCT G3'; reverse primer 5'TAG CGG CCG CTA TTA GGG GGG GAA GTG GGC CTT3'. Other mutant constructs were similarly obtained similarly : the truncated form HA-SUSD4-ΔN_T corresponding to aminoacids 294-490, and the extracellular form of *Susd4* HA-SUSD4-N_T corresponding to aminoacids 2-299. The HA-SUSD4-ΔPY contained a mutation in aminoacids 411 and 414 changing PPAY to APAA, HA-SUSD4-ΔLY in aminoacids 376 and 379 changing LPTY to APTA. Mutagenesis was performed using the QuikChange Lightning Multi site directed mutagenesis kit (agilent, Cat#210513) according to the manufacturer's instructions. The plasmid pIRES2-eGFP (Addgene, Cat#6029-1) was used as transfection control. The plasmid SEPGluA2 (Addgene, Cat#24001) was used to follow GLUA2. The control transmembrane protein PVRL3α was cloned into the mammalian expression vector pCAG-mGFP (Addgene, Cat#14757) to express the protein under the pCAG promoter (pCAG-PVRL3α). Rab4a-GFP, Rab5a-GFP, Rab7a-GFP and Rab11a-GFP were kindly provided by Dr. Bruno Goud.

Viral mediated *in vivo* expression of HA-SUSD4

AAV2 particles were generated using a hSYN-DIO-HA-SUSD4-2A-eGFP-WPRE construct (Vector biolabs, Malvern, USA) and injected stereotaxically in cerebella of adult mice expressing the CRE recombinase in cerebellar Purkinje cells (using the L7Cre mice). In the absence of Cre expression, the transgene is not produced. In the presence of Cre expression, the transgene will be "FLip-EXchanged" leading to expression of the transgene.

***In situ* hybridization**

Fresh frozen 20μm thick-sections were prepared using a cryostat from brains of *Susd4* WT and KO mice at P0, P7 or P21. The probe sequence corresponded to the nucleotide residues 287-1064 bp for mouse *Susd4* (NM_144796.4) cDNA. The riboprobes were used at a final concentration of 0,05 μg/μL, and hybridization was done overnight at a temperature of 72°C. The anti-digoxigenin-AP antibody (for details see antibodies in supplemental information) was used at a dilution of 1:5000. Alkaline phosphatase detection was done using BCIP/NBT colorimetric revelation (Roche, Cat#11681451001).

Behavioral Study

12-14 weeks old male mice were used in this study. They were housed in groups of 3-5 in standard conditions: 12h. light/dark cycle, with *ad libitum* food and water access. Seven days before the beginning of behavioral test, mice were housed individually to limit inter-houses variability resulting from social relationships. All behavioral test took place in the light cycle.

S.H.I.R.P.A. protocol: Mice performed a series of tests to ensure their general good health and motor performance and habituate them to being manipulated (Crawley, 2006). The test includes observation of appearance, spontaneous behavior, neurological reflexes, anxiety, motor coordination, balance rotarod and muscular strength tests and were performed within five days. Individuals presenting deficits during the S.H.I.R.P.A. protocol were not used for other behavioral tests.

Footprint analysis: The fore and hind paws of mice were dipped in blue and pink non-toxic paint, respectively. Mice were allowed to walk through a rectangular plastic tunnel (9cm W x 57cm L x 16cm H), whose floor was covered with a sheet of white paper. Habituation was done the day before the test. 5 footsteps were considered for the analysis. Footprints were scanned and length measurements were made using ImageJ.

Rotarod: Mice were first habituated to the rotarod apparatus, three days before the acceleration test. The habituation protocol consists of 5 minutes at 4 r.p.m. To evaluate the motor coordination, mice were placed on immobile rotarod cylinders, which ramped up from 0 to 45 rotations per minute in 10 minutes. The timer was stopped when the mouse fell off the cylinder or did a whole turn with it. For a given session, this procedure was repeated three times per day separated by 60 minutes. The session was repeated during five consecutive days.

Whole-cell patch-clamp on acute cerebellar slices

Responses to PF and CF stimulation were recorded in Purkinje cells of the lobule VI in acute parasagittal and horizontal (LTP experiments) cerebellar slices from *Susd4* KO juvenile (from P25 to P35) or adult (~P60) mice. *Susd4* WT littermates were used as controls. Mice were anesthetized using isoflurane 4% and sacrificed by decapitation. The cerebellum was dissected in ice cold oxygenated (95% O₂ and 5% CO₂) Bicarbonate Buffered Solution (BBS) containing (in mM): NaCl 120, KCl 3, NaHCO₃ 26, NaH₂PO₄ 1.25, CaCl₂ 2, MgCl₂ 1 and D(+)-glucose 35. 300µm-thick cerebellar slices were cut with a vibratome (Microm 650 V; Thermo Scientific Microm, Massachusetts, USA) in slicing solution (in mM): N-Methyl-D-Glucamine 93, KCl 2.5, NaH₂PO₄ 1.2, NaHCO₃ 30, HEPES 20, D(+)-Glucose 25, MgCl₂ 10, sodium ascorbate 5, Thiourea 2, sodium pyruvate 3, N-acetyl-cystein 1, Kynurenic acid 1 and CaCl₂ 0.5 (pH 7.3). Immediately after cutting, slices were allowed to briefly recover at 37°C in the oxygenated sucrose-based buffer (in mM): sucrose 230, KCl 2.5, NaHCO₃ 26, NaH₂PO₄ 1.25, D(+)-glucose 25, CaCl₂ 0.8 and MgCl₂ 8. D-APV and minocycline at a final concentration of 50µM and 50nM respectively were added to the sucrose-based buffer. Slices were allowed to fully recover in bubbled BBS at 37°C for at least 40 minutes before starting the experiment. Patch clamp borosilicate glass pipettes with 3-6MΩ resistance were filled with the following internal solutions:

1. Cesium metanesulfonate solution (CsMe solution, for EPSC elicited from CF and PF), containing (in mM) CsMeSO₃ 135, NaCl 6, MgCl₂ 1, HEPES 10, MgATP 4, Na₂GTP 0.4, EGTA 1.5, QX314Cl 5, TEA 5 and Biocytin 2.6 (pH 7.3).

2. CsMe S-solution (for delayed EPSC quanta events), containing (in mM): CsMeSO₃ 140, MgCl₂ 0.5, HEPES 10, MgATP 4, Na₂GTP 0.5, BAPTA 10 and Neurobiotin 1% (pH 7.35).

3. Potassium Gluconate solution (KGLu solution, for PF long-term plasticity), containing (in mM): K Gluconate 136, KCl 10, HEPES 10, MgCl₂ 1, Sucrose 16, MgATP 4 and Na₂GTP 0.4 (pH 7.35).

Stimulation electrodes with ~5 MΩ resistances were pulled from borosilicate glass pipettes and filled with BBS. Recordings were performed at room temperature on slices continuously perfused with oxygenated BBS. The experiment started at least 20 minutes after the whole-cell configuration was established. The Digitimer DS3 (Digitimer Ltd, Hertfordshire, UK) stimulator was used to elicit CF and PF and neuronal connectivity responses in Purkinje cells. Patch-clamp experiments were conducted in voltage clamp mode (except for the LTP and LTD induction protocols that were made under current clamp mode) using a MultiClamp 700B amplifier (Molecular Devices, California, USA) and acquired using the freeware WinWCP written by John Dempster (<https://pureportal.strath.ac.uk/en/datasets/strathclyde-electrophysiology-software-winwcp-winedr>). Series resistance was compensated by 60-100% and cells were discarded if significant changes were detected. Currents were low-pass filtered at 2.2kHz and digitized at 20kHz.

CF and PF-EPSC experiments: To isolate the AMPARs current, the BBS was supplemented with (in mM) picrotoxin 0.1, D-AP5 10, CGP52432 0.001, JNJ16259685 0.002, DPCPX 0.0005 and AM251 0.001. CF and PF EPSCs were monitored at a holding potential of -10mV. During CF recordings, the stimulation electrode was placed in the granule cell layer below the clamped cell; CF-mediated responses were identified by the typical all-or-none response and strong depression displayed by the second response elicited during paired pulse stimulations (20Hz). The number of CFs innervating the recorded PC was estimated from the number of discrete CF-EPSC steps. PF stimulation was achieved by placing the stimulation electrode in the molecular layer at the minimum distance required to avoid direct stimulation of the dendritic tree of the recorded PC. The input-output curve was obtained by incrementally increasing the stimulation strength. Peak EPSC values for PF were obtained following averaging of three consecutive recordings, values for CF-EPSC correspond to the first recording. Short-term plasticity experiments were analyzed using a software written in Python by Antoine Valera (<http://synaptiqs.wixsite.com/synaptiqs>).

PF-Long-term plasticity experiments: Purkinje cells (PCs) were clamped at -60 mV. Each PF-induced response was monitored by a test protocol of paired stimulation pulses (20Hz) applied every 20 seconds. A baseline was established during 10 minutes of paired-pulse stimulation in the voltage clamp configuration. After that, an induction protocol was applied in current-clamp mode with cells held at -60mV. During LTD induction, the PFs were stimulated with two pulses at high frequency (200Hz) and, after 100ms, the CF was stimulated with four pulses at high frequency (200Hz) repeated every 2 seconds for a period of 10 minutes. During LTP induction, the PFs were stimulated with bursts of 15 pulses at high frequency (100 Hz) repeated every 3 seconds for a period of 5 minutes (Binda *et al.*, 2016). Then, PCs were switched to the voltage clamp mode and paired stimulation pulses applied again, lasting 40 minutes. All the data were normalized to the mean baseline. Long-term plasticity was analyzed with the software Igor Pro 6.05 (WaveMetrics INC, Oregon, USA).

PF and CF delayed EPSC quanta events: were detected and analyzed using the software Clampfit 10.7 (Molecular Devices). PF- and CF-delayed EPSC quanta superposed events were discarded manually based on the waveform. A threshold of 10pA for minimal amplitude was used to select the CF events. 100 (PF) and 300 (CF) events for each neuron were studied by analyzing consecutive traces.

High density microelectrode array (MEA) analysis of Purkinje cell spiking in acute cerebellar slices

Experiments were performed on acute cerebellar slices obtained from 3-6 months-old mice in artificial cerebrospinal fluid (ACSF) containing (in mM): NaCl 125, KCl 2.5, D(+)Glucose 25, NaHCO₃ 25, NaH₂PO₄ 1.25, CaCl₂ 2, and MgCl₂ 1 and oxygenated (95% O₂ and 5% CO₂). Parasagittal slices (320µm) were cut at 30°C (Huang and Uusisaari, 2013) with a Campden Ci 7000 smz microtome at an advance speed of 0.03mm/s and vertical vibration set to 0.1 – 0.3µm. Slices were then transferred to a chamber filled with oxygenated ACSF at 37°C and allowed to recover for 1h before recordings.

For recording, the slices were placed over a high-density micro electrode array of 4096 electrodes (electrode size, 21 × 21µm; pitch, 42µm; 64 × 64 matrix; Biocam X, 3Brain, Wädenswil, Switzerland), and constantly perfused with oxygenated ACSF at 37°C. Extracellular activity was digitized at 17 kHz and data were analyzed with the Brainwave software from 3Brain. The signal was filtered with a butterworth high-pass filter at 200 Hz, spikes were detected with a hard threshold set at -100µV, and unsupervised spike sorting was done by the software. We selected units with a firing rate between 15 and 100 spikes per second and we excluded units presenting more than 5% of refractory period violation (set to 3ms). Recordings were performed on two slices per animal, each slice containing between 20 and 200 active neurons, and results were then pooled for each animal.

To quantify the average variability in the firing rate, the coefficient of variation (CV) of the ISI (interspike interval in seconds) was calculated as the ratio of the standard deviation (SD) of ISIs to the mean ISI of a given cell. To measure the firing pattern variability within a short period of two ISIs, CV2 was calculated [$CV2 = 2|ISI_{n+1} - ISI_n| / (ISI_{n+1} + ISI_n)$] (Holt and Douglas, 1996).

Affinity-purification of SUSD4 interactors from synaptosome preparations

HEK293H (Gibco, Cat#11631-017) were maintained at 37°C in a humidified incubator with 5% CO₂ in Dulbecco's Modified Eagle's Medium (DMEM; containing high glucose and glutamax, Life Technologies, Cat#31966047) supplemented with 10% fetal bovine serum (Gibco, Cat#16141-079), and 1% penicillin/streptomycin (Gibco, Cat#15140122). 10⁶ cells were plated per well in a 6-well plate and transfected 24 hours after plating with the indicated plasmids (1µg plasmid DNA per well) using Lipofectamine 2000 (Life Technologies, Cat#11668) according to manufacturer's instructions.

Forty-eight hours after transfection, cells were lysed and proteins were solubilized for 1h at 4°C under gentle rotation in lysis buffer (10 mM Tris-HCl pH7.5, 10 mM EDTA, 150 mM NaCl, 1% Triton X100, 0.1% SDS) supplemented with a protease inhibitor cocktail (1:100; Sigma, Cat#110205) and MG132 (100µM; Sigma, Cat#C2211). Lysates were sonicated for 10 seconds, further solubilized for one hour at 4°C and clarified by centrifugation at 6,000 rpm during 8 minutes. Supernatants were collected, incubated with 5 µg of rat monoclonal anti-HA antibody (for details see antibodies), together with 60 µL of protein G-sepharose beads (Sigma;

Cat#10003D) for 3 hours at 4°C, to coat the beads with the HA-tagged SUSD4 proteins. When SUSD4-GFP was expressed for affinity-pulldowns, GFP-Trap was done according to the instructions of GFP-Trap®_A (Chromotek, New York, USA, Cat#ABIN509397). Coated beads were washed 3 times with 1 mL lysis buffer.

To prepare synaptosome fractions, cerebella from WT mice (P30) were homogenized at 4°C in 10 volumes (w/v) of 10mM Tris buffer (pH7.4) containing 0.32M sucrose and protease inhibitor cocktail (1:100). The resulting homogenate was centrifuged at 800 g for 5min at 4°C to remove nuclei and cellular debris. Synaptosomal fractions were purified by centrifugation for 20 min at 20,000 r.p.m. (SW41Ti rotor) at 4°C using Percoll-sucrose density gradients (2-6-10-20%; v/v). Each fraction from the 10–20% interface was collected, washed in 10 mL of a 5 mM HEPES buffer pH 7.4 (NaOH) containing 140 mM NaCl, 3 mM KCl, 1.2 mM MgSO₄, 1.2 mM CaCl₂, 1 mM NaH₂PO₄, 5 mM NaHCO₃, 10 mM D(+)-Glucose by centrifugation. The suspension was immediately centrifuged at 1x10⁴ g at 4°C for 10min. Synaptosomes in the pellet were resuspended in 100 µL in lysis buffer (10 mM Tris-HCl pH7.5, 10 mM EDTA, 150 mM NaCl, 1% Tx) supplemented with a protease inhibitor cocktail (1:100) and MG132 (100µM). Lysates were sonicated for 10 seconds, and further incubated for one hour at 4°C. HA-SUSD4 or GFP-SUSD4 coated beads were then incubated with the synaptosomal lysates for three hours at 4°C. Beads were washed three times with lysate buffer supplemented with 0.1% SDS. Bound proteins were eluted for 10 minutes at 75°C using Laemmli buffer (160mM Tris pH6.8, 4% SDS, 20% glycérol, 0.008% BBP) with 5% beta mercaptoethanol.

Co-Immunoprecipitation of HA-SUSD4 in HEK293 cells

Proteins from HEK293 cell lysates were solubilized in lysis buffer (1 M Tris-HCl pH8, 10 mM EDTA, 1.5 M NaCl, 1% Tergitol™ (sigma; Cat#NP40), 2% Na azide, 10% SDS and 10% Na deoxycholate) supplemented with a protease inhibitor cocktail (1%) and MG132 (1%). Then, lysates were sonicated for 15 seconds, further clarified by a centrifugation at 14,000 rpm for 10min. Supernatants were collected and incubated with Dynabeads protein G (life technologies, Cat#10004D) and 28.8 µg of rat monoclonal anti-HA antibody (for details see antibodies) under gentle rotation for 1h at 4°C. Precipitates were washed 3 times in lysis buffer and then eluted by boiling (65°C) the beads 15 min in βME-reducing sample buffer before SDS-PAGE.

Mass spectrometry analysis

Proteins were separated by SDS-PAGE on 10 % polyacrylamide gels (Mini-PROTEAN® TGX™ Precast Gels, Bio-Rad, Hercules USA) and stained with Protein Staining Solution (Euromedex, Souffelweyersheim France). Gel lanes were cut into 5 pieces and destained with 50 mM triethylammonium bicarbonate (TEABC) and three washes in 100% acetonitrile. Proteins were digested in-gel using trypsin (1.2 µg/band, Gold, Promega, Madison USA), as previously described(Thouvenot *et al.*, 2008). Digest products were dehydrated in a vacuum centrifuge.

Nano-flow liquid chromatography coupled to tandem mass spectrometry (NanoLC-MS/MS):

Peptides, resuspended in 3 µL formic acid (0.1%, buffer A), were loaded onto a 15 cm reversed phase column (75 mm inner diameter, Acclaim Pepmap 100® C18, Thermo Fisher Scientific) and separated with an Ultimate 3000 RSLC system (Thermo Fisher Scientific) coupled to a Q Exactive Plus (Thermo Fisher Scientific) *via* a nano-electrospray source, using a 120-min gradient of 5 to 40% of buffer B (80% ACN, 0.1% formic acid) and a flow rate of 300 nl/min.

MS/MS analyses were performed in a data-dependent mode. Full scans (375 – 1,500 m/z) were acquired in the Orbitrap mass analyzer with a 70,000 resolution at 200 m/z. For the full scans, 3×10^6 ions were accumulated within a maximum injection time of 60 ms and detected in the Orbitrap analyzer. The twelve most intense ions with charge states ≥ 2 were sequentially isolated to a target value of 1×10^5 with a maximum injection time of 45 ms and fragmented by HCD (Higher-energy collisional dissociation) in the collision cell (normalized collision energy of 28%) and detected in the Orbitrap analyzer at 17,500 resolution.

MS/MS data analysis: Raw spectra were processed using the MaxQuant environment ((Cox and Mann, 2008), v.1.5.5.1) and Andromeda for database search (Cox *et al.*, 2011). The MS/MS spectra were matched against the UniProt Reference proteome (Proteome ID UP00000589) of *Mus musculus* (release 2017_03; <http://www.uniprot.org>) and 250 frequently observed contaminants (MaxQuant contaminants database) as well as reversed sequences of all entries. The following settings were applied for database interrogation: mass tolerance of 7 ppm (MS) and 0.5 Th (MS/MS), trypsin/P enzyme specificity, up to two missed cleavages allowed, only peptides with at least seven amino acids in length considered, and Oxidation (Met) and acetylation (protein N-term) as variable modifications. The “match between runs” (MBR) feature was allowed, with a matching time window of 0.7 min. FDR was set at 0.01 for peptides and proteins.

A representative protein ID in each protein group was automatically selected using an in-house bioinformatics tool (leading v2.1). First, proteins with the most numerous identified peptides are isolated in a “match group” (proteins from the “Protein IDs” column with the maximum number of “peptides counts”). For the match groups where more than one protein ID are present after filtering, the best annotated protein in UniProtKB (reviewed entries rather than automatic ones), highest evidence for protein existence, most annotated protein according to the number of Gene Ontology Annotations (GOA Mouse version 151) is defined as the “leading” protein. Only proteins identified with a minimum of two unique peptides, without MS/MS in control immunoprecipitation and exhibiting more than 4-fold enrichment (assessed by spectral count ratio) in Sushi domain-containing protein 4 (SUSD4) immunoprecipitation, *vs.* control immunoprecipitation, in the two biological replicates, were considered as potential partners of SUSD4 (**Table 1**).

Gene Ontology analysis: The statistically enriched gene ontology (GO) categories for the 28 candidate proteins were determined by Cytoscape (v3.6) plugin ClueGO v2.5.3 (Bindea *et al.*, 2009). The molecular function category was considered (release 18.12.2018, <https://www.ebi.ac.uk/GOA>), except evidences inferred from electronic annotations. Terms are selected by different filter criteria from the ontology source: 3-8 GO level intervals, minimum of 4 genes per GO term and 10% of associated genes/term. A two-sided hypergeometric test for enrichment analysis (Benjamini-Hochberg standard correction used for multiple testing) was applied against the whole identified protein as reference set. Other predefined settings were used. Each node representing a specific GO term is color-coded based on enrichment significance (p-value). Edge thickness represents the calculated score (kappa) to determine the association strength between the terms.

Chemical LTD in cerebellar acute slices

300 μm -thick parasagittal cerebellar slices were obtained from P31-P69 WT and *Susd4* KO mice following the same protocol as for patch-clamp recordings. Slices were then incubated for 2h at 37°C in oxygenated BBS with or without proteasome (50 μM MG132) and protease inhibitors (100 $\mu\text{g}/\text{mL}$ Leupeptine, Sigma, Cat#11017101001). Chemical LTD was induced by incubating the slices for 5 minutes at 37°C in BBS containing 50 mM K^+ and 10 μM Glutamate, followed by a recovery period in BBS for 30 minutes at 37°C; in presence or not of inhibitors. Slices were then homogenized in lysis buffer, containing: 50mM Tris-HCl, 150mM NaCl, 0.1% SDS, 0.02% Na Azide, 0.5% Na Deoxycholate, 1% NP-40 and protease inhibitor cocktail (1:100). Homogenates were incubated 45 minutes at 4°C, then sonicated and centrifuged at 14000 r.p.m. for 10 minutes at 4°C. Supernatants were then heated at 65°C in 2X sample buffer prior to western blot analysis for detection of GLUA2 and GRID2.

Immunofluorescence

Labeling of primary hippocampal neurons: Hippocampi were dissected from E18 mice embryos and dissociated. 1.2×10^5 neurons were plated onto 18 mm diameter glass cover-slips precoated with 80 $\mu\text{g}/\text{mL}$ poly-L-ornithine (Sigma, Gothenburg, Sweden, Cat#P3655) and maintained at 37°C in a 5% CO_2 humidified incubator in neurobasal medium (Gibco, Massachusetts, USA, Cat#21103049) supplemented with 2% B-27 supplement (Gibco, Cat#17504044) and 2mM Glutamax (Gibco, Cat#35050-038). Fresh culture medium (neurobasal medium supplemented with 2% B-27, 2mM L-glutamine (Gibco, Cat#A2916801) and 5% horse serum (Gibco, Cat#26050088) was added every week for maintenance of the neuronal cultures.

Hippocampal neurons at days in vitro 13 (DIV13) were transfected using Lipofectamine 2000 and 0.5 μg plasmid DNA per well. After transfection, neurons were maintained in the incubator for 24h, then fixed with 100% methanol for 10 minutes at -20°C. After rinsing with PBS, non-specific binding sites were blocked using PBS containing 4% donkey serum (DS, Abcam, Cat#ab7475) and 0.2% Triton X-100 (Tx; Sigma, Cat#x100). Primary and secondary antibodies were diluted in PBS 1% DS / 0.2% Tx and incubated one hour at room temperature. Three PBS 0.2% Tx washes were performed before and after each antibody incubation. Nuclear counterstaining was performed with Hoechst 33342 (Sigma, Cat#H6024) for 15 min at room temperature.

Labeling of brain sections: 30 μm -thick parasagittal sections were obtained using a freezing microtome and brains obtained after intracardiac perfusion of mice with 4% PFA in PBS solution. Sections were washed three times for five minutes in PBS, then blocked with PBS 4% DS for 30 minutes. The primary antibodies were diluted in PBS, 1% DS, 1% Triton X-100. The sections were incubated in the primary antibody solution overnight at 4°C and then washed three times for five minutes in PBS 1% Tx. Sections were incubated in the secondary antibody, diluted in PBS 1% DS 1% Tx solution, for 1 hour at room temperature. The sections were then incubated for 15 minutes at room temperature with the nuclear marker Hoechst 33342 (Thermo Fisher Scientific, Cat#H1399) in PBS 0.2% Tx. Finally, the sections were washed three times for five minutes in PBS 1% Tx, recovered in PBS and mounted with Prolong Gold (Thermo Fisher Scientific, Massachusetts, USA, Cat#P36934) between microscope slides and coverslips (Menzel-gläser, Brunswick, Germany, Cat#15165252).

RT-PCR and quantitative RT-PCR

For standard RT-PCR, total RNA was isolated from the cortex, cerebellum and brainstem of 2-month-old *Susd4*^{-/-} knockout mice and *Susd4*^{+/+} control littermates, using the RNeasy mini kit

(Qiagen, Venlo, Netherlands, Cat#74104). Equivalent amounts of total RNA (100 ng) were reverse-transcribed according to the protocol of SuperScript® VILO™ cDNA Synthesis kit (Life Technologies, California, USA, Cat#11754-250) according to manufacturer's instructions. The primers used were forward 5'TGT TAC TGC TCG TCA TCC TGG3' and reverse 5'GAG AGT CCC CTC TGC ACT TGG3'. PCR was performed with an annealing temperature of 61°C, for 39 cycles, using the manufacturer's instructions (*Taq* polymerase; New England Biolabs, Massachusetts, USA, Cat#M0273S). Quantitative PCR was performed using the TaqMan universal master mix II with UNG (Applied Biosystems, Cat# 4440038) and the following TaqMan probes: *Rpl13a* (#4331182_Mm01612986_gH) and *Susd4* (#4331182_Mm01312134_m1).

Western Blot analysis

Proteins were resolved by electrophoresis on a 4-12% NuPAGE Bis-Tris-Gel according to Invitrogen protocols, then electrotransferred using TransBlot® Transfer Medium (Bio-Rad) to PVDF membrane (Immobilon-P transfer membrane, Millipore, Cat#IPVH00010). Membranes were blocked in PBS supplemented with Tween 0.2% (PBST) and non-fat milk 5% and incubated with primary antibodies in PBST- milk 5%. After washing in PBST, membranes were incubated with Horseradish Peroxidase-conjugated secondary antibodies in PBST-milk 5%. Bound antibodies were revealed using Immobilon Western (Millipore, Cat#WBKLS) or Western Femto Maximum Sensitivity (Thermo Fisher Scientific, Cat#34095) chemiluminescent solutions and images acquired on a Fusion FX7 system (Vilber Lourmat, Île-de-France, France).

Image acquisition and quantification

In situ hybridization images were acquired using an Axio Zoom. V16 (Zeiss, Oberkochen, Germany) microscope equipped with a digital camera (AxioCam HRm) using a 10x objective (pixel size 0,650µm). Immunofluorescence image stacks were acquired using a confocal microscope (SP5, Leica, Wetzlar, Germany), using a 63x objective (1,4NA, oil immersion, pixel size: 57nm for cell culture imaging, pixel size: 228nm for 63x; 76nm, 57nm, 45nm for higher magnifications for *in vivo* imaging). The pinhole aperture was set to 1 Airy Unit and a z-step of 200 nm was used. Laser intensity and photomultiplier tube (PMT) gain was set so as to occupy the full dynamic range of the detector. Images were acquired in 16-bit range.

Deconvolution was performed for the VGLUT1 images with Huygens 4.1 software (Scientific Volume Imaging) using Maximum Likelihood Estimation algorithm from Matlab. 40 iterations were applied in classical mode, background intensity was averaged from the voxels with lowest intensity, and signal to noise ratio values were set to a value of 25.

VGLUT1 and VGLUT2 puncta were analyzed using the Matlab software and a homemade code source (Dr. Andréa Dumoulin). The number, area and intensity of puncta were quantified using the mask of each puncta generated by the Multidimensional Image analysis software (MIA) from Metamorph. For each animal, puncta parameters were measured from four equidistant images within a 35-image stack at 160 nm interval, acquired from three different lobules (n=12).

Statistical analysis

Data from all experiments were imported in Prism (GraphPad Software, California, USA) for statistical analysis, except for electrophysiology data that were imported to Igor Pro 6.05 (WaveMetrics INC) for statistical analysis.

In the case of two column analyses of means, the differences between the two groups were assessed using two-tailed Student's t-test. Normality of populations were assessed using D'Agostino &

Pearson, Shapiro-Wilk and Kolmogorov-Smirnov normality tests. When groups did not fit the normal distribution, the Mann-Whitney non-parametric test was used. For the rotarod behavioral test (two variables, genotype and trial), two-way repeated measures ANOVA followed by Bonferroni post hoc test was performed. The two-tailed Student's one sample t-test (when normality criterion was met) or the two-tailed Wilcoxon Signed Rank Test was used to compare ratios to a null hypothesis of 1 for biochemical experiments or 100 for long-term plasticity (Fay, 2013). The two-tailed Mann-Whitney test was used to compare two populations of ratios. Differences in cumulative probability were assessed with the Kolmogorov-Smirnov distribution test, and differences in distribution were tested using the chi-squared test.

Supplementary references

- Bindea, G. *et al.* (2009) 'ClueGO : a Cytoscape plug-in to decipher functionally grouped gene ontology and pathway annotation networks', 25(8), pp. 1091–1093. doi: 10.1093/bioinformatics/btp101.
- Cox, J. *et al.* (2011) 'Andromeda: A peptide search engine integrated into the MaxQuant environment', *Journal of Proteome Research*, 10(4), pp. 1794–1805. doi: 10.1021/pr101065j.
- Cox, J. and Mann, M. (2008) 'MaxQuant enables high peptide identification rates, individualized p.p.b.-range mass accuracies and proteome-wide protein quantification.', *Nature biotechnology*, 26(12), pp. 1367–72. doi: 10.1038/nbt.1511.
- Crawley, J. N. (2006) *What's Wrong With My Mouse?: Behavioral Phenotyping of Transgenic and Knockout Mice: Second Edition*, *What's Wrong With My Mouse?: Behavioral Phenotyping of Transgenic and Knockout Mice: Second Edition*. doi: 10.1002/9780470119051.
- Fay, D. S. (2013) 'A biologist's guide to statistical thinking and analysis', *WormBook*. doi: 10.1895/wormbook.1.159.1.
- Holt, G. R. and Douglas, J. (1996) 'Comparison of Discharge Variability Visual Cortex Neurons', *Journal of Neurophysiology*, 75(5), pp. 1806–1814.
- Huang, S. and Uusisaari, M. Y. (2013) 'Elevated temperature during slicing enhances acute slice preparation quality', *Frontiers in Cellular Neuroscience*, 7(APR), pp. 1–8. doi: 10.3389/fncel.2013.00048.
- Thouvenot, E. *et al.* (2008) 'Enhanced Detection of CNS Cell Secretome in Plasma Protein-Depleted Cerebrospinal Fluid research articles', pp. 4409–4421.

Résumé :

La schizophrénie, pathologie psychiatrique neurodéveloppementale parmi les plus invalidantes, est maintenant considérée comme une synaptopathie, une maladie des synapses. Cependant, les mécanismes développementaux menant à la formation et la régulation fine de la circuiterie synaptique n'ont été que peu étudiés. Le réseau olivo-cérébelleux, de par son architecture synaptique stéréotypée et bien connue, est un modèle de choix pour étudier les mécanismes du développement synaptique. De plus, bien qu'initialement connu pour ses fonctions motrices, le cervelet est aussi impliqué dans des tâches cognitives plus complexes, et pourrait jouer un rôle dans l'étiologie de la schizophrénie.

Dans ce projet de thèse, j'ai utilisé deux modèles murins mimant deux facteurs de risque associés à la schizophrénie : le modèle génétique LgDel, mimant la délétion 22q11 chez l'homme, associée à un fort surrisque de développer la schizophrénie, et le modèle pharmacologique chronique néonatal phencyclidine (PCP), en tant que perturbation environnementale du développement postnatal. J'ai étudié dans ces deux modèles la morphologie et les propriétés électrophysiologiques globales du cervelet, ainsi que l'organisation de chacune des afférences synaptiques de la cellule de Purkinje, le principal neurone du cortex cérébelleux. Ces propriétés étaient toutes normales dans le modèle génétique LgDel. Cependant, le modèle PCP a montré un déficit spécifique de la fibre grimpanche, à savoir une baisse du volume des boutons synaptiques, ainsi qu'une augmentation locale de leur densité. Ces déficits sont associés à une dérégulation transitoire de l'expression de gènes pouvant interférer avec le développement des synapses du cervelet, dont le gène codant pour la protéine sécrétée CTGF, fortement surexprimée dans le cervelet des souris durant l'injection de PCP. Cette protéine est particulièrement prometteuse, de par sa fonction, et ses interactions avec de nombreux acteurs du développement synaptique. De plus, j'ai montré qu'une augmentation de l'activité des neurones granulaires du cervelet durant la seconde semaine postnatale est suffisante pour induire une augmentation de l'expression de *Ctgf*. Enfin, les résultats de cette thèse suggèrent qu'une dérégulation d'origine environnementale de l'activité neuronale durant une période critique du développement peut perturber la mise en place et l'organisation de la microcircuiterie synaptique dans le cervelet, pouvant potentiellement jouer un rôle dans les pathologies neurodéveloppementales telles que la schizophrénie.

Mots clés : synapses, cervelet, schizophrénie, Purkinje, développement, fibre grimpanche

Abstract:

Schizophrenia, one of the most debilitating neurodevelopmental psychiatric pathologies, is now considered is a synaptopathy, a disease of the synapse. However, the developmental mechanisms leading to the formation and fine-tuning of synaptic circuitry have been poorly studied. The olivo-cerebellar network, because of its stereotypical and well-known synaptic architecture, is a useful model for studying the mechanisms of synaptic development. In addition, although initially known for its motor functions, the cerebellum is also involved in more complex cognitive tasks, and may play a role in the etiology of schizophrenia. In this thesis project, I used two murine models mimicking two risk factors associated with schizophrenia: the LgDel genetic model, mimicking the 22q11 deletion in humans associated with a high risk of developing schizophrenia, and the pharmacological model chronic neonatal phencyclidine (PCP), as an environmental disruption of postnatal development. In these two models, I studied the overall morphology and electrophysiological properties of the cerebellum, as well as the organization of each synaptic afferent of the Purkinje cell, the main neuron of the cerebellar cortex. These properties were all normal in the LgDel genetic model. The PCP model showed a specific deficit of cerebellar climbing fiber morphology, while other afferents were unaffected. The injection of PCP during the second postnatal week is associated with a transient deregulation of the expression of genes that can interfere with the development of cerebellar synapses, including the gene encoding the secreted protein CTGF, strongly transiently overexpressed in the cerebellum of PCP mice. This protein is particularly promising, because of its function and its functional interactions with many players in synaptic development. In addition, I have shown that an increase in the activity of cerebellar granule cells during the second postnatal week is sufficient to induce an increase in *Ctgf* expression. Finally, the results of this thesis suggest that an environmental deregulation of neuronal activity during a critical period of synaptic development can disrupt the establishment and organization of the synaptic microcircuitry in the cerebellum, potentially playing a role in neurodevelopmental pathologies such as schizophrenia.

Keywords: synapses, cerebellum, schizophrenia, Purkinje, development, climbing fiber